The complex inositol metabolism of *Corynebacterium glutamicum* and its application for the production of rare inositols

Inaugural Dissertation

for the attainment of the title of doctor
in the Faculty of Mathematics and Natural Sciences
at the Heinrich Heine University Düsseldorf

presented by

Paul Ramp

Born in Frankfurt am Main

Jülich, September 2022

This thesis in hand has been performed at the Institute of Bio- and Geosciences, IBG-1: Biotechnology, Forschungszentrum Jülich GmbH, from April 2019 until September 2022 under the supervision of Prof. Dr. Michael Bott and Dr. Meike Baumgart.

Printed with the permission of
the Faculty of Mathematics and Natural Sciences
of the Heinrich Heine University Düsseldorf

Examiner: **Prof. Dr. Michael Bott**
Institute of Bio- and Geosciences, IBG-1: Biotechnology
Forschungszentrum Jülich GmbH

Co-examiner: **Prof. Dr. Vlada Urlacher**
Institute of Biochemistry II
Heinrich Heine Universität Düsseldorf

Date of the oral examination: 23.03.2023

„DON’T PANIC“

— **Douglas Adams, 1979**. The Hitchhiker´s Guide to the Galaxy

Results described in this dissertation have been published in the following original publications or are summarized in manuscripts that will be submitted soon:

Ramp, P., Lehnert, A., Matamouros, S., Wirtz, A., Baumgart, M., & Bott, M. (2021). Metabolic engineering of Corynebacterium glutamicum for production of scyllo-inositol, a drug candidate against Alzheimer's disease. *Metabolic Engineering*, *67*, 173-185.

Ramp, P., Pfleger C., Dittrich J., Mack, C., Gohlke, H., Bott, M. (2022). Physiological, biochemical, and structural bioinformatic analysis of the multiple inositol dehydrogenases from *Corynebacterium glutamicum*. – accepted in *Microbiology Spectrum*, August 24, 2022

Ramp, P., Mack, C., Wirtz, A., Bott, M. (2022). Production of D-*chiro*-inositol with *Corynebacterium glutamicum* via two different synthesis routes. – to be submitted

Further publications not discussed in this thesis:

Davoudi, C. F., Ramp, P., Baumgart, M., & Bott, M. (2019). Identification of Surf1 as an assembly factor of the cytochrome bc_1-aa_3 supercomplex of Actinobacteria. *Biochimica et Biophysica Acta (BBA)-Bioenergetics*, *1860* (10), 148033.

Bakkes, P. J., Ramp, P., Bida, A., Dohmen-Olma, D., Bott, M., & Freudl, R. (2020). Improved pEKEx2-derived expression vectors for tightly controlled production of recombinant proteins in *Corynebacterium glutamicum*. *Plasmid*, *112*, 102540.

Content

Summary

Inositols (cyclohexanehexols) comprise nine isomeric cyclic sugar alcohols, several of which occur in all domains of life with various functions. The most abundant isomer is *myo*-inositol (MI). Its rare isomers, *scyllo*- (SI) and D-*chiro*-inositol (DCI) are promising drug candidates for treating Alzheimer's disease, diabetes type 2 and polycystic ovary syndrome. Therefore, cost efficient processes for the production of these compounds are desirable. Many bacteria can utilize inositols as carbon and energy source via a specific pathway involving inositol dehydrogenases (IDHs) as the first step of catabolism, followed by the actions of inosose isomerases. The microbial cell factory *Corynebacterium glutamicum* can grow on MI as sole carbon source and possesses many uncharacterized genes that are annotated to contribute to inositol degradation. It also has the innate ability to synthesize MI from glucose-6-phosphate. This thesis aimed to elucidate the function of the undescribed genes for inositol metabolism and exploit the potential of *C. glutamicum* to be engineered as a suitable host for the biotechnological production of SI and DCI.

Throughout the studies reported in this thesis, *C. glutamicum* was found to grow on *myo*-, *scyllo*-, D-*chiro*- and L-*chiro*-inositol as single carbon and energy source. Overall, seven IDHs were identified of which the five: IolG, OxiB, IdhA3, OxiD and OxiE were characterized as NAD^+-dependent and contribute differently to growth on the tested inositols. OxiC was without function while IolW proved to be an NADPH-dependent *scyllo*-IDH. Sequence alignments, crystal structure elucidation, structure modeling and molecular docking experiments revealed cofactor and substrate binding sites that can partially explain the reason behind inositol selectivity and different activities for the identified IDHs.

To generate an efficient *C. glutamicum* chassis strain that cannot degrade inositols, 21 genes spread among two gene clusters had to be deleted. Overexpression of *iolG* and *iolW* in the generated chassis strain enabled efficient biotransformation of MI to SI, which could be optimized to 100% efficiency by changing media conditions. Combined expression of *iolG* with the newly discovered inosose isomerase cg0212 enabled production of DCI from MI. The heterologous expression of the plant-derived D-ononitol and D-pinitol dehydrogenase genes *MtOEPa* and *MtOEPb* enabled a novel biosynthesis route for DCI. Combining these processes with the overexpression of the *myo*-inositol-1-phosphate synthase *ino1* in the *C. glutamicum* chassis strain enabled the production of 4.4.g/L SI and 1.2 g/L DCI starting directly from 20 g/L glucose or 20 g/L sucrose.

Zusammenfassung

Inositole (Cyclohexanhexole) umfassen neun zyklische Zuckeralkohol-Isomere, von denen mehrere in allen Bereichen des Lebens mit unterschiedlichen Funktionen vorkommen. Das am häufigsten vorkommende Isomer ist *myo*-Inositol (MI). Seine seltenen Isomere, *scyllo*- (SI) und D-*chiro*-Inositol (DCI), sind vielversprechende Arzneimittelkandidaten für die Behandlung der Alzheimer-Krankheit, von Diabetes Typ 2 und des polyzystischen Ovarsyndroms. Aufgrund dessen existiert die Nachfrage nach kosteneffizienten Verfahren für die Herstellung dieser Verbindungen. Viele Bakterien können Inositole als Kohlenstoff- und Energiequelle über einen spezifischen Abbauweg verstoffwechseln, an dem Inositol-Dehydrogenasen (IDHs) als erster Schritt des Katabolismus beteiligt sind, gefolgt von Inosose-Isomerasen. Die mikrobielle Zellfabrik *Corynebacterium glutamicum* kann auf MI als einzige Kohlenstoffquelle wachsen und besitzt viele noch nicht charakterisierte Gene, die zum Inositol-Abbau beitragen sollen. Es besitzt ebenfalls die Fähigkeit, MI aus Glucose-6-phosphat zu synthetisieren. Ziel dieser Arbeit war es, die Funktion der unbeschriebenen Gene für den Inositol-Stoffwechsel aufzuklären und das Potenzial von *C. glutamicum* als geeigneten Wirt für die biotechnologische Produktion von SI und DCI zu nutzen.

In den Studien, über die in dieser Arbeit berichtet wird, wurde festgestellt, dass *C. glutamicum* auf *myo*-, *scyllo*-, D-*chiro*- und L-*chiro*-Inositol als einzige Kohlenstoff- und Energiequelle wächst. Insgesamt wurden sieben IDHs identifiziert, von denen die fünf: IolG, OxiB, IdhA3, OxiD und OxiE als NAD^+-abhängig charakterisiert wurden und unterschiedlich zum Wachstum auf den getesteten Inositolen beitragen. OxiC war ohne Funktion, während IolW sich als NADPH-abhängige *scyllo*-IDH erwies. Sequenzalignments, Kristallstrukturaufklärung, Strukturmodellierung und molekulare Docking-Experimente ergaben Kofaktor- und Substratbindungsstellen, die den Grund für die Inositolselektivität und die unterschiedlichen Aktivitäten der identifizierten IDHs teilweise erklären können.

Um einen effizienten *C. glutamicum*-Chassis-Stamm zu erzeugen, der keine Inositole abbauen kann, mussten 21 Gene, verteilt auf zwei Gencluster, deletiert werden. Die Überexpression von *iolG* und *iolW* in dem erzeugten Chassis-Stamm ermöglichte eine effiziente Biotransformation von MI zu SI, die durch Anpassen der Medienbedingungen auf 100 % Effizienz optimiert werden konnte. Die kombinierte Expression von *iolG* mit der neu entdeckten Inosose-Isomerase cg0212 ermöglichte die Produktion von DCI aus MI. Die heterologe Expression der pflanzlichen D-ononitol- und D-pinitol-Dehydrogenasen *MtOEPa* und *MtOEPb* ermöglichte einen neuen Biosyntheseweg für DCI. Die Kombination dieser Prozesse mit der Überexpression der *myo*-Inositol-1-Phosphat-Synthase *ino1* im *C. glutamicum*-Chassis-Stamm ermöglichte die Produktion von bis zu 4,4 g/L SI und 1,2 g/L DCI direkt aus 20 g/L Glucose oder 20 g/L Saccharose.

Abbreviations

1KDCI	1-keto-D-*chiro*-inositol
2KMI	2-keto-*myo*-inositol
5DG	5-deoxy-D-glucuronic acid
a.u.	Arbitrary units
AD	Alzheimer's Disease
APH-1	Anterior pharynx defective 1
APP	Amyloid precursor protein
ATCC	American Type Culture Collection
ATP	Adenosine triphosphate
Aβ	Amyloid-β
BACE	Membrane-anchored β-secretase
CDP-DAG	Cytidine diphosphate diacylglycerol
DCI	D-*chiro*-inositol
DHAP	Dihydroxyacetone phosphate
DKG	2-deoxy-5-keto-D-gluconic acid
DKGP	2-deoxy-5-keto-6-phosphogluconic acid
DNA	Deoxyribonucleic acid
DPIN	D-pinitol
DT2	Diabetes type 2
FSH	Follicle stimulating hormone
G6P	Glucose-6-phosphate
GlcN-Ins	1D-*myo*-inositol-2-amino-2-deoxy-α-D-glucopyranoside
GPI	Glycosylphosphatidylinositol
HMIT	H^+/*myo*-inositol transporter
IMT	Inositol methyl transferase
Ino1	*myo*-inositol-1-phosphate synthase
IPG	Inositol phoshoglycans
IPTG	Isopropyl-β-D-thiogalactopyranoside
IR	Insulin receptor
IRS	IR substrates
LAM	Lipoarabinomannan
LCI	L-*chiro*-inositol

LM	Lipomannan
MI	*myo*-inositol
mIDH	*myo*-inositol dehydrogenase
MIOX	*myo*-inositol monooxygenase
MIP1	L-*myo*-inositol-1-phosphate
MIP6	*myo*-inositol hexakisphosphate
MIPS	*myo*-inositol-1-phosphate synthase
MSA	Malonic semialdehyde
NAD	Nicotinamide adenine dinucleotide
NIC	Nicastrin
ONO	D-ononitol
PCOS	Polycystic ovarian syndrome
PD	Parkinson's disease
PEN-2	Presenilin enhancer 2
PI	Phosphatidylinositol
PIM	Phosphatidylinositol mannosides
PIP	Phosphatidylinositol phosphate
PRES-1/2	Presenilin 1 or 2
RBS	Ribosome binding site
SI	*scyllo*-inositol
sIDH	*scyllo*-inositol dehydrogenase
SMIT	Sodium-*myo*-inositol cotransporter
TCA	Tricarboxylic acid
THcHDO	3D-(3,5/4)-trihydroxy-cyclohexane-1,2-dione
TSH	Thyroid stimulating hormone
wt	Wild type
wt/vol	Weight per volume
Δ	Deletion

Further abbreviations not included in this section are according to international standards, as, for example listed in the author guidelines of the *FEBS Journal*.

1. Introduction

1.1 Inositol isomers and derivatives

Inositol (1,2,3,4,5,6-cyclohexanol) is a cyclic carbohydrate with six hydroxyl groups, one on each carbon atom. The oldest known inositol is *myo*-inositol (MI), which was initially isolated in 1850 from muscle extracts and named after the greek word for muscle (μῦς: mys) (Majumder and Biswas, 2006; Scherer, 1850). MI is one of nine possible stereoisomers, as the six secondary hydroxyl groups can be arranged either axial or equatorial. Including MI, eight stereoisomers are known to occur in nature: *myo*-, *scyllo*-, D-*chiro*, L-*chiro*, *allo*-, *muco*-, *epi*- and *neo*-inositol (Fig. 1.1). Only the isomer *cis*-inositol, with all hydroxyl groups arranged in the axial position, was not found in nature and is only accessible by chemical synthesis (López-Gambero et al., 2020; Thomas et al., 2016). Inositols are found in all domains of life (Michell, 2008; Wakelam and Michell, 2007) as the inositol moiety is utilized as a precursor for a variety of compounds with a diverse portfolio of biological functions, such as signal transduction (Tsui and York, 2010), membrane biogenesis and cell wall formation (Fagone and Jackowski, 2009), ion channel physiology (Parys and De Smedt, 2012), phosphate storage, osmoregulation, and anti-oxidative activity (Al-Suod et al., 2017; Loewus and Murthy, 2000; Thomas et al., 2016).

Biosynthesis of all inositol-containing compounds starts with MI (Fig. 1.1). It is the only inositol isomer that is synthesized *de novo* from glucose-6-phosphate (G6P), which is first converted to L-*myo*-inositol-1-phosphate (MIP1) by an NAD^+-dependent *myo*-inositol-1-phosphate synthase (MIPS or Ino1) (Bachhawat and Mande, 1999; Loewus and Kelly, 1962; Stieglitz et al., 2005). The reaction starts with the open ring form of G6P by oxidation of C5 via hydride transfer to the cofactor NAD^+ (Ramos-Figueroa and Palmer, 2022). The next two steps consists of an enolization and an aldol reaction resulting in a cyclization via C6–C1 bond formation. Finally, a hydride transfer from NADH to the C5 carbonyl group generates the product MIP1 and regenerates the cofactor NAD^+. Afterwards, MIP1 is dephosphorylated to MI by a *myo*-inositol phosphatase (Nigou and Besra, 2002; Stieglitz et al., 2007). The other naturally occuring inositol isomers are obtained by epimerization of one or two hydroxyl groups of MI (Hipps et al., 1982; Hipps et al., 1973) (Fig. 1.1).

Inositols are incorporated in phosphatidylinositol (PI) by esterification of inositol to cytidine diphosphate diacylglycerol (CDP-DAG) via a phosphodiester linkage (Blunsom and Cockcroft, 2020a) (Fig. 1.1). PI is a vital lipid and structural component of cellular membranes and participates in essential metabolic processes in all plants and animals (Gardocki et al., 2005).

The most abundant stereochemical forms are *myo*-PI and D-*chiro*-PI, but in some plants *scyllo*-PI isomers have been identified (Kinnard et al., 1995). PIs can further function as precursors for various glycosylphosphatidylinositols (GPIs), which are synthesized by glycosidically binding glucosamine and mannose to the inositol residue (Ferguson, 1999; Majumder and Biswas, 2006). GPIs can be attached to the C-terminus of a protein during post-translational modification. The resulting GPI-anchored proteins can be displayed on the cell surface and play key roles in various biological processes (Eisenhaber et al., 2003; Paulick and Bertozzi, 2008).

In higher eukaryotic cells, PIs can also be further phosphorylated to PI phosphates (or phosphoinositides, PIP) that are incorporated in cell membranes where they function as important cell signaling compounds (Balla, 2013; Di Paolo and De Camilli, 2006). Several lipid kinases and phosphatases selectively insert and remove monoester phosphates in three of the remaining free positions of the inositol ring (C3, C4, C5) (Tolias and Cantley, 1999), generating the seven currently known PIP species (PI(3,4,5)P1-3: number of phosphates varies between one and three) (Blunsom and Cockcroft, 2020a). An important representative is PI-4,5-bisphosphate (PIP2), a substrate of phospholipase C that hydrolyzes the phosphodiester bond to yield diacylglycerol (DAG) and free inositol-1,4,5-triphosphate (IP3), which acts as a second messenger (Taylor and Machaca, 2019).

In plants, even higher phosphorylated IPs are found, with the number of substituted phosphate groups on the inositol ring varying between one and six (IP_{1-6}). *Myo*-inositol hexakisphosphate (MIP6), also known as phytic acid, is the most abundant form and functions as phosphate storage mostly in seeds (Gerke, 2015; Loewus and Murthy, 2000; Wang et al., 2022). Its synthesis starts with MIP1, which is sequentially phosphorylated by several kinases, each adding one phosphate group (Rasmussen et al., 2010). However, IP3 released from PIP2 can also be channeled into phytic acid synthesis (Suzuki et al., 2007). Besides MIP1-6, mono-, di- and multi-phosphate derivatives of *neo*-, *scyllo*- and D-*chiro*-inositol phosphates were identified in terrestrial and aquatic environments, however, their exact origins remain unknown (Cosgrove and Irving, 1980; Turner et al., 2002). In the biogeochemical cycle, MIPs accumulate in soil by rotting dead plant matter, animal wastes, and released IPs from microbial biomass. It is hypothesized that inositol-utilizing microorganisms are responsible for epimerization and dephosphorylation of MIPs to *neo*-, *scyllo*- and D-*chiro*-inositol phosphates (L'Annunziata et al., 2007; Turner et al., 2002).

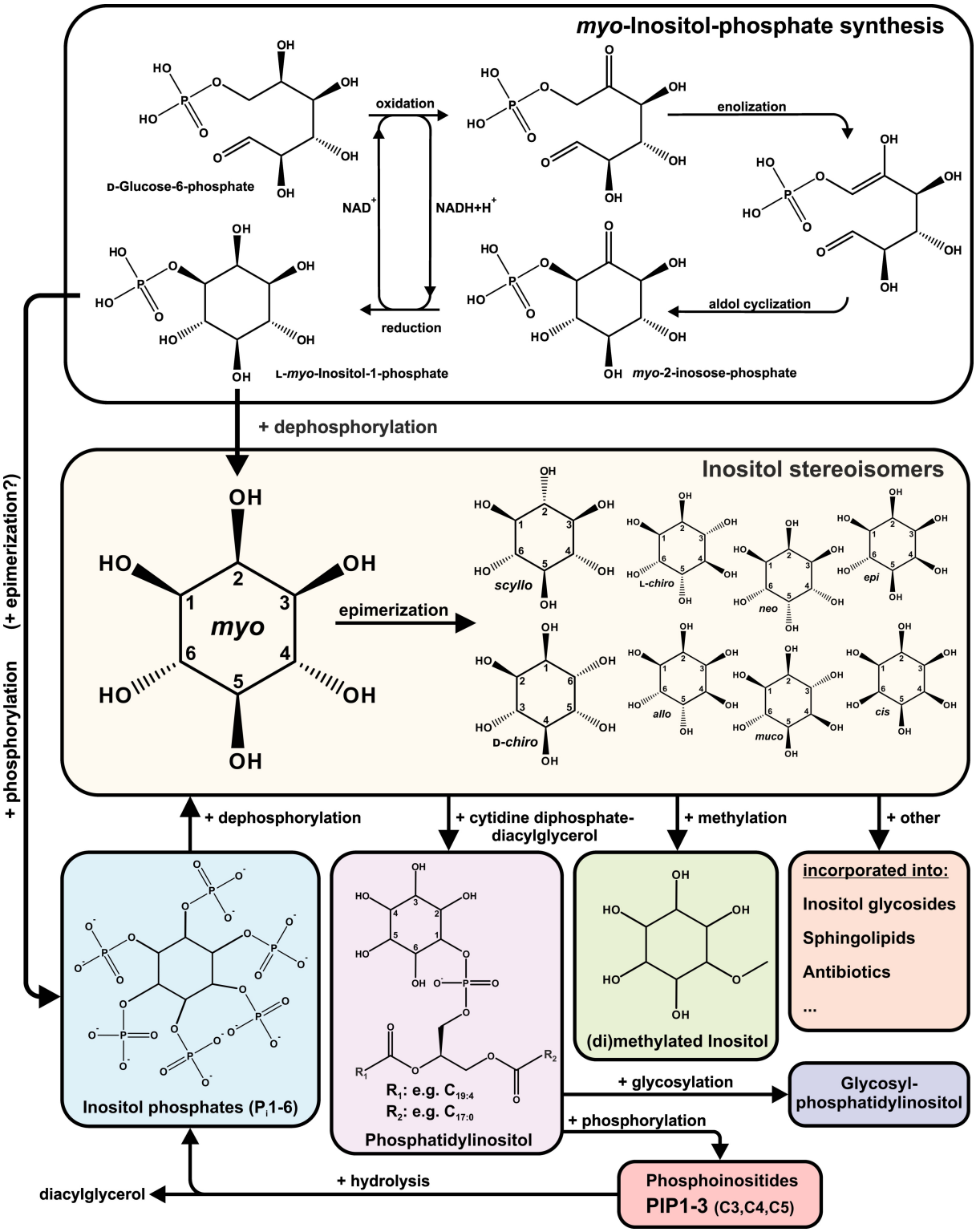

Fig. 1.1. Inositols and derivatives. L-*myo*-inositol-1-phosphate (MIP1) is synthesized from D-glucose-6-phosphate via NAD^+-dependent *myo*-inositol-1-phosphate synthase. MIP1 is dephosphorylated to *myo*-inositol (MI), which can be converted to other stereoisomers via epimerization of one or two hydroxyl groups. Inositols are incorporated into many different compounds, including phosphatidylinositol (PI), inositol (poly-)phosphates with phosphate groups varying between 1 and 6, (di-)methylated inositols, and further metabolites. PIs are phosphorylated at C3, C4 and C5 to yield phosphoinositides, which can be hydrolyzed to recover inositol phosphates.

Other inositol derivatives identified are secondary plant metabolites consisting of mono- and dimethylated inositols, which mainly function as osmolytes in response to abiotic stress. S-adenosylmethionine-dependent inositol methyltransferases methylate specific hydroxyl groups resulting in several isomers such as 4-*O*-methyl-*myo*-inositol (D-ononitol) (Pupel et al., 2019), 3-*O*-methyl-D-*chiro*-inositol (D-pinitol; DPIN) (Sanchez-Hidalgo et al., 2021), 3-*O*,6-*O*-dimethyl-D-*chiro*-inositol (pinpollitol) (Sureshan et al., 2009), and more (Al-Suod et al., 2017). Further inositol derivatives consist of inositol glycosides-like sphingolipids (Tartaglio et al., 2017) and ceramides (Buré et al., 2014). Inositols also function as building blocks of aminoglycoside antibiotics produced by *Streptomyces* species, such as streptomycin or kasugamycin (Kudo and Eguchi, 2009).

1.2 Inositols in human metabolism and their pharmaceutical relevance

Inositols occur in all domains of life, so naturally, they play a central role in various cellular processes in the human body. The most abundant isomer in human tissue is MI representing approximately 99% of the inositol pool. The remaining 1% mainly consists of DCI and traces of SI identified in some tissue cells (Özturan et al., 2019). In the past, MI was considered an essential nutrient belonging to the vitamin B family. However, discovering inositol biosynthesis in liver and kidney tissue took away the title (Regidor and Schindler, 2016). Yet, the necessary amount of MI for the human body can be obtained via dietary uptake. A western diet has been estimated to provide about 1 g/day of MI (Bizzarri et al., 2016; Goodhart and Shils, 1980), with animal-based food containing mainly free MI and PIs, while plant-derived food contains MI preferentially as phytic acid (Caputo et al., 2020). Phytic acid is partially degraded by a combination of brush border membrane-associated endogenous phytases, phosphatases, pancreatic phospholipases, and microbial phytases, which results in the release of lower MIPs and even free MI in the intestine (Holub, 1986; Huber, 2016) (Fig. 1.2). Although the other inositol isomers are mainly derived from MI, DCI was also found to be obtained from its methylated derivative DPIN. DPIN is demethylated to free DCI under acidic conditions in the gastrointestinal tract (Kiani et al., 2021) (Fig. 1.2).

After intestinal absorption, MI is distributed to different tissue via the bloodstream (Lewin et al., 1976). Transport of inositol compounds from blood plasma into cells is an active and saturable carrier-mediated process (Bizzarri et al., 2016) performed by the sodium- and proton-dependent inositol transporters SMIT1 (Berry et al., 1995), SMIT2 (Coady et al., 2002), and

the H^+/*myo*-inositol transporter HMIT (Uldry et al., 2001) (Fig. 1.2). SMIT1 and SMIT2 have been identified in many body tissues. Still, they are predominantly present in the intestine, kidney tissue and brain tissue (Schneider, 2015), while HMIT is exclusively present in the latter (Uldry et al., 2001).

The inositol concentration in blood plasma and tissue cells is regulated by a complex balance between dietary MI uptake, incorporation into derivatives, *de novo* synthesis, excretion, and catabolic utilization as energy source (Dinicola et al., 2017). MI degradation mainly occurs in kidney cells (Chang et al., 2015; Howard Jr and Anderson, 1967), a process that is initiated by the *myo*-inositol monooxygenase (MIOX), a non-heme iron enzyme that converts MI to D-glucuronic acid (Arner et al., 2001). The subsequent steps include the conversion of D-glucuronic acid to D-xylulose-5-phosphate, which enters the pentose phosphate pathway (Arner et al., 2004) (Fig. 1.2). Kidney and liver cell tissues also synthesize up to 4 g MI per day via the elaborated mechanism (chapter 1.1) (Clements Jr and Diethelm, 1979).

As stated before in chapter 1.1, inositols are important substrates for the synthesis of PI. In eukaryotic cells, PI synthesis takes place at the endoplasmatic reticulum (ER) where MI or DCI are joined with CDP-DAG, catalyzed by the PI synthase (Blunsom and Cockcroft, 2020b). Through the ER, PIs undergo glycosylation to produce GPIs (Michell, 2018), which are then incorporated into the cell membrane. PI is also transported directly to the cell membrane by PI transport proteins, where it makes up 10–15% of mammalian membrane phospholipids (Vance, 2015). There, a complex array of different kinases phosphorylate *myo*-PI to yield PIPs (Blunsom and Cockcroft, 2020a). In mammals, hormones and neurotransmitters regulate phospholipase C, which is responsible for the release of the second messengers IP3 and DAG from PIP2 (Kadamur and Ross, 2013; Nakamura and Fukami, 2017) (Fig. 1.2). IP3 induces Ca^{2+} release in many tissues, which initiates the regulation of hormones such as thyroid stimulating hormone (TSH), follicle stimulating hormone (FSH), and insulin (Alberts et al., 2015; Bizzarri and Carlomagno, 2014).

As inositols are involved in many metabolic and signaling processes throughout the human body, improper biosynthesis, distribution, uptake, or degradation is associated with metabolic diseases. Hence, many studies deal with investigating the potential pharmaceutical applications of inositols. Administration of MI, DCI, SI, and their phosphate derivatives is tested against diseases that are directly connected to an improper inositol balance, but also the applications of isomers and derivatives not natural to the human body are studied. This thesis focuses on the

inositols MI, DCI and SI. Therefore, only explicit examples for their pharmaceutical use will be covered. The following chapters explain the roles of MI and DCI in the treatment of insulin resistance as well as the application of SI for the treatment of neurodegenerative diseases like Alzheimer's disease (AD).

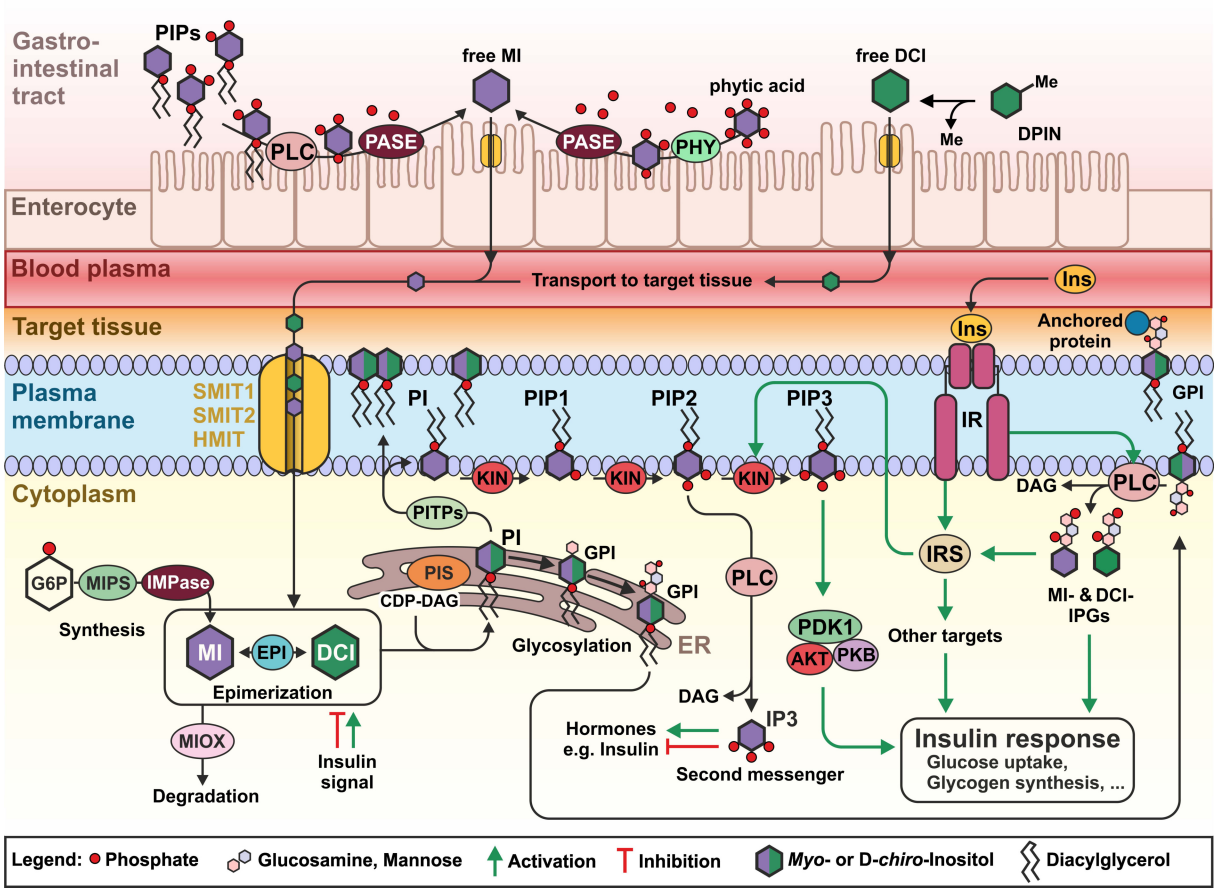

Fig. 1.2. Inositol uptake, metabolism and further processing with impact on insulin signaling. Phytic acid and phosphoinositides (PIP) are degraded to free *myo*-inositol (MI) by phytases (PHY), phospholipase C (PLC), and phosphatases (PASE). D-pinitol (DPIN) is demethylated to free D-*chiro*-inositol (DCI). Inositols are taken up by Na^+-dependent MI transporters (SMIT1 and SMIT2) and an H^+-dependent MI importer (HMIT). Inositols are transported to target tissue cells. MI and DCI can be degraded by *myo*-inositol monooxygenase (MIOX). MI can be synthesized from glucose-6-phosphate (G6P) by *myo*-inositol-1-phosphate synthase (MIPS) and inositol phosphatases (IMPase). Interconversion of MI and DCI catalyzed by an inositol epimerase (EPI) is regulated by an insulin signal. Inositols are linked to cytidine diphosphate diacylglycerol (CDP-DAG) at the endoplasmatic reticulum (ER) by phosphatidylinositol synthase (PIS) to yield phosphatidylinositol (PI). PIs are transported to the cell membrane by phosphatidylinositol transporter proteins (PITPs). *Myo*-PI is further phosphorylated by specific kinases (KIN) to PIP1-3. PIs are glycosylated with glucosamines and mannosides to glycosylphosphatylinositol (GPI). GPIs are transported to the cell membrane and can function as membrane anchor for proteins. Insulin (Ins) binds to the insulin receptor (IR) and activate IR substrates (IRS). IRS activates a kinase that catalyzes the phosphorylation of PIP2 to PIP3. PIP3 activates PDK1 that subsequently activates PKB/AKT, which mediate insulin responses. PIP2 can be cleaved by PLC to generate DAG and inositol-triphosphate (IP3), which regulates insulin and other hormones. Inositolphosphoglycans (IPG) are cleaved from GPI by PLC under insulin stimulus and stimulate IRS and other insulin response reactions.

1.2.1 Role in insulin signaling and treatment of insulin resistance

Diabetes mellitus type 2 (DT2) affects over 400 million adults with numbers increasing. It is mainly caused by an obesity epidemic in highly developed countries. Diabetes and its associated complications are the fourth leading cause of mortality worldwide and with its increasing cases becomes a major economic burden for health care systems. These complications can include increased risk for cardiovascular diseases, blindness, kidney failure, and more (Deshpande et al., 2008; Owczarczyk-Saczonek et al., 2018). The development of DT2 is caused by a combination of lifestyle and genetic factors. One preceding effect is the development of insulin resistance, in which target tissues are not able to maintain a coordinated response to a normal insulin plasma level (Petersen and Shulman, 2018).

Insulin is a peptide hormone produced by beta (β) cells in the Islets of Langerhans in pancreas tissue (Mears, 2004). It regulates glucose uptake from the bloodstream and its further metabolism in peripheral tissues. Insulin output is tightly regulated by blood glucose concentration to maintain a constant blood sugar level (Wilcox, 2005). In insulin-resistant patients, blood glucose uptake is impaired as cells are not or less stimulated by insulin. The main reasons and mechanism leading to insulin resistance are still uncertain. However, in most cases it is hypothesized that insulin resistance manifests at the cellular level via post-receptor defects in the insulin signaling pathway (Wheatcroft et al., 2003; Wilcox, 2005).

The canonical insulin signaling is based on insulin binding to the insulin receptor (IR) in target tissues, promoting tyrosine autophosphorylation of IR (Fig. 1.2). This acts as a signal for the recruitment of different IR substrates (IRS), which are then phosphorylated by IR. Activated IRS proteins stimulate, among others, the generation of PIP3, which then activates the phosphoinositide-dependent kinase Pdk-1 and subsequently Pkb/Akt. Pkb and Akt account for most of the intracellular actions of insulin, for example, increased expression and translocation of glucose transporter genes or activation of glycogen synthesis (Boucher et al., 2014; Cheatham et al., 1994; Lizcano and Alessi, 2002).

The model of inositols acting in the insulin signaling pathway changed with the discovery of inositol phosphoglycans (IPG), which are released from GPIs upon insulin-promoted phospholipase C activity (Saltiel and Cuatrecasas, 1986; Saltiel et al., 1982). IPGs act as insulin modulators downstream of the signaling pathway via direct and indirect mechanisms, through the Pdk-1/Akt pathway (Fig. 1.2). IPGs are therefore described to exhibit insulin-mimetic effects and are differentiated between MI-IPG and DCI-IPG (Kessler et al., 1998). Both exhibit

different effects. MI-IPG regulates glucose transporters and glucose utilization, while DCI-IPG is involved in the regulation of glycogen synthesis and is part of a mediator in maintaining insulin sensitivity (Larner, 2002; Ortmeyer et al., 1993).

As inositols greatly contribute to insulin signaling and regulating blood-glucose levels, deviations in inositol homeostasis are one factor that can lead to insulin-resistance. In insulin-resistant and first-degree DT2 patient tissues, elevated MI and significantly reduced DCI excretion paired with overall deficient DCI bioactivity was observed (Asplin et al., 1993; Larner et al., 2010). The biosynthesis of DCI is based on an NAD^+/NADH-dependent epimerization of MI, stimulated by insulin. Under normal insulin signaling, this results in tissue or organ-specific ratios between MI and DCI. In insulin-resistant patients, this epimerization is diminished (Heimark et al., 2013; Unfer et al., 2014). Permanent insulin resistance is a sign of risk for developing DT2 and it accompanies a variety of other disorders, like nonalcoholic fatty liver disease (Marchesini et al., 1999), lipodystrophy (Petersen et al., 2002), and polycystic ovarian syndrome (PCOS). PCOS is the most common gynecological disorder, with 5% to 10% of women of reproductive age being afflicted (Thomas et al., 2016). It is a heterogeneous, multifaceted disorder characterized by infertility, chronic anovulation (irregular menstrual cycles), hyperandrogenism, and polycystic ovaries (Homburg, 2008).

Due to their insulin-mimetic effects, MI, DCI, and other inositol isomers are tested for treatment of insulin resistance by trying to counter the defective inositol homeostasis. Studies showed that concentrations of 1 mM DCI and different inositol isomers could stimulate glucose transporter translocation to the plasma membrane of cells of diabetic rats and therefore induce glucose uptake (Yap et al., 2007). Furthermore, low concentrations of MI and DCI promoted the phosphorylation of Akt and other insulin signaling cascade proteins in human vascular endothelial cells (D'Oria et al., 2017). Whole rat and mice trials showed that MI could inhibit intestinal glucose absorption and increase muscle glucose uptake (Chukwuma et al., 2016), while supplemented DCI-IPG acted as an insulin sensitizer leading to decreasing food intake and body weight (Jeon et al., 2016).

Furthermore, human clinical trials report that oral administration of DCI alone and in combination with MI could increase general insulin sensitivity in tissues of DT2 patients (Gambioli et al., 2021; Pintaudi et al., 2016). At doses ranging between 2 and 10 g/day, MI and DCI had favorable effects on glucose and insulin homeostasis, lipid profile, and arterial blood pressure in people with prediabetes or dyslipidemia. Administration of low DCI concentrations

could decrease blood pressure, serum androgens, and plasma triglycerides and promote ovulation in PCOS patients (Monastra et al., 2017; Ortmeyer et al., 1993). These direct and indirect evidences suggest that administration of MI, DCI, and derivatives has beneficial effects on the treatment of insulin resistance.

1.2.2 Role in treatment of Alzheimer's disease

The development of modern medicine increases the average life expectancy in many countries, however, this is associated with new challenges in the form of neurodegenerative diseases. Prominent examples are Alzheimer's disease (AD) and Parkinson's disease (PD). It is estimated that 35.6 million people worldwide were affected by AD in the year 2010, whereby the given number tends to double every 20 years, giving approximately 115 million affected people by the year 2050 (Prince et al., 2013). Most AD cases occur at higher age, surpassing 65 years, with symptoms varying from loss of memory and mood changes to learning deficits and changes in behavior (Bature et al., 2017). Yet, a small percentage of people exhibit AD symptoms much earlier in life, in their mid-30s (Van Cauwenberghe et al., 2016). The primary causes that ultimately lead to the clinical AD phenotype are not fully understood, however, many different factors like cholinergic dysfunctions (DeKosky et al., 1992), inflammatory reactions (Griffin et al., 1989), or DNA damage seem to contribute.

The most noted hypothesis for AD development is the Aβ hypothesis, in which the aggregation of amyloid-β (Aβ) plaques causing neural damage is thought to be the leading cause of the phenotypical manifestation of AD (Fig. 1.3). In brain tissue cells, the amyloid precursor protein (APP) is digested by β- and γ-secretase to yield Aβ peptides, whose natural functions are also not entirely certain. In more detail, the extracellular moiety of APP is first cleaved by the membrane-anchored β-secretase (BACE) (Yan et al., 1999). This process reveals a soluble APPβ protein and a membrane-integrated C99 fragment (Pulina et al., 2019; Seubert et al., 1993). C99 is cut within its transmembrane domain by the γ-secretase, a multi-subunit protease complex, consisting of presenilin 1 or 2 (PRES-1/2), nicastrin (NIC), presenilin enhancer 2 (PEN-2) and the stability factor "anterior pharynx defective 1" (APH-1). PRES1/2 provide the active center (De Strooper, 2003). The γ-secretase-mediated cut of C99 releases the high-molecular Aβ peptide. Aberrant activity of γ-secretase can lead to further processing of the Aβ peptide to the highly self-aggregating Aβ40 or Aβ42 fragments (Takami et al., 2009). Extracellularly, these peptides can accumulate to Aβ oligomers, which can form insoluble

fibrils, ultimately leading to aggregating of Aβ plaques around brain tissue cells (Ashrafian et al., 2021). Aggregation around neurons can result in disruption of signaling processes (Salehi et al., 2004), which leads to loss of brain functions, like memory. Aβ plaques can also start immune responses leading to inflammation in brain tissue, causing damage of surrounding neurons (Sigurdsson et al., 2004) (Fig. 1.3).

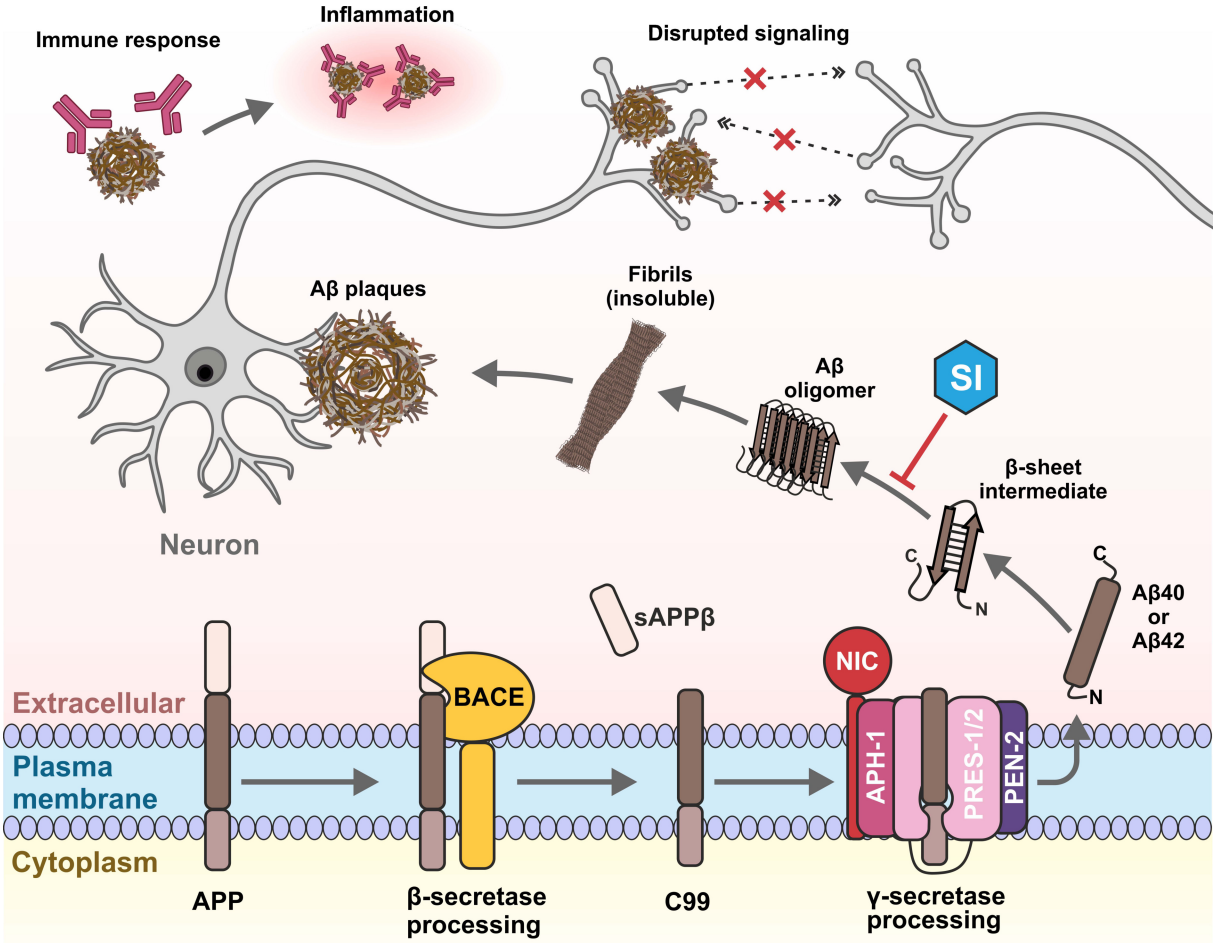

Fig. 1.3. Impact of *scyllo*-inositol on preventing amyloid β peptide aggregation and Aβ plaque formation. Amyloid precursor protein (APP) is digested by β-secretase (BACE) to yield soluble APPβ peptides and membrane-integrated C99 fragment. The γ-secretase multi-enzyme complex, consisting of presenilin 1 or 2 (PRES-1/2), nicastrin (NIC), presenilin enhancer 2 (PEN-2), and the stability factor anterior pharynx defective 1 APH-1, hydrolyses C99 to release Aβ40 or Aβ42 peptides. Aβ40/42 tend to form β-sheet intermediates that organize to Aβ oligomers. Aβ oligomers can aggregate to insoluble fibrils that accumulate to form Aβ-plaques, a distinct factor of Alzheimer's disease. *Scyllo*-inositol (SI) was shown to inhibit Aβ oligomer formation by stabilizing β-sheet conformation of Aβ-peptides.

In early onset AD patients, a significantly increased production of Aβ40/42 peptides is observed. The cause is traced back to mutations that mainly reside in the genes of the APP and the presenilin proteins (Chartier-Harlin et al., 1991; Holmes and Lovestone, 2002). Therefore,

the development of drug candidates against AD focused on compounds that could prevent Aβ42 peptides aggregation. Among the tested compounds are the inositols MI, SI, and *epi*-inositol, of which SI showed promising effects.

SI prevented the oligomerization of Aβ peptides via the formation of an inositol-Aβ complex *in vitro* (McLaurin et al., 2000) (Fig. 1.3) and successfully rescued Aβ oligomer-induced cognitive deficits and ameliorated disease pathology caused by Aβ oligomers in mice models (Fenili et al., 2007; Townsend et al., 2006). In clinical trials in humans, SI significantly reduced the amount of Aβ42 oligomers in cerebrospinal fluid or treated patients due to its good pharmacokinetic properties (Salloway et al., 2011). Moreover, SI could reduce the occurrence of neuropsychiatric symptoms (NPS) in AD significantly in a phase II clinical trial (Tariot et al., 2012). All taken together make SI a promising candidate in treatment against AD.

1.3 Bacterial inositol metabolism

1.3.1 Inositol catabolism

Inositols are not only implemented in diverse metabolic and signaling processes in eukaryotes, but are also found in microorganisms that utilize them as energy source or as building blocks for various metabolites. In the biogeochemical cycle, microorganisms are believed to be responsible for the accumulation of different inositol phosphate isomers besides MIP in soil (Turner et al., 2002). Research on bacterial inositol metabolism achieved its first breakthrough already over 50 years ago with the elucidation of the general inositol degradation pathway in *Klebsiella aerogenes* by Boris Magasanik and coworkers (Anderson and Magasanik, 1971; Berman and Magasanik, 1966a; Berman and Magasanik, 1966b; Magasanik, 1953). This pathway was later found to be highly conserved among inositol-utilizing bacteria. Over the years, many other microorganisms have been identified that can use inositols as sole carbon and energy source, for example, *Rhizobium leguminosarum* (Fry et al., 2001), *Bacillus subtilis* (Yoshida et al., 2008), *Sinorhizobium meliloti* (Kohler et al., 2010), *Paracoccus laeviglucosivorans* (Fukano et al., 2018; Shimizu et al., 2012), or *Legionella pneumophila* (Manske et al., 2016).

Nowadays, inositol catabolism has been best studied in *B. subtilis*, in which the whole catabolic pathway for not only MI, but also SI and DCI was explored and the corresponding genes identified (Fig. 1.4). Inositol catabolism starts with the uptake of inositol via specific inositol

transporters. For *B. subtilis*, the three transporters IolF, IolT, and YfiG have been identified (Bettaney et al., 2013; Morinaga et al., 2010b; Yoshida et al., 2002). After entering the cell, MI is first oxidized via the *myo*-inositol-2-dehydrogenase (mIDH) IolG at C2, resulting in the keto-intermediate 2-keto-*myo*-inositol (2KMI), also termed *myo*-inosose-2/*scyllo*-inosose. 2KMI enters the catabolic pathway via dehydration by the 2KMI dehydratase IolE yielding 3D-(3,5/4)-trihydroxy-cyclohexane-1,2-dione (THcHDO) and a water molecule (Yoshida et al., 2004). This intermediate is unstable, and via the addition of a water molecule catalyzed by the THcHDO acylhydrolase IolD the ring structure opens to yield 5-deoxy-D-glucuronic acid (5DG). 5DG is then isomerized by the 5DG isomerase IolB to 2-deoxy-5-keto-D-gluconic acid (DKG). The DKG kinase IolC transfers a phosphate from ATP to DKG to generate 2-deoxy-5-keto-6-phosphogluconic acid (DKGP). The DKGP aldolase IolJ cleaves DKGP into dihydroxyacetone phosphate (DHAP), which can directly enter the glycolytic pathway, and malonic semialdehyde (MSA). IolA, a malonate semialdehyde dehydrogenase, oxidizes malonate semialdehyde to acetyl-CoA with concomitant reduction of NAD^+ to $NADH+H^+$ and release of a CO_2 molecule. The resulting acetyl-CoA can then enter the tricarboxylic acid (TCA) cycle (Yoshida et al., 2008).

The inositol degradation pathway-encoding genes are often organized in a large operon, such as the *iolABCDEFGHIJ* operon in *B. subtilis* (Fig. 1.4) (Yoshida et al., 1997). Expression of the operon is typically regulated by a repressor called IolR, which often is encoded upstream of the inositol operon in the opposite direction, like in *B. subtilis* (Yoshida et al., 1999). In the presence of inositols, IolR forms a complex with the accumulating intermediate DKGP, which causes dissociation of IolR from its operator and induction of gene expression (Fig. 1.4) (Yoshida et al., 2008). Besides the large inositol operon, IolR also regulates the expression of genes encoding inositol transporters that are usually located elsewhere in the genome, like reported for *iolT* in *B. subtilis* (Yoshida et al., 2002).

Besides MI, *B. subtilis* was also shown to utilize SI and DCI. In the case of SI, the inositol transporter responsible for uptake is unknown, but three inositol dehydrogenases showing activity for SI were identified (Morinaga et al., 2010a; Kang et al., 2017b). The NAD^+-dependent *scyllo*-inositol 2-dehydrogenase (sIDH) IolX was found to be responsible for growth in minimal medium containing SI as single carbon and energy source. IolX oxidizes any C-atom of SI, thereby generating 2KMI, which can enter the degradation pathway (Fig. 1.4). In the genome of *B. subtilis, iolX* is preceded by the gene *iolQ* encoding its transcriptional repressor (Kang et al., 2017a). The two other sIDHs identified are IolW and IolU, NADPH-

dependent enzymes that catalyzes the opposite reaction, i.e., the reduction of 2KMI to SI (Fig. 1.4). The physiological meaning of this reaction is unclear.

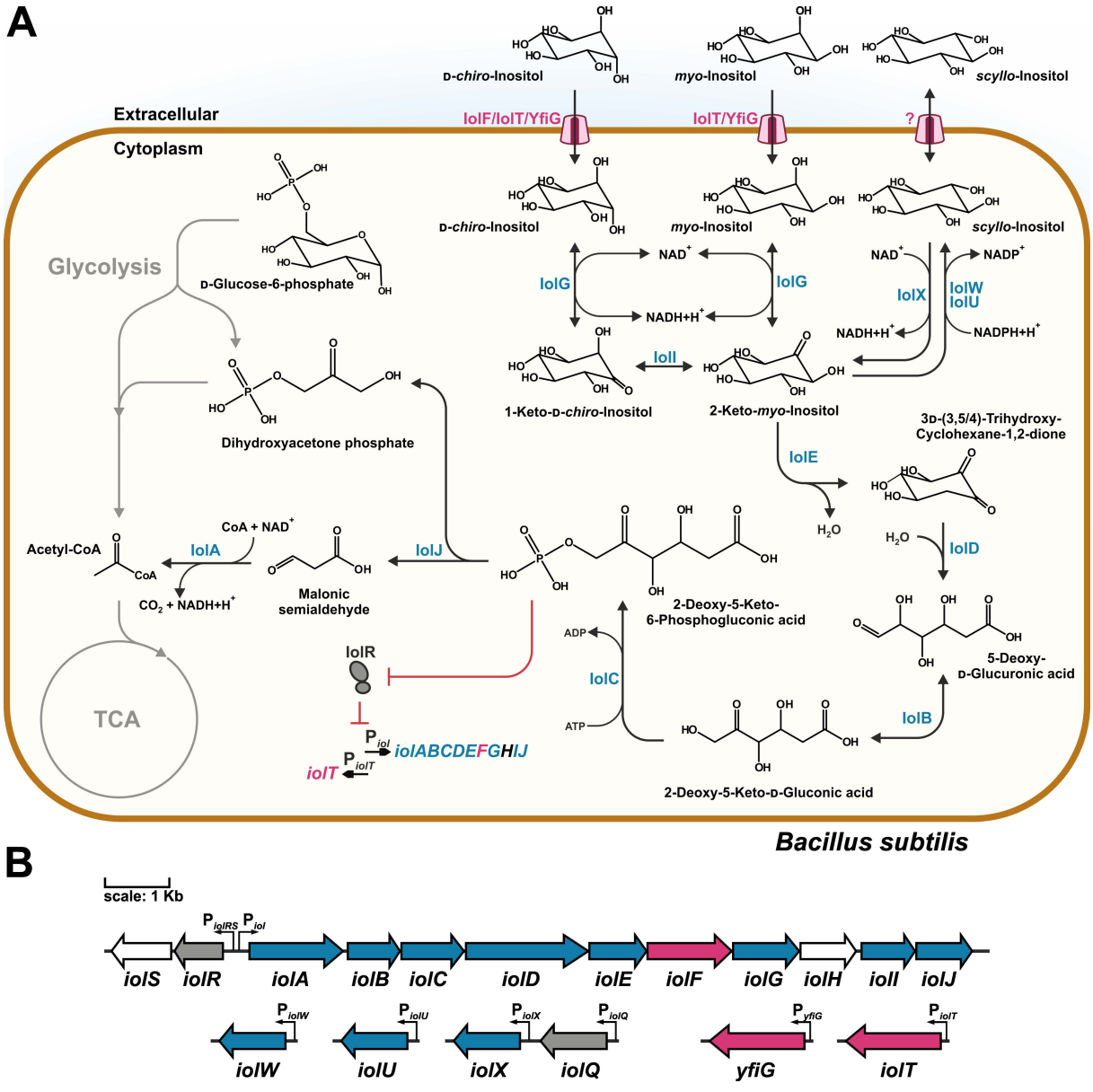

Fig. 1.4. Schematic overview of the inositol catabolism in *B. subtilis*. (A) Inositol catabolism starts with uptake via three specific secondary transporters (IolF, IolT, YfiG). MI and DCI are oxidized by the NAD^+-dependent inositol dehydrogenase IolG forming 2-keto-*myo*-inositol (2KMI) and 1-keto-D-*chiro*-inositol, respectively. The latter is isomerized to 2KMI by the inosose isomerase IolI. SI is oxidized by the NAD^+-dependent inositol dehydrogenase IolX to 2KMI. The inositol catabolic enzymes encoded in the large *iolABCDEFGHIJ* operon further degrade 2KMI to intermediates of central metabolism, dihydroxyacetone phosphate, acetyl-CoA, and CO_2. The NADPH-dependent sIDHs IolW and IolU reduce 2KMI to SI. Accumulating 2-deoxy-5-keto-6-phosphogluconic acid (DKGP) binds to IolR causing dissociation from its operator and induction of gene expression. **(B)** The *iolABCDEFGHIJ* operon and additional genes that show upregulation in presence of MI. The genes encoding enzymes involved in inositol catabolism are highlighted in blue, genes coding for inositol transporters are colored in magenta. Genes coding for transcriptional regulators are colored in grey and genes shown in white encode proteins of yet unknown function.

DCI was found to be taken up by all three inositol transporters (Bettaney et al., 2013). DCI is also oxidized by IolG, but at the C1 or C6, resulting in the intermediate 1-keto-D-*chiro*-inositol (1KDCI). It is hypothesized that 1KDCI must first be isomerized to 2KMI before being further degraded. This reaction is catalyzed by the inosose isomerase IolI, which is part of the large inositol operon in *B. subtilis* (Yoshida et al., 2006).

The two NAD^+-dependent IDH IolG and IolX of *B. subtilis* show different activities for either MI and DCI or for SI. In other inositol-degrading bacteria, multiple paralogous IDHs were identified that show overlapping substrate specificities (Aamudalapalli et al., 2018; Yoshida et al., 2012; Zhang et al., 2010). Some species containing multiple IDH-encoding genes were identified, although the inositol catabolic pathway is absent (Kohler and Rossbach, 2013; Zhang et al., 2010). Most IDHs accept a broad substrate spectrum, but remain highly stereoselective. The model enzyme of this class is the mIDH BsIolG of *B. subtilis,* which like the other known IDHs belongs to the GFO (glucose–fructose oxidoreductase)/IDH/MocA family of dehydrogenases. BsIolG oxidizes the inositols MI and DCI, but not the all-equatorial stereoisomer SI. Moreover, BsIolG also oxidizes the monosaccharides α-D-glucose and α-D-xylose, but not β-D-glucose, D-mannose, and D-galactose (Ramaley et al., 1979). The molecular reaction is based on a Bi Bi mechanism, with NAD^+ binding first and then inositol. The two products are released in opposite sequential order (van Straaten et al., 2010). The crystal structure of BsIolG showed that NAD^+ binds close to the GXGXXG consensus sequence motif for NAD(H)-binding proteins and the catalytic triad consisting of Lys97, Asp172, and His176 (*B. subtilis* numbering), similar to other members of the GFO/IDH/MocA family. The reaction mechanism is believed to be initiated by proton abstraction from His176, which would facilitate equatorial hydride transfer from C2 of inositol to C4 of the nicotinamide group of NAD^+ (van Straaten et al., 2010).

Crystal structure analysis of IDHs from *Lactobacillus casei* dealt with finding reasons behind inositol stereoselectivity and positioning in the active site. *L. casei* contains two homologous IDHs: LcIDH1, a mIDH with activity for MI and DCI, and LcIDH2, a sIDH showing activity for MI, DCI and SI with preference for the latter. Both IDHs bind MI with a conserved Asp residue, but in LcIDH1 His155 orients MI close to NAD^+ with an angular displacement of 22° compared to SI bound by Arg15 in LcIDH2. In LcIDH1 the equatorial OH group at the C2 position of SI would sterically clash with the nicotinamide ring (Aamudalapalli et al., 2018). Follow-up studies also reported that LcIDH2 does not necessarily oxidize MI at the C2, which would lead to the formation of 2KMI. LcIDH2 simultaneously oxidizes MI either at C5, C3, or

C1, resulting in *neo*-inosose (ratio 70%) as the major product, along with the minor products 1D-*chiro*-inosose (ratio 20%) and 1L-*chiro*-inosose (ratio 10%) (Ramos-Figueroa et al., 2020). These findings suggest that the inositol catabolism of microorganisms is more complex than described previously and that further enzymes involved in the initial steps of the degradation of other inositol isomers exist.

1.3.2 Role of inositols in *Actinobacteria*

In some bacteria, inositol is not necessarily used as a carbon and energy source, but serves as a precursor of structural and stress-response compounds. Members of the phylum *Actinobacteria* are exceptional in that they contain a diverse repertoire of essential inositol derivatives (Jackson et al., 2000; Newton et al., 2008; Vercellone et al., 1998). *Actinobacteria* are a large and diverse group of Gram-positive bacteria encountered in soil and seawater, but also in the skin, lungs, and gastrointestinal tract of humans. Some are used for the production of commercial products, including amino acids and antibiotics (Kalinowski et al., 2003; Weber et al., 2003), while others are responsible for causing human diseases, such as diphtheria (*Corynebacterium diphtheriae*) (Murphy, 1996; Sangal and Hoskisson, 2016) or tuberculosis (*Mycobacterium tuberculosis*) (Koch and Mizrahi, 2018). These bacteria can synthesize MI from G6P via the pathway described in chapter 1.1 catalyzed by a bacterial *myo*-inositol-1-phosphate synthase (Ino1) and inositol phosphatases.

MI serves as a precursor of several characteristic molecules of *Actinobacteria*. One important example is mycothiol (1-D-*myo*-inositol-2-(N-acetyl-L-cysteinylamino)-2-deoxy-α-D-glucopyranoside; MSH), the major thiol serving as a substitute of glutathione, which is the dominant thiol in other bacteria and eukaryotes, but absent in *Actinobacteria*. Like glutathione, MSH can prevent cellular damage caused by oxidative and other stresses (Liu et al., 2013; Vetting et al., 2008). MSH synthesis starts with MIP1 being fused to *N*-acetylglucosamine catalyzed by the *N*-acetylglucosaminyl transferase MshA (Fig. 1.5A). The phosphatase MshA2 removes the phosphate moiety from this intermediate before the deacetylase MshB releases acetic acid from the *N*-acetylglucosamine moiety yielding 1D-*myo*-inositol-2-amino-2-deoxy-α-D-glucopyranoside (GlcN-Ins). The last two steps include the ATP-dependent ligase MshC linking cysteine via a peptide bond with the amino group of the glucosamine moiety and the acetylation of the amino group of the cysteine moiety by the acetyltransferase MshD using acetyl-CoA as a donor to yield MSH (Guo et al., 2018; Newton et al., 2008; Vilchèze et al.,

2008). Another important inositol-derived compound found in some *Actinobacteria* is phosphatidylinositol (PI). MI is linked to cytidine diphosphate diacylglycerol (CDP-DAG) to synthesize PI (chapter 1.1 and Fig. 1.5A), which acts as an abundant phospholipid in the cytoplasmic membrane. PI is also a precursor of more complex lipids of the cell envelope, such as phosphatidylinositol mannosides (PIM), lipomannan (LM), and lipoarabinomannan (LAM) (Morita et al., 2011) (Fig. 1.5A). PIs and PIMs are essential for membrane stability and cell viability (Jackson et al., 2000). In pathogenic *Actinobacteria*, LAM is a crucial modulator of the immune response in the course of tuberculosis and leprosy (Chatterjee and Khoo, 1998; Mishra et al., 2011). In some *Streptomyces* species, MI and SI are converted to aminocyclitols, which are core structures in some aminoglycoside antibiotics, including streptomycin, spectinomycin, kasugamycin, fortimicin, and hygromycin A (Ahlert et al., 1997; Kasuga et al., 2017; Kudo and Eguchi, 2009; Lamichhane et al., 2014; Palaniappan et al., 2009).

1.3.3 Features of *Corynebacterium glutamicum*

A prominent member of the phylum *Actinobacteria* is the soil-dwelling *Corynebacterium glutamicum*, which has become a model organism in industrial biotechnology. Originally isolated in 1956 in Japan for its capability of secreting L-glutamate (Kinoshita et al., 1957), much work was put into developing strains for the production of L-glutamate and other amino acids, particularly L-lysine. A particular boost in research of *C. glutamicum* was triggered by the determination of the genome sequence of the type strain ATCC 13032 in 2003 (Ikeda and Nakagawa, 2003; Kalinowski et al., 2003), which was rapidly followed by the establishment of the transcriptomics (Hüser et al., 2003; Polen and Wendisch, 2004) and proteomics (Bendt et al., 2003; Schaffer et al., 2001), and further systems biology approaches (Wendisch et al., 2006). A large number of genetic tools is available, including many different kinds of plasmids with constitutive or inducible promoters (Kirchner and Tauch 2003 Journal of Biotechnology 104: 287-299, (Kortmann et al., 2015), riboswitches (Zhou and Zeng, 2015), transcription factor-based biosensors (Binder et al., 2012; Mahr et al., 2015; Mustafi et al., 2012), CRISPR/Cas-based tools (Jiang et al., 2017; Wang et al., 2021), and further engineering tools (Bott and Eggeling, 2017). Using these tools, a large variety of producer strains for value-added products has been generated, many of which fulfill the GRAS criteria (“generally recognized as safe”) (Baritugo et al., 2018). Nowadays, *C. glutamicum* strains are used industrially for the annual production of about three million tons of the flavor

enhancer L-glutamate and more than two million tons of the feed additive L-lysine (Becker et al., 2011; Wendisch et al., 2014). Bioprocesses using *C. glutamicum* have also been developed for the production of vitamins (Hüser et al., 2005), diamines (Nguyen et al., 2015), terpenoids (Henke et al., 2018), organic acids (Krause et al., 2010; Okino et al., 2005; Okino et al., 2008), alcohols (Inui et al., 2004; Yamamoto et al., 2013), proteins (Freudl, 2017), and further compounds (Becker et al., 2018; Eggeling and Bott, 2005; Wolf et al., 2021).

C. glutamicum possesses many features that make it an attractive production host for industrial processes, such as growth to high cell densities with a high biomass-specific production rate. It possesses high resistance against a variety of stress factors, like oxidative stress, shear stress, toxic compounds, high osmotic pressure, or phages (Becker and Wittmann, 2016; Eggeling and Bott, 2005; Follmann et al., 2009; Lee et al., 2016; Stella et al., 2019). Another economically relevant feature is that *C. glutamicum* can utilize a broad variety of carbon sources alongside glucose, fructose, and sucrose (Becker and Wittmann, 2016), including organic acids (propionic acid, lactic acid, acetic acid, gluconic acid, and citric acid) (Claes et al., 2002; Gerstmeir et al., 2003; Stansen et al., 2005; Vallino and Stephanopoulos, 1994), alcohols (ethanol) (Arndt et al., 2008), and other diverse carbohydrates like mannose, maltose (Blombach and Seibold, 2010; Kiefer et al., 2002), arabitol (Laslo et al., 2012), or MI (Krings et al., 2006).

1.3.4 Inositol metabolism and its regulation in *C. glutamicum*

In *C. glutamicum*, MI is embedded in many metabolic processes. As mentioned before, *C. glutamicum* uses MI as precursor for mycothiol and PI synthesis (Fig. 1.5A). The *myo*-inositol phosphate synthase (Ino1, Cg3323) is responsible for MIP1 formation (Chen et al., 2019) and at least two monophosphatases (ImpA, Cg2298 and SuhB, Cg2090) have the ability to dephosphorylate MIP1 to yield MI (Kulis-Horn et al., 2017). Biosynthesis of MI in *C. glutamicum* is tightly regulated. Expression of the *ino1* gene is activated by the LacI-type transcriptional regulator IpsA, which was found to act both as an activator and repressor for diverse targets. Binding to excessive MI inactivates IpsA, leading to dissociation from its DNA targets, which enables control of MI synthesis via a negative feedback loop (Fig. 1.5A) (Baumgart et al., 2013).

C. glutamicum is not only able to synthesize MI, but also utilizes it as single carbon and energy source via the conserved bacterial degradation route (Fig. 1.5A) (Krings et al., 2006). More

than 20 genes showed increased expression when MI was present in the culture medium. Most of these genes are located in two clusters on the genome (*iol1* and *iol2*) (Fig. 1.5B).

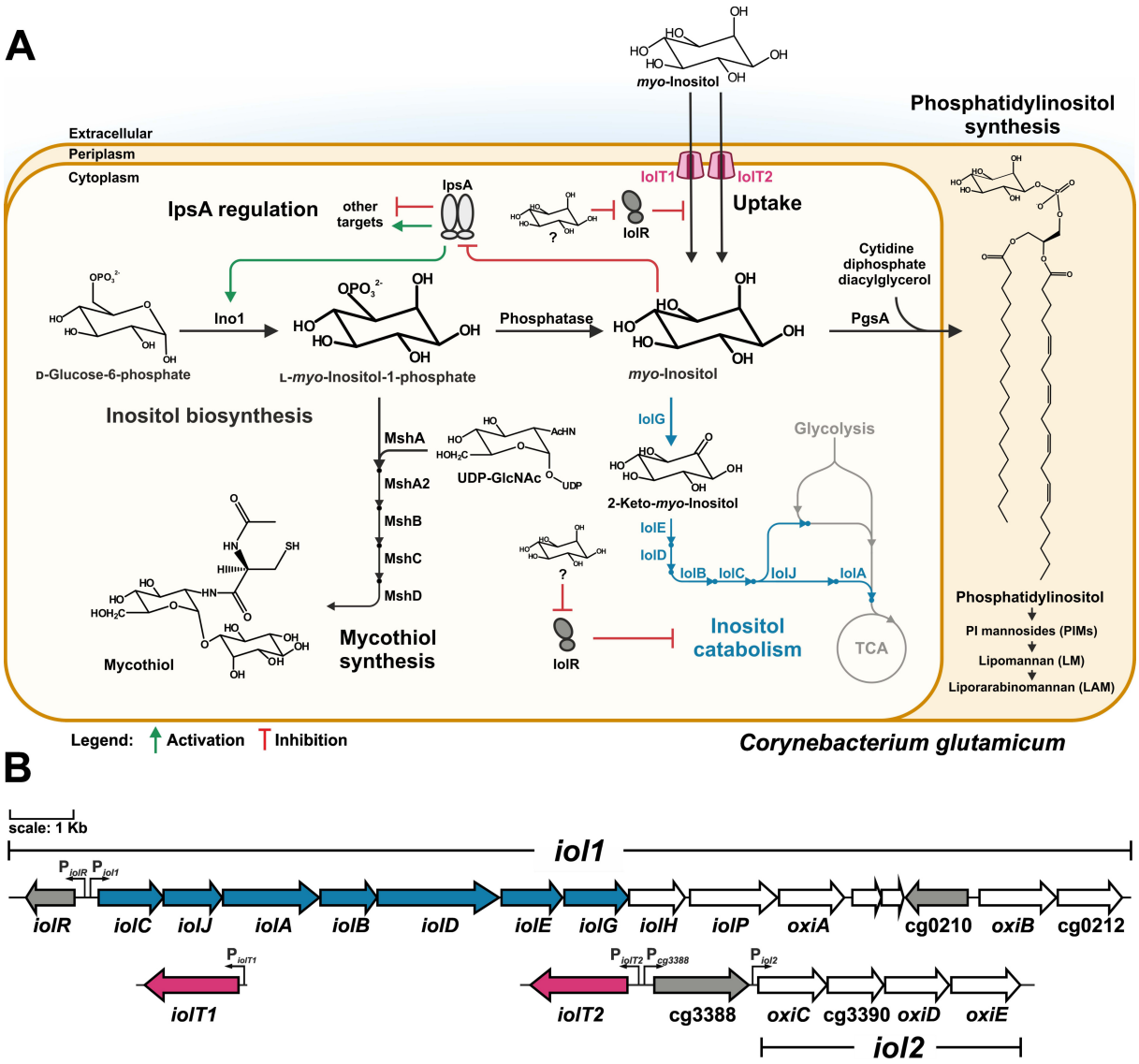

Fig. 1.5. Schematic overview of *myo*-inositol utilization in *C. glutamicum*. (A) *myo*-inositol (MI) can be synthesized, taken up, assimilated, and degraded by *C. glutamicum*. L-*myo*-inositol-1-phosphate (MIP1) is synthesized from D-glucose-6-phosphate by Ino1. Together with UDP-GlcNAc and L-cysteine it is one of the precursors for the dominant thiol mycothiol. MIP1 is dephosphorylated to free MI via an inositol phosphatase. Synthesis of MI is regulated via a negative feedback loop. Binding of MI to the transcriptional regulator IpsA inactivates its function as repressor and activator. Free MI is linked to cytidine diphosphate diacylglycerol to generate phosphatidylinositol, which can be converted to more complex inositol-containing lipids. External MI enters the cell through the specific secondary transporters IolT1 and IolT2 and degradation follows the conserved pathway shown in Fig. 1.4. IolR represses expression of the genes encoding the MI catabolic pathway and *iolT1*. Repression is abolished by binding of intermediate of inositol catabolism to IolR, causing dissociation from its operator sites. **(B)** Gene clusters (*iol1* and *iol2*) and single genes that show increased expression in the presence of MI. The genes involved in the conserved inositol degradation pathway are highlighted in blue, genes encoding inositol transporters are colored in magenta. Genes for transcriptional regulators are colored in grey and genes shown in white have not yet been characterized.

Cluster *iol1* contains the genes encoding the catabolic pathway organized in an operon (*iolCJABDEGH*), similar to *B. subtilis*. An *iolI*-like equivalent gene is missing in this cluster, but it includes two more putative oxidoreductases *oxiA* and *oxiB* as well as genes for a putative permease (cg0206, *iolP*) and a putative sugar phosphate isomerase (cg0212). Cluster *iol2* encodes three additional oxidoreductases, *oxiC*, *oxiD*, and *oxiE*, as well as the putative sugar isomerase cg3390. Although the genes of the *iol2* cluster were upregulated during growth on MI, they could be deleted without having an impact on growth on MI (Krings et al., 2006). Interestingly, upon deletion of the *iolG* gene encoded in cluster *iol1*, cluster *iol2* could sustain growth on MI and thus must encode at least one additional mIDH (Krings et al., 2006). *C. glutamicum* possesses two secondary transporters for MI, IolT1 (Cg0223) and IolT2 (Cg3387). IolT1 and IolT2 share 55% sequence identity and comparable kinetic constants (Krings et al. 2006). Similar to other inositol-degrading bacteria, the expression of the genes responsible for MI degradation and of *iolT1* is repressed by the GntR-type transcriptional regulator IolR in the absence of MI (Klaffl et al., 2013). Cluster *iol2* might be regulated by the LacI-type transcriptional regulator Cg3388 encoded upstream of *oxiC* in the same direction.

1.4 Inositol market and production

In humans, inositols and their derivatives are studied to understand their role in metabolism and simultaneously investigated for their promising health-promoting properties. They are tested for pharmaceutical applications in therapies against several metabolic and neurodegenerative diseases. However, the overall inositol market includes many more industrial applications and demands. In the cosmetic industry, e.g., MI is added to skin products as it promotes cell growth and prohibits cell aging. Inositols find use in the beverage and food industry. They are applied as additives in energy drinks and foods because of their nutraceutical and sweetening function (Li et al., 2021). MI is also an important feed additive and health supplement in the aquaculture industry. For some species of aquatic animals, like Atlantic salmon, Common carp but also Juvenile grass shrimp or Chinese mitten crab, *de novo* synthesis of MI is insufficient to meet their metabolic demands. Especially in fish, exogenous supplementation of MI improves salinity tolerance, growth, immunity, and stress alleviation (Cui et al., 2022). Finally, MI is also used as an important starting compound for the production of other valuable chemicals besides its more expensive isomers. It is used, for example, as a substrate to produce glucaric acid (Liu et al., 2016), one of the US Department of Energy's top 12 renewable chemical compounds

(Werpy and Petersen, 2004). The market for inositols is expected to grow over the years. The current global market is estimated at 15,000 tons per year, with a value of around 94 million USD by 2019, corresponding to a price of about 6.3 $/kg MI. The global market size is expected to reach 140 million USD by 2024, with Europe and China being the main consumer regions (Benvenga et al., 2019). China, together with Japan, is also the leading country for inositol production, primarily MI.

1.4.1 Conventional production

The traditional method of producing MI is based on pressurized acid hydrolysis of phytic acid, which is obtained from corn and rice bran-soaking water during the processing of agricultural products. First, phytic acid is extracted through multiple steps: acid soaking, neutralization and filtration. Using inorganic acids under high pressure and high-temperature, phytic acid is hydrolyzed to release MI and free phosphate. Pure MI is obtained after concentration and crystallization (Li et al., 2021).

Other inositol isomers can also be obtained via chemical production processes. DCI is mainly obtained from plants rich in D-pinitol (DPIN), like legumes and pinewood (Sanchez-Hidalgo et al., 2021). Industrial preparation of DCI is achieved by removing the 3-*O*-methyl group from DPIN via chemical hydrolysis with high concentrations of inorganic acid. Another example is the preparation of SI that starts with MI or MI orthoformate as initial substrates (Sarmah and Shashidhar, 2003). The substrate is selectively benzoylated and tosylated to a 2-hydroxy intermediate, which is then Swern oxidized (Omura and Swern, 1978) and reduced to SI.

Although these production methods are based on abundant resources of raw materials and decades of development, they have many disadvantages. Especially the production of MI suffers from low yields. The direct extraction from raw materials comes with large amounts of various impurities, which increase the costs of downstream processing. The demanding use of high amounts of inorganic acid under high pressure and high temperature comes with strict equipment and waste disposal requirements. Recently developed processes enable atmospheric phytic acid hydrolysis via the use of various catalysts, which loosens the requirements for the equipment. However, separating the product MI from these catalysts also adds to a high production cost (Li et al., 2021). To address these challenges and especially avoid the inorganic waste accumulation and the resulting ecological burdens, biotechnological processes have been established for the production of inositols.

1.4.2 Biotechnological production of inositols

The biotechnological production of inositols is based on the innate ability of some microorganisms to produce enzymes that enable the *de novo* synthesis of MI from cheaper starting compounds. Over the years, many biotechnological processes for the synthesis of MI have been established with production hosts like *Saccharomyces cerevisiae* (White et al., 1991) and *Escherichia coli* (Hansen et al., 1999; Yi et al., 2020). The process with *S. cerevisiae* is based on the organism's natural ability to synthesize MI from G6P as it encodes a MIPS and IMPase. The transfer of *S. cerevisiae* MIPS to *E.coli* allowed the generation of heterologous production processes (Tang et al., 2020; Yi et al., 2020). As G6P is the starting compound of glycolysis, the pentose phosphate pathway, and saccharide biosynthesis, many studies dealt with redirecting carbon flux towards inositol production. This led to the development of strains able to produce over 100 g/L MI (You et al., 2020). In addition, the need for a microbial host was removed entirely as many *in vitro* processes based on cascades of purified MIPS and IMPases have been developed (Lu et al., 2018) (Patent: WO2018004307A1). Hence, no competing metabolic pathway consumes G6P, which led to a highly efficient synthesis of MI. Further research on cell-free MI production involves the combination of these processes with enzymes like phosphorylases, kinases, isomerases, epimerases, ketolases and aldolases which allowed the production of MI from much cheaper carbon sources than G6P like glucose, starch (Fujisawa et al., 2017), cellulose (Meng et al., 2018), and even pentoses like xylose (Cheng et al., 2019).

In contrast to MI, biotechnological production processes for other inositol isomers are as scarce as the isomers themselves. The conventional methods mentioned earlier (chapter 1.4.1), including chemical hydrolysis and syntheses are still more prominent, but plant-based natural sources for many inositol isomers are rare. As stated in chapter 1.1, free and phosphorylated derivatives of SI, DCI, and *neo*-inositol were identified in soil, and it is speculated that they are of microbial origin. For the development of biotechnological production processes for inositol isomers, application of the (*myo*-)inositol metabolism of microorganisms is an obvious starting point. The first steps of inositol degradation are catalyzed by IDHs, enzymes with high stereoselectivity, and inosose isomerases, which interconvert keto-inositol intermediates. By employing bacterial IDHs and inosose isomerases as biocatalysts, biotechnological processes have been developed for SI and DCI (Yamaoka et al., 2011; Yoshida et al., 2006). Yoshida et al. reported an engineered *B. subtilis* strain that is unable to degrade inositol by deleting the corresponding pathway. Overexpression of the mIDH gene *iolG* together with *iolI* allowed

production of DCI from MI. First, IolG oxidizes MI to 2KMI with formation of $NADH+H^+$. Secondly, IolI isomerizes 2KMI to 1KDCI with a ratio of 86:14 2KMI:1KDCI, and finally, due to the reaction equilibrium, IolG reduces 1KDCI to DCI with $NADH+H^+$ as reductant. In this process, 6% of the total MI was converted to DCI.

Similar processes have also been established for the production of SI. Tanaka et. al reported a *B. subtilis* strain unable to catabolize MI that constitutively overproduced IolG, which oxidized MI to 2KMI, and the NADPH-dependent sIDH IolW, which subsequently reduced 2KMI to SI (Tanaka et al., 2013). This process achieved 100% conversion. Such two-step conversion processes have also been established in other microbial hosts via heterologous expression of IDH genes (Li et al., 2020). Further engineering included the implementation of the biosynthesis of MI from glucose-6-phosphate via heterologous expression of the *myo*-inositol phosphate synthase gene *mips* from *M. tuberculosis* in the same microbial host. This enabled production of SI directly from glucose (Michon et al., 2020). Biotechnological production of inositol isomers using IDHs and inosose isomerases in suitable microbial hosts offers the opportunity to supply the growing need for inositols.

1.5 Aims of this thesis

This thesis combines fundamental and applied research in the model organism *C. glutamicum* aiming for a detailed knowledge of the inositol metabolism and the enzymes involved as well as for the development of biotechnological production processes for rare inositols. As stated in chapters 1.3.3 and 1.3.4, *C. glutamicum* possesses the natural ability to synthesize MI and degrade it via the established catabolic pathway. Still, the function of more than 12 genes present in clusters *iol1* and *iol2* are unknown, although showing upregulated expression in the presence of MI. This leads to the hypothesis that inositol metabolism in *C. glutamicum* might be more complex than currently known. So the principal objective of this thesis is to profoundly investigate the potential hidden in the uncharacterized parts of the inositol gene clusters and use the gained insights to generate inositol producer strains.

Through metabolic engineering, I aimed to construct *C. glutamicum* strains that are unable to degrade inositols and simultaneously possess an increased ability for MI biosynthesis. These strains should serve as chassis for multiple inositol production processes. By combining molecular, genetic, physiological, and biochemical analysis, I aimed to elucidate the physiological function of the uncharacterized genes and their role in inositol metabolism. A further aspect aimed at understanding the inositol selectivity of the relevant enzymes and at utilizing the promiscuity of these enzyme classes to establish novel inositol synthesis routes.

2. Results

The central topic of this doctoral thesis was the investigation of the inositol catabolism of *C. glutamicum*, analysis of the acting enzymes and application of metabolic engineering for the development of biotechnological production processes for inositols. The results of these studies have been summarized in two peer-reviewed publications and a manuscript, which will be submitted soon.

In the publication "Metabolic engineering of *Corynebacterium glutamicum* for production of *scyllo*-inositol, a drug candidate against Alzheimer's disease" the generation of *C. glutamicum* chassis strains as hosts for the biotechnological production of the rare inositol *scyllo*-inositol (SI) is described. Following the model of *B. subtilis*, the genome of *C. glutamicum* was analyzed for the presence of genes encoding NAD^+/NADPH-dependent IDHs. Using Blastp analysis with *B. subtilis* mIDH and sIDHs sequences as templates, seven inositol dehydrogenases were identified, among them one NADPH-dependent sIDH. Growth experiments with MI as single carbon and energy source revealed that *C. glutamicum* naturally produces, exports, takes up and degrades SI. Both gene clusters associated with inositol catabolism needed to be deleted to completely abolish inositol degradation. Overexpressing the well-characterized IDH *iolG* together with the newly identified NADPH-dependent IDH enabled efficient production of SI from MI in defined media. Using rich medium for the biotransformation resulted in complete conversion of MI to SI. Overexpressing the genes for innate MI synthesis from G6P in *C. glutamicum* together with the established IDH-based system enabled the production of SI directly from glucose and sucrose. In summary, this study demonstrated *C. glutamicum* as an efficient host for the production of SI.

The publication "Physiological, biochemical, and structural bioinformatics analysis of the multiple inositol dehydrogenases from *Corynebacterium glutamicum*" describes the further characterization of the previously identified IDHs, their role in inositol catabolism and the attempt to understand the reasons behind different activity towards different inositols. Growth experiments revealed that *C. glutamicum* can utilize SI and DCI as single carbon and energy source. Both previously identified inositol transporters are responsible for uptake. Complementation experiments testing a deletion strain lacking all identified IDH genes revealed four different IDH with overlapping activity towards MI, SI and DCI. Enzymatic activity assays characterized their activity towards all tested inositols. CgIDHs were compared to other characterized IDH from other organisms and molecular docking experiments allowed

determination of substrate binding sites. Potential sites responsible for inositol selectivity were identified. Overall, this study elucidated the complex inositol catabolism of *C. glutamicum* and established a bioinformatic approach to analyze substrate acceptance of IDH. The insights in this study were extended through additional growth experiments on L-*chiro*-inositol and the solving of the crystal structure of a sIDH, both further explained in the Appendix.

The manuscript "Production of D-*chiro*-inositol with *Corynebacterium glutamicum* via two different synthesis routes" deals with further investigation of the DCI catabolism of *C. glutamicum* and the parallel development of novel biotechnological production processes for DCI. According to previous studies on DCI catabolism in *B. subtilis*, an inosose isomerase is mandatory for DCI degradation. For *C. glutamicum* we identified two so far uncharacterized genes encoding inosose isomerases acting on inositol-keto-compounds. The overexpression of one isomerase gene with the mIDH *iolG* in a *C. glutamicum* strain unable to degrade inositols enabled the biotransformation of MI to DCI. Surprisingly, production and growth complementation experiments revealed that *C. glutamicum* possesses at least two more paralogous inosose isomerase genes, of which one was identified. In parallel, a novel DCI synthesis route was developed by utilizing the promiscuous activity of two plant-derived methyl-inositol dehydrogenases. An NAD^+/NADPH-dependent process for the biotransformation of MI to DCI was established. Co-expression of both dehydrogenases with the *myo*-inositol-1-phosphate synthase *ino1* enabled the novel production of DCI directly from glucose. By constructing a new bicistronic expression vector the final yield was further increased. This study once more highlighted the potential of *C. glutamicum* as an efficient host for the production of rare inositols like SI or DCI.

2.1 Metabolic engineering of *Corynebacterium glutamicum* for production of *scyllo*-inositol, a drug candidate against Alzheimer's disease.

Ramp, P., Lehnert, A., Matamouros, S., Wirtz, A., Baumgart, M., & Bott, M. (2021). *Metabolic Engineering*, *67*, 173-185.

Author contributions

PR: Conceptualization, Methodology, Investigation, Writing – Initial Draft, Visualization.

AL: Investigation, Methodology.

SM: Supervision, Methodology.

AW: Investigation, Methodology.

MBa: Methodology, Writing – original draft, Supervision.

MBo: Conceptualization, Supervision, Writing – review & editing, Funding acquisition.

Overall contribution: 45%

Metabolic Engineering 67 (2021) 173–185

Contents lists available at ScienceDirect

Metabolic Engineering

journal homepage: www.elsevier.com/locate/meteng

Metabolic engineering of *Corynebacterium glutamicum* for production of *scyllo*-inositol, a drug candidate against Alzheimer's disease

Paul Ramp, Alexander Lehnert, Susana Matamouros, Astrid Wirtz, Meike Baumgart, Michael Bott *

IBG-1: Biotechnology, Institute of Bio- and Geosciences, Forschungszentrum Jülich, Jülich, Germany

ARTICLE INFO

Keywords:
Corynebacterium glutamicum
Metabolic engineering
Myo-inositol
Scyllo-inositol
Sucrose
Alzheimer's disease

ABSTRACT

Scyllo-inositol has been identified as a potential drug for the treatment of Alzheimer's disease. Therefore, cost-efficient processes for the production of this compound are desirable. In this study, we analyzed and engineered *Corynebacterium glutamicum* with the aim to develop competitive *scyllo*-inositol producer strains. Initial studies revealed that *C. glutamicum* naturally produces *scyllo*-inositol when cultured with *myo*-inositol as carbon source. The conversion involves NAD^+-dependent oxidation of *myo*-inositol to 2-keto-*myo*-inositol followed by NADPH-dependent reduction to *scyllo*-inositol. Use of *myo*-inositol for biomass formation was prevented by deletion of a cluster of 16 genes involved in *myo*-inositol catabolism (strain MB001(DE3)Δ*iol1*). Deletion of a second cluster of four genes (*oxiC*-cg3390-*oxiD*-*oxiE*) related to inositol metabolism prevented conversion of 2-keto-*myo*-inositol to undesired products causing brown coloration (strain MB001(DE3)Δ*iol1*Δ*iol2*). The two chassis strains were used for plasmid-based overproduction of *myo*-inositol dehydrogenase (IolG) and *scyllo*-inositol dehydrogenase (IolW). In BHI medium containing glucose and *myo*-inositol, a complete conversion of the consumed *myo*-inositol into *scyllo*-inositol was achieved with the Δ*iol1*Δ*iol2* strain. To enable *scyllo*-inositol production from cheap carbon sources, *myo*-inositol 1-phosphate synthase (Ino1) and *myo*-inositol 1-phosphatase (ImpA), which convert glucose 6-phosphate into *myo*-inositol, were overproduced in addition to IolG and IolW using plasmid pSI. Strain MB001(DE3)Δ*iol1*Δ*iol2* (pSI) produced 1.8 g/L *scyllo*-inositol from 20 g/L glucose and even 4.4 g/L *scyllo*-inositol from 20 g/L sucrose within 72 h. Our results demonstrate that *C. glutamicum* is an attractive host for the biotechnological production of *scyllo*-inositol and potentially further *myo*-inositol-derived products.

1. Introduction

Scyllo-inositol, one of nine structural isomers of inositol (1,2,3,4,5,6-cyclohexanehexol), is under study as a promising therapeutic agent for Alzheimer's disease, because of its inhibitory effect on amyloid β protein (Aβ) aggregation and reduction of cerebral Aβ pathology (Fenili et al., 2007; McLaurin et al., 2006; Salloway et al., 2011; Townsend et al., 2006). Therefore, an efficient process for *scyllo*-inositol production is desirable. Although chemical production has been described (Sarmah and Shashldhar, 2003), a biotechnological route might be more promising, as it can start from cheaper precursors such as glucose, avoids the use of hazardous chemicals and high temperatures, and may allow higher yields (Li et al., 2021; Wenda et al., 2011). A pathway for epimerization of *myo*-inositol to *scyllo*-inositol was first proposed using extracts of the fat body of the desert locust *Schistocerca gregaria*, which involved the initial oxidation of *myo*-inositol with NAD^+ to 2-keto--*myo*-inositol (*myo*-inosose) followed by an NADPH-dependent reduction of 2-keto-*myo*-inositol to *scyllo*-inositol (Candy, 1967). The formation of the intermediate 2-keto-*myo*-inositol in this two-step process was confirmed by labeling studies using cells of *Streptomyces griseus* (Horner and Thaker, 1968).

In the past years, several studies were dedicated to the production of *scyllo*-inositol with *Bacillus subtilis*, which is naturally able to catabolize *myo*-inositol (Yoshida et al., 1997). The first step in the degradation pathway is the oxidation of *myo*-inositol to 2-keto-*myo*-inositol by the dehydrogenase IolG, followed by dehydration to 3D-(3,5/4)-trihydroxycyclohexane-1,2-dione (THcHDO) by IolE (Yoshida et al., 2004). This intermediate is converted in subsequent steps to dihydroxyacetone phosphate, acetyl-CoA and CO_2 (Yoshida et al., 2008). Besides *myo*-inositol, *B. subtilis* can also grow with *scyllo*-inositol as sole carbon

* Corresponding author.
E-mail address: m.bott@fz-juelich.de (M. Bott).

https://doi.org/10.1016/j.ymben.2021.06.011
Received 9 April 2021; Received in revised form 17 June 2021; Accepted 30 June 2021
Available online 2 July 2021

source and two *scyllo*-inositol dehydrogenases were identified, IolX and IolW (Morinaga et al., 2010). IolX was shown to be essential for growth with *scyllo*-inositol and to catalyze the NAD^+-dependent oxidation of *scyllo*-inositol to 2-keto-*myo*-inositol, which then is degraded via the same pathway used for *myo*-inositol. IolW was dispensable for growth on *scyllo*-inositol and preferably catalyzed the NADPH-dependent reduction of 2-keto-*myo*-inositol to *scyllo*-inositol (Morinaga et al., 2010). Based on this knowledge a *B. subtilis* strain was constructed that allowed bioconversion of 10 g/L *myo*-inositol to about 4 g/L *scyllo*-inositol (Yamaoka et al., 2011). An improved strain enabled complete conversion of 10 g/L *myo*-inositol into *scyllo*-inositol within 48 h (Tanaka et al., 2013). In a further study, an increase of the Bacto soytone concentration in the medium allowed conversion of 50 g/L *myo*-inositol into 27.6 g/L *scyllo*-inositol (Tanaka et al., 2017). Most recently, further *B. subtilis* strains were constructed that allowed production of 2 g/L *scyllo*-inositol from 20 g/L glucose (Michon et al., 2020). These strains contained *myo*-inositol phosphate synthase from *Mycobacterium tuberculosis*, which converts glucose 6-phosphate to L-*myo*-inositol 1-phosphate, which is then dephosphorylated to *myo*-inositol by the intrinsic inositol monophosphatase YktC.

Corynebacterium glutamicum is a Gram-positive actinobacterium that has become a model organism in industrial biotechnology due its use in large-scale amino acid production (Eggeling and Bott, 2005, 2015; Wendisch et al., 2016). Meanwhile, *C. glutamicum* strains for the synthesis of many other products besides amino acids have been developed (Becker and Wittmann, 2012; Freudl, 2017; Heider and Wendisch, 2015; Wieschalka et al., 2013). *C. glutamicum* can utilize a broad variety of carbon sources, including *myo*-inositol (Krings et al., 2006). When cultivated with *myo*-inositol, more than 20 genes showed increased expression, the majority of which was located in two clusters on the genome. Cluster I contains genes that are essential for growth on *myo*-inositol, whereas the genes of cluster II are dispensable for *myo*-inositol degradation (Krings et al., 2006). Cluster II encodes amongst others several putative oxidoreductases that had the ability to compensate loss of the IolG function encoded in cluster I and thus must contain at least one gene encoding an additional *myo*-inositol dehydrogenase (Krings et al., 2006). Two secondary transporters for *myo*-inositol were identified in *C. glutamicum* and characterized, called IolT1 (Cg0223) and IolT2 (Cg3387). IolT1 and IolT2 share 55% sequence identity and comparable kinetic constants with K_m values of 0.22 and 0.45 mM and V_{max} values of 1.22 and 2.90 nmol min^{-1} (mg cells)$^{-1}$, respectively (Krings et al., 2006). The expression of the genes of cluster I and of *iolT1* is repressed by the GntR-type transcriptional regulator IolR in the absence of *myo*-inositol (Klaffl et al., 2013).

In contrast to *B. subtilis*, *C. glutamicum* is not only able to degrade *myo*-inositol, but also has the intrinsic capability to synthesize *myo*-inositol from glucose 6-phosphate. In the order *Corynebacteriales*, which includes the genus *Mycobacterium*, *myo*-inositol is required for the synthesis of mycothiol, the analog of glutathione in this bacterial group (Newton et al., 2008), and of phosphatidylinositol, an abundant phospholipid in the cytoplasmic membrane and the precursor of more complex lipids of the cell envelope such as phosphatidylinositol mannosides, lipomannan, and lipoarabinomannan (Morita et al., 2011). *Myo*-inositol is formed by first converting glucose 6-phosphate to L-*myo*-inositol 1-phosphate with *myo*-inositol phosphate synthase (Ino1, Cg3323) followed by dephosphorylation with *myo*-inositol phosphate monophosphatase (ImpA, Cg2298). Expression of the *ino1* gene is activated by the LacI-type transcriptional regulator IpsA, which itself is inactivated by binding of *myo*-inositol, causing dissociation of IpsA from its DNA targets (Baumgart et al., 2013).

Based on the available knowledge on *myo*-inositol metabolism and a preliminary bioinformatic analysis of the multiple inositol dehydrogenase genes encoded in the genome, we considered *C. glutamicum* as an interesting alternative host for *scyllo*-inositol production. In this study, we show the natural ability of *C. glutamicum* to produce and consume *scyllo*-inositol when cultivated in the presence of *myo*-inositol and

Table 1
Bacterial strains and plasmids used in this study.

Strain or plasmid	Relevant characteristics	Source or reference
E. coli		
DH5α	F$^-$ Φ80*dlac*Δ(*lacZ*)M15 Δ(*lacZYA-argF*) U169 *endA1 recA1 hsdR17* (r_K^-, m_K^+) *deoR thi-1 phoA supE44* λ^- *gyrA96 relA1*; strain used for cloning procedures	Hanahan (1983)
C. glutamicum		
MB001(DE3)	prophage-free derivate of ATCC 13032 with chromosomal expression of T7 RNA polymerase gene under control of P_{lacUV5} (IPTG-inducible)	Kortmann et al. (2015)
MB001(DE3)Δ*iol1*	MB001(DE3) derivative with deletion of the genes cg0196-cg0212	This work
MB001(DE3)Δ*iol1* Δ*iol2*	MB001(DE3)Δ*iol1* derivative with deletion of the genes cg3389-cg3392	This work
Plasmids		
pK19*mobsacB*	Kan^R; plasmid for allelic exchange in *C. glutamicum*; (pK18 *ori*$V_{E.c.}$, *sacB*, *lacZα*)	Schäfer et al. (1994)
pK19*mobsacB*Δ*iol1*	Kan^R; pK19*mobsacB* derivative containing two 1-kb PCR products which cover the upstream flanking region of *iolR* (cg0196) and the downstream flanking region of *iolE2* (cg0212)	This work
pK19*mobsacB*Δ*iol2*	Kan^R; pK19*mobsacB* derivative containing two 1-kb PCR products which cover the upstream flanking region of *oxiC* (cg3389) and the downstream flanking region of *oxiE* (cg3392)	This work
pMKEx2	Kan^R; *E. coli-C. glutamicum* shuttle vector (*lacI*, P_{T7}, lacO1, pHM1519 ori $_{Cg}$; pACYC177 ori $_{Ec}$) for expression of target genes under control of the T7 promoter	Kortmann et al. (2015)
pMKEx2-*eyfp*	Kan^R; pMKEx2 derivative containing the *eyfp* gene under control of P_{T7}	Kortmann et al. (2015)
pIolGW	Kan^R; pMKEx2 derivative containing the *C. glutamicum* genes *iolG* (cg0204) and *iolW* (cg0207) as a synthetic operon under control of the T7 promoter	This work
pSI	Kan^R; pMKEx2 derivative containing the *C. glutamicum* genes *ino1* (cg3323), *impA* (cg2298), *iolG* (cg0204) and iolW (cg0207) as synthetic operon under control of the T7 promoter	This work
pMKEx2-*iolG*	Kan^R; pMKEx2 derivative containing the *C. glutamicum* gene *iolG* (cg0204) under control of P_{T7}	This work
pMKEx2-*iolW*	Kan^R; pMKEx2 derivative containing the *C. glutamicum* gene *iolW* (cg0207) under control of P_{T7}	This work
pMKEx2-*oxiC*	Kan^R; pMKEx2 derivative containing the *C. glutamicum* gene *oxiC* (cg3389) under control of P_{T7}	This work
pMKEx2-*oxiD*	Kan^R; pMKEx2 derivative containing the *C. glutamicum* gene *oxiD* (cg3391) under control of P_{T7}	This work
pMKEx2-*oxiE*	Kan^R; pMKEx2 derivative containing the *C. glutamicum* gene *oxiE* (cg3392) under control of P_{T7}	This work
pMKEx2-*idhA3*	Kan^R; pMKEx2 derivative containing the *C. glutamicum* gene *idhA3* (cg2313) under control of P_{T7}	This work
pMKEx2-cg3390	Kan^R; pMKEx2 derivative containing the *C. glutamicum* gene cg3390 under control of P_{T7}	This work
pMKEx2-*iolG-oxiC*	Kan^R; pMKEx2 derivative containing the *C. glutamicum* genes *iolG* (cg0204) and *oxiC* (cg3389) as a synthetic operon under control of the T7 promoter	This work
pMKEx2-*iolG*-cg3390	Kan^R; pMKEx2 derivative containing the *C. glutamicum* genes *iolG* (cg0204) and cg3390 as a synthetic operon under control of the T7 promoter	This work

Table 2
Oligonucleotides used in this study.

Oligonucleotide name	Oligonucleotide sequence (5'→ 3')
Construction pK19mobsacBΔ*iol1*	
P001_Δiol1_FW1	GAGGATCCCCGGGTACCGAGCTCGTTCCGCCAACTCAACC
P002_Δiol1_RV1	TGAAACCACTCTGGTGGCCAGGTAAG
P003_Δiol1_FW2	CTTACCTGGCCACCAGAGTGGTTTCAGAAGAGTCCCTGGTTTC
P004_Δiol1_RV2	CGTTGTAAAACGACGGCCAGTGAATTTCCTTGGTCACCAGATC
P005_Seq_pK19_FW	AGCGGATAACAATTTCACACAGGA
P006_Seq_pK19_RV	CGCCAGGGTTTTCCCAGTCAC
Construction pK19mobsacBΔ*iol2*	
P007_ΔoxiC-E_FW1	GAGGATCCCCGGGTACCGAGCTCGGGAACCCAATTCACCTTCG
P008_ΔoxiC-E_RV1	GCCTAGCAGGCCAACAAC
P009_ΔoxiC-E_FW2	AAATTGTTGTTGGCCTGCTAGGCTGCGCTGGTTCCATCTGC
P010_ΔoxiC-E_RV2	CGTTGTAAAACGACGGCCAGTGAATTGGACCAACCAGAAACTTC
P005_Seq_pK19_FW	AGCGGATAACAATTTCACACAGGA
P006_Seq_pK19_RV	CGCCAGGGTTTTCCCAGTCAC
Construction of individual pMKEx2 plasmids	
P011_iolW_pMKEx2_FW	ACTTTAAGAAGGAGATATACCATGACTATTCGAATCGGACTCG
P012_iolW_pMKEx2_RV	TGGCACCAGAGCGAGCTCTGCGGCCTTAGCTCAACTCAATGGTGCG
P013_iolG_pMKEx2_FW	ACTTTAAGAAGGAGATATACCATGAGCAAGAGCCTTCGC
P014_iolG_pMKEx2_RV	TGGCACCAGAGCGAGCTCTGCGGCCTTAAGCGTAGAAATCTGGGCG
P015_impA_pMKEx2_FW	CTTTAAGAAGGAGATATACCATGGATGCTCGTGGGATGTTG
P016_impA_pMKEx2_RV	GGTGGCTCCAGCTTGCCATGTTACTTGTACTCCTCATTTAACG
P041_oxiC_pMKEx2_FW	CTTTAAGAAGGAGATATACCATGAGTGATCAAAAAATTG
P042_oxiC_pMKEx2_RV	CCAGAGCGAGCTCTGCGGCCTTAGATGTTTACGGAAATGCC
P043_cg3390_pMKEx2_FW	CTTTAAGAAGGAGATATACCATGAAACCACAACTTATTG
P044_cg3390_pMKEx2_RV	GAGCGAGCTCTGCGGCCTCAGTTAGTGGAGGGGGC
P045_oxiD_pMKEx2_FW	CTTTAAGAAGGAGATATACCATGACTCTTCGTATCGCC
P046_oxiD_pMKEx2_RV	CCAGAGCGAGCTCTGCGGCCCTAAACGTTGGCAGGGTTGAG
P047_oxiE_pMKEx2_FW	CTTTAAGAAGGAGATATACCATGAAAAACATCACCATCGG
P048_oxiE_pMKEx2_RV	CCAGAGCGAGCTCTGCGGCCTTAAGCAGATGGAACCAGCG
P049_idhA3_pMKEx2_FW	CTTTAAGAAGGAGATATACCATGTCAGTCAAACTTGCCCTC
P050_idhA3_pMKEx2_RV	CCAGAGCGAGCTCTGCGGCCTTAAACCTCGATGCTTTCAG
P017_Seq_pMKEx2_FW	AGGAGATGGCGCCCAACAG
P018_Seq_pMKEx2_RV	ACTTTGCGCAGCTCAGG
Construction of pIolG-W	
P013_iolG_pMKEx2_FW	ACTTTAAGAAGGAGATATACCATGAGCAAGAGCCTTCGC
P019_iolG_iolG-IolW_RV	TGTCGCTCAGAGACCTGAGGTTAAGCGTAGAAATCTGGGCGAG
P020_iolW_iolG-IolW_FW	CCTCAGGTCTCTGAGCGACAGAAGGAGATATACCATG
P012_iolW_pMKEx2_RV	CCAGAGCGAGCTCTGCGGCCTTAGCTCAACTCAATGGTG
P021_Seq_iolG1	GTGTTGGTGAGAGCTAC
P022_Seq_iolW1	AAAGCAGCCGTTGCAG
P023_Seq_iolW2	CGGCTCCTACGTATC
P017_Seq_pMKEx2_FW	AGGAGATGGCGCCCAACAG
P018_Seq_pMKEx2_RV	ACTTTGCGCAGCTCAGG
Construction of pSI	
P024_ino1_ino1-impA-iolG-iolW_FW	CTTTAAGAAGGAGATATACCATGAGCACGTCCACCATCAG
P025_ino1_ino1-impA-iolG-iolW_RV	GCAGGTGCACAATGATACGATTACGCCTCGATGATGAATG
P026_impA_ino1-impA-iolG-iolW_FW	TCGTATCATTGTGCACCTGCGAAGGAGATATACCATG
P027_impA_ino1-impA-iolG-iolW_RV	ACATCGTTGAGTGGTCACCGTTACTTGTACTCCTCATTTAAC
P028_iolG_ino1-impA-iolG-iolW_FW	CGGTGACCACTCAACGATGTGAAGGAGATATACCATG
P029_iolG_ino1-impA-iolG-iolW_RV	TGTCGCTCAGAGACCTGAGGTTAAGCGTAGAAATCTGGGCGAG
P030_iolW_ino1-impA-iolG-iolW_FW	CCTCAGGTCTCTGAGCGACAGAAGGAGATATACCATG
P012_iolW_pMKEx2_RV	TGGCACCAGAGCGAGCTCTGCGGCCTTAGCTCAACTCAATGGTGCG
P021_Seq_iolG1	GTGTTGGTGAGAGCTAC
P022_Seq_oxiA1	AAAGCAGCCGTTGCAG
P023_Seq_oxiA2	CGGCTCCTACGTATC
P017_Seq_pMKex2_FW	AGGAGATGGCGCCCAACAG
P018_Seq_pMKex2_RV	ACTTTGCGCAGCTCAGG
P031_ino1_pSI_Seq	TTGGTGTCCTACCTCC
P032_impA_pSI_Seq1	AGCAGCTTCCAGACGATG
P033_impA_pSI_Seq2	AGCATGCGTATCGTTTAG
Construction of pMKEx2-*iolG-oxiC*	
P013_iolG_pMKEx2_FW	ACTTTAAGAAGGAGATATACCATGAGCAAGAGCCTTCGC
P051_iolG_iolG-oxiC_RV	CTTTCAGAAGTGGGTTTCTCCTTAAGCGTAGAAATC
P052_iolG-oxiC_pMKEx2-FW	GAGAAACCCACTTCTGAAAGGAGAATTCCCATGAGTGATC
P042_oxiC_pMKEx2_RV	CCAGAGCGAGCTCTGCGGCCTTAGATGTTTACGGAAATGCC
Construction of pMKEx2-*iolG*-cg3390	
P013_iolG_pMKEx2_FW	ACTTTAAGAAGGAGATATACCATGAGCAAGAGCCTTCGC
P019_iolG_iolG-IolW_RV	TGTCGCTCAGAGACCTGAGGTTAAGCGTAGAAATCTGGGCGAG
P053_cg3390_iolG-cg3390_FW	CTCAGGTCTCTGAGCGACAAGAGGAGCACTCCATG
P044_cg3390_pMKEx2_RV	GAGCGAGCTCTGCGGCCTCAGTTAGTGGAGGGGGC
Recombination analysis Δ*iol1*	
P034_Col_deliol_FW	GGGATTTCGTTGCCATG
P035_Col_deliolR-E2_RV	GGTTGCGGCAATCTTCC
P036_Seq_deliol1	CTGGACCAAACCAGGTG

(*continued on next page*)

Table 2 (*continued*)

Oligonucleotide name	Oligonucleotide sequence (5'→ 3')
Recombination analysis Δ*iol2*	
P037_Col_deloxiC-E_FW	ACACCATCCGGGACAC
P038_Col_deloxiC-E_RV1	CGTTCAAGACGTCATC
P039_Col_deloxiC-E_RV2	ACTGCAATGCTGGCCTG
P040_Seq_delOxiC-E_1	CGTGGAACTGATCCTG

identified the responsible enzymes. By metabolic engineering, we obtained strains enabling efficient conversion of *myo*-inositol into *scyllo*-inositol. Finally, we designed strains that were able to produce high titers of *scyllo*-inositol from the cheap carbon source sucrose.

2. Materials and methods

2.1. Bacterial strains, plasmids and growth conditions

All bacterial strains and plasmids used in this work are listed in Table 1. All cloning steps were performed with *Escherichia coli* DH5α as host. *E. coli* strains were cultivated at 37 °C on LB agar plates or in lysogeny broth (LB) (Bertani, 1951) with 50 μg/mL kanamycin. *C. glutamicum* was cultivated in baffled shake flasks at 130 rpm and 30 °C using either brain heart infusion (BHI) medium (Difco Laboratories, Detroit, USA) or defined CGXII medium (Keilhauer et al., 1993) with 0.03 g/L protocatechuic acid, which were supplemented with either 20 g/L glucose, 20 g/L *myo*-inositol, 20 g/L each of glucose and *myo*-inositol, or 20 g/L sucrose as carbon and energy sources. Where appropriate, 25 μg/mL kanamycin was added to the medium. Bacterial growth was followed by measuring the optical density at 600 nm (OD_{600}). To start cultivation, 10 mL BHI medium in a 100 mL baffled shake flask was inoculated with a single colony from an agar plate and incubated overnight at 30 °C and 130 rpm. The main culture was inoculated to an initial OD_{600} of 0.5. Main cultures in BHI medium were inoculated directly from overnight precultures. For inoculation of main cultures in CGXII medium, cells of the preculture were harvested and washed twice in CGXII medium. Target gene expression was induced via addition of isopropyl-β-D-thiogalactoside (IPTG) as indicated in the results sections.

2.2. Recombinant DNA work and construction of deletion mutants

All plasmids and oligonucleotides used in this study are listed in Tables 1 and 2, respectively. Routine methods such as PCR and DNA restriction were performed using established protocols (Green and Sambrook, 2012). Transformation of *E. coli* was performed according to an established protocol (Hanahan, 1983). Transformation of *C. glutamicum* was performed by electroporation (van der Rest et al., 1999). Plasmids were constructed via Gibson assembly (Gibson et al., 2009). DNA sequencing and oligonucleotide synthesis were performed by Eurofins Genomics (Ebersberg, Germany). The deletion mutant *C. glutamicum* MB001(DE3)Δ*iol1* was constructed via double homologous recombination as described previously using pK19mobsacBΔ*iol1* (Niebisch and Bott, 2001). The double deletion mutant *C. glutamicum* MB001(DE3)Δ*iol1*Δ*iol2* was constructed in the same way using plasmid pK19mobsacBΔ*iol2*. The chromosomal deletions were confirmed via colony-PCR using oligonucleotides annealing outside of the deleted region. For both deletions, 25% of the tested clones after the second recombination event contained the desired deletion, whereas 75% showed the wild-type situation, showing that none of deleted genes was essential for growth in the media used.

Table 3
C. glutamicum proteins showing homology to the *B. subtilis* inositol dehydrogenases IolG, IolW, and IolX. The analysis was performed with BLAST function of the ERGO Bioinformatics suite (Igenbio Inc., Chicago, USA).

Query protein of *B. subtilis*	Homologs in *C. glutamicum* (with cg number)	Alignment length (amino acids)	E-value	% Identity
IolG (344 aa)	IolG (Cg0204)	335	2e-78	39.10
	IdhA3 (Cg2313)	352	3e-33	29.55
	OxiD (Cg3391)	332	3e-28	26.81
	OxiE (Cg3392)	309	8e-21	27.18
IolW (358 aa)	IolW (OxiA) (Cg0207)	353	1e-45	30.88
	OxiC (Cg3389)	309	5e-12	24.60
IolX (342 aa)	IdhA3 (Cg2313)	334	8e-56	36.83
	OxiD (Cg3391)	332	1e-50	32.83
	OxiE (Cg3392)	304	4e-45	31.58

For the construction of the expression plasmids pIolGW and pSI, all corresponding genes were first cloned separately into the plasmid pMKEx2 downstream of the *C. glutamicum* consensus ribosome binding site (RBS). All genes were then again amplified together with the RBS using the designated primer pairs and cloned as synthetic operons in pMKEx2 via Gibson assembly. For the expression plasmids, pMKEx2-*oxiC*, pMKEx2-*oxiD*, pMKEx2-*oxiE*, pMKEx2-*idhA3* and pMKEx2-cg3390 the corresponding genes were amplified by PCR from chromosomal DNA and then cloned via Gibson assembly into pMKEx2 downstream of the *C. glutamicum* consensus RBS.

2.3. Inositol analysis by HPLC

1 mL culture was centrifuged at 17,000 *g* for 20 min, the supernatant was filtered (0.2 μm syringe filter, Whatman™, GE Healthcare, Freiburg, Germany) and frozen at −20 °C until further analysis. Thawed samples were diluted with deionized water and applied for HPLC analysis. A 10 μL sample was measured using an Agilent LC-1100 system (Agilent, Santa Clara, CA, USA) equipped with a Carbo-Ca Guard Catridge (Phenomenex, Aschaffenburg, Germany) and a Rezex RCM-Monosaccharide 300 × 7.8 mm column (Phenomenex, Aschaffenburg, Germany). Separation was performed at 80 °C with water as eluent at a flow rate of 0.6 mL/min. Sugar and sugar alcohols were detected with a refraction index detector operated at 35 °C. The retention times were 11 min for glucose, 8.5 min for sucrose, 14.5 min for *myo*-inositol, and 12.1 min for *scyllo*-inositol.

2.4. Protein overproduction, SDS-PAGE and inositol dehydrogenase activity assays

C. glutamicum MB001(DE3)Δ*iol1*Δ*iol2* was transformed with pMKEx2-based plasmids for expression of various inositol dehydrogenases and cultivated in BHI medium supplemented with 20 g/L glucose. Overexpression of the target genes was induced after 3 h with 100 μM IPTG and cells were harvested after 24 h of cultivation via centrifugation (30 min at 5100 *g* and 4 °C). Cell pellets were washed and resuspended in 4 mL lysis buffer (100 mM Tris-HCl pH 7.5, 1 mM $MgSO_4$) per g cell wet weight and disrupted using 0.1 mm zirconia/silica beads (BioSpec Products Inc., Bartlesville, USA) in a MM2 mixer mill (Retsch GmbH, Haan, Germany). Whole cell lysates were cleared by centrifugation at 13,000 *g* and 4 °C for 20 min. Equal amounts of protein (10 μg per lane) were analyzed by SDS-PAGE according to standard procedures (Green and Sambrook, 2012). Proteins were visualized by Coomassie Brilliant Blue staining. The inositol dehydrogenase activity assay was performed as described previously (Bakkes et al., 2020) with final concentrations of 25 mM *myo*-inositol or *scyllo*-inositol as substrates and 1 mM NAD^+ or 1 mM $NADP^+$ as coenzymes.

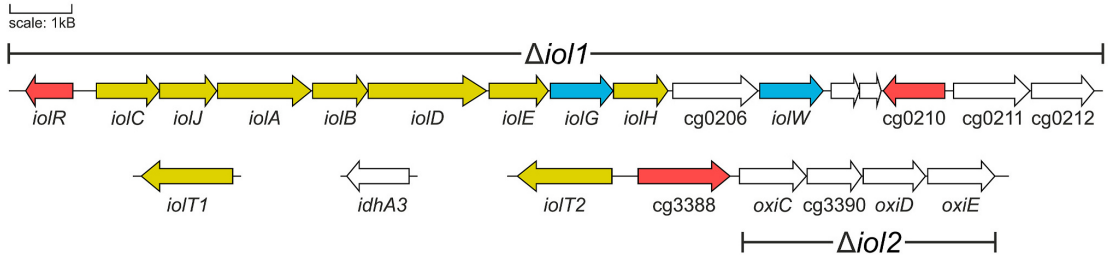

Fig. 1. Genes related to inositol catabolism in *C. glutamicum*. The genomic regions deleted in this work are indicated as Δ*iol1* and Δ*iol2*. Genes shown in red encode transcriptional regulators, genes in yellow have a known or predicted function, and genes in white have putative or unknown functions. The genes *iolG* and *iolW* used in this study for the production of *scyllo*-inositol are highlighted in blue.

3. Results and discussion

3.1. Bioinformatic analysis of the C. glutamicum protein repertoire for the presence of inositol dehydrogenases

The conversion of *myo*-inositol to *scyllo*-inositol involves *myo*-inositol dehydrogenase and *scyllo*-inositol dehydrogenase. Analysis of the proteins encoded by the *C. glutamicum* genome with the *B. subtilis myo*-inositol dehydrogenase $IolG_{Bs}$ as query resulted in the identification of four proteins with an identity >26%, which have been annotated as IolG (Cg0204), IdhA3 (Cg2313), OxiE (Cg3392), and OxiD (Cg3391) (Table 3, Fig. 1). IolG was recently purified and shown to have a specific NAD^+-dependent *myo*-inositol dehydrogenase activity of 27 μmol min^{-1} (mg protein)$^{-1}$ (Bakkes et al., 2020). In addition, IolG also catalyzes the oxidation of D-xylose to D-xylonate (Tenhaef et al., 2018). Expression of *iolG*, *oxiE*, and *oxiD* was strongly upregulated in *myo*-inositol-grown cells (Krings et al., 2006), whereas expression of *idhA3* was not altered, suggesting a different regulation. As the *iolG* inactivation mutant WT:p*iolG'* was still able to grow with *myo*-inositol, but not a WTΔ*oxiII*:p*iolG'* double mutant lacking also *oxiC*, *oxiD*, and *oxiE* (Krings et al., 2006), OxiD and/or OxiE most likely have *myo*-inositol dehydrogenase activity. With the *scyllo*-inositol dehydrogenase IolW of *B. subtilis* as query two proteins were identified in *C. glutamicum*, which are OxiA, renamed IolW now (Cg0207), and OxiC (Cg3389). With the *scyllo*-inositol dehydrogenase IolX of *B. subtilis* as query three related proteins were found in *C. glutamicum*, which are IdhA3 (Cg2313), OxiD (Cg3391), and OxiE (Cg3392) (Table 3).

3.2. Scyllo-inositol formation from myo-inositol by C. glutamicum

The results of the bioinformatic analysis suggested that *C. glutamicum* might possess the capabilities to synthesize and to degrade *scyllo*-inositol. Therefore, we performed a shake flask experiment in which *C. glutamicum* MB001(DE3) was cultivated in CGXII minimal medium with either 20 g/L glucose, or 20 g/L *myo*-inositol, or 20 g/L of each glucose and *myo*-inositol as carbon and energy source. Growth was similar for all three conditions (Fig. 2A, D, and G), except that the cultures with both carbon sources reached a higher final OD_{600}. When cultivated with *myo*-inositol, *C. glutamicum* secreted up to 1 g/L *scyllo*-inositol within the first 10 h, which was depleted again after 24 h (Fig. 2F). In contrast, no *scyllo*-inositol was formed during growth with glucose (Fig. 2C). When cultivated with a mixture of glucose and *myo*-inositol, a maximal titer of 2 g/L *scyllo*-inositol was formed after 24 h, which disappeared within the next 24 h (Fig. 2I). These results show that *C. glutamicum* naturally produces *scyllo*-inositol when cultivated in the presence of *myo*-inositol.

3.3. Construction and characterization of C. glutamicum chassis strains for scyllo-inositol production from myo-inositol

For an efficient biotechnological production of *scyllo*-inositol from *myo*-inositol by *C. glutamicum*, a strain which is unable to catabolize *myo*-inositol is mandatory. Previous studies showed that genes of cluster I (cg0196-cg0223) are required for inositol catabolism, whereas the genes of cluster II (cg3385-cg3395) are not (Krings et al., 2006). Based on this information, we constructed two deletion mutants. *C. glutamicum* MB001(DE3)Δ*iol1* lacks 16 genes (cg0196-cg0212) present in cluster I and *C. glutamicum* MB001(DE3)Δ*iol1*Δ*iol2* additionally lacks four genes (cg3389-3392) located in cluster II (Fig. 1). Growth, *myo*-inositol consumption, and *scyllo*-inositol production of these strains were analyzed during cultivation in shake flasks with CGXII medium containing either 20 g/L glucose, 20 g/L *myo*-inositol, or 20 g/L each of glucose and *myo*-inositol (Fig. 2). Both deletion mutants grew slightly faster (μ = 0.44 h^{-1}) than the parental strain (μ = 0.37 h^{-1}) when cultivated on glucose (Fig. 2A), which correlated with a faster glucose consumption (Fig. 2B). This difference is presumably caused by the strongly increased expression of *iolT1* (>70-fold increased mRNA level) caused by the deletion of *iolR* (Fig. 1) encoding the transcriptional regulator IolR (Cg0196), which represses *iolT1* in the absence of *myo*-inositol (Klaffl et al., 2013). IolT1 is a secondary transporter with a relaxed substrate specificity, which does not only transport *myo*-inositol, but also glucose (Ikeda et al., 2011; Lindner et al., 2011) and xylose (Brüsseler et al., 2018). IolT1 provides an additional pathway for glucose uptake besides the glucose-specific phosphotransferase system PtsG. The overall glucose uptake capacity is thus increased.

When cultivated with *myo*-inositol as sole carbon and energy source, the *C. glutamicum* chassis strains MB001(DE3)Δ*iol1* and MB001(DE3)Δ*iol1*Δ*iol2* showed no growth (Fig. 2D), as all seven genes proposed to be involved in the catabolism of *myo*-inositol to dihydroxyacetone phosphate, acetyl-CoA and CO_2 (*iolG*, *iolE*, *iolD*, *iolB*, *iolC*, *iolJ*, and *iolA*) were removed by the Δ*iol1* deletion (Fig. 1). Accordingly, *myo*-inositol was not consumed and no *scyllo*-inositol was formed (Fig. 2F). When cultivated in medium with 20 g/L glucose and 20 g/L *myo*-inositol, the two chassis strains showed impaired growth (μ = 0.18 h^{-1}) and slowed glucose consumption compared to the parental strain MB001(DE3) (μ = 0.41 h^{-1}) (Fig. 2G and H). One reason for this difference is probably the reduced uptake of glucose via IolT1 in the presence of *myo*-inositol. The K_m value for *myo*-inositol of IolT1 was determined as 0.22 mM (Krings et al., 2006), whereas for glucose a K_s value of 2.3 mM was reported (Lindner et al., 2011). Therefore, glucose uptake via IolT1 is expected to be outcompeted by *myo*-inositol. However, this difference does not explain the strongly reduced growth rate, as glucose can still be taken up by PtsG. We assume that accumulation of *myo*-inositol or products formed from *myo*-inositol within the cells of strains MB001(DE3)Δ*iol1* and MB001(DE3)Δ*iol1*Δ*iol2* cause inhibitory effects on metabolism, which are responsible for slowed growth and glucose consumption.

Interestingly, strain MB001(DE3)Δ*iol1* consumed ~5 g/L *myo*-

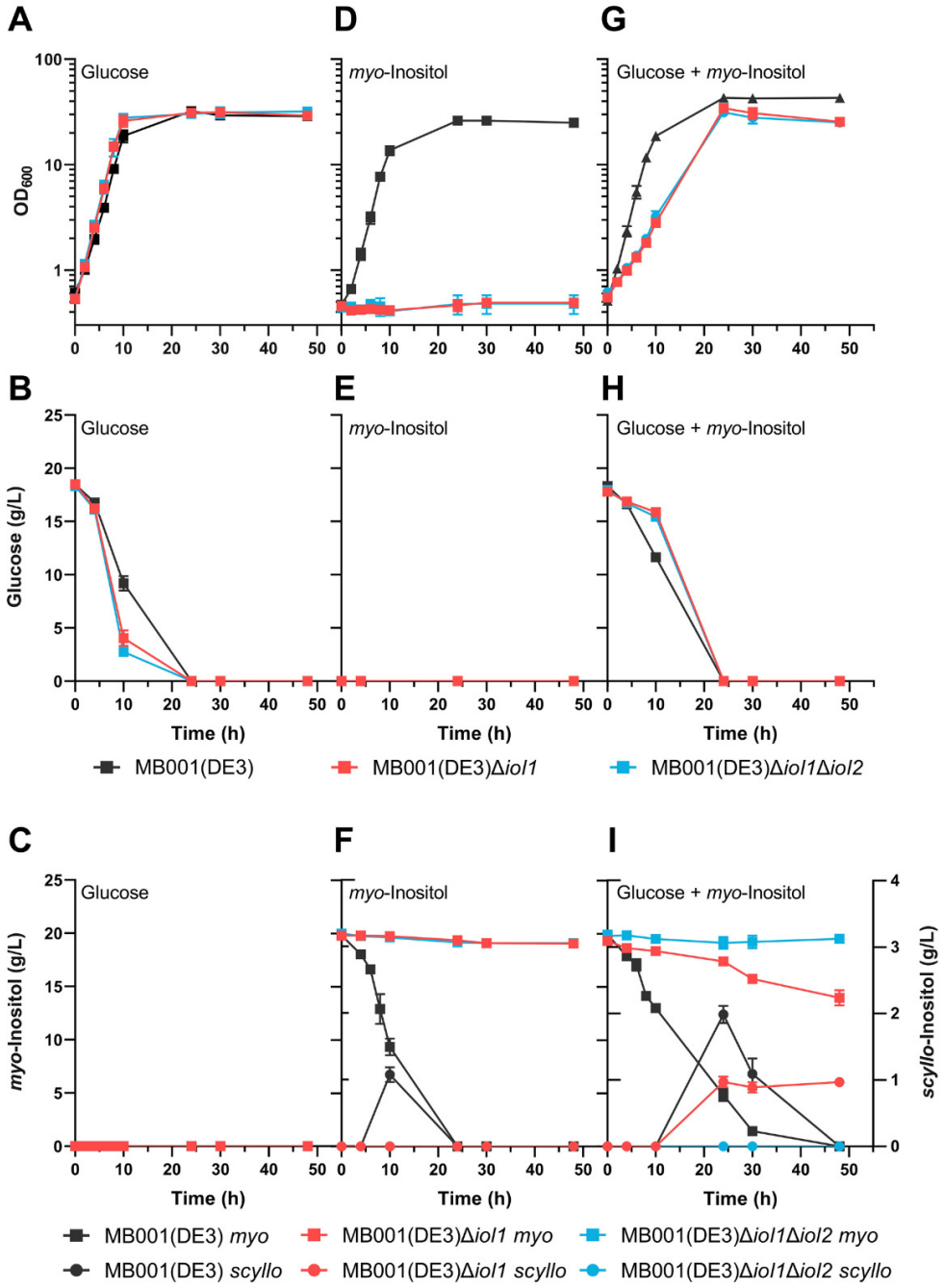

Fig. 2. Growth (OD_{600}), glucose consumption, *myo*-inositol consumption (*myo*) and *scyllo*-inositol formation (*scyllo*) of the indicated *C. glutamicum* strains in CGXII medium containing either 20 g/L glucose (panels A, B, C), or 20 g/L *myo*-inositol (panels D, E, F), or 20 g/L each of glucose and *myo*-inositol (panels G, H, I). Mean values of biological triplicates and standard deviations are shown.

inositol and formed ~1 g/L *scyllo*-inositol within 24 h, which was not degraded later on (Fig. 2I). Concomitantly, the medium became brown. In contrast, the mutant MB001(DE3)Δ*iol1*Δ*iol2* did not consume *myo*-inositol or produce *scyllo*-inositol (Fig. 2I) and the medium did not become brown. These results suggest that one or several of the three dehydrogenases (OxiC, OxiD, OxiE) encoded in the Δ*iol2* region are responsible for the conversion of *myo*-inositol to *scyllo*-inositol in strain MB001(DE3)Δ*iol1*. Only about 20% of the *myo*-inositol consumed by strain MB001(DE3)Δ*iol1* was converted to *scyllo*-inositol and therefore also other products must have been formed. Since strain MB001(DE3)Δ

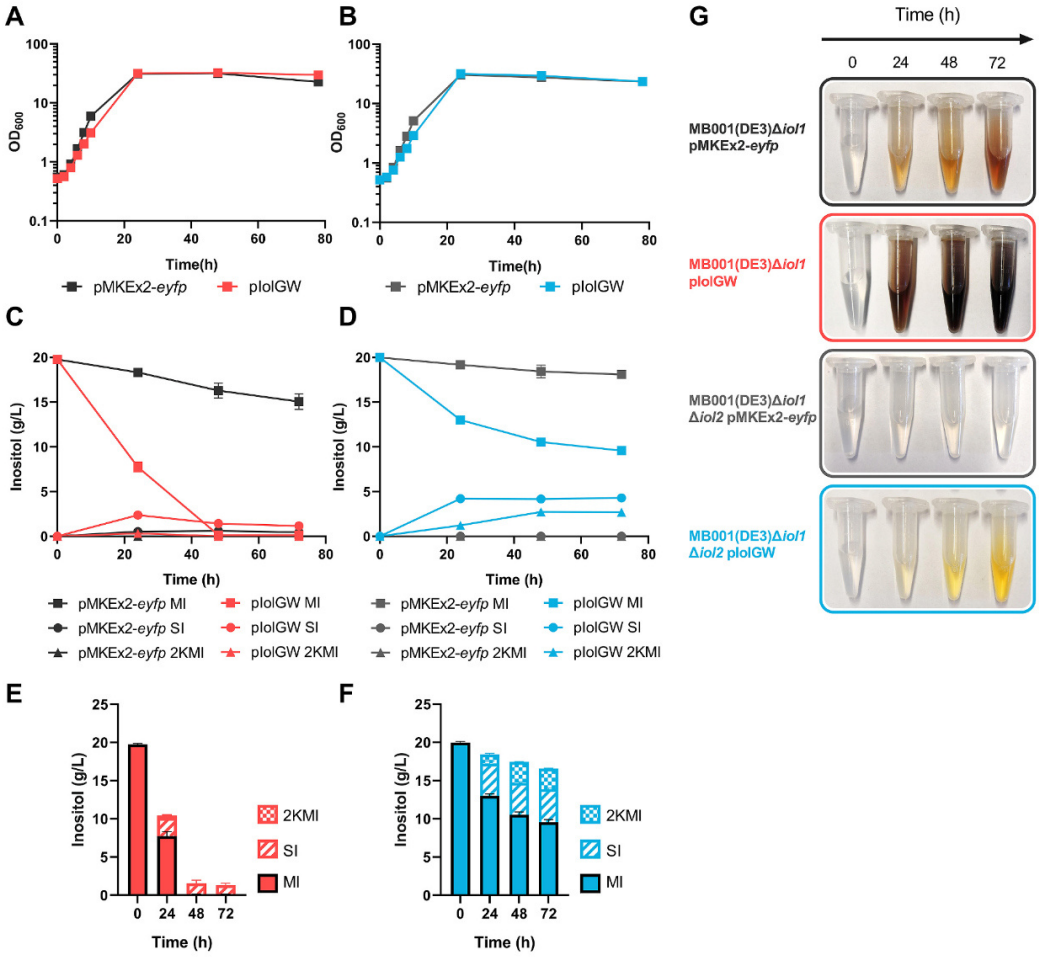

Fig. 3. Production of *scyllo*-inositol from *myo*-inositol in CGXII medium with 20 g/L each of glucose and *myo*-inositol. Panels A and B show growth, panels C and D the kinetics of *myo*-inositol (MI) consumption and formation of *scyllo*-inositol (SI) and 2-keto-*myo*-inositol (2KMI) of the *C. glutamicum* strains MB001(DE3)Δ*iol1* (panels A and C) and MB001(DE3)Δ*iol1*Δ*iol2* (panels B and D) carrying either pMKEx2-*eyfp* or pIolGW. Panels E and F show the sum of the different inositol concentrations detected at the indicated time points for strain MB001(DE3)Δ*iol1* with pIolGW (E) and MB001(DE3)Δ*iol1*Δ*iol2* with pIolGW (F). Panel G shows photographs of supernatant samples of the indicated strain at the indicated time points during cultivation. For A-F, mean values and standard deviations of three biological replicates are shown.

*iol1*Δ*iol2* did not consume appreciable amounts of *myo*-inositol, its utilization for the synthesis of mycothiol, phosphatidylinositol and derived lipids cannot explain the missing 80% of *myo*-inositol. As shown below, the conversion of 2-keto-*myo*-inositol to unknown products causing brown coloration is presumably responsible for the difference between *myo*-inositol consumption and *scyllo*-inositol production by strain MB001(DE3)Δ*iol1*.

3.4. Production of scyllo-inositol from myo-inositol in defined medium

In the next step for efficient *scyllo*-inositol production from *myo*-inositol, we used the *myo*-inositol dehydrogenase IolG, whose activity has been confirmed (Bakkes et al., 2020), and the putative *scyllo*-inositol dehydrogenase IolW, since it showed the highest identity to $IolW_{Bs}$ of *B. subtilis* (Tanaka et al., 2013). The other putative inositol dehydrogenases were not included, since they showed similar identities to several reference proteins (Table 3), among them IolX, which is an NAD^+-dependent *scyllo*-inositol dehydrogenase responsible for *scyllo*-inositol oxidation (Morinaga et al., 2010). We cloned the genes *iolG* (cg0204) and *iolW* (cg0207) of *C. glutamicum* as a synthetic operon into the plasmid pMKEx2 under control of the T7 promoter to enable strong, IPTG-inducible expression in the MB001(DE3) background (Kortmann et al., 2015). The resulting plasmid pIolGW and the control plasmid pMKEx2-*eyfp* were transferred into MB001(DE3)Δ*iol1* and MB001(DE3)Δ*iol1*Δ*iol2* and the recombinant strains were cultivated in CGXII medium with 20 g/L each of glucose and *myo*-inositol. The strains with pIolGW showed a slightly diminished growth rate compared to the strains with pMKEx2-*eyfp* (Fig. 3A and B). Expression of *iolG* and *iolW* was induced at the start of the cultivation with 100 μM IPTG. Whereas the two strains with pMKEx2-*eyfp* displayed a comparable behavior with respect to *myo*-inositol consumption as the plasmid-free strains (Fig. 2), the strains with pIolGW showed remarkable differences (Fig. 3C–F). Strain MB001(DE3)Δ*iol1* with pIolGW completely consumed *myo*-inositol within 48 h and formed a maximal titer of 2.5 g/L *scyllo*-inositol after 24 h, which subsequently decreased to 1.2 g/L after 72 h (Fig. 3C and E). Strain MB001(DE3)Δ*iol1*Δ*iol2* with pIolGW consumed only 11

Table 4
Specific *myo*-inositol and *scyllo*-inositol dehydrogenase activities in cell-free extracts of *C. glutamicum* MB001(DE3)Δ*iol1*Δ*iol2* overproducing six known or putative inositol dehydrogenases. Dehydrogenase activity was determined in a spectrophotometric assay by measuring the absorbance increase at 340 nm in an assay mixture containing cell-free extract, 1 mM of cofactor (either NAD^+ or $NADP^+$) and either 25 mM *myo*-inositol or 25 mM *scyllo*-inositol. Mean values and standard deviations of three technical replicates are shown.

Protein overproduced	Coenzyme	Specific activity for *myo*-inositol (μmol min^{-1} mg^{-1})	Specific activity for *scyllo*-inositol (μmol min^{-1} mg^{-1})
eYFP (negative control)	NAD^+	n. d.	n. d.
	$NADP^+$	n. d.	n. d.
OxiC	NAD^+	n. d.	n. d.
	$NADP^+$	n. d.	n. d.
OxiD	NAD^+	22.59 ± 0.03	n. d.
	$NADP^+$	1.11 ± 0.12	n. d.
OxiE	NAD^+	2.68 ± 0.04	11.06 ± 0.18
	$NADP^+$	n. d.	0.32 ± 0.05
IdhA3	NAD^+	n. d.	n. d.
	$NADP^+$	n. d.	n. d.

n.d.: not detected.

g/L *myo*-inositol within 72 h, but formed a titer of 4.4 g/L *scyllo*-inositol within 24 h, which remained constant until the end of the cultivation (Fig. 3D and F). Moreover, this strain also accumulated 2.7 g/L 2-keto-*myo*-inositol after 72 h. This intermediate was not detectable in the Δ*iol1* strain. When looking at the balance, the fate of 18.8 g/L *myo*-inositol consumed by strain MB001(DE3)Δ*iol1* remains unknown, whereas for strain MB001(DE3)Δ*iol1*Δ*iol2* it is 3.9 g/L. This suggested that in MB001(DE3)Δ*iol1* further products are formed, e.g. by the enzymes encoded in the Δ*iol2* region and elsewhere in the genome, as also for MB001(DE3)Δ*iol1*Δ*iol2* the balance was not closed.

As shown in Fig. 3G, the two strains with pIolGW also differed with respect to the color of the cultures. The supernatant of strain MB001 (DE3)Δ*iol1* became brown within 24 h and the intensity increased further at 48 h. We speculate that the brown coloration is caused by Maillard reaction products that are formed by reactions of reducing sugars and free amino groups (Ajandouz et al., 2001; Ledl and Schleicher, 1990; Stadler et al., 2002). As this color was not observed in the supernatant of strain MB001(DE3)Δ*iol1*Δ*iol2*, enzymes encoded in the Δ*iol2* region are probably responsible for the formation of the brown color. The supernatant of strain MB001(DE3)Δ*iol1*Δ*iol2* showed only a slight change of color within 24 h and became yellow-orange within 48 h. This color is due to the formation of 2-keto-*myo*-inositol, as it was also observed when this compound (obtained by Sigma Aldrich) was dissolved in CGXII medium, while dissolved *scyllo*-inositol caused no color change (data not shown).

3.5. Analysis of proteins encoded by the Δiol2 region and by idhA3

To investigate if one or more of the residual dehydrogenases are responsible for the loss of *myo*- and *scyllo*-inositol observed in the experiments shown in Fig. 3, we individually overproduced the putative inositol dehydrogenases OxiC, OxiD, OxiE, and IdhA3 in *C. glutamicum* MB001(DE3)Δ*iol1*Δ*iol2* using the pMKEx2 expression vector (Fig. S1). Subsequently we determined the specific dehydrogenase activity for *myo*-inositol and *scyllo*-inositol using cell-free extracts and NAD^+ or $NADP^+$ as coenzyme (Table 4). Extracts containing OxiC and IdhA3 showed no activity for either tested inositol. In contrast, extracts containing OxiD and OxiE catalyzed the NAD^+-dependent oxidation of *myo*-inositol with specific activities of 22.59 ± 0.03 μmol min^{-1} mg^{-1} and 2.68 ± 0.04 μmol min^{-1} mg^{-1}. Therefore, the consumption of *myo*-inositol by strain MB001(DE3)Δ*iol1* observed in Fig. 2I and the residual growth observed for a *iolG* mutant in a previous study (Krings et al., 2006) can be explained by the *myo*-inositol dehydrogenase activity of OxiD and OxiE.

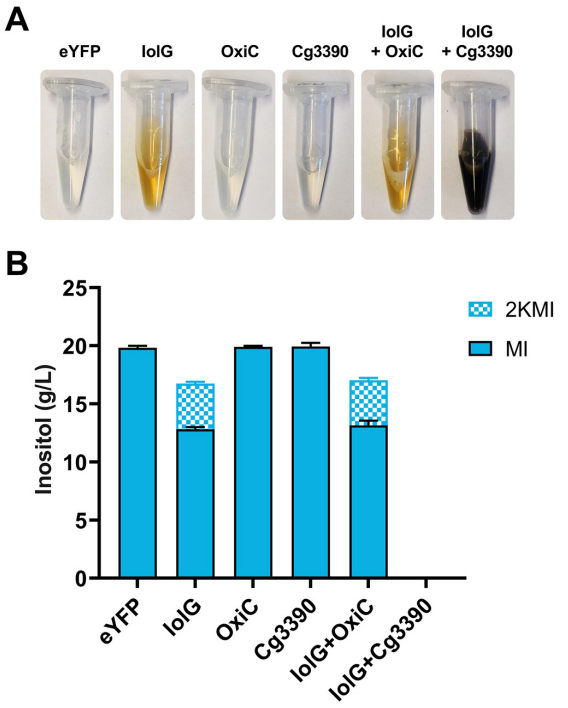

Fig. 4. Influence of plasmid-based overproduction of the indicated proteins in *C. glutamicum* MB001(DE3)Δ*iol1*Δ*iol2* on the color of the medium (A) and the concentrations of *myo*-inositol (MI) and 2-keto-*myo*-inositol (2KMI) (B) after 72 h of growth at 30 °C in CGXII medium with 20 g/L glucose and 20 g/L *myo*-inositol.

Interestingly, OxiE showed an even higher specific activity for *scyllo*-inositol with NAD^+ as favored cofactor (11.06 ± 0.18 μmol min^{-1} mg^{-1}), revealing a function similar to the catabolic *scyllo*-inositol dehydrogenase IolX of *B. subtilis* (Morinaga et al., 2010). This suggests that OxiE mainly functions in oxidizing *scyllo*-inositol to 2-keto-*myo*-inositol and thus counteracts *scyllo*-inositol formation by IolW. Therefore, it can be assumed that OxiE contributes to *scyllo*-inositol consumption observed in the *C. glutamicum* strains possessing the *iol2* cluster (Fig. 2F and I and Fig. 3C).

As 2-keto-*myo*-inositol was only detected in the MB001(DE3)Δ*iol1*Δ*iol2* strain, but not in the Δ*iol1* strain although the latter consumed much more *myo*-inositol (Fig. 3), we assumed that 2-keto-*myo*-inositol is converted to other products in the Δ*iol1* strain by enzymes encoded in the Δ*iol2* region, resulting in the proposed Maillard products and the dark brown coloration. Since we showed that OxiD and OxiE function as *myo*- and/or *scyllo*-inositol dehydrogenases (Table 4), we considered them unlikely to be responsible for a different kind of 2-keto-*myo*-inositol conversion and brown coloration. Rather, we focused on the putative sugar phosphate isomerase Cg3390 and OxiC as potential causes for the conversion of 2-keto-*myo*-inositol to further, unknown products. To test their role in the formation of the brown color, we cloned *oxiC* and cg3390 individually and in combination with *iolG* into pMKEx2, introduced the resulting plasmids in *C. glutamicum* MB001 (DE3)Δ*iol1*Δ*iol2*, and cultivated the strains at 30 °C in CGXII medium with 20 g/L glucose and 20 g/L *myo*-inositol. Gene expression was induced via addition of 100 μM IPTG at the beginning of the cultivation. After 72 h, we examined the color and determined the concentrations of *myo*-inositol and 2-keto-*myo*-inositol (Fig. 4). Cultures in which cg3390,

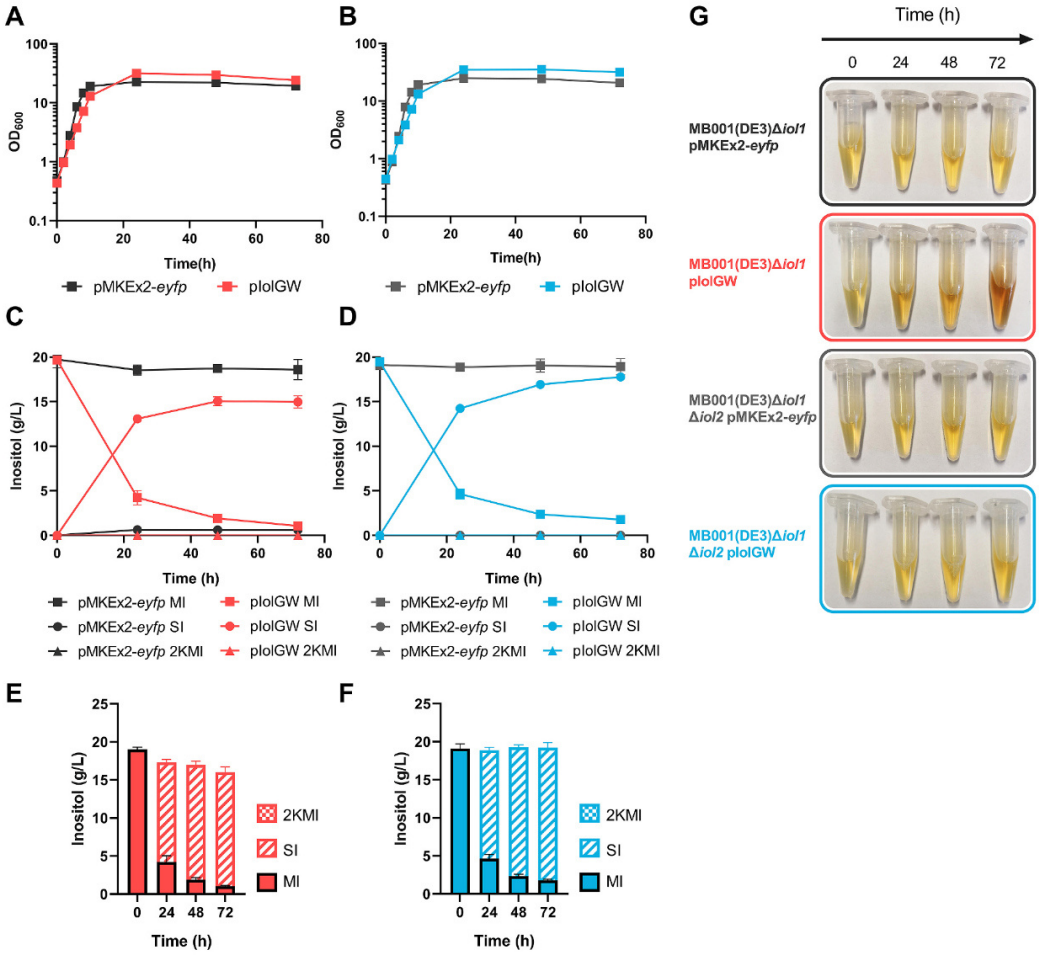

Fig. 5. Production of *scyllo*-inositol from *myo*-inositol in BHI medium with 20 g/L each of glucose and *myo*-inositol. Panels A and B show growth, panels C and D show the kinetics of *myo*-inositol (MI) consumption and formation of *scyllo*-inositol (SI) and 2-keto-*myo*-inositol (2KMI) of the *C. glutamicum* strains MB001(DE3)Δ*iol1* (panels A and C) and MB001(DE3)Δ*iol1*Δ*iol2* (panels B and D) carrying either pMKEx2-*eyfp* or pIolGW. Panels E and F show the sum of the different inositol concentrations detected at the indicated time points for strain MB001(DE3)Δ*iol1* with pIolGW (B) and MB001(DE3)Δ*iol1*Δ*iol2* with pIolGW (D). Panel G shows photographs of supernatant samples of the indicated strain at the indicated time points during cultivation. For A-F, mean values and standard deviations of three biological replicates are shown.

oxiC, or as control *eyfp* were overexpressed showed no color change and no *myo*-inositol consumption. Strains expressing either *iolG* or *iolG-oxiC* consumed part of the *myo*-inositol and formed approximately 4.0 g/L of 2-keto-*myo*-inositol, associated with yellow coloration, but not *scyllo*-inositol. Most interestingly, the strain expressing *iolG* together with cg3390 showed dark brown coloration (Fig. 4A) and no residual *myo*-inositol or 2-keto-*myo*-inositol was present after 72 h (Fig. 4B). This result proves that Cg3390 is responsible for the conversion of 2-keto-*myo*-inositol to unknown products causing brown coloration.

3.6. Production of scyllo-inositol from myo-inositol in rich medium

As the *scyllo*-inositol yield from *myo*-inositol in CGXII medium was maximally 0.4 g/g, we tested whether the use of rich BHI medium, which is often used for cultivation of *C. glutamicum*, could increase the yield. Previous studies with *B. subtilis* reported a positive effect of increased peptone concentrations on *scyllo*-inositol formation from *myo*-inositol (Tanaka et al., 2017). We analyzed *scyllo*-inositol formation by *C. glutamicum* MB001(DE3)Δ*iol1* and MB001(DE3)Δ*iol1*Δ*iol2* containing either pIolGW or pMKEx2-*eyfp* during growth in BHI medium containing 20 g/L each of glucose and *myo*-inositol. Expression of the target genes was induced at the start of the cultivation with 100 μM IPTG. Again, the strains with pIolGW showed a slightly diminished growth rate compared to the strains with pMKEx2-*eyfp* (Fig. 5A and B). Strain MB001(DE3)Δ*iol1* with pIolGW produced ~15 g/L *scyllo*-inositol from 20 g/L *myo*-inositol after 72 h, with ~1 g/L *myo*-inositol remaining in the medium. 4 g/L *myo*-inositol was converted into unknown products (Fig. 5C, E). Increasingly brown coloration of medium supernatants was observed during the cultivation, but much less intense than in CGXII medium (Fig. 5G). Based on the results described in the previous section, conversion of 2-keto-*myo*-inositol by the Cg3390 enzyme is probably responsible for synthesis of the unknown products and the brown color. Strain MB001(DE3)Δ*iol1*Δ*iol2* with pIolGW formed 18 g/L *scyllo*-inositol from 18 g/L consumed *myo*-inositol and the residual 2 g/L *myo*-inositol remained unmetabolized. Thus, the entire *myo*-inositol consumed was converted into *scyllo*-inositol (Fig. 5D, F). In these

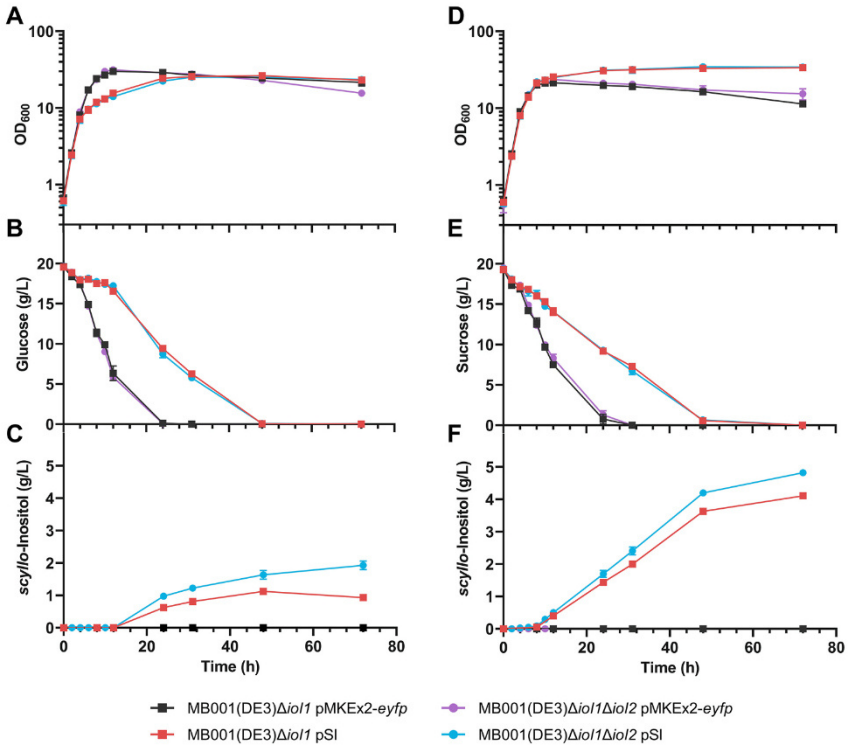

Fig. 6. Growth (A, D), glucose and sucrose consumption (B, E), and production of *scyllo*-inositol (C, F) of the indicated *C. glutamicum* strains during cultivation in BHI medium with 20 g/L glucose (A–C) or with 20 g/L sucrose (D–F). Target gene expression was induced at an OD_{600} of 2 with 200 μM IPTG. Mean values of three biological replicates and standard deviations are shown.

cultures, the color of the medium remained almost unchanged (Fig. 5G).

In conclusion, the deletion of the *iol2* region proved to be important for the biotechnological production of *scyllo*-inositol with *C. glutamicum*, since the activities of at least two enzymes encoded in this region counteract *scyllo*-inositol formation. OxiE oxidizes *scyllo*-inositol formed in an NADPH-dependent reaction by IolW back to 2-keto-*myo*-inositol using NAD^+ as coenzyme. The putative isomerase Cg3390 converts 2-keto-*myo*-inositol to a yet unknown product that is probably further converted to Maillard products. Besides the Δ*iol2* deletion, the use of BHI instead of CGXII medium enabled a much better conversion of *myo*-inositol into *scyllo*-inositol and strongly reduced the formation of compounds assumed to be Maillard products. Furthermore, no accumulation of 2-keto-*myo*-inositol was observed for strain MB001(DE3)Δ*iol1*Δ*iol2* with pIolGW in BHI medium in contrast to CGXII medium. This suggests that the reduction of 2-keto-*myo*-inositol to *scyllo*-inositol is a bottleneck in CGXII medium. A possible explanation for the difference is a lowered NADPH demand for biomass synthesis in BHI medium compared to CGXII medium. BHI medium contains amino acids and peptides, which are taken up by the cells and used for the synthesis of proteins, which make up about 50% of the cell dry weight. In CGXII medium, all amino acids need to be synthesized from glucose and ammonia, which is associated with a high NADPH demand. For example, synthesis of one mol lysine from oxaloacetate requires 4 mol NADPH. Therefore, during cultivation in CGXII medium a large fraction of the NADPH formed in the oxidative PPP and a few other reactions is used for biomass synthesis and not available for reduction of 2-keto-*myo*-inositol to *scyllo*-inositol.

3.7. Production of scyllo-inositol from glucose and sucrose

The experimental setup described above allowed efficient production of *scyllo*-inositol from *myo*-inositol, but as this compound is still quite expensive, we aimed to replace it by cheaper carbon sources such as glucose or sucrose. As described in the introduction, *C. glutamicum* has the natural ability to synthesize *myo*-inositol from glucose 6-phosphate in a two-step pathway involving *myo*-inositol 1-phosphate synthase (Ino1) and *myo*-inositol 1-phosphatase (ImpA). We therefore constructed the pMKEx2-based expression plasmid pSI, which contains a synthetic operon comprising the genes *ino1*, *impA*, *iolG*, and *iolW* under the control of the T7 promoter. The *C. glutamicum* strains MB001(DE3)Δ*iol1* and MB001(DE3)Δ*iol1*Δ*iol2* were transformed with pSI or the control plasmid pMKEx2-*eyfp* and cultivated in BHI medium with 20 g/L glucose or 20 g/L sucrose.

When cultivated in the presence of glucose or sucrose, the strains containing the control plasmid pMKEx2-*eyfp* consumed glucose or sucrose completely within 24 h or 32 h, respectively, and did not form *scyllo*-inositol (Fig. 6). The strains containing pSI showed decelerated growth (after ~4 h) on glucose, but not on sucrose (Fig. 6A, D), whereas consumption was slowed down for both, glucose and sucrose (Fig. 6B, E). The reason for the negative effect of the presence of the pSI plasmid is not clear yet. One explanation could be an unspecific dephosphorylation of phosphorylated metabolites besides *myo*-inositol 1-phosphate by the overproduced phosphatase ImpA, causing a deceleration of central metabolism. Examples for such unspecific activities have been reported e.g. for the 3′-phosphoadenosine-5′-phosphatase CysQ of *Mycobacterium tuberculosis*, which besides the natural substrate also dephosphorylates *myo*-inositol 1-phosphate and fructose 1,6-bisphosphate (Hatzios et al., 2008).

Production of *scyllo*-inositol from glucose started after 12 h and reached titers of 0.8 g/L for MB001(DE3)Δ*iol1* pSI and 1.8 g/L for MB001(DE3)Δ*iol1*Δ*iol2* pSI after 72 h (Fig. 6C). A slight drop of the

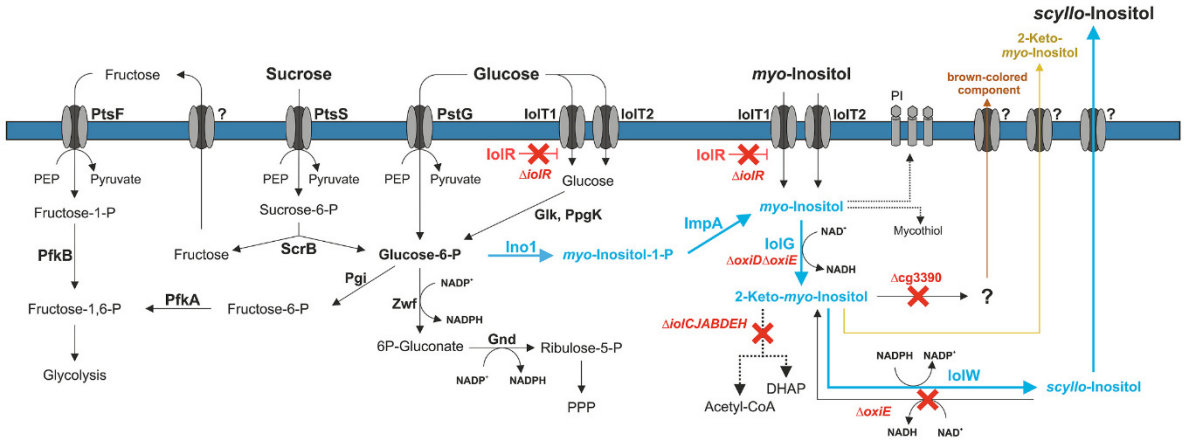

Fig. 7. Scheme of metabolism relevant for *scyllo*-inositol production from glucose, sucrose, and *myo*-inositol by *C. glutamicum*. The genes required for catabolizing of *myo*-inositol or catalyzing further conversions of inositol-derived metabolites (grey) and the gene encoding the transcriptional regulator IolR (red) were deleted in the strain MB001(DE3)Δ*iol1*Δ*iol2*. Highlighted in blue is the engineered pathway for *scyllo*-inositol production from either *myo*-inositol, glucose or sucrose employing *myo*-inositol 1-phosphate synthase (Ino1), *myo*-inositol 1-monophosphatase (ImpA), *myo*-inositol dehydrogenase (IolG), and *scyllo*-inositol dehydrogenase (IolW). IolT1 and IolT2: transporters for *myo*-inositol and glucose; PtsG, PtsF, PtsS: EII components of the PEP-dependent phosphotransferase system for uptake of glucose, fructose, and sucrose, respectively; PfkA: 6-phosphofructokinase; PfkB: 1-phosphofructokinase; ScrB: sucrose 6-phosphate hydrolase; Pgi: glucose 6-phosphate isomerase; Zwf: glucose 6-phosphate dehydrogenase; Gnd: 6-phosphogluconate dehydrogenase; Glk: glucokinase; PpgK: polyphosphate-dependent glucokinase; OxiD: enzyme with *myo*-inositol dehydrogenase activity; OxiE: enzyme with *scyllo*-inositol and *myo*-inositol dehydrogenase activity; Cg3390: enzyme converting 2-keto-*myo*-inositol to a yet unknown product responsible for brown coloration; PEP: phosphoenolpyruvate; DHAP: dihydroxyacetone phosphate; PI: phosphatidylinositol.

scyllo-inositol concentration was observed between 48 h and 72 h for the Δ*iol1* strain, whereas it still increased in that period for the Δ*iol1*Δ*iol2* strain. This effect and difference in titers are most likely due to the activities of OxiE and Cg3390 (see above). Production of *scyllo*-inositol from sucrose started after ~8 h and reached titers of 3.9 g/L for MB001(DE3)Δ*iol1* pSI and 4.4 g/L for MB001(DE3)Δ*iol1*Δ*iol2* pSI after 72 h (Fig. 6F). The majority of *scyllo*-inositol was formed when the cultures were in the stationary growth phase. No 2-keto-*myo*-inositol formation was observed in supernatant samples and no color change occurred for both strains cultivated on either glucose or sucrose.

The increase in *scyllo*-inositol production with sucrose as substrate instead of glucose is presumably linked to the differences in the metabolism of these sugars (Blombach and Seibold, 2010), shown in Fig. 7. Glucose is taken up by PtsG forming glucose 6-phosphate, or by IolT1 followed by phosphorylation via Glk (Cg2399) or PpgK (Cg2091) to glucose 6-phosphate. Sucrose is taken up by the sucrose-specific PTS (PtsS), forming sucrose 6-phosphate, which is then hydrolyzed by ScrB into fructose and glucose 6-phosphate. Fructose is exported by an unknown carrier and then reimported by the fructose-specific PTS (PtsF) to form fructose 1-phosphate, which is phosphorylated by fructose 1-phosphate kinase (PfkB) to fructose 1,6-bisphosphate. In a study on the carbon flux of sucrose in a lysine-producing strain of *C. glutamicum*, the glucose part of sucrose was completely channeled into the PPP, whereas the fructose part was predominantly metabolized in glycolysis (Wittmann et al., 2004). When cells are grown on glucose alone, a large fraction of glucose 6-phosphate is channeled into glycolysis, which varies between 73% and 26% depending on the NADPH demand of the cells (Marx et al., 1997). We speculate that there is a higher concentration and availability of glucose 6-phosphate in sucrose-grown cells, which is responsible for the increased *scyllo*-inositol production. The first enzyme for channeling glucose 6-phosphate into the inositol pathway is *myo*-inositol 1-phosphate synthase (Ino1). For Ino1 of *C. glutamicum* a K_m value of 12 mM for glucose 6-phosphate and a k_{cat} of 2.24 min^{-1} have been reported (Chen et al., 2019). In contrast, the competing glucose 6-phosphate dehydrogenase (G6PDH) of *C. glutamicum*, which catalyzes the irreversible oxidation to 6-phosphogluconolactone, has a K_m value of 169 μM for glucose 6-phosphate and a specific activity of 160 U/mg (Moritz et al., 2000). In view of these differences, an increased glucose 6-phosphate concentration might be a major reason for increased *scyllo*-inositol production from sucrose by enabling higher Ino1 activity.

4. Conclusions

The results of this study identify *C. glutamicum* as a promising host for the production of *scyllo*-inositol, a potential drug against Alzheimer's disease. Using strains defective in *myo*-inositol and *scyllo*-inositol metabolism that overexpressed the genes *iolG* and *iolW* we could achieve a complete conversion of *myo*-inositol to *scyllo*-inositol in rich medium. Additional overexpression of the genes *ino1* and *impA* enabled *scyllo*-inositol production from glucose with a yield (1.8 g/20 g glucose) comparable to the one reported for *B. subtilis* (Michon et al., 2020). However, sucrose turned out to be a better substrate than glucose, as 4.4 g *scyllo*-inositol were formed from 20 g sucrose. Our next studies aim at a further increase of the production of *scyllo*-inositol and other *myo*-inositol-derived compounds from cheap carbon sources by metabolic engineering approaches aiming at a redirection of carbon flux towards *myo*-inositol, examples of which were reported e.g. for glucarate production in *E. coli* (Brockman and Prather, 2015; Doong et al., 2018).

Declaration of competing interest

The authors declare no conflict of interests.

Acknowledgments

This project was financially supported by the CLIB-Competence Center Biotechnology (CKB) funded by the European Regional Development Fund ERDF [grant number 34.EFRE-0300097] and by the German Federal Ministry of Education and Research (BMBF) [grant number 031B0918A], as part of the project "BioökonomieREVIER".

Appendix A. Supplementary data

Supplementary data to this article can be found online at https://doi.org/10.1016/j.ymben.2021.06.011.

Author statement

Paul Ramp: Conceptualization, Methodology, Investigation, Writing – Initial Draft, Visualization. Alexander Lehnert: Investigation, Methodology. Susana Matamouros: Supervision, Methodology. Astrid Wirtz: Methodology, Investigation. Meike Baumgart: Methodology, Writing – original draft, Supervision. Michael Bott: Conceptualization, Supervision, Writing – review & editing, Funding acquisition.

References

Ajandouz, E.H., Tchiakpe, L.S., Dalle Ore, F., Benajiba, A., Puigserver, A., 2001. Effects of pH on caramelization and Maillard reaction kinetics in fructose-lysine model systems. J. Food Sci. 66, 926–931.

Bakkes, P.J., Ramp, P., Bida, A., Dohmen-Olma, D., Bott, M., Freudl, R., 2020. Improved pEKEx2-derived expression vectors for tightly controlled production of recombinant proteins in *Corynebacterium glutamicum*. Plasmid 112, 102540.

Baumgart, M., Luder, K., Grover, S., Gätgens, C., Besra, G.S., Frunzke, J., 2013. IpsA, a novel LacI-type regulator, is required for inositol-derived lipid formation in Corynebacteria and Mycobacteria. BMC Biol. 11, 122.

Becker, J., Wittmann, C., 2012. Bio-based production of chemicals, materials and fuels–*Corynebacterium glutamicum* as versatile cell factory. Curr. Opin. Biotechnol. 23, 631–640.

Bertani, G., 1951. Studies on lysogenesis. The mode of phage liberation by lysogenic *Escherichia coli*. J. Bacteriol. 62, 293–300.

Blombach, B., Seibold, G.M., 2010. Carbohydrate metabolism in *Corynebacterium glutamicum* and applications for the metabolic engineering of L-lysine production strains. Appl. Microbiol. Biotechnol. 86, 1313–1322.

Brockman, I.M., Prather, K.L.J., 2015. Dynamic knockdown of *E. coli* central metabolism for redirecting fluxes of primary metabolites. Metab. Eng. 28, 104–113.

Brüsseler, C., Radek, A., Tenhaef, N., Krumbach, K., Noack, S., Marienhagen, J., 2018. The *myo*-inositol/proton symporter IolT1 contributes to D-xylose uptake in *Corynebacterium glutamicum*. Bioresour. Technol. 249, 953–961.

Candy, D.J., 1967. Occurrence and metabolism of *scyllo*-inositol in the locust. Biochem. J. 103, 666–671.

Chen, C., Chen, K., Su, T., Zhang, B., Li, G., Pan, J., Si, M., 2019. *Myo*-inositol-1-phosphate synthase (Ino-1) functions as a protection mechanism in *Corynebacterium glutamicum* under oxidative stress. MicrobiologyOpen 8, e00721.

Doong, S.J., Gupta, A., Prather, K.L.J., 2018. Layered dynamic regulation for improving metabolic pathway productivity in *Escherichia coli*. Proc. Natl. Acad. Sci. U.S.A. 115, 2964–2969.

Eggeling, L., Bott, M., 2005. Handbook of *Corynebacterium glutamicum*. CRC Press, Boca Raton.

Eggeling, L., Bott, M., 2015. A giant market and a powerful metabolism: L-lysine provided by *Corynebacterium glutamicum*. Appl. Microbiol. Biotechnol. 99, 3387–3394.

Fenili, D., Brown, M., Rappaport, R., McLaurin, J., 2007. Properties of *scyllo*-inositol as a therapeutic treatment of AD-like pathology. J. Mol. Med. 85, 603–611.

Freudl, R., 2017. Beyond amino acids: use of the *Corynebacterium glutamicum* cell factory for the secretion of heterologous proteins. J. Biotechnol. 258, 101–109.

Gibson, D.G., Young, L., Chuang, R.Y., Venter, J.C., Hutchison, C.A., Smith, H.O., 2009. Enzymatic assembly of DNA molecules up to several hundred kilobases. Nat. Methods 6, 343–345.

Green, M.R., Sambrook, J., 2012. Molecular Cloning. A Laboratory Manual. Cold Spring Harbor Laboratory Press, Cold Spring Harbor, New York.

Hanahan, D., 1983. Studies on transformation of *Escherichia coli* with plasmids. J. Mol. Biol. 166, 557–580.

Hatzios, S.K., Iavarone, A.T., Bertozzi, C.R., 2008. Rv2131c from *Mycobacterium tuberculosis* is a CysQ 3'-phosphoadenosine-5'-phosphatase. Biochemistry 47, 5823–5831.

Heider, S.A., Wendisch, V.F., 2015. Engineering microbial cell factories: metabolic engineering of *Corynebacterium glutamicum* with a focus on non-natural products. Biotechnol. J. 10, 1170–1184.

Horner, W.H., Thaker, I.H., 1968. Metabolism of *scyllo*-inositol in *Streptomyces griseus*. Biochim. Biophys. Acta 165, 306–308.

Ikeda, M., Mizuno, Y., Awane, S., Hayashi, M., Mitsuhashi, S., Takeno, S., 2011. Identification and application of a different glucose uptake system that functions as an alternative to the phosphotransferase system in *Corynebacterium glutamicum*. Appl. Microbiol. Biotechnol. 90, 1443–1451.

Keilhauer, C., Eggeling, L., Sahm, H., 1993. Isoleucine synthesis in *Corynebacterium glutamicum*: molecular analysis of the *ilvB-ilvN-ilvC* operon. J. Bacteriol. 175, 5595–5603.

Klaffl, S., Brocker, M., Kalinowski, J., Eikmanns, B.J., Bott, M., 2013. Complex regulation of the phosphoenolpyruvate carboxykinase gene *pck* and characterization of its GntR-type regulator IolR as a repressor of *myo*-inositol utilization genes in *Corynebacterium glutamicum*. J. Bacteriol. 195, 4283–4296.

Kortmann, M., Kuhl, V., Klaffl, S., Bott, M., 2015. A chromosomally encoded T7 RNA polymerase-dependent gene expression system for *Corynebacterium glutamicum*: construction and comparative evaluation at the single-cell level. Microb. Biotechnol. 8, 253–265.

Krings, E., Krumbach, K., Bathe, B., Kelle, R., Wendisch, V.F., Sahm, H., Eggeling, L., 2006. Characterization of *myo*-inositol utilization by *Corynebacterium glutamicum*: the stimulon, identification of transporters, and influence on L-lysine formation. J. Bacteriol. 188, 8054–8061.

Ledl, F., Schleicher, E., 1990. New aspects of the Maillard reaction in foods and in the human body. Angew. Chem. Int. Ed. 29, 565–594.

Li, Y., Han, P., Wang, J., Shi, T., You, C., 2021. Production of *myo*-inositol: recent advances and prospective. Biotechnol. Appl. Biochem. 1–11.

Lindner, S.N., Seibold, G.M., Henrich, A., Krämer, R., Wendisch, V.F., 2011. Phosphotransferase system-independent glucose utilization in *Corynebacterium glutamicum* by inositol permeases and glucokinases. Appl. Environ. Microbiol. 77, 3571–3581.

Marx, A., Striegel, K., de Graaf, A.A., Sahm, H., Eggeling, L., 1997. Response of the central metabolism of *Corynebacterium glutamicum* to different flux burdens. Biotechnol. Bioeng. 56, 168–180.

McLaurin, J., Kierstead, M.E., Brown, M.E., Hawkes, C.A., Lambermon, M.H.L., Phinney, A.L., Darabie, A.A., Cousins, J.E., French, J.E., Lan, M.F., Chen, F.S., Wong, S.S.N., Mount, H.T.J., Fraser, P.E., Westaway, D., St George-Hyslop, P., 2006. Cyclohexanehexol inhibitors of Aβ aggregation prevent and reverse Alzheimer phenotype in a mouse model. Nat. Med. 12, 801–808.

Michon, C., Kang, C.M., Karpenko, S., Tanaka, K., Ishikawa, S., Yoshida, K.I., 2020. A bacterial cell factory converting glucose into *scyllo*-inositol, a therapeutic agent for Alzheimer's disease. Comm. Biol. 3, 93.

Morinaga, T., Ashida, H., Yoshida, K., 2010. Identification of two *scyllo*-inositol dehydrogenases in *Bacillus subtilis*. Microbiology 156, 1538–1546.

Morita, Y.S., Fukuda, T., Sena, C.B., Yamaryo-Botte, Y., McConville, M.J., Kinoshita, T., 2011. Inositol lipid metabolism in mycobacteria: biosynthesis and regulatory mechanisms. Biochim. Biophys. Acta 1810, 630–641.

Moritz, B., Striegel, K., De Graaf, A.A., Sahm, H., 2000. Kinetic properties of the glucose-6-phosphate and 6-phosphogluconate dehydrogenases from *Corynebacterium glutamicum* and their application for predicting pentose phosphate pathway flux *in vivo*. Eur. J. Biochem. 267, 3442–3452.

Newton, G.L., Buchmeier, N., Fahey, R.C., 2008. Biosynthesis and functions of mycothiol, the unique protective thiol of Actinobacteria. Microbiol. Mol. Biol. Rev. 72, 471–494.

Niebisch, A., Bott, M., 2001. Molecular analysis of the cytochrome bc_1-aa_3 branch of the *Corynebacterium glutamicum* respiratory chain containing an unusual diheme cytochrome c_1. Arch. Microbiol. 175, 282–294.

Salloway, S., Sperling, R., Keren, R., Porsteinsson, A.P., van Dyck, C.H., Tariot, P.N., Gilman, S., Arnold, D., Abushakra, S., Hernandez, C., Crans, G., Liang, E., Quinn, G., Bairu, M., Pastrak, A., Cedarbaum, J.M., ELND005-AD201 Investigators, 2011. A phase 2 randomized trial of ELND005, *scyllo*-inositol, in mild to moderate Alzheimer disease. Neurology 77, 1253–1262.

Sarmah, M.P., Shashidhar, M.S., 2003. Sulfonate protecting groups. Improved synthesis of *scyllo*-inositol and its orthoformate from *myo*-inositol. Carbohydr. Res. 338, 999–1001.

Schäfer, A., Tauch, A., Jäger, W., Kalinowski, J., Thierbach, G., Pühler, A., 1994. Small mobilizable multi-purpose cloning vectors derived from the *Escherichia coli* plasmids pK18 and pK19: selection of defined deletions in the chromosome of *Corynebacterium glutamicum*. Gene 145, 69–73.

Stadler, R.H., Blank, I., Varga, N., Robert, F., Hau, J., Guy, P.A., Robert, M.C., Riediker, S., 2002. Acrylamide from Maillard reaction products. Nature 419, 449–450.

Tanaka, K., Natsume, A., Ishikawa, S., Takenaka, S., Yoshida, K., 2017. A new-generation of *Bacillus subtilis* cell factory for further elevated *scyllo*-inositol production. Microb. Cell Factories 16.

Tanaka, K., Tajima, S., Takenaka, S., Yoshida, K., 2013. An improved *Bacillus subtilis* cell factory for producing *scyllo*-inositol, a promising therapeutic agent for Alzheimer's disease. Microb. Cell Factories 12, 124.

Tenhaef, N., Brüsseler, C., Radek, A., Hilmes, R., Unrean, P., Marienhagen, J., Noack, S., 2018. Production of D-xylonic acid using a non-recombinant *Corynebacterium glutamicum* strain. Bioresour. Technol. 268, 332–339.

Townsend, M., Cleary, J.P., Mehta, T., Hofmeister, J., Lesne, S., O'Hare, E., Walsh, D.M., Selkoe, D.J., 2006. Orally available compound prevents deficits in memory caused by the Alzheimer amyloid-beta oligomers. Ann. Neurol. 60, 668–676.

van der Rest, M.E., Lange, C., Molenaar, D., 1999. A heat shock following electroporation induces highly efficient transformation of *Corynebacterium glutamicum* with xenogeneic plasmid DNA. Appl. Microbiol. Biotechnol. 52, 541–545.

Wenda, S., Illner, S., Mell, A., Kragl, U., 2011. Industrial biotechnology—the future of green chemistry? Green Chem. 13, 3007–3047.

Wendisch, V.F., Jorge, J.M., Pérez-García, F., Sgobba, E., 2016. Updates on industrial production of amino acids using *Corynebacterium glutamicum*. World J. Microbiol. Biotechnol. 32, 105.

Wieschalka, S., Blombach, B., Bott, M., Eikmanns, B., 2013. Bio-based production of organic acids with *Corynebacterium glutamicum*. Microb. Biotechnol. 6, 87–102.

Wittmann, C., Kiefer, P., Zelder, O., 2004. Metabolic fluxes in *Corynebacterium glutamicum* during lysine production with sucrose as carbon source. Appl. Environ. Microbiol. 70, 7277–7287.

Yamaoka, M., Osawa, S., Morinaga, T., Takenaka, S., Yoshida, K., 2011. A cell factory of *Bacillus subtilis* engineered for the simple bioconversion of *myo*-inositol to *scyllo*-inositol, a potential therapeutic agent for Alzheimer's disease. Microb. Cell Factories 10.

Supplementary information

Metabolic engineering of *Corynebacterium glutamicum* for production of *scyllo*-inositol, a drug candidate against Alzheimer's disease

Paul Ramp, Alexander Lehnert, Susanna Matamouros, Astrid Wirtz, Meike Baumgart, Michael Bott[#]

IBG-1: Biotechnology, Institute of Bio- and Geosciences, Forschungszentrum Jülich, Jülich, Germany

[#]Corresponding author: m.bott@fz-juelich.de

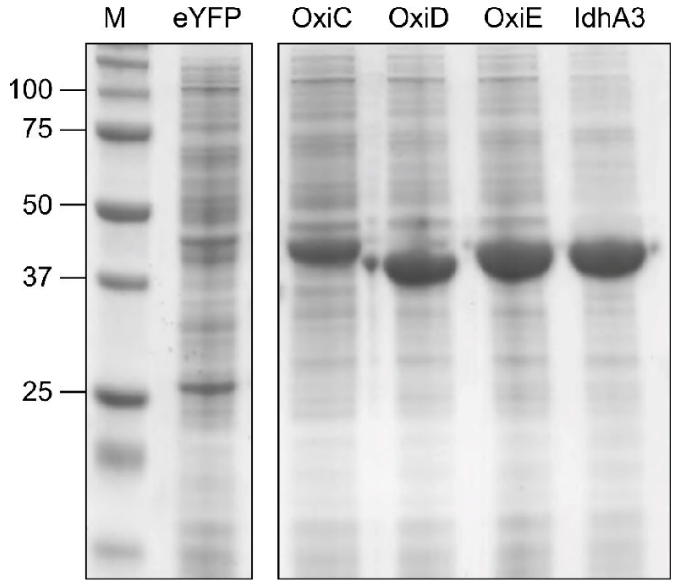

Fig. S1. Coomassie-stained SDS-polyacrylamide gel showing the overproduction of the *C. glutamicum* proteins OxiC (Cg3389, 39.58 kDa), OxiD (Cg3391, 36.23 kDa), OxiE (Cg3392, 38.03 kDa) and IdhA3 (Cg2313, 35.21 kDa). The proteins were overexpressed with the vector pMKEx2 in the *C. glutamicum* strain MB001(DE3)Δ*iol1*Δ*iol2* as described in the Methods section. Cell-free extracts of the different strains were prepared and 10 µg protein were separated by SDS-PAGE. M, marker proteins with molecular masses indicated in kDa.

2.2 Physiological, biochemical, and structural bioinformatics analysis of the multiple inositol dehydrogenases from *Corynebacterium glutamicum*

Ramp, P., Pfleger C., Dittrich J., Mack, C., Gohlke, H., Bott, M. (2022). – accepted in Microbiology Spectrum, August 24, 2022

Author contributions

PR: Conceptualization, Methodology, Investigation, Writing – Initial Draft, Visualization, Funding acquisition

CP: Methodology, Investigation, Writing – Manuscript, Visualization,

JD: Methodology, Investigation, Writing – Manuscript, Visualization, Funding acquisition

CM: Methodology, Investigation,

HG: Supervision, Writing – review & editing, Funding acquisition

MB: Conceptualization, Supervision, Writing – review & editing, Funding acquisition

Overall contribution: 40%

AMERICAN SOCIETY FOR MICROBIOLOGY | Microbiology Spectrum

RESEARCH ARTICLE

Physiological, Biochemical, and Structural Bioinformatic Analysis of the Multiple Inositol Dehydrogenases from *Corynebacterium glutamicum*

Paul Ramp,[a,b] Christopher Pfleger,[c] Jonas Dittrich,[b,c] Christina Mack,[a] Holger Gohlke,[b,c,d,e,f,g] Michael Bott[a,b]

[a]IBG-1: Biotechnology, Institute of Bio- and Geosciences, Forschungszentrum Jülich, Jülich, Germany
[b]The Bioeconomy Science Center (BioSC), Forschungszentrum Jülich, Jülich, Germany
[c]Institut für Pharmazeutische und Medizinische Chemie, Heinrich-Heine-Universität Düsseldorf, Düsseldorf, Germany
[d]John von Neumann Institute for Computing (NIC), Forschungszentrum Jülich GmbH, Jülich, Germany
[e]Jülich Supercomputing Centre (JSC), Forschungszentrum Jülich GmbH, Jülich, Germany
[f]Institute of Biological Information Processing (IBI-7: Structural Biochemistry), Forschungszentrum Jülich GmbH, Jülich, Germany
[g]Institute of Bio- and Geosciences (IBG-4: Bioinformatics), Forschungszentrum Jülich GmbH, Jülich, Germany

ABSTRACT Inositols (cyclohexanehexols) comprise nine isomeric cyclic sugar alcohols, several of which occur in all domains of life with various functions. Many bacteria can utilize inositols as carbon and energy sources via a specific pathway involving inositol dehydrogenases (IDHs) as the first step of catabolism. The microbial cell factory *Corynebacterium glutamicum* can grow with *myo*-inositol as a sole carbon source. Interestingly, this species encodes seven potential IDHs, raising the question of the reason for this multiplicity. We therefore investigated the seven IDHs to determine their function, activity, and selectivity toward the biologically most important isomers *myo*-, *scyllo*-, and D-*chiro*-inositol. We created an ΔIDH strain lacking all seven IDH genes, which could not grow on the three inositols. *scyllo*- and D-*chiro*-inositol were identified as novel growth substrates of *C. glutamicum*. Complementation experiments showed that only four of the seven IDHs (IolG, OxiB, OxiD, and OxiE) enabled growth of the ΔIDH strain on two of the three inositols. The kinetics of the four purified enzymes agreed with the complementation results. IolG and OxiD are NAD^+-dependent IDHs accepting *myo*- and D-*chiro*-inositol but not *scyllo*-inositol. OxiB is an NAD^+-dependent *myo*-IDH with a weak activity also for *scyllo*-inositol but not for D-*chiro*-inositol. OxiE on the other hand is an NAD^+-dependent *scyllo*-IDH showing also good activity for *myo*-inositol and a very weak activity for D-*chiro*-inositol. Structural models, molecular docking experiments, and sequence alignments enabled the identification of the substrate binding sites of the active IDHs and of residues allowing predictions on the substrate specificity.

IMPORTANCE *myo*-, *scyllo*-, and D-*chiro*-inositol are C_6 cyclic sugar alcohols with various biological functions, which also serve as carbon sources for microbes. Inositol catabolism starts with an oxidation to keto-inositols catalyzed by inositol dehydrogenases (IDHs). The soil bacterium *C. glutamicum* encodes seven potential IDHs. Using a combination of microbiological, biochemical, and modeling approaches, we analyzed the function of these enzymes and identified four IDHs involved in the catabolism of inositols. They possess distinct substrate preferences for the three isomers, and modeling and sequence alignments allowed the identification of residues important for substrate specificity. Our results expand the knowledge of bacterial inositol metabolism and provide an important basis for the rational development of producer strains for these valuable inositols, which show pharmacological activities against, e.g., Alzheimer's disease, polycystic ovarian syndrome, or type II diabetes.

Editor Amelia-Elena Rotaru, University of Southern Denmark

Address correspondence to Michael Bott, m.bott@fz-juelich.de, or Holger Gohlke, h.gohlke@fz-juelich.de.

The authors declare no conflict of interest.

Received 1 June 2022
Accepted 24 August 2022

KEYWORDS inositol metabolism, *myo*-inositol, *scyllo*-inositol, D-*chiro*-inositol, enzyme kinetics, structural models, molecular docking, *Corynebacterium glutamicum*, inositols, inositol dehydrogenase

Inositols (cyclohexanehexols) comprise a group of nine isomeric forms of C_6-sugar alcohols having a cyclic structure formed by the six carbon atoms, each linked to a hydroxyl group. Depending on the orientation of the hydroxyl groups, nine isomers are possible, termed *myo*-, *scyllo*-, *epi*-, *allo*-, *muco*-, *neo*-, D-*chiro*, L-*chiro*-, and *cis*-inositol, all of which except the last occur in nature (1, 2). *myo*-Inositol (MI) is the predominant isomer used in biology and occurs in all kingdoms of life (3). It is synthesized from glucose 6-phosphate, which is converted by inositol 1-phosphate synthase (Ino1) to *myo*-inositol 1-phosphate followed by dephosphorylation to MI by an inositol monophosphatase (4–6). The other naturally occurring isomers are known or assumed to be derived from MI via epimerization (7, 8).

Numerous biological functions have been identified for inositols. For example, MI-containing phospholipids are constituents of the membranes of many archaea and all eukaryotes (3). Also, *scyllo*-inositol (SI) and D-*chiro*-inositol (DCI) were identified in lipids in some plant species (9, 10). Polyphosphorylated inositols ($IP_{1–3}$) are key components of eukaryotic signaling pathways (3, 11), and MI hexakisphosphate (IP_6), also known as phytic acid, is an abundant plant constituent serving as the main storage form of phosphate in seeds (12). In the bacterial kingdom, inositols play a prominent role, particularly in *Actinobacteria*. In this large phylum, MI is one of the precursors for the synthesis of mycothiol, a metabolite substituting for glutathione (13), and a precursor of phosphatidylinositol, an abundant phospholipid in the cytoplasmic membrane and the precursor of more complex lipids of the cell envelope such as phosphatidylinositol mannosides, lipomannan, and lipoarabinomannan (14).

Many bacteria are able to utilize MI as a carbon and energy source, such as *Klebsiella aerogenes* (15), *Rhizobium leguminosarum* (16), *Bacillus subtilis* (17, 18), *Sinorhizobium meliloti* (19, 20), *Paracoccus laeviglucosivorans* (21, 22), *Legionella pneumophila* (23), or *Thermotoga maritima* (24). After uptake via specific inositol transporters, MI is first oxidized by an inositol dehydrogenase (IDH) to yield the intermediate 2-keto-*myo*-inositol (2KMI), which is dehydrated to 3D-(3,5/4)-trihydroxycyclohexane-1,2-dione (THcHDO) by a 2KMI dehydratase (25, 26). This intermediate is converted in subsequent steps to dihydroxyacetone phosphate, acetyl coenzyme A (acetyl-CoA), and CO_2 (15). The genes encoding the responsible enzymes are organized in large operons (27–29), which are usually regulated by a repressor called IolR that dissociates from its operator and enables gene expression when it forms a complex with intermediates of MI catabolism (30, 31).

Corynebacterium glutamicum is a soil-dwelling Gram-positive actinobacterium that is used as an industrial cell factory, in particular for large-scale production of L-glutamate and L-lysine (32–34). It can grow with MI as the sole carbon source (35). During growth on MI, more than 20 genes showed increased expression, most of which were located in two clusters on the genome. Cluster *iol1* (Fig. 1) contains 16 genes, which include a putative operon comprising 10 genes (cg0197 to cg0207), including those for the seven enzymes assumed to be responsible for MI conversion to dihydroxyacetone, acetyl-CoA, and CO_2. Whereas many genes of cluster *iol1*, such as *iolD*, are essential for growth on MI, the genes of cluster *iol2* are dispensable (35). Two secondary transporters for MI uptake were identified in *C. glutamicum*, called IolT1 and IolT2 (35). In the absence of MI, expression of the genes involved in MI transport and degradation was shown to be repressed by the GntR-type transcriptional regulator IolR (36). *C. glutamicum* not only is able to degrade MI but also has the intrinsic capability to synthesize MI via MI phosphate synthase (Ino1, Cg3323) and MI phosphate monophosphatase (ImpA, Cg2298) (37). Expression of the *ino1* gene is activated by the LacI-type transcriptional regulator IpsA in response to the cytoplasmic MI concentration. When sufficient MI is present, it binds to IpsA and abolishes activation of *ino1* expression (38).

In many inositol-degrading bacteria, multiple paralogous genes annotated or shown

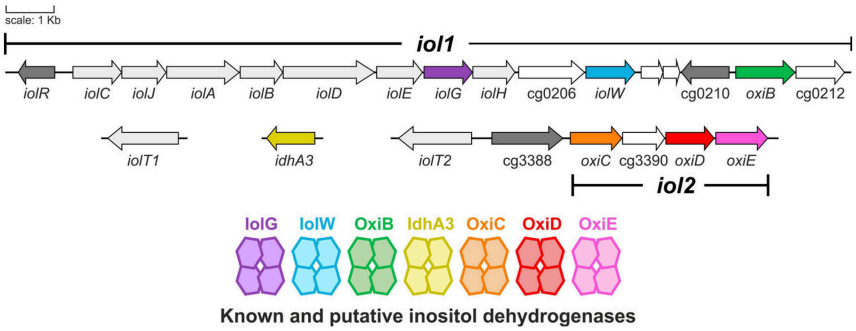

FIG 1 Organization of *C. glutamicum* genes involved in inositol transport and metabolism with the seven different IDH genes highlighted in color. The gene clusters *iol1* and *iol2* comprising genes involved in inositol metabolism are indicated.

to encode IDHs were identified (39–41), which, in the case of *B. subtilis*, for example, enable growth not only on MI but also on SI and DCI (42, 43). In *C. glutamicum*, seven potential inositol oxidoreductases were annotated, three in cluster *iol1* (IolG, IolW, and OxiB), three in cluster *iol2* (OxiC, OxiD, and OxiE), and another one elsewhere in the genome (IdhA3) (Fig. 1). This work aimed at a detailed characterization of the IDHs of *C. glutamicum*. Using a ΔIDH strain lacking the genes for all seven potential IDHs as a host for overexpression of the seven genes individually, we could show that four of the seven IDHs enable growth with MI, SI, or DCI (see Fig. S1 in the supplemental material) as the sole carbon and energy source. Biochemical characterization of the four purified enzymes revealed different activity profiles for the tested inositol isomers. We used structural modeling and molecular docking to elucidate the molecular basis responsible for the various substrate specificities of the four enzymes that may be helpful in predicting the substrate specificity of yet-uncharacterized inositol dehydrogenases in other organisms.

RESULTS

Growth on different inositols. *C. glutamicum* can grow in minimal medium with MI as the sole carbon and energy source (35). The IDH IolG was shown to be important for growth on MI, as inactivation of *iolG* led to a reduced growth rate. Additional deletion of the gene cluster comprising *oxiC*-cg3390-*oxiD*-*oxiE* abolished the growth on MI, suggesting redundant MI dehydrogenase activities in *C. glutamicum* (35). To determine the potential of *C. glutamicum* to utilize further inositols besides MI for growth, we cultivated *C. glutamicum* MB001(DE3) in CGXII medium with either glucose, MI, SI, or DCI as the sole carbon and energy source using a BioLector microcultivation system. Growth was monitored by measuring backscatter at 620 nm over a time period of 48 h. This experiment showed that *C. glutamicum* is able to grow not only with MI but also with DCI and SI (Fig. 2A). The growth rate (μ) on MI (0.42 h^{-1}) and DCI (0.42 h^{-1}) was comparable to that on glucose (0.46 h^{-1}), while the growth rate on SI was lower (0.26 h^{-1}).

C. glutamicum possesses the two inositol transporters IolT1 and IolT2, both contributing to the uptake of MI (35). To test if DCI and SI enter the cells the same way, we analyzed the growth of the Δ*iolT1*, Δ*iolT2*, and Δ*iolT1*Δ*iolT2* transporter deletion mutant strains on glucose, MI, SI, and DCI. Indeed, both transporters contributed to the uptake of all tested inositols (Fig. 2B to D). With MI as the carbon source, the Δ*iolT1* and Δ*iolT2* strains showed comparable growth rates (0.42 h^{-1}). In the case of DCI and SI, the Δ*iolT1* strain grew slightly slower (DCI, 0.38 h^{-1}; SI, 0.24 h^{-1}) than the Δ*iolT2* strain (DCI, 0.41 h^{-1}; SI, 0.26 h^{-1}), suggesting that IolT1 has a higher activity for DCI and SI uptake than IolT2 (Fig. 2B and C). Deletion of both *iolT1* and *iolT2* abolished growth on each of the three inositols completely (Fig. 2D), indicating that *C. glutamicum* does not possess an additional transporter for the uptake of inositols.

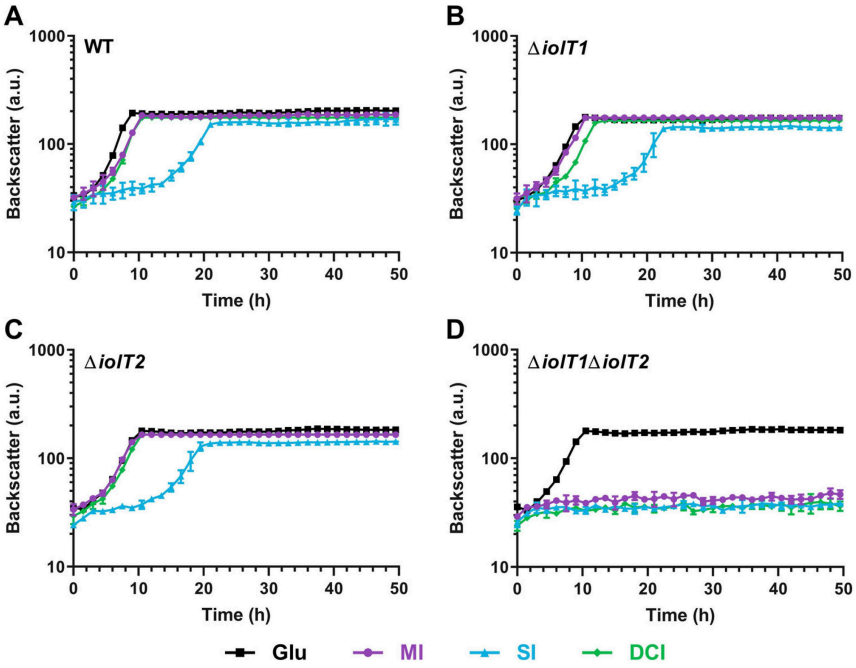

FIG 2 Growth of the *C. glutamicum* strains MB001(DE3) (A), ATCC 13032 Δ*iolT1* (B), ATCC 13032 Δ*iolT2* (C), and ATCC 13032 Δ*iolT1*Δ*iolT2* (D) on different inositols compared to glucose. The strains were cultivated in a BioLector system using CGXII minimal medium supplemented with glucose, MI, SI, or DCI at 10 g/L. The cultures were incubated for 48 h at 30°C, 1,200 rpm, and 85% humidity. Mean values and standard deviations for three biological replicates are shown. a.u., arbitrary units.

As an efficient approach for investigating the role of the seven annotated IDHs of *C. glutamicum* for growth on MI, SI, and DCI, we constructed the *C. glutamicum* ΔIDH strain, in which all seven IDH genes and the putative sugar phosphate isomerase gene cg3390, which is part of the *oxiC*-cg3390-*oxiD*-*oxiE* operon, were deleted (Fig. 1). *C. glutamicum* ΔIDH was transformed with pMKEx2-based expression plasmids encoding one of the seven IDHs and tested for growth on the different inositols. The successful synthesis of the individual IDH proteins was confirmed by SDS-PAGE (Fig. S2). As controls, the parent strain *C. glutamicum* MB001(DE3) and the ΔIDH strain were transformed with pMKEx2-*eyfp*. Target gene expression was induced by adding 20 μM isopropyl-β-D-thiogalactopyranoside (IPTG) to the second, overnight preculture and the main culture to enable an immediate start of growth.

In contrast to strain MB001(DE3)(pMKEx2-*eyfp*), the ΔIDH(pMKEx2-*eyfp*) strain was unable to grow on MI, SI, and DCI, confirming that this mutant is suitable to test the functionality of the different IDHs. Growth of the ΔIDH strain on MI comparable to that of the positive control was obtained by expressing either *iolG* or *oxiD* (Fig. 3). Expression of *oxiB* and *oxiE* also enabled growth on MI but at lower growth rates of 0.24 h^{-1} and 0.11 h^{-1}, respectively. Expression of *iolW*, *oxiC*, and *idhA* did not restore growth on MI and showed the same profile as the negative control expressing *eyfp*.

Similar to the growth with MI, the growth of the ΔIDH strain with DCI was made possible by the expression of either *iolG* or *oxiD* (Fig. 3) and enabled the same growth rate (0.45 h^{-1}) as that of the positive-control strain. In contrast to growth with MI, no growth on DCI was observed for the ΔIDH strain expressing *oxiB* or *oxiE*. Growth of the ΔIDH strain on SI was enabled only by expressing *oxiE* or *oxiB* (Fig. 3). Plasmid-based expression of *oxiE*, even at low induction levels, enabled faster growth (0.40 h^{-1}) than that of the positive-control strain (0.26 h^{-1}), indicating that native *oxiE* expression

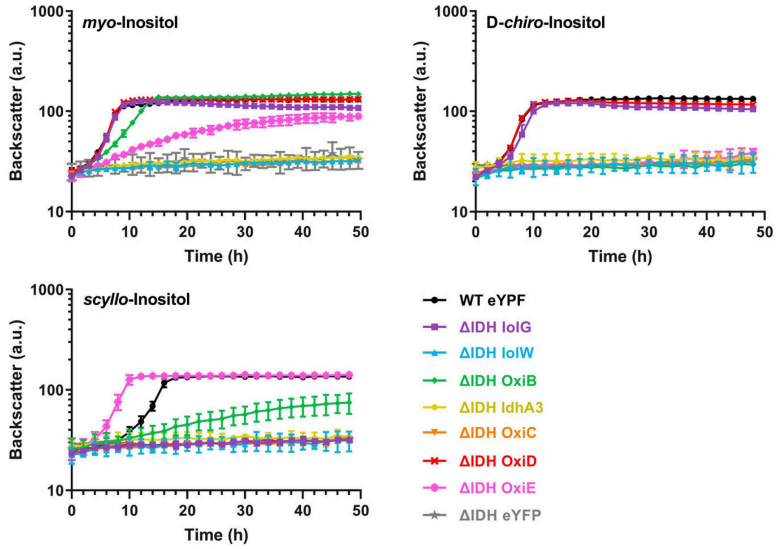

FIG 3 Growth on MI, SI, and DCI of *C. glutamicum* ΔIDH expressing one of the seven IDH genes or as negative-control enhanced yellow fluorescent protein (*eyfp*) using the corresponding pMKEx2-based plasmids. *C. glutamicum* MB001(DE3) transformed with pMKEx2-*eyfp* was used as a positive control. The strains were cultivated in a BioLector cultivation system for 48 h at 30°C, 1,200 rpm, and 85% humidity in CGXII minimal medium supplemented with 10 g/L of MI, DCI, SI, or glucose. Mean values and standard deviations for three biological replicates are shown. a.u., arbitrary units.

limited growth on SI. The expression of *oxiB* led to slower growth on SI (0.09 h^{-1}) and a lower final backscatter after 48 h of cultivation.

The results of the growth experiments suggest that IolG and OxiD function as efficient MI and DCI dehydrogenases. OxiB and OxiE also possess MI dehydrogenase activity but apparently not DCI dehydrogenase activity. OxiE probably has a high SI dehydrogenase activity, whereas OxiB has a weak activity for SI.

Kinetic properties of the enzymes IolG, OxiD, OxiE, and OxiB. To confirm the conclusions derived from the growth experiments, we biochemically characterized those IDHs that enabled growth on the tested inositols, i.e., IolG, OxiD, OxiB, and OxiE. The enzymes were overproduced with a C-terminal Strep-tag II in *C. glutamicum* MB001(DE3) using the newly constructed pPREx6 vector. It enables the direct fusion of the target protein to a C-terminal Strep-tag II and strong inducible overexpression under the control of the T7 promoter. Enzymes were purified via StrepTactin Sepharose affinity chromatography followed by size exclusion chromatography. The purity of the proteins was confirmed by SDS-PAGE and Coomassie blue staining (Fig. S3).

The purified proteins were used for enzyme activity measurements via spectrophotometric assays measuring the decrease in absorbance of NADH at 340 nm with MI, SI, and DCI as the substrates. The results of these experiments agreed with the conclusions derived from the growth experiments and revealed clear differences in substrate preferences and activities (Table 1 and Fig. S4). IolG and OxiD both accept MI and DCI as the substrates with a preference for MI. OxiD showed a 2.5-times-higher turnover number for MI than IolG. Also, the K_m of OxiD for MI was 3 times lower than that of IolG. OxiB showed activity for MI and SI but not for DCI. The specific activity of OxiB for MI was 4 times lower than that of IolG and 10 times lower than that of OxiD, corresponding to the slower growth of the ΔIDH(pMKEx2-OxiB) strain on MI (Fig. 3). The K_m values of OxiB for MI and SI were similar and comparable to the K_m values of IolG for MI. OxiE was the only IDH that showed activity for all three tested inositols with the highest activity and lowest K_m for SI. The activity for DCI was more than 1,000-fold

TABLE 1 Role of the indicated IDHs for growth on MI, DCI, and SI and kinetic constants for oxidation of MI, DCI, and SI by purified IolG, OxiB, OxiD, and OxiE

Enzyme	Substrate	Growth[a]	V_{max} (μmol min^{-1} mg^{-1})	K_m (mM)	k_{cat} (s^{-1})	k_{cat}/K_m (M^{-1} s^{-1})
IolG	*myo*-Inositol	+++	23.1 ± 3.2	60.9 ± 13.7	14.0 ± 1.9	235.1 ± 23.4
	D-*chiro*-Inositol	+++	14.3 ± 0. 9	61.93 ± 5.61	8.66 ± 0.54	140.39 ± 7.4
	scyllo-Inositol	−	ND[b]			
OxiD	*myo*-Inositol	+++	59.0 ± 2.3	19.6 ± 1.8	35.6 ± 1.4	1,831.8 ± 107.4
	D-*chiro*-Inositol	+++	25.5 ± 2.7	50.6 ± 8.7	15.4 ± 1.7	307.6 ± 20.0
	scyllo-Inositol	−	ND			
OxiB	*myo*-Inositol	++	5.8 ± 0.5	62.1 ± 12.5	4.2 ± 0.4	69.1 ± 7.3
	D-*chiro*-Inositol	−	ND			
	scyllo-Inositol	+	0.05 ± 0.01	28.8 ± 7.1	0.03 ± 0.00	1.03 ± 0.11
OxiE	*myo*-Inositol	+	3.1 ± 0.2	51.6 ± 3.6	3.9 ± 0.3	76.7 ± 5.2
	D-*chiro*-Inositol	−	0.005 ± 0.001	54.1 ± 8.0	0.003 ± 0.00	0.06 ± 0.00
	scyllo-Inositol	+++	13.4 ± 0.1	12.4 ± 0.8	8.5 ± 0.1	688.6 ± 41.5

[a]Growth of ΔIDH strain expressing the genes encoding the indicated IDHs, with +++ indicating very good growth and − indicating no growth.
[b]ND, no detectable activity.

lower than that for MI and SI. This low activity was apparently not sufficient to enable the growth of the ΔIDH(pMKEx2-OxiE) strain on DCI.

Analysis of the *C. glutamicum* IDHs by sequence alignments. Explanations for the substrate specificity of different IDHs are scarce. Previous studies dealt with the structure elucidation of IDHs in complex with inositols to understand the interactions between the enzyme, the substrate, and the cofactor. For OxiD of *C. glutamicum*, a crystal structure (PDB ID 3EUW) with a resolution of 2.3 Å has been deposited in the Protein Data Bank (PDB) (44, 45) but without a bound cofactor or a substrate. The structure of IolG of *B. subtilis* complexed with NAD^+ and MI enabled the identification of important residues for cofactor and substrate binding. Structure-based sequence alignments led to the definition of six conserved sequence motifs (46). Motifs I and II contain amino acid residues that are important for cofactor binding, whereas motifs III to VI contain residues responsible for substrate binding and the catalytic triad consisting of Lys97, Asp172, and His176 (BsIolG numbering).

We compared the amino acid sequences of all seven annotated IDHs of *C. glutamicum* with the sequences of the biochemically characterized inositol dehydrogenases reported in the literature (Table S1) and sorted them into four groups (Fig. S5): (i) NAD^+-dependent IDHs known to have activity for MI and DCI, (ii) NAD^+-dependent IDHs known to have activity for MI and SI, (iii) $NADP^+$-dependent IDHs catalyzing the reduction of 2KMI to SI, and (iv) IDHs with no activity for any tested inositol. In our comparison, we focused on the previously reported motifs to identify differences in functionally important residues within motifs I to VI. In group i, which includes CgIolG and CgOxiD, the sequences G_{124}FM/NRRY/FD_{130} in motif III and $Y_{233}GY_{235}$ in motif V (BsIolG numbering) seem to be more conserved than in the other groups. $F_{125}M/N_{126}R_{127}$ and Y235 were reported as substrate binding sites for BsIolG. In group ii, the sequence G_{124}FM/NRRY/FD_{130} can also be found in some cases; however, the $Y_{233}GY_{235}$ sequence does not occur in any representative. In most cases, the second Tyr residue is replaced by a positively charged amino acid (H>R>K). As shown below, this residue is involved in substrate binding and, therefore, can serve as a marker to discriminate between IDHs specific for SI and DCI, although exceptions are possible (Fig. 4).

We previously identified IolW as an $NADP^+$-dependent *scyllo*-IDH that catalyzes the reduction of 2KMI to SI (47) and therefore assigned it to group iii. At position 35, IolW contains an Ala residue, while most other IDHs contain an Asp or Glu residue. Asp or Glu residues at this position are conserved in NAD^+-dependent IDHs, in which they form hydrogen bonds with the ribose moiety of NAD^+. $NADP^+$-dependent enzymes typically replace Asp or Glu with a small, neutral residue, as the negatively charged carboxylate of Asp or Glu would effectively repel the phosphate group in this position. Often, a basic residue follows the small neutral residue, like Arg36 in IolW, which can

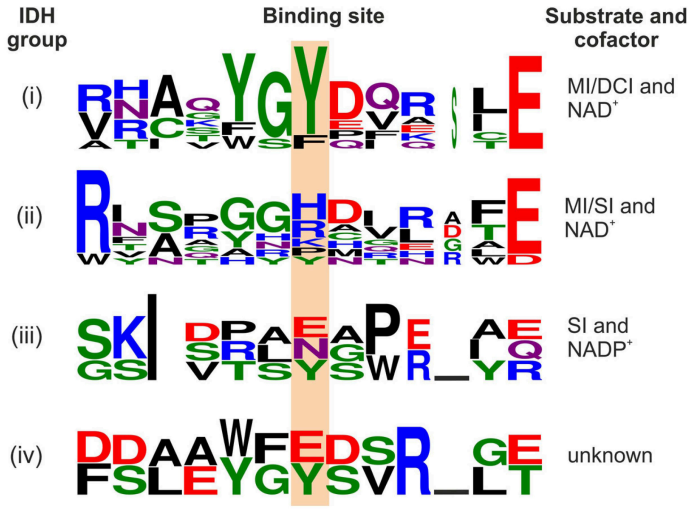

FIG 4 Consensus sequences for motif V of the four IDH subgroups with the substrate binding site highlighted. Letter height is proportional to the relative abundance of that residue at each position, and letter width is proportional to the fraction of valid symbols at that position. Letter color corresponds to the chemical properties of the amino acid (black, hydrophobic; red, acidic; blue, basic; green, polar; purple, carboxamides). The figure was generated using WebLogo 3 (WebLogo 3 - About [https://threeplusone.com]).

interact with the 2′-phosphate group of NADPH (48–50). Also, BsIolW and BsIolU, both of which have been characterized as NADPH-dependent KMI reductases, possess a Ser or Thr residue rather than Asp or Glu at position 35 (BsIolG numbering) (51). This difference between NAD^+- and $NADP^+$-dependent IDHs suggests that IolW is the only IDH of *C. glutamicum* favoring NADPH as a cofactor.

Among all analyzed IDHs, the motifs of CgOxiC differ the most from the published ones (Fig. S5). It is the only protein within the annotated IDHs of *C. glutamicum* that does not contain a complete GxGxxG consensus sequence in motif I. Additionally, instead of Asp179, a residue of the catalytic triad, OxiC contains an Ile residue. The lack of Asp179 suggests that OxiC is not active as an IDH, which is supported by the fact that expression of *oxiC* did not enable the growth of the ΔIDH strain on MI, DCI, or SI (Fig. 3). IdhA3 also differs at the corresponding position 172, as it contains a Glu residue instead of Asp, similar to the *myo*-IDH Gk1899, for which activity toward MI was reported previously (40). Despite being a conservative exchange, the difference in size might prevent IDH activity of IdhA3. As in the case of OxiC, the expression of *idhA3* did not allow growth of the ΔIDH strain on MI, DCI, or SI (Fig. 3). We constructed an IdhA3 variant in which we replaced Glu172 by Asp. However, the expression of *idhA3*-E172D also did not allow growth of *C. glutamicum* ΔIDH on MI, DCI, or SI (data not shown).

Structural models of *C. glutamicum* IDHs and inositol docking. Amino acid sequence comparisons of IDHs allow the prediction of cofactors and potential substrates when looking at highly conserved motifs. However, structural models and docking experiments are required to further understand inositol preferences and binding mechanisms. To this end, we generated structural models with their corresponding cofactor of the IDHs IolG, OxiB, OxiC, OxiD, OxiE, and IdhA3 (Table S2). All structures show an intermediate to good global model quality (Table S2) and good local model quality near the inositol binding sites (Fig. S6), with regions of lower quality located mainly in the loops and the central tetrameric interface.

The models served as input for docking experiments using AutoDock3 (52) in combination with DrugScore^{2018} (53) to probe the potential interaction between MI, SI, or DCI and the catalytic site of each IDH. To test if a docked solution likely adopts a favorable position in the catalytic site, we measured the distance *d* between the C-2 atom in MI, the C-1 or C-6 atom in DCI, or any C atom in SI and the C-4 atom of the nicotinamide

group from the NAD^+ cofactor. As the orientation of the reactive carbon atoms toward the cofactor and the distance between these atoms is crucial for the reaction to take place, we considered a binding pose valid only if *d* was ≤ 5 Å. For validation of the docking approach, we performed redocking experiments using the X-ray structures of *Lactobacillus casei* IDH1 (PDB ID 4MIO) and *L. casei* IDH2 (PDB ID 4N54) in complex with MI and SI, respectively. All dockings converged perfectly, and the poses show root mean square deviation (RMSD) values of <2.0 Å to the respective bound MI and SI in the X-ray structures (Fig. S7A and B). Furthermore, the docked solutions of the inositols showed *d* of <5 Å for both IDHs (Fig. S7C and D), even if the docked MI poses are slightly rotated in a counterclockwise manner.

Of the systems investigated here, the two dehydrogenases, OxiC and IdhA3, served as negative controls as both show no activity for either MI or SI (47). The two IDHs differ markedly in the structure of the entrance region to the catalytic site. In OxiC, the presence of the α-helix V159 to Q169 narrows the catalytic site's accessibility, thus hampering the interaction of the inositols and the enzyme (Fig. 5A). This helical element is missing in IolG, OxiD, OxiE, and IdhA3. The last shows an open catalytic site (Fig. 5B). In OxiB, an extended loop region is located at the same position as the helix in OxiC. However, the loop does not narrow the entrance to the catalytic site.

We obtained converged docking results for all combinations of these IDHs and the investigated inositols, indicating that the docking method finds a single most favorable binding pose for each inositol, except for the combinations of IdhA3 with MI and of OxiE with DCI, where two binding poses were found (Table S3). All docked solutions of the inositols in OxiC showed distances *d* >5 Å (Fig. 5C), since helix V159 to Q169 blocks the catalytic site. Despite the accessible catalytic site in IdhA3, we also observed no valid docking pose ($d > 5$ Å). This finding is remarkable as both IDHs showed no activity for MI or SI in previous experiments (47) and also could not recover growth of *C. glutamicum* ΔIDH on any tested inositol.

In the case of OxiE, valid docking poses were found for MI ($d = 4.4$ Å) and SI ($d = 5.0$ Å), which agrees with the activity data from experiments (Fig. 5C). Furthermore, the hydroxyl groups of docked inositol poses of MI and SI form interactions with the charged amino acids R13, K101, R130, D160, D178, H182, and H243 (Fig. 5D and E). Interestingly, we observed a slight incline of the docked MI compared to the SI orientation, which, though less pronounced, agrees with results reported previously for *L. casei* IDH1 (39). The docking with OxiE failed to generate valid docking poses for DCI, although purified OxiE showed very weak activity for DCI (Table 1), which was insufficient to enable growth on DCI.

For OxiD, we observed valid docking poses for MI ($d = 3.9$ Å) but not for SI ($d = 9.7$ Å), which agrees with the enzymatic activity data (Fig. 5C and Fig. S8). Here, the computed pose of MI interacts with the charged amino acids K94, D153, and H175 and the hydroxyl groups Y235 and Y280 (Fig. 5F and G). Compared to the orientation of the docked MI in OxiE, the incline is more pronounced in OxiD and similar to the orientation reported before for *L. casei* IDH1 (39). Surprisingly, for OxiD no valid docking pose was found for DCI (Fig. 5C), even though purified OxiD shows high activity for DCI as the substrate (Table 1).

For IolG, our docking results agree with the enzyme activity data (Fig. 5C). Here, MI and DCI produced valid docking poses ($d = 4.5$ Å for both inositols), whereas for SI no valid docking pose was found ($d = 5.7$ Å) (Fig. S8). Nevertheless, MI, SI, and DCI show the same interactions in our docking experiments with the amino acids H155, H176, S173, and Y235 (Fig. S9). The larger distance between SI and the cofactor is due to a wrong orientation of the inositol that shows an incline similar to that observed for MI. Finally, SI is located further away from the cofactor than MI and DCI.

In the case of OxiB, the predicted binding poses agree only for SI with the enzyme activity data (Fig. 5C). For SI, we observed a valid docking pose with a distance *d* of 3.8 Å (Fig. S8). The positions of all docked inositols are strongly overlapping, thus interacting with the same amino acids Y138, Y166, D193, H197, and N278 (Fig. S9). The

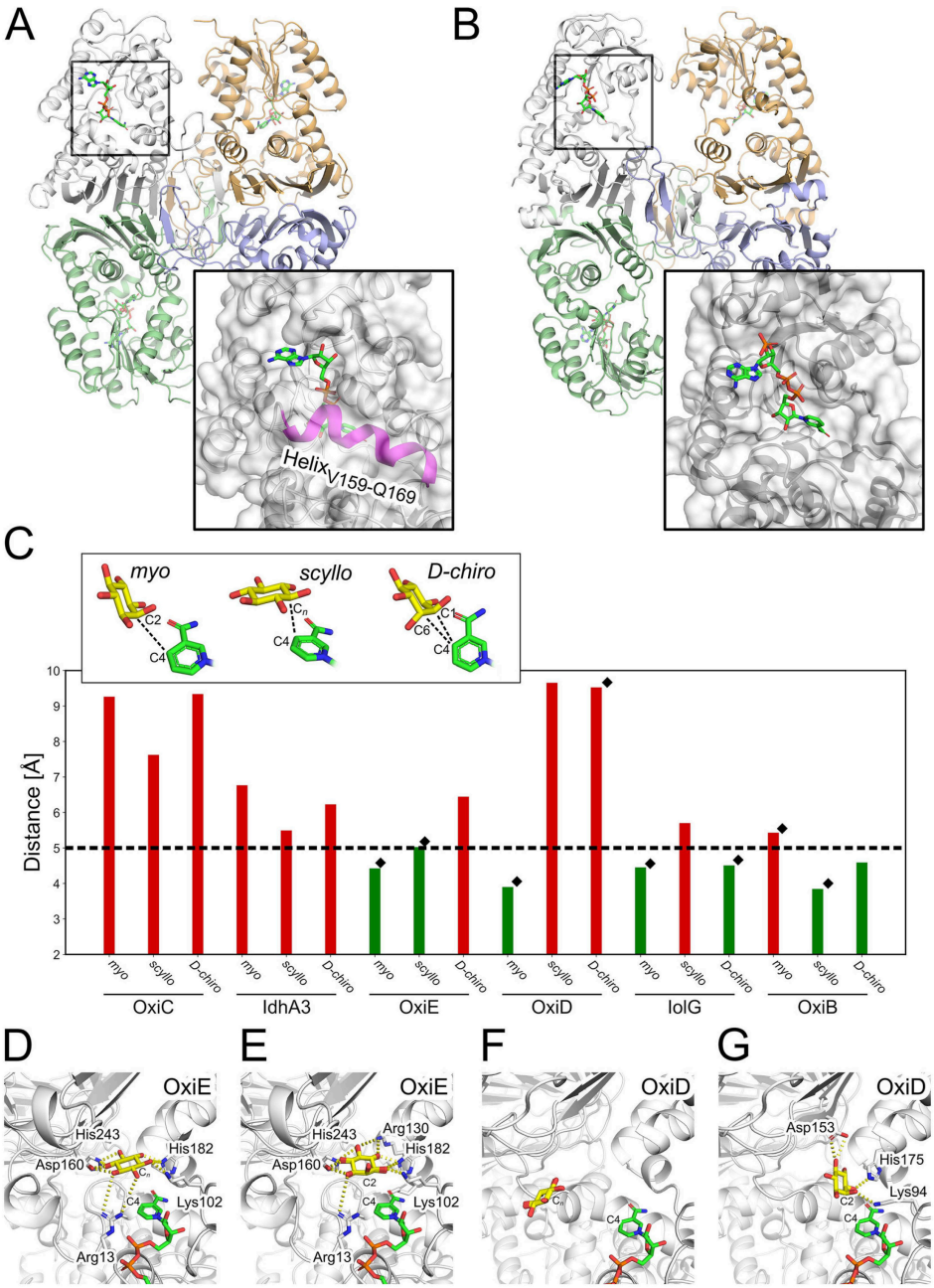

FIG 5 Docking results for *myo*-, *scyllo*-, and D-*chiro*-inositol into structural models of *C. glutamicum* IDHs. (A and B) Structural comparison between IdhA3 (A) and OxiC (B) shows an α-helix (magenta) blocking the entrance to the catalytic site of OxiC. Compared to active IDHs, the catalytic site in IdhA3 is more exposed. (C) Distances were measured for the docked inositol poses between the reactive carbon atom from each inositol and the C-4 atom of the cofactor nicotinamide group; black diamonds depict those inositols that result in growth. The horizontal dashed line indicates the threshold for considering a valid docking pose. The bar color depicts whether the distance is within the threshold (green) or outside (red). (D to G) Comparison of the docked solutions for MI and SI into OxiE and OxiD.

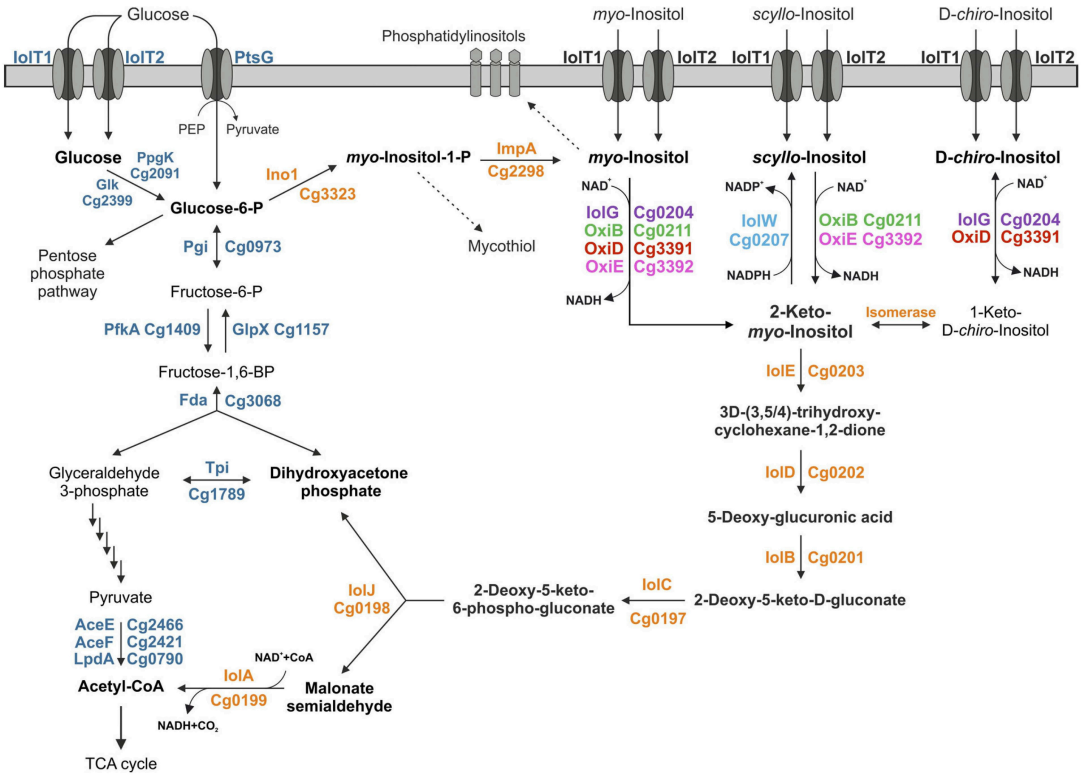

FIG 6 Schematic overview of *myo*-, *scyllo*-, and D-*chiro*-inositol catabolism in *C. glutamicum*. Reactions leading to cell constituents requiring L-*myo*-inositol-1-phosphate or *myo*-inositol for synthesis are indicated with dashed arrows. TCA, tricarboxylic acid.

larger distance between MI and the cofactor results from the misplaced C-2 atom of the inositol. Here, the C-2 atom points away from the cofactor and reveals a parallel orientation of the carbocyclic ring and the nicotinamide group of the cofactor. In the case of DCI, the C-1/C-6 atoms are oriented toward the cofactor and show a slight incline, suggesting an optimal interaction between DCI and the cofactor. Here, the docking result deviates from the enzyme activity data, as OxiB showed no activity with DCI as the substrate (Table 1). Overall, we were able to identify valid binding poses for MI, SI, and DCI in six IDHs in 15 out of 18 docking experiments.

DISCUSSION

The genome of *C. glutamicum* harbors seven genes that potentially encode IDHs. In this study, we characterized the physiological functions and biochemical properties of these IDHs and employed bioinformatics and molecular modeling to obtain more detailed information on their structural differences and substrate preferences. Our initial growth experiments with the strain MB001(DE3) derived from *C. glutamicum* ATCC 13032 revealed that it can grow not only with MI but also with SI and DCI as sole carbon and energy sources. In Fig. 6, we present an overview of our current knowledge of the inositol metabolism in *C. glutamicum*. We showed that both inositol transporters, IolT1 and IolT2, catalyze the uptake not only of MI but also of DCI and SI, which further underlines the fact that these transporters have a broad substrate specificity including not only inositols but also glucose, fructose, and xylose (54–57). According to the observed growth rates, IolT1 seems to have a higher activity for DCI and SI uptake than IolT2, while the two transporters are comparably effective with respect to MI uptake (35). Studies on the three inositol transporters of *B. subtilis* showed that they exhibit different preferences for different inositols (58).

By creating the ΔIDH strain of *C. glutamicum*, which lacks all seven known or putative IDH genes, we were able to test the role of each of the IDHs individually for their ability to enable growth on MI, SI, and DCI. The experiments showed that, besides IolG, also OxiD allows for fast growth on MI. OxiB and OxiE also enabled growth on MI but at a much lower rate. These results agree with the kinetic properties of the purified enzymes with MI as the substrate: IolG and OxiD showed V_{max} values about 5- to 10-fold-higher than those of OxiB and OxiE (Table 1). Growth on DCI was possible only with IolG and OxiD, and the kinetic properties confirmed a high activity of these enzymes with DCI as the substrate. OxiE showed superior growth and faster kinetics for SI than for MI, suggesting that this enzyme primarily functions as a *scyllo*-IDH. OxiB also allowed growth on SI but at a much lower rate. The kinetic properties of OxiE and OxiB for SI were in agreement with the growth data (Table 1). The observation that the IDHs possess activity for more than one inositol isomer has also been reported for IDHs of other bacteria. They are often classified either as *myo*-IDH with the highest activity for MI and lower activity for DCI or as *scyllo*-IDH with a preference for SI and lower activity for MI (21, 22, 39). OxiB is unusual in that it shows activity for SI and MI but has a strong preference for MI.

Expression of *iolW*, *oxiC*, and *idhA3* did not allow growth of the ΔIDH strain on MI, DCI, or SI, indicating that these proteins do not possess the required enzymatic activities. For IolW, this result was expected as our previous studies showed that this enzyme catalyzes the NADPH-dependent reduction of 2KMI to SI (47). In the case of OxiC, several reasons for the lack of enzymatic activity were identified. OxiC lacks the Asp179 residue, which is part of the catalytic triad, and contains an incomplete GxGxxG motif. Furthermore, the structural model shows that the substrate binding site of OxiC is blocked by an α-helix (Fig. 5A). Also, the docking experiments revealed no valid binding poses for the tested inositols. Therefore, all evidence argues against an enzymatic activity of OxiC as an IDH, and the function of this protein remains unknown. In the case of IdhA3, the Asp172 residue of the catalytic triad is replaced by a Glu residue and the exchange of the Glu residue with Asp did not enable growth on MI, SI, or DCI (data not shown). The structural model of IdhA3 shows that the catalytic site is more exposed than the binding pockets of active IDHs (Fig. 5B), and the docking experiments revealed no valid binding poses. As in the case of OxiC, the function of IdhA3 is currently unclear.

The structural models generated for the *C. glutamicum* IDHs in this study were used in blind docking experiments, which in 15 out of 18 cases were in good agreement with the experimental growth and kinetic data when the distance between the reactive carbon atom from each inositol and the C-4 atom of the cofactor's nicotinamide group was evaluated as a criterion for activity. Only for the pairs OxiD/DCI and OxiB/MI, we obtained false-negative and, for OxiB/DCI, false-positive docking solutions, which might be due to treating the protein and the cofactor as rigid. Using computationally more demanding investigations including molecular dynamics simulations may overcome these limitations.

Amino acid sequence alignments and the predicted interactions of the inositols with the residues of the binding pocket suggested that motif V plays a role in the selectivity of IDHs. In group i, in which IDHs use MI and DCI as the substrates, a YGY_{245} motif (BsIolG numbering) with Y245 serving as a substrate binding site is highly conserved, whereas this motif is absent in group ii, in which IDHs use MI or SI as the substrate and in group iii, in which IDHs serve as 2KMI reductases. In group ii, Y245 is exchanged mainly for a positively charged residue (H>R>K) and the model proposes H243 as a substrate interaction site in OxiE (Fig. 5D and E). Therefore, this position can be used to estimate the substrate preferences of IDHs (Fig. 4).

As several inositols were reported to show pharmacological activities against, e.g., Alzheimer's disease, polycystic ovarian syndrome, or type II diabetes (2), the biotechnological production of these sugar alcohols is of high interest and was shown, e.g., for SI production with *B. subtilis* (59) and *C. glutamicum* (47). These processes require the activity of IDHs for epimerization of MI to the desired inositol, and the knowledge of

biochemical properties of the IDHs is a prerequisite for the design of appropriate synthesis pathways and chassis strains preventing, for example, the reoxidation of the target inositol. The structural models enable rational engineering of the IDHs to change the substrate or cofactor selectivity, which can provide new synthetic routes for the interconversion of inositol isomers. Besides MI, DCI, and SI, also other inositols were reported to have pharmacological activities (2). Our strategy for analyzing the properties of IDHs can be employed to identify novel IDHs suitable for production of rare inositols.

Our study revealed the functions of four of the seven putative IDHs present in *C. glutamicum* (IolG, OxiD, OxiB, and OxiE), not including the 2KMI reductase IolW reported previously (47). The functions of OxiC and IdhA3 remain unknown, and especially, OxiC is unlikely to be an active IDH. The overlapping substrate specificities of several of the four active NAD^+-dependent IDHs might provide an advantage for scavenging inositols in the natural habitat. The oxidation product of MI and SI is 2KMI (or *scyllo*-inosose), which is subsequently converted by a 2KMI dehydratase (IolE) to 3D-(3,5/4)-trihydroxy-cyclohexane-1,2-dione (Fig. 6). The oxidation product of DCI, however, is 1-keto-D-*chiro*-inositol, which in *B. subtilis* is converted by the isomerase IolI to 2KMI (43). Current studies aim at identifying the *C. glutamicum* isomerase involved in growth on DCI.

MATERIALS AND METHODS

Bacterial strains, plasmids, and growth conditions. All bacterial strains and plasmids used in this work are listed in Table 2. All cloning steps were performed with *Escherichia coli* DH5α as host. *E. coli* strains were cultivated at 37°C on LB agar plates or in lysogeny broth (LB) (60) with 50 μg/mL kanamycin. For growth characterization, *C. glutamicum* was cultivated in a BioLector microcultivation system (m2p-labs, Baesweiler, Germany). Single colonies were transferred in brain heart infusion (BHI) medium and cultivated for 8 h at 30°C as a first preculture. The second preculture containing defined CGXII medium (61) with 0.03 g/L protocatechuic acid and 2% (wt/vol) glucose was inoculated with 10% (vol/vol) of the first preculture and cultivated for 16 h at 30°C. Before inoculation of the main cultures, cells were washed once with CGXII medium without a carbon source. BioLector microcultivation was performed in 800 μL CGXII medium, which was supplemented with 1% (wt/vol) of the indicated carbon source in 48-well FlowerPlates (m2p-labs, Baesweiler, Germany) at 1,200 rpm at 30°C. Growth in this system was measured online as scattered light at 620 nm (62). For protein production, *C. glutamicum* was cultivated in 200 mL BHI medium supplemented with 2% (wt/vol) glucose in 2-L baffled shake flasks at 100 rpm and 30°C. When appropriate, 25 μg/mL kanamycin was added to the medium. Gene expression was induced via the addition of isopropyl-β-D-thiogalactoside (IPTG) at the indicated concentrations. Bacterial growth was followed by measuring the optical density at 600 nm (OD_{600}).

Recombinant DNA work and construction of deletion mutants. Plasmids and oligonucleotides used in this study are listed in Table 2 and in Table S4 in the supplemental material, respectively. PCRs, DNA restrictions, and plasmid constructions were performed according to established protocols (63, 64). DNA sequencing and oligonucleotide synthesis were performed by Eurofins Genomics (Ebersberg, Germany). Chemically competent *E. coli* cells were transformed according to an established protocol (65). *C. glutamicum* was transformed via electroporation as described previously (66). The deletion mutant *C. glutamicum* MB001(DE3)ΔIDH was constructed via consecutive double homologous recombination as described previously (67) using the plasmids pK19mobsacBΔiol2, pK19mobsacBΔiolG, pK19mobsacBΔiolW, pK19mobsacBΔidhA3, and pK19mobsacBΔoxiB. The chromosomal deletions were confirmed via colony PCR using oligonucleotides annealing outside the deleted region.

For the construction of the pMKEx2-based expression plasmids, the corresponding target genes were cloned downstream of the *C. glutamicum* consensus ribosome binding site (RBS) via Gibson assembly. For protein overproduction and purification, the inositol dehydrogenase genes were cloned into the newly constructed pPREx6 plasmid, which is a derivative of pPREx2 (68) in which the promoter P_{tac} was replaced by the T7 promoter. For promoter exchange, the plasmid backbone was amplified using oligonucleotides P027 and P028, and the T7 promoter was amplified from pMKEx2 with oligonucleotides P029 and P030. DNA fragments were joined via Gibson assembly, yielding pPREx6.

Protein overproduction and purification. *C. glutamicum* MB001(DE3) was transformed with pPREx6-based expression plasmids for inositol dehydrogenase production and cultivated in 200 mL BHI medium supplemented with 20 g/L glucose. Gene overexpression was induced with 250 μM IPTG after 3 h, and cells were harvested after 24 h of cultivation via centrifugation at 5,000 $\times$ *g* for 20 min at 4°C. Cell pellets were washed and resuspended in 4 mL lysis buffer (100 mM KPO_4, pH 7.5, 150 mM NaCl, 1 mM $MgSO_4$) per g (wet weight) of cells and lysed by five passages through a French press at 124 MPa. The resulting cell extract was first centrifuged at 5,000 $\times$ *g* and 4°C for 20 min, and the supernatant was then subjected to ultracentrifugation at 45,000 $\times$ *g* and 4°C for 1 h. The resulting supernatant was incubated with avidin (25 μg/mg protein) for 30 min on ice before performing purification on an Äkta pure protein purification system (Cytiva) via StrepTactin Sepharose affinity chromatography and subsequent size exclusion chromatography.

TABLE 2 Bacterial strains and plasmids used in this study

Strain or plasmid	Relevant characteristics	Reference or source
Strains		
E. coli DH5α	F$^-$ ϕ80d*lac*Δ(*lacZ*)M15 Δ(*lacZYA-argF*)*U169 endA1 recA1 hsdR17* (r_K^- m_K^+) *deoR thi-1 phoA supE44* λ^- *gyrA96 relA1*; strain used for cloning procedures	65
C. glutamicum		
MB001(DE3)	Derivative of the prophage-free strain MB001 with a chromosomally encoded *E. coli lacI* gene under control of its native promoter followed by the T7 RNA polymerase gene under control of the *lacUV5* promoter	78
MB001(DE3)ΔIDH	MB001(DE3) derivative with deletion of the genes *oxiC*-cg3390-*oxiD*-*oxiE* (cg3389–cg3392), *iolG* (cg0204), *iolW* (cg0207), *idhA3* (cg2313), and *oxiB* (cg0211)	This work
ATCC 13032 Δ*iolT1*	Derivative of the wild-type ATCC 13032 in which the inositol transporter *iolT1* was deleted	35
ATCC 13032 Δ*iolT2*	Derivative of the wild-type ATCC 13032 in which the inositol transporter *iolT2* was deleted	35
ATCC 13032 Δ*iolT1*Δ*iolT2*	Derivative of the wild-type ATCC 13032 in which the inositol transporters *iolT1* and *iolT2* were deleted	35
Plasmids		
pK19mobsacB	Kan^r; plasmid for allelic exchange in *C. glutamicum*; pK18 *oriV*$_{E.c.}$ *sacB lacZ*α	79
pK19mobsacBΔ*iol2*	Kan^r; plasmid for deletion of the genes cg3389–cg3392 containing two 1-kb PCR products which cover the upstream flanking region of *oxiC* (cg3389) and the downstream flanking region of *oxiE* (cg3392)	47
pK19mobsacBΔ*iolG*	Kan^r; plasmid for deletion of *iolG* (cg0204)	80
pK19mobsacBΔ*iolW*	Kan^r; plasmid for deletion of *iolW* (cg0207)	57
pK19mobsacBΔ*oxiB*	Kan^r; plasmid for deletion of *oxiB* (cg0211)	This work
pK19mobsacBΔ*idhA3*	Kan^r; plasmid for deletion of *idhA3* (cg2313)	This work
pMKEx2	Kan^r; *E. coli-C. glutamicum* shuttle vector (*lacI* P_{T7} *lacO1* pHM1519 *ori*$_{Cg}$; pACYC177 *ori*$_{Ec}$) for expression of target genes under control of the T7 promoter	78
pMKEx2-*eyfp*	Kan^r; pMKEx2 derivative containing the *eyfp* gene under control of P_{T7}	78
pMKEx2-IolG	Kan^r; pMKEx2 derivative containing the *iolG* gene under control of P_{T7}	This work
pMKEx2-IolW	Kan^r; pMKEx2 derivative containing the *iolW* gene under control of P_{T7}	This work
pMKEx2-OxiB	Kan^r; pMKEx2 derivative containing the *oxiB* gene under control of P_{T7}	This work
pMKEx2-IdhA3	Kan^r; pMKEx2 derivative containing the *idhA3* gene under control of P_{T7}	47
pMKEx2-OxiC	Kan^r; pMKEx2 derivative containing the *oxiC* gene under control of P_{T7}	47
pMKEx2-OxiD	Kan^r; pMKEx2 derivative containing the *oxiD* gene under control of P_{T7}	47
pMKEx2-OxiE	Kan^r; pMKEx2 derivative containing the *oxiE* gene under control of P_{T7}	47
pPREx2	Kan^r; *E. coli-C. glutamicum* shuttle vector (P_{tac} *lacI*^{q} pBL1 *ori*$_{Cg}$; ColE1 *ori*$_{Ec}$ with a Strep-tag II-encoding sequence	68
pPREx6	Kan^r; pPREx2 derivative with P_{tac} exchanged for P_{T7} promoter	This work
pPREx6-IolG	Kan^r; pPREx6 derivative containing the *iolG* gene under control of P_{T7} and fused to Strep-tag II sequence	This work
pPREx6-OxiB	Kan^r; pPREx6 derivative containing the *oxiB* gene under control of P_{T7} and fused to Strep-tag II sequence	This work
pPREx6-OxiD	Kan^r; pPREx6 derivative containing the *oxiD* gene under control of P_{T7} and fused to Strep-tag II sequence	This work
pPREx6-OxiE	Kan^r; pPREx6 derivative containing the *oxiE* gene under control of P_{T7} and fused to Strep-tag II sequence	This work

A StrepTrap HP 1-mL column was equilibrated with binding buffer (100 mM KPO_4, pH 7.5, 150 mM NaCl, 1 mM $MgSO_4$) before loading the protein extract. The column was washed with 10 column volumes (CV) of binding buffer, and the remaining proteins were then eluted in six 0.5-mL fractions with elution buffer I (100 mM KPO_4, pH 7.5, 150 mM NaCl, 1 mM $MgSO_4$, 2.5 mM dethiobiotin). The protein-containing elution fractions were combined and concentrated by using a 10-kDa Amicon filter and centrifuging at 3,500 $\times$ *g* and 4°C to a final volume of 500 μL. The concentrated protein was then applied to a Superdex 200 Increase size exclusion chromatography column that had been equilibrated with 2 CV of elution buffer II (100 mM KPO_4, pH 7.5, 1 mM $MgSO_4$). Protein was eluted with 1.5 CV of elution buffer II and collected in 2-mL fractions. The purity and apparent molecular mass of the proteins after both purification steps were determined by 12% (wt/vol) SDS-PAGE according to standard procedures (64). Protein concentrations were determined using the Bradford assay (69).

Inositol dehydrogenase activity assays. Inositol dehydrogenase activity was determined as described before with some adjustments (68). Measurements were performed in a 600-μL reaction volume using 1-mL cuvettes containing 0.25 to 600 μg purified enzyme in elution buffer II at 30°C. A reaction mixture without the substrate was used as a blank, and the reaction was initiated by the addition of the substrate. Kinetic assays were performed with various concentrations of MI, DCI, and SI (0.5 to 50 mM) at a constant concentration of 5 mM NAD^+. Kinetic constants were determined via a nonlinear regression fit based on the Michaelis-Menten equation with the GraphPad Prism software.

Structural bioinformatics methods. Homology models of the IDHs were generated with the protein structure homology modeling server of SWISS-MODEL (70, 71). The template search against the SWISS-MODEL template library (SMTL; last update 2 October 2021, last included PDB release 2 May 2021) was performed with BLAST (72) and HHblits (73): Initially, the target sequence was searched with BLAST against the primary amino acid sequences contained in the SMTL. A total of 23 (OxiC), 79 (IdhA3), 42 (OxiE), 61 (OxiD), 28 (IolG), and 19 (OxiB) templates were found. An initial HHblits profile was built using the procedure outlined in reference 73, followed by one iteration of HHblits against Uniclust30 (74). Next, the obtained profile was searched against all profiles of the SMTL. A total of 1,846 (OxiC), 3,608 (IdhA3), 2,552 (OxiE), 3,393 (OxiD), 3,946 (IolG), and 2,505 (OxiB) templates were found. Based on the found template structures, we chose the ones that included a bound cofactor and showed the highest sequence identity (Table S2). Models are built based on the target-template alignment using ProMod3 (75). Coordinates conserved between the target and the template are copied from the template to the model. Insertions and deletions are remodeled using a fragment library. Side chains are then rebuilt. Finally, the resulting model's geometry is regularized using a force field. The global and per-residue model quality was assessed using the QMEANDisCo scoring function (76) (Fig. S6). The cofactors' position was determined from the template structures and carried over to the structural models using PyMOL Molecular Graphics System, version 2.3.0 (Schrödinger, LLC, New York, NY) (77).

For the molecular docking, the three-dimensional (3D) structures of the substrates MI, SI, and DCI were generated based on their corresponding SMILES codes using RDKit: Open-source Chemoinformatics (https://doi.org/10.5281/zenodo.3732262). The substrates were subsequently docked into the catalytic sites of the respective IDH utilizing a combination of AutoDock3 (52) as a docking engine and DrugScore^{2018} (53) as an objective function. Docking grids were generated with DrugScore^{2018} using converged pair-potentials for all atom pairs. The position and dimension of the grids were calculated using the positions of inositols in crystal structures as reference points. Accounting for a margin of 8 Å in every direction, the final docking grid shows box dimensions of approximately 23 Å by 23 Å by 20 Å and is centered in the pocket of the IDHs (Fig. S7A and B). Following an established procedure (53), the docking protocol considered 100 independent runs for each ligand using an initial population size of 100 individuals, a maximum number of 27.0×10^3 generations, a maximum number of 5.0×10^6 energy evaluations, a mutation rate of 0.02, a crossover rate of 0.8, and an elitism value of 1. The Lamarckian genetic algorithm was chosen for sampling in all approaches. The distance between the reactive carbon of the docked substrates and the cofactor was measured using the PyMOL Molecular Graphics System.

Data availability. The strains and plasmids used in this work will be made available by the corresponding author (M.B.) upon request.

SUPPLEMENTAL MATERIAL

Supplemental material is available online only.

SUPPLEMENTAL FILE 1, PDF file, 4 MB.

ACKNOWLEDGMENTS

This project was financially supported by the CLIB-Competence Center Biotechnology (CKB) funded by the European Regional Development Fund ERDF (grant number 34.EFRE-030096 and 34.EFRE-030097) and by the German Federal Ministry of Education and Research (BMBF) (grant number 031B0918A) as part of the innovation lab "AutoBiotech" within the project "BioökonomieREVIER." The study is part of the scientific activities of the Bioeconomy Science Center (BioSC), which is financially supported by the Ministry of Innovation, Science and Research of the German Federal State of North Rhine-Westphalia (313/323-400-00213); project PhD_MP_2021_08).

We are grateful for computational support and infrastructure provided by the "Zentrum für Informations- und Medientechnologie" (ZIM) at the Heinrich Heine University Düsseldorf and the computing time provided by the John von Neumann Institute for Computing (NIC) to H.G. on the supercomputer JUWELS at the Jülich Supercomputing Centre (JSC) (user ID: HKF7, VSK33).

REFERENCES

1. Thomas MP, Mills SJ, Potter BV. 2016. The "other" inositols and their phosphates: synthesis, biology, and medicine. Angew Chem Int Ed Engl 55:1614–1650. https://doi.org/10.1002/anie.201502227.
2. Lopez-Gambero AJ, Sanjuan C, Serrano-Castro PJ, Suarez J, Rodriguez de Fonseca F. 2020. The biomedical uses of inositols: a nutraceutical approach to metabolic dysfunction in aging and neurodegenerative diseases. Biomedicines 8:295. https://doi.org/10.3390/biomedicines8090295.
3. Michell RH. 2008. Inositol derivatives: evolution and functions. Nat Rev Mol Cell Biol 9:151–161. https://doi.org/10.1038/nrm2334.
4. Donahue TF, Henry SA. 1981. *myo*-Inositol-1-phosphate synthase. Characteristics of the enzyme and identification of its structural gene in yeast. J Biol Chem 256:7077–7085. https://doi.org/10.1016/S0021-9258(19)69102-7.
5. Bachhawat N, Mande SC. 1999. Identification of the INO1 gene of *Mycobacterium tuberculosis* H37Rv reveals a novel class of inositol-1-phosphate synthase enzyme. J Mol Biol 291:531–536. https://doi.org/10.1006/jmbi.1999.2980.
6. Nigou J, Besra GS. 2002. Characterization and regulation of inositol monophosphatase activity in *Mycobacterium smegmatis*. Biochem J 361:385–390. https://doi.org/10.1042/bj3610385.

7. Pak Y, Huang LC, Lilley KJ, Larner J. 1992. *In vivo* conversion of [3H]myoinositol to [3H]chiroinositol in rat tissues. J Biol Chem 267:16904–16910. https://doi.org/10.1016/S0021-9258(18)41870-4.
8. Hipps PP, Ackermann KE, Sherman WR. 1982. Inositol epimerase - inosose reductase from bovine brain. Methods Enzymol 89:593–598. https://doi.org/10.1016/S0076-6879(82)89102-7.
9. Kinnard RL, Narasimhan B, Pliska-Matyshak G, Murthy PP. 1995. Characterization of *scyllo*-inositol-containing phosphatidylinositol in plant cells. Biochem Biophys Res Commun 210:549–555. https://doi.org/10.1006/bbrc.1995.1695.
10. Majumder AL, Biswas BB. 2006. Biology of inositols and phosphoinositides. Springer, New York, NY.
11. Mikoshiba K. 2007. IP3 receptor/Ca2+ channel: from discovery to new signaling concepts. J Neurochem 102:1426–1446. https://doi.org/10.1111/j.1471-4159.2007.04825.x.
12. Lott JNA, Ockenden I, Raboy V, Batten GD. 2000. Phytic acid and phosphorus in crop seeds and fruits: a global estimate. Seed Sci Res 10:11–33. https://doi.org/10.1017/S0960258500000039.
13. Fahey RC. 2013. Glutathione analogs in prokaryotes. Biochim Biophys Acta 1830:3182–3198. https://doi.org/10.1016/j.bbagen.2012.10.006.
14. Morita YS, Fukuda T, Sena CB, Yamaryo-Botte Y, McConville MJ, Kinoshita T. 2011. Inositol lipid metabolism in mycobacteria: biosynthesis and regulatory mechanisms. Biochim Biophys Acta 1810:630–641. https://doi.org/10.1016/j.bbagen.2011.03.017.
15. Anderson WA, Magasanik B. 1971. The pathway of *myo*-inositol degradation in *Aerobacter aerogenes*. Conversion of 2-deoxy-5-keto-D-gluconic acid to glycolytic intermediates. J Biol Chem 246:5662–5675. https://doi.org/10.1016/S0021-9258(18)61857-5.
16. Fry J, Wood M, Poole PS. 2001. Investigation of *myo*-inositol catabolism in *Rhizobium leguminosarum* bv. *viciae* and its effect on nodulation competitiveness. Mol Plant Microbe Interact 14:1016–1025. https://doi.org/10.1094/MPMI.2001.14.8.1016.
17. Yoshida KI, Yamaguchi M, Morinaga T, Kinehara M, Ikeuchi M, Ashida H, Fujita Y. 2008. *myo*-Inositol catabolism in *Bacillus subtilis*. J Biol Chem 283:10415–10424. https://doi.org/10.1074/jbc.M708043200.
18. Ramaley R, Fujita Y, Freese E. 1979. Purification and properties of *Bacillus subtilis* inositol dehydrogenase. J Biol Chem 254:7684–7690. https://doi.org/10.1016/S0021-9258(18)36000-9.
19. Kohler PR, Zheng JY, Schoffers E, Rossbach S. 2010. Inositol catabolism, a key pathway in *Sinorhizobium meliloti* for competitive host nodulation. Appl Environ Microbiol 76:7972–7980. https://doi.org/10.1128/AEM.01972-10.
20. Galbraith MP, Feng SF, Borneman J, Triplett EW, de Bruijn FJ, Rossbach S. 1998. A functional *myo*-inositol catabolism pathway is essential for rhizopine utilization by *Sinorhizobium meliloti*. Microbiology 144:2915–2924. https://doi.org/10.1099/00221287-144-10-2915.
21. Shimizu T, Takaya N, Nakamura A. 2012. An L-glucose catabolic pathway in *Paracoccus* species 43P. J Biol Chem 287:40448–40456. https://doi.org/10.1074/jbc.M112.403055.
22. Fukano K, Ozawa K, Kokubu M, Shimizu T, Ito S, Sasaki Y, Nakamura A, Yajima S. 2018. Structural basis of L-glucose oxidation by *scyllo*-inositol dehydrogenase: implications for a novel enzyme subfamily classification. PLoS One 13:e0198010. https://doi.org/10.1371/journal.pone.0198010.
23. Manske C, Schell U, Hilbi H. 2016. Metabolism of *myo*-inositol by *Legionella pneumophila* promotes infection of amoebae and macrophages. Appl Environ Microbiol 82:5000–5014. https://doi.org/10.1128/AEM.01018-16.
24. Rodionova IA, Leyn SA, Burkart MD, Boucher N, Noll KM, Osterman AL, Rodionov DA. 2013. Novel inositol catabolic pathway in *Thermotoga maritima*. Environ Microbiol 15:2254–2266. https://doi.org/10.1111/1462-2920.12096.
25. Berman T, Magasanik B. 1966. The pathway of *myo*-inositol degradation in *Aerobacter aerogenes*. Dehydrogenation and dehydration. J Biol Chem 241:800–806. https://doi.org/10.1016/S0021-9258(18)96836-5.
26. Yoshida KI, Yamaguchi M, Ikeda H, Omae K, Tsurusaki KI, Fujita Y. 2004. The fifth gene of the *iol* operon of *Bacillus subtilis, iolE*, encodes 2-keto-*myo*-inositol dehydratase. Microbiology (Reading) 150:571–580. https://doi.org/10.1099/mic.0.26768-0.
27. Kawsar HI, Ohtani K, Okumura K, Hayashi H, Shimizu T. 2004. Organization and transcriptional regulation of *myo*-inositol operon in *Clostridium perfringens*. FEMS Microbiol Lett 235:289–295. https://doi.org/10.1016/j.femsle.2004.04.047.
28. Yoshida KI, Aoyama D, Ishio I, Shibayama T, Fujita Y. 1997. Organization and transcription of the *myo*-inositol operon, *iol*, of *Bacillus subtilis*. J Bacteriol 179:4591–4598. https://doi.org/10.1128/jb.179.14.4591-4598.1997.
29. Yebra MJ, Zuniga M, Beaufils S, Perez-Martinez G, Deutscher J, Monedero V. 2007. Identification of a gene cluster enabling *Lactobacillus casei* BL23 to utilize *myo*-inositol. Appl Environ Microbiol 73:3850–3858. https://doi.org/10.1128/AEM.00243-07.
30. Yoshida KI, Shibayama T, Aoyama D, Fujita Y. 1999. Interaction of a repressor and its binding sites for regulation of the *Bacillus subtilis iol* divergon. J Mol Biol 285:917–929. https://doi.org/10.1006/jmbi.1998.2398.
31. Kohler PR, Choong EL, Rossbach S. 2011. The RpiR-like repressor IolR regulates inositol catabolism in *Sinorhizobium meliloti*. J Bacteriol 193:5155–5163. https://doi.org/10.1128/JB.05371-11.
32. Becker J, Rohles CM, Wittmann C. 2018. Metabolically engineered *Corynebacterium glutamicum* for bio-based production of chemicals, fuels, materials, and healthcare products. Metab Eng 50:122–141. https://doi.org/10.1016/j.ymben.2018.07.008.
33. Eggeling L, Bott M. 2015. A giant market and a powerful metabolism: L-lysine provided by *Corynebacterium glutamicum*. Appl Microbiol Biotechnol 99:3387–3394. https://doi.org/10.1007/s00253-015-6508-2.
34. Wendisch VF. 2020. Metabolic engineering advances and prospects for amino acid production. Metab Eng 58:17–34. https://doi.org/10.1016/j.ymben.2019.03.008.
35. Krings E, Krumbach K, Bathe B, Kelle R, Wendisch VF, Sahm H, Eggeling L. 2006. Characterization of *myo*-inositol utilization by *Corynebacterium glutamicum*: the stimulon, identification of transporters, and influence on L-lysine formation. J Bacteriol 188:8054–8061. https://doi.org/10.1128/JB.00935-06.
36. Klaffl S, Brocker M, Kalinowski J, Eikmanns BJ, Bott M. 2013. Complex regulation of the phosphoenolpyruvate carboxykinase gene *pck* and characterization of its GntR-type regulator IolR as a repressor of *myo*-inositol utilization genes in *Corynebacterium glutamicum*. J Bacteriol 195:4283–4296. https://doi.org/10.1128/JB.00265-13.
37. Chen C, Chen K, Su T, Zhang B, Li G, Pan J, Si M. 2019. *Myo*-inositol-1-phosphate synthase (Ino-1) functions as a protection mechanism in *Corynebacterium glutamicum* under oxidative stress. Microbiologyopen 8:e00721. https://doi.org/10.1002/mbo3.721.
38. Baumgart M, Luder K, Grover S, Gätgens C, Besra GS, Frunzke J. 2013. IpsA, a novel LacI-type regulator, is required for inositol-derived lipid formation in *Corynebacteria* and *Mycobacteria*. BMC Biol 11:122. https://doi.org/10.1186/1741-7007-11-122.
39. Aamudalapalli HB, Bertwistle D, Palmer DRJ, Sanders DAR. 2018. *myo*-Inositol dehydrogenase and *scyllo*-inositol dehydrogenase from *Lactobacillus casei* BL23 bind their substrates in very different orientations. Biochim Biophys Acta Proteins Proteom 1866:1115–1124. https://doi.org/10.1016/j.bbapap.2018.08.011.
40. Yoshida K, Sanbongi A, Murakami A, Suzuki H, Takenaka S, Takami H. 2012. Three inositol dehydrogenases involved in utilization and interconversion of inositol stereoisomers in a thermophile, *Geobacillus kaustophilus* HTA426. Microbiology (Reading) 158:1942–1952. https://doi.org/10.1099/mic.0.059980-0.
41. Zhang WY, Sun ZH, Yu DL, Airideng C, Chen W, Meng H, Zhang HP. 2010. Comparative analysis of *iol* clusters in *Lactobacillus casei* strains. World J Microbiol Biotechnol 26:1949–1955. https://doi.org/10.1007/s11274-010-0375-x.
42. Morinaga T, Ashida H, Yoshida K. 2010. Identification of two *scyllo*-inositol dehydrogenases in *Bacillus subtilis*. Microbiology (Reading) 156:1538–1546. https://doi.org/10.1099/mic.0.037499-0.
43. Yoshida K, Yamaguchi M, Morinaga T, Ikeuchi M, Kinehara M, Ashida H. 2006. Genetic modification of *Bacillus subtilis* for production of D-*chiro*-inositol, an investigational drug candidate for treatment of type 2 diabetes and polycystic ovary syndrome. Appl Environ Microbiol 72:1310–1315. https://doi.org/10.1128/AEM.72.2.1310-1315.2006.
44. Berman HM, Westbrook J, Feng Z, Gilliland G, Bhat TN, Weissig H, Shindyalov IN, Bourne PE. 2000. The protein data bank. Nucleic Acids Res 28:235–242. https://doi.org/10.1093/nar/28.1.235.
45. Kumaran D, Mahmood A, Burley SK, Swaminathan S. 2021. 3EUW. Crystal structure of a *myo*-inositol dehydrogenase from *Corynebacterium glutamicum* ATCC 13032. Protein Data Bank https://doi.org/10.2210/pdb3euw/pdb.
46. van Straaten KE, Zheng H, Palmer DR, Sanders DA. 2010. Structural investigation of *myo*-inositol dehydrogenase from *Bacillus subtilis:* implications for catalytic mechanism and inositol dehydrogenase subfamily classification. Biochem J 432:237–247. https://doi.org/10.1042/BJ20101079.
47. Ramp P, Lehnert A, Matamouros S, Wirtz A, Baumgart M, Bott M. 2021. Metabolic engineering of *Corynebacterium glutamicum* for production of *scyllo*-inositol, a drug candidate against Alzheimer's disease. Metab Eng 67:173–185. https://doi.org/10.1016/j.ymben.2021.06.011.

48. Carugo O, Argos P. 1997. NADP-dependent enzymes. II: evolution of the mono- and dinucleotide binding domains. Proteins 28:29–40. https://doi.org/10.1002/(SICI)1097-0134(199705)28:1%3C29::AID-PROT3%3E3.0.CO;2-E.
49. Carugo O, Argos P. 1997. NADP-dependent enzymes. I: conserved stereochemistry of cofactor binding. Proteins 28:10–28. https://doi.org/10.1002/(SICI)1097-0134(199705)28:1%3C10::AID-PROT2%3E3.0.CO;2-N.
50. Zheng H, Bertwistle D, Sanders DA, Palmer DR. 2013. Converting NAD-specific inositol dehydrogenase to an efficient NADP-selective catalyst, with a surprising twist. Biochemistry 52:5876–5883. https://doi.org/10.1021/bi400821s.
51. Kang DM, Tanaka K, Takenaka S, Ishikawa S, Yoshida K. 2017. *Bacillus subtilis iolU* encodes an additional $NADP^+$-dependent *scyllo*-inositol dehydrogenase. Biosci Biotechnol Biochem 81:1026–1032. https://doi.org/10.1080/09168451.2016.1268043.
52. Morris GM, Goodsell DS, Halliday RS, Huey R, Hart WE, Belew RK, Olson AJ. 1998. Automated docking using a Lamarckian genetic algorithm and an empirical binding free energy function. J Comput Chem 19:1639–1662. https://doi.org/10.1002/(SICI)1096-987X(19981115)19:14%3C1639::AID-JCC10%3E3.0.CO;2-B.
53. Dittrich J, Schmidt D, Pfleger C, Gohlke H. 2019. Converging a knowledge-based scoring function: DrugScore^{2018}. J Chem Inf Model 59:509–521. https://doi.org/10.1021/acs.jcim.8b00582.
54. Bäumchen C, Krings E, Bringer S, Eggeling L, Sahm H. 2009. *Myo*-inositol facilitators IolT1 and IolT2 enhance D-mannitol formation from D-fructose in *Corynebacterium glutamicum*. FEMS Microbiol Lett 290:227–235. https://doi.org/10.1111/j.1574-6968.2008.01425.x.
55. Ikeda M, Mizuno Y, Awane S, Hayashi M, Mitsuhashi S, Takeno S. 2011. Identification and application of a different glucose uptake system that functions as an alternative to the phosphotransferase system in *Corynebacterium glutamicum*. Appl Microbiol Biotechnol 90:1443–1451. https://doi.org/10.1007/s00253-011-3210-x.
56. Lindner SN, Seibold GM, Henrich A, Krämer R, Wendisch VF. 2011. Phosphotransferase system-independent glucose utilization in *Corynebacterium glutamicum* by inositol permeases and glucokinases. Appl Environ Microbiol 77:3571–3581. https://doi.org/10.1128/AEM.02713-10.
57. Brüsseler C, Radek A, Tenhaef N, Krumbach K, Noack S, Marienhagen J. 2018. The myo-inositol/proton symporter IolT1 contributes to D-xylose uptake in *Corynebacterium glutamicum*. Bioresour Technol 249:953–961. https://doi.org/10.1016/j.biortech.2017.10.098.
58. Bettaney KE, Sukumar P, Hussain R, Siligardi G, Henderson PJ, Patching SG. 2013. A systematic approach to the amplified expression, functional characterization and purification of inositol transporters from *Bacillus subtilis*. Mol Membr Biol 30:3–14. https://doi.org/10.3109/09687688.2012.729093.
59. Michon C, Kang CM, Karpenko S, Tanaka K, Ishikawa S, Yoshida K. 2020. A bacterial cell factory converting glucose into *scyllo*-inositol, a therapeutic agent for Alzheimer's disease. Commun Biol 3:93. https://doi.org/10.1038/s42003-020-0814-7.
60. Bertani G. 1951. Studies on lysogenesis. The mode of phage liberation by lysogenic *Escherichia coli*. J Bacteriol 62:293–300. https://doi.org/10.1128/jb.62.3.293-300.1951.
61. Keilhauer C, Eggeling L, Sahm H. 1993. Isoleucine synthesis in *Corynebacterium glutamicum*: molecular analysis of the *ilvB-ilvN-ilvC* operon. J Bacteriol 175:5595–5603. https://doi.org/10.1128/jb.175.17.5595-5603.1993.
62. Kensy F, Zang E, Faulhammer C, Tan RK, Büchs J. 2009. Validation of a high-throughput fermentation system based on online monitoring of biomass and fluorescence in continuously shaken microtiter plates. Microb Cell Fact 8:31. https://doi.org/10.1186/1475-2859-8-31.
63. Gibson DG, Young L, Chuang RY, Venter JC, Hutchison CA, Smith HO. 2009. Enzymatic assembly of DNA molecules up to several hundred kilobases. Nat Methods 6:343–345. https://doi.org/10.1038/nmeth.1318.
64. Green MR, Sambrook J. 2012. Molecular cloning. A laboratory manual, 3rd ed. Cold Spring Harbor Laboratory Press, Cold Spring Harbor, NY.
65. Hanahan D. 1983. Studies on transformation of *Escherichia coli* with plasmids. J Mol Biol 166:557–580. https://doi.org/10.1016/s0022-2836(83)80284-8.
66. van der Rest ME, Lange C, Molenaar D. 1999. A heat shock following electroporation induces highly efficient transformation of *Corynebacterium glutamicum* with xenogeneic plasmid DNA. Appl Microbiol Biotechnol 52:541–545. https://doi.org/10.1007/s002530051557.
67. Niebisch A, Bott M. 2001. Molecular analysis of the cytochrome bc_1-aa_3 branch of the *Corynebacterium glutamicum* respiratory chain containing an unusual diheme cytochrome c_1. Arch Microbiol 175:282–294. https://doi.org/10.1007/s002030100262.
68. Bakkes PJ, Ramp P, Bida A, Dohmen-Olma D, Bott M, Freudl R. 2020. Improved pEKEx2-derived expression vectors for tightly controlled production of recombinant proteins in *Corynebacterium glutamicum*. Plasmid 112:102540. https://doi.org/10.1016/j.plasmid.2020.102540.
69. Bradford MM. 1976. A rapid and sensitive method for the quantitation of microgram quantities of protein utilizing the principle of protein-dye binding. Anal Biochem 72:248–254. https://doi.org/10.1006/abio.1976.9999.
70. Waterhouse A, Bertoni M, Bienert S, Studer G, Tauriello G, Gumienny R, Heer FT, de Beer TAP, Rempfer C, Bordoli L, Lepore R, Schwede T. 2018. SWISS-MODEL: homology modelling of protein structures and complexes. Nucleic Acids Res 46:W296–W303. https://doi.org/10.1093/nar/gky427.
71. Bienert S, Waterhouse A, de Beer TA, Tauriello G, Studer G, Bordoli L, Schwede T. 2017. The SWISS-MODEL repository - new features and functionality. Nucleic Acids Res 45:D313–D319. https://doi.org/10.1093/nar/gkw1132.
72. Camacho C, Coulouris G, Avagyan V, Ma N, Papadopoulos J, Bealer K, Madden TL. 2009. BLAST+: architecture and applications. BMC Bioinformatics 10:421. https://doi.org/10.1186/1471-2105-10-421.
73. Steinegger M, Meier M, Mirdita M, Vohringer H, Haunsberger SJ, Soding J. 2019. HH-suite3 for fast remote homology detection and deep protein annotation. BMC Bioinformatics 20:473. https://doi.org/10.1186/s12859-019-3019-7.
74. Mirdita M, von den Driesch L, Galiez C, Martin MJ, Soding J, Steinegger M. 2017. Uniclust databases of clustered and deeply annotated protein sequences and alignments. Nucleic Acids Res 45:D170–D176. https://doi.org/10.1093/nar/gkw1081.
75. Studer G, Tauriello G, Bienert S, Biasini M, Johner N, Schwede T. 2021. ProMod3 - a versatile homology modelling toolbox. PLoS Comput Biol 17:e1008667. https://doi.org/10.1371/journal.pcbi.1008667.
76. Studer G, Rempfer C, Waterhouse AM, Gumienny R, Haas J, Schwede T. 2020. QMEANDisCo-distance constraints applied on model quality estimation. Bioinformatics 36:1765–1771. https://doi.org/10.1093/bioinformatics/btz828.
77. DeLano WL. 2002. The PyMOL molecular graphics system. www.pymol.org. Version 2.3.0.
78. Kortmann M, Kuhl V, Klaffl S, Bott M. 2015. A chromosomally encoded T7 RNA polymerase-dependent gene expression system for *Corynebacterium glutamicum*: construction and comparative evaluation at the single-cell level. Microb Biotechnol 8:253–265. https://doi.org/10.1111/1751-7915.12236.
79. Schäfer A, Tauch A, Jäger W, Kalinowski J, Thierbach G, Pühler A. 1994. Small mobilizable multi-purpose cloning vectors derived from the *Escherichia coli* plasmids pK18 and pK19: selection of defined deletions in the chromosome of *Corynebacterium glutamicum*. Gene 145:69–73. https://doi.org/10.1016/0378-1119(94)90324-7.
80. Tenhaef N, Brüsseler C, Radek A, Hilmes R, Unrean P, Marienhagen J, Noack S. 2018. Production of D-xylonic acid using a non-recombinant *Corynebacterium glutamicum* strain. Bioresour Technol 268:332–339. https://doi.org/10.1016/j.biortech.2018.07.127.

SUPPORTING INFORMATION

Physiological, biochemical, and structural bioinformatic analysis of the multiple inositol dehydrogenases from *Corynebacterium glutamicum*

Paul Ramp[1,2], Christopher Pfleger[3], Jonas Dittrich[2,3], Christina Mack[1], Holger Gohlke[2,3,4,#], and Michael Bott[1,2,#]

[1]IBG-1: Biotechnology, Institute of Bio- and Geosciences, Forschungszentrum Jülich, Jülich, Germany
[2]The Bioeconomy Science Center (BioSC), Forschungszentrum Jülich, Jülich, Germany
[3]Institut für Pharmazeutische und Medizinische Chemie, Heinrich-Heine-Universität Düsseldorf, 40225 Düsseldorf, Germany
[4]John von Neumann Institute for Computing (NIC), Jülich Supercomputing Centre (JSC), Institute of Biological Information Processing (IBI-7: Structural Biochemistry) & Institute of Bio- and Geosciences (IBG-4: Bioinformatics), Forschungszentrum Jülich GmbH, 52425 Jülich, Germany

[#]Corresponding authors: m.bott@fz-juelich.de and h.gohlke@fz-juelich.de

Running title: Inositol dehydrogenases of *Corynebacterium glutamicum*

Table S1. Identifiers and references for the characterized IDHs aligned in Fig. S5.

Name	Uniprot number	Organism	Reference
BsIolG	P26935	*B. subtilis*	(1)
BsIolW	O32223	*B. subtilis*	(2)
BsIolX	P40332	*B. subtilis*	(2)
BsIolU	O05265	*B. subtilis*	(3)
Gk1897	Q5KYQ4	*Geobacillus kaustophilus* strain HTA426	(4)
Gk1898	Q5KYQ3	*Geobacillus kaustophilus* strain HTA426	(4)
Gk1899	Q5KYQ2	*Geobacillus kaustophilus* strain HTA426	(4)
LcIDH1	E1U887	*Lactobacillus casei* strain Bl23	(5)
LcIDH2	E1U888	*Lactobacillus casei* strain Bl23	(5)
TmIolG	Q9WYP5	*Thermotoga maritima*	(6)
SMc01163	Q92SL5	*Rhizobium meliloti* strain 1021 (*Sinorhizobium meliloti* strain 1021)	(7)
SmIdhA	O68965	*Rhizobium meliloti* strain 1021 (*Sinorhizobium meliloti* strain 1021)	(8)
PllgdA	K7ZP76	*Paracoccus laeviglucosivorans*	(9)

Table S2. Used templates for generating structural models of the IDHs and global assessment of the model quality.

IDH	Template PDB	Sequence identity [%]	Resolution [Å]	QMEANDisCo Global (10)
IdhA3	4l8v	33.99	2.1	0.52
OxiC	3cea	23.05	2.4	0.55
OxiB	5ya8	33.33	2.3	0.67
OxiD	4mio	25.47	1.5	0.62
OxiE	4n54	35.88	2.1	0.65
IolG	4l8v	38.44	2.1	0.75

Table S3. Convergence of docking results[1]

IDH	*myo*-Inositol	*scyllo*-Inositol	D-*chiro*-Inositol
IdhA3	Cl 1: 98% (-6.31 kcal mol^{-1}) Cl 2: 2% (-6.28 kcal mol^{-1})	Cl 1: 100% (-6.23 kcal mol^{-1})	Cl 1: 100% (-6.40 kcal mol^{-1})
OxiC	Cl 1: 100% (-6.97 kcal mol^{-1})	Cl 1: 100% (-6.85 kcal mol^{-1})	Cl 1: 100% (-6.97 kcal mol^{-1})
OxiB	Cl 1: 100% (-7.11 kcal mol^{-1})	Cl 1: 100% (-7.02 kcal mol^{-1})	Cl 1: 100% (-6.96 kcal mol^{-1})
OxiD	Cl 1: 100% (-6.71 kcal mol^{-1})	Cl 1: 100% (-6.51 kcal mol^{-1})	Cl 1: 100% (-6.51 kcal mol^{-1})
OxiE	Cl 1: 100% (-7.32 kcal mol^{-1})	Cl 1: 100% (-7.37 kcal mol^{-1})	Cl 1: 65% (-6.98 kcal mol^{-1}) Cl 2: 35% (-6.93 kcal mol^{-1})
IolG	Cl 1: 100% (-7.24 kcal mol^{-1})	Cl 1: 100% (-7.23 kcal mol^{-1})	Cl 1: 100% (-7.18 kcal mol^{-1})

[1] RMSD-based clustering of docked inositols; percentage convergence of docked inositol poses; average energies shown in parentheses.

Table S4. Oligonucleotides used in this study

Oligonucleotide name	Oligonucleotide sequence (5'→ 3')
pK19mobsacB plasmids	
P001_ΔoxiB_1	GCATGCCTGCAGGTCGACTCTAGAGTTGTCGTCGATGGTGGTG
P002_ΔoxiB_2	AAGTTCTTGCTGAGTCAC
P003_ΔoxiB_3	GGTCATAGTGACTCAGCAAGAACTTATCCCTGCAAACAACTAG
P004_ΔoxiB_4	CGTTGTAAAACGACGGCCAGTGAATTTCCTTGGTCACCAGATC
P005_Δcg2313_1	GAGGATCCCCGGGTACCGAGCTCGCCTCAAGCGGAACCTGAAG
P006_Δcg2313_2	CTTGCTGAAAGCATCGAGG
P007_Δcg2313_3	GTTAAACCTCGATGCTTTCAGCAAGGAGGGCAAGTTTGACTGAC
P008_Δcg2313_4	CGTTGTAAAACGACGGCCAGTGAATTATGGTGGTCAAGCCGATG
Recombination analysis	
P009_ΔiolG_1	CGACGTTGCTGGTCTTGCTTCCAAG
P010_ΔiolG_2	GGTTAGTGATGTAGCGCAGGCCGTG
P011_ΔiolW_1	AAGTGCTGCGGTGGTATGCGGTTTT
P012_ΔiolW_2	CTTGCGCGGGCGAGGAACTAACTCG
P013_ΔoxiB_1	ATGCATGATCTCCGGGTG
P014_ΔoxiB_2	CGGATATGACAACACTCC
P015_Δcg2313_1	GGAATGGGCTGCGTTG
P016_Δcg2313_2	GCAGAAGTTTCGGTGTG
P017_Δiol2_1	ACACCATCCGGGACAC
P018_Δiol2_2	ACTGCAATGCTGGCCTG
pMKEx2 plasmids	
P019_iolG_1	TTAACTTTAAGAAGGAGATATACCATGAGCAAGAGCCTTCGC
P020_iolG_2	CTTTCAGAAGTGGGTTTCTCCTTAAGCGTAGAAATC
P021_iolW_1	GATTTCTACGCTTAAGGAGAAACCCACTTCTGAAAG
P022_iolW_2	TGGCACCAGAGCGAGCTCTGCGGCCTTAGCTCAACTCAATGGTG
P023_oxiB_1	TTTAACTTTAAGAAGGAGATATACCATGACTCAGCAAGAACTTC
P024_oxiB_2	GCACCAGAGCGAGCTCTGCGGCCGCCTAGTTGTTTGCAGGGATC
P025_idhA3_E172D_1	GGACCATCTTCCTGGATACCCTCATCCACGATTTC
P026_idhA3_E172D_2	GAAATCGTGGATGAGGGTATCCAGGAAGATGGTCC
pPREx6 plasmids	
P027_pPREx2_1	GAAGGAGATATACATATGACCTGAGCTAGC
P028_pPREx2_2	GCCAGAACCGTTATGATG
P029_T7_ 1	CATCATAACGGTTCTGGCATGCGTCCGGCGTAGAG
P030_T7 _2	CTAGCTCAGGTCATATGTATATCTCCTTCTTAAAGTTAAACAAAATTATTTC
P031_x6_IolG_1	GCCTGCAGAAGGAGATATACAATGAGCAAGAGCCTTCGC
P032_x6_IolG_2	TTACTTCTCGAACTGTGGGTGGGACCAGCTAGCAGCGTAGAAATCTGGGCGAGG
P033_x6_OxiB_1	TTAACTTTAAGAAGGAGATATACATATGACTCAGCAAGAACTTC
P034_x6_OxiB_2	CGAACTGTGGGTGGGACCAGCTAGCCTAGTTGTTTGCAGGGATC
P035_x6_OxiD_1	TTTAAGAAGGAGATATACATATGACTCTTCGTATCGCC
P036_x6_OxiD_2	TGTGGGTGGGACCAGCTAGCCTAAACGTTGGCAGGGTTGAG
P037_x6_OxiE_1	TTTAAGAAGGAGATATACATATGAAAAACATCACCATCGG
P038_x6_OxiE_2	TGTGGGTGGGACCAGCTAGCTTAAGCAGATGGAACCAGCG

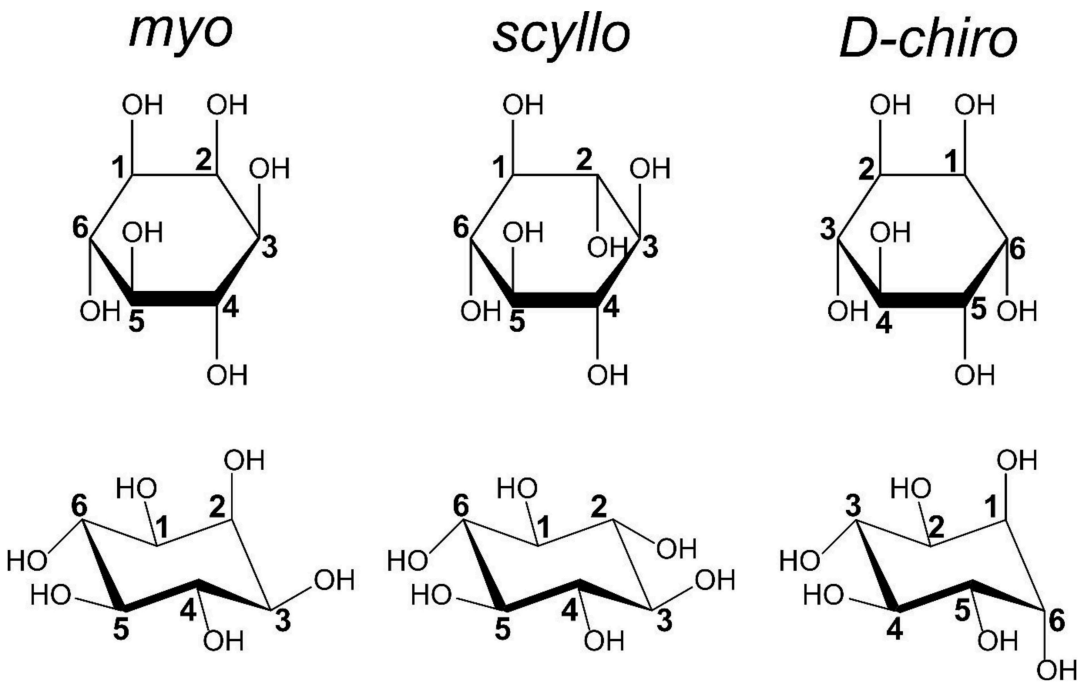

Fig. S1. Haworth projection and chair form of MI, SI, and DCI according to (11).

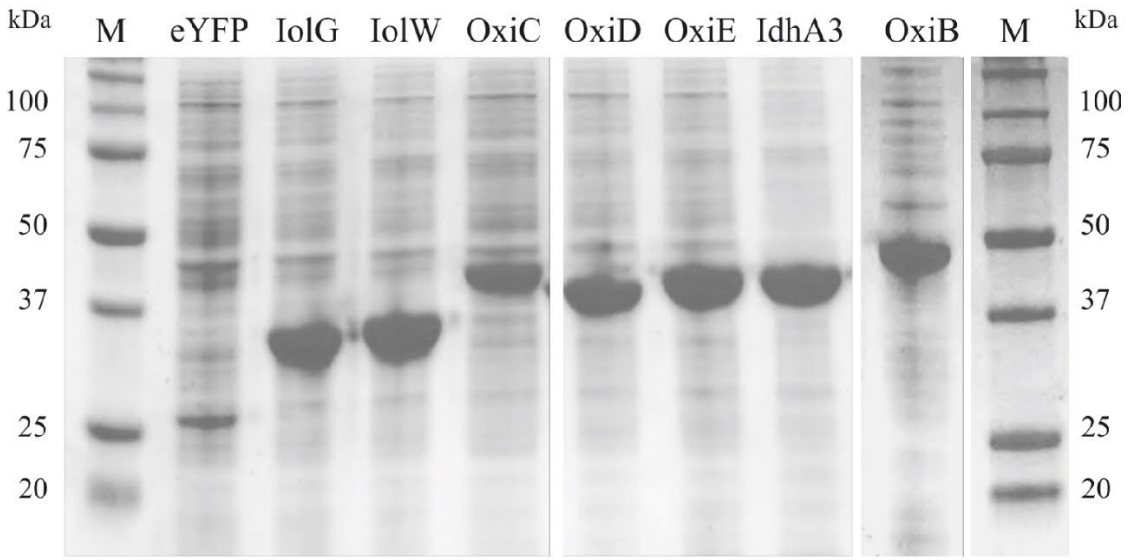

Fig. S2. SDS-PAGE of supernatant fractions of lysed *C. glutamicum* ΔIDH cells overproducing the indicated IDHs using pMKEx2-based expression plasmids. The gels were stained with Coomassie blue. M, protein standards; eYFP, control strain overproducing the eYFP protein (27 kDa).

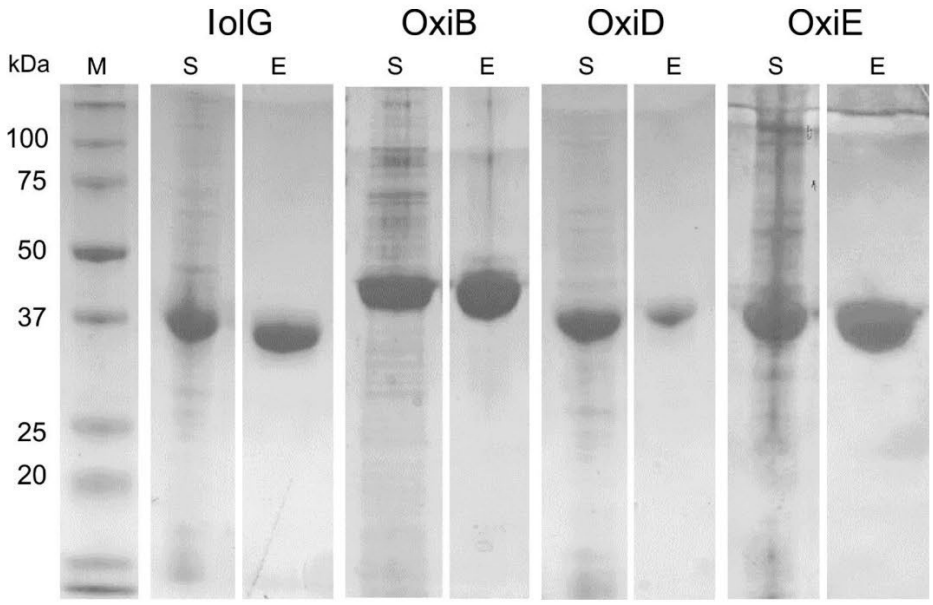

Fig. S3. Coomassie-stained SDS-polyacrylamide gels of purified IolG, OxiB, OxiD and OxiE. Shown are supernatant fractions of lysed *C. glutamicum* cells overexpressing the mentioned IDH (S) and final elution fractions after purification by affinity and size-exclusion chromatography.

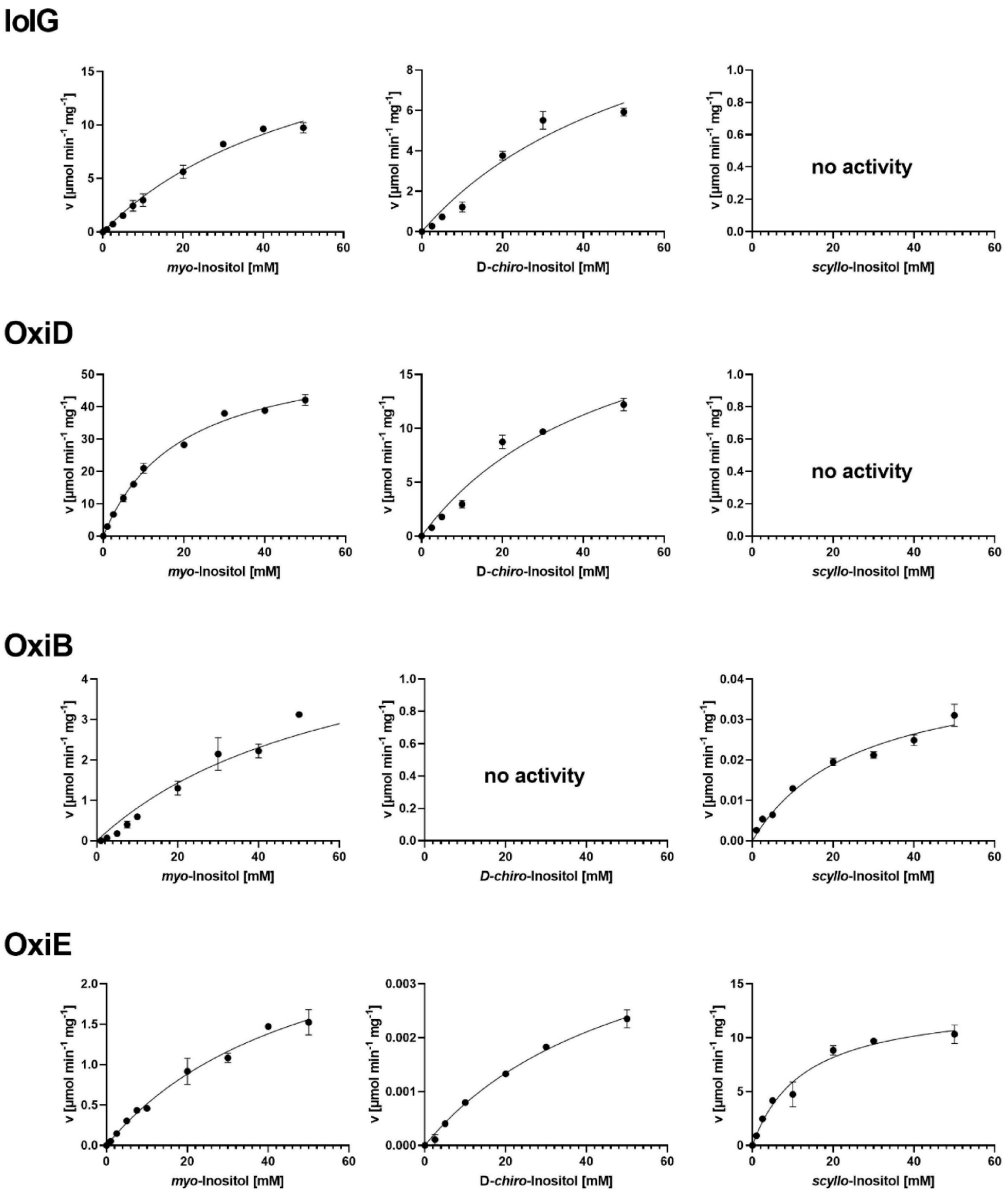

Fig. S4. Michaelis-Menten plots for the four indicated IDHs and the three different substrates MI, DCI, and SI. Kinetic constants were determined via a non-linear regression fit based on the Michaelis-Menten equation performed with the GraphPad Prism software.

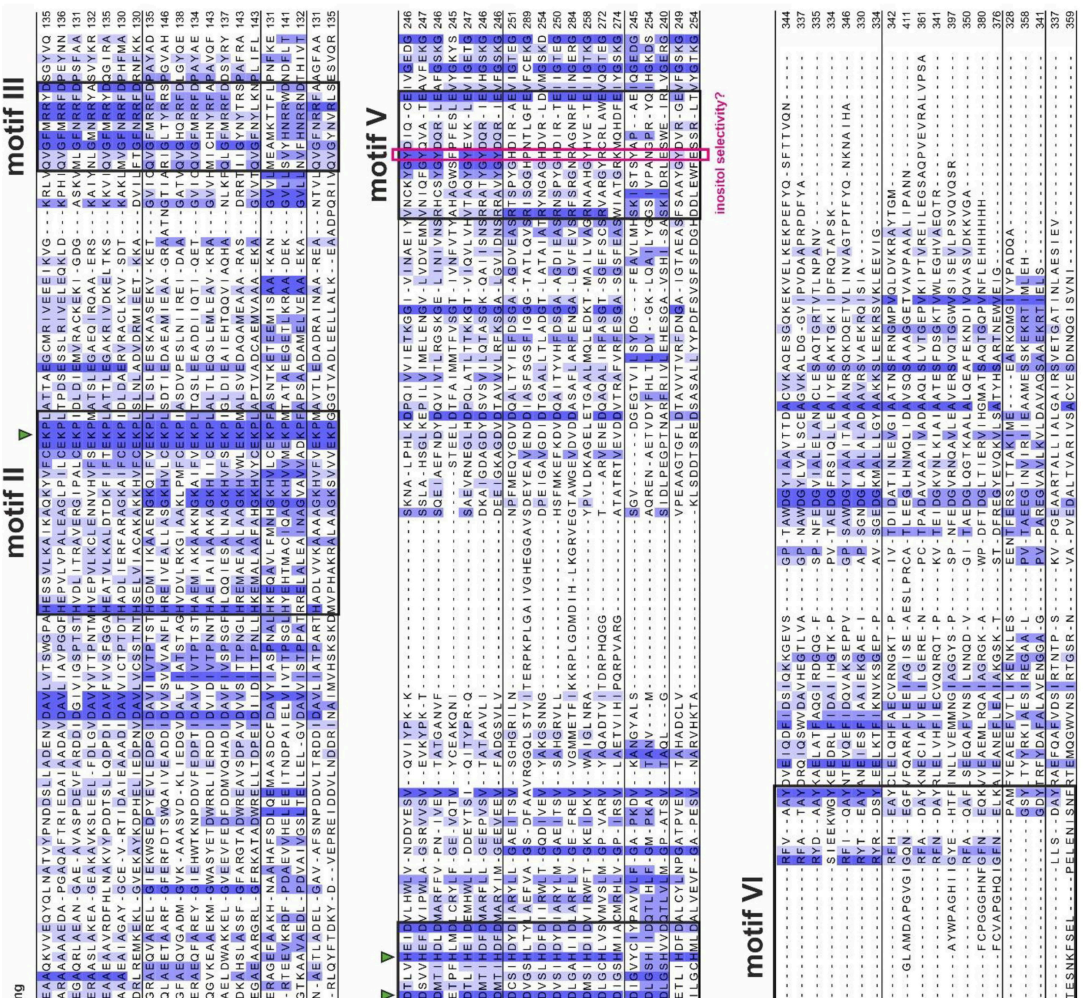
motif I
NAD(P) binding
motif II
motif III
GxGxxG consensus
motif IV
motif V
motif VI
inositol selectivity?
myo/gluco/scyllo + NAD+ (I)
myo/scyllo + NAD+ (II)
scyllo + NADP+ (III)
none (IV)

Fig. S5. Amino acid sequence alignment of the seven known or putative inositol dehydrogenases of *C. glutamicum* with characterized IDHs from other bacteria using Clustal Omega. Amino acid conservation for each subgroup is highlighted in blue color with intensity representing conservation rate. Highlighted are important residues and motifs for cofactor binding (motifs I and II with GxGxxG consensus sequence and residues 45-46) and for substrate binding and catalysis (motifs III-VI). The residues of the catalytic triade are highlighted by green arrows. The residue highlighted with a pink frame was identified to enable estimations of the substrate preferences of the IDHs (see text). The identifiers and references for the sequences from characterized IDHs of other bacteria are shown in Table S1.

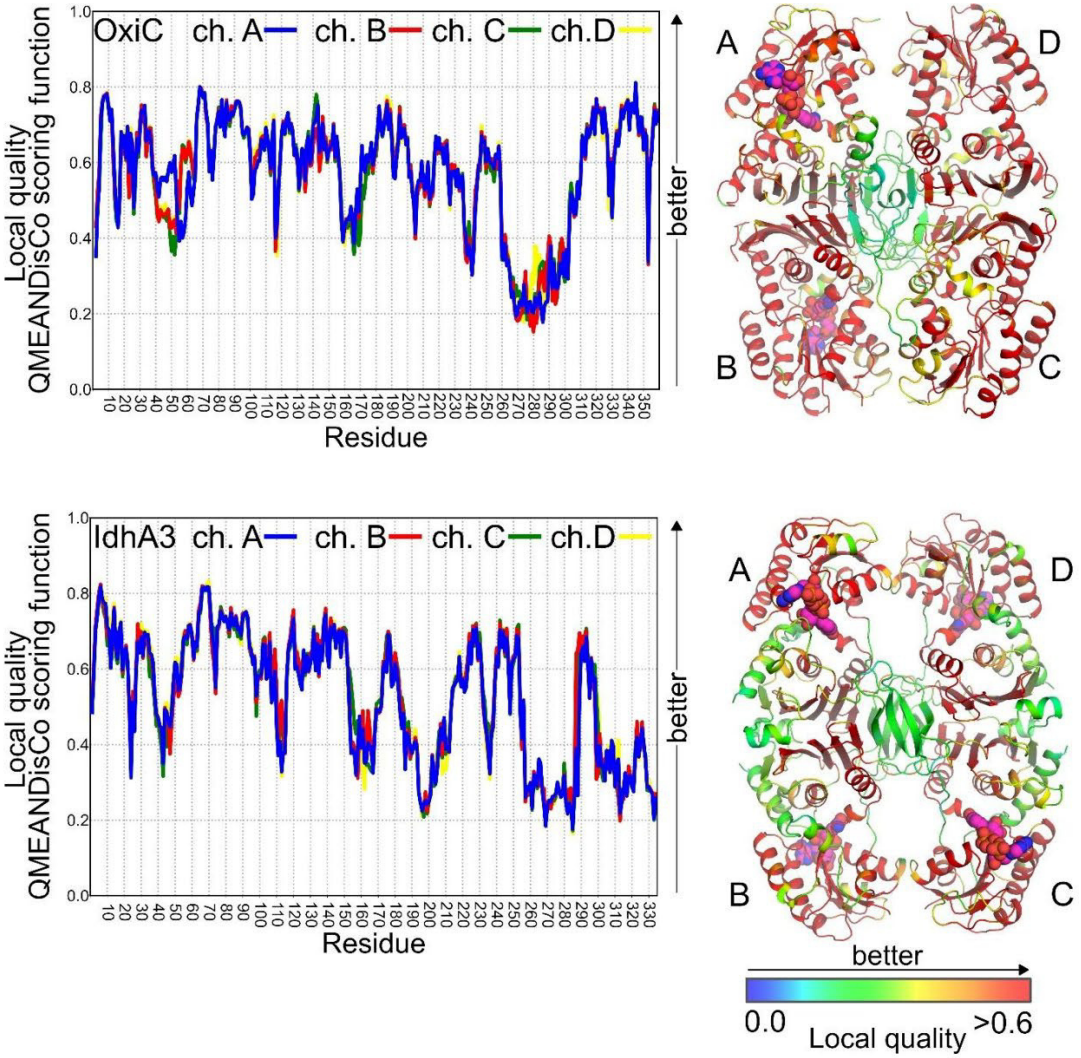

Continued next page

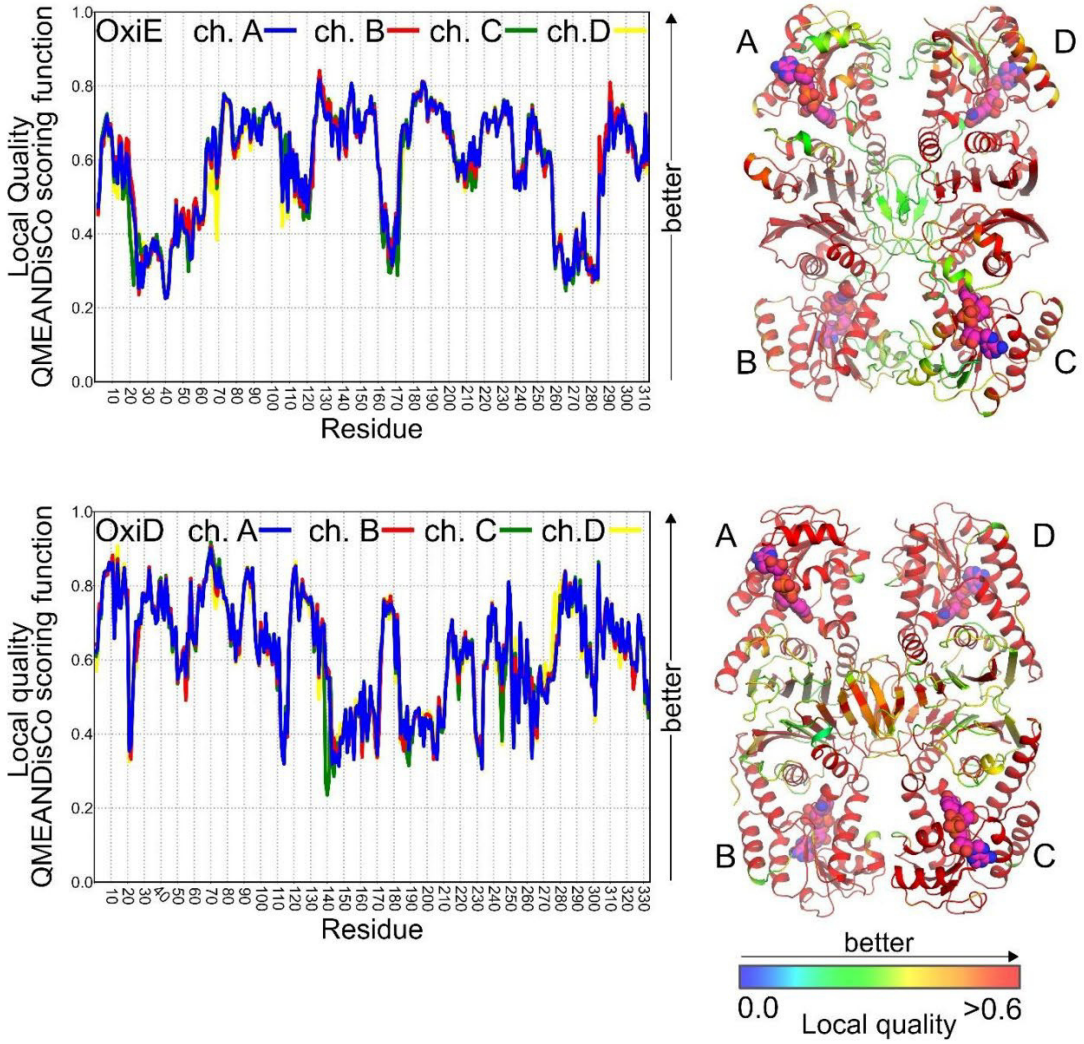

Continued next page

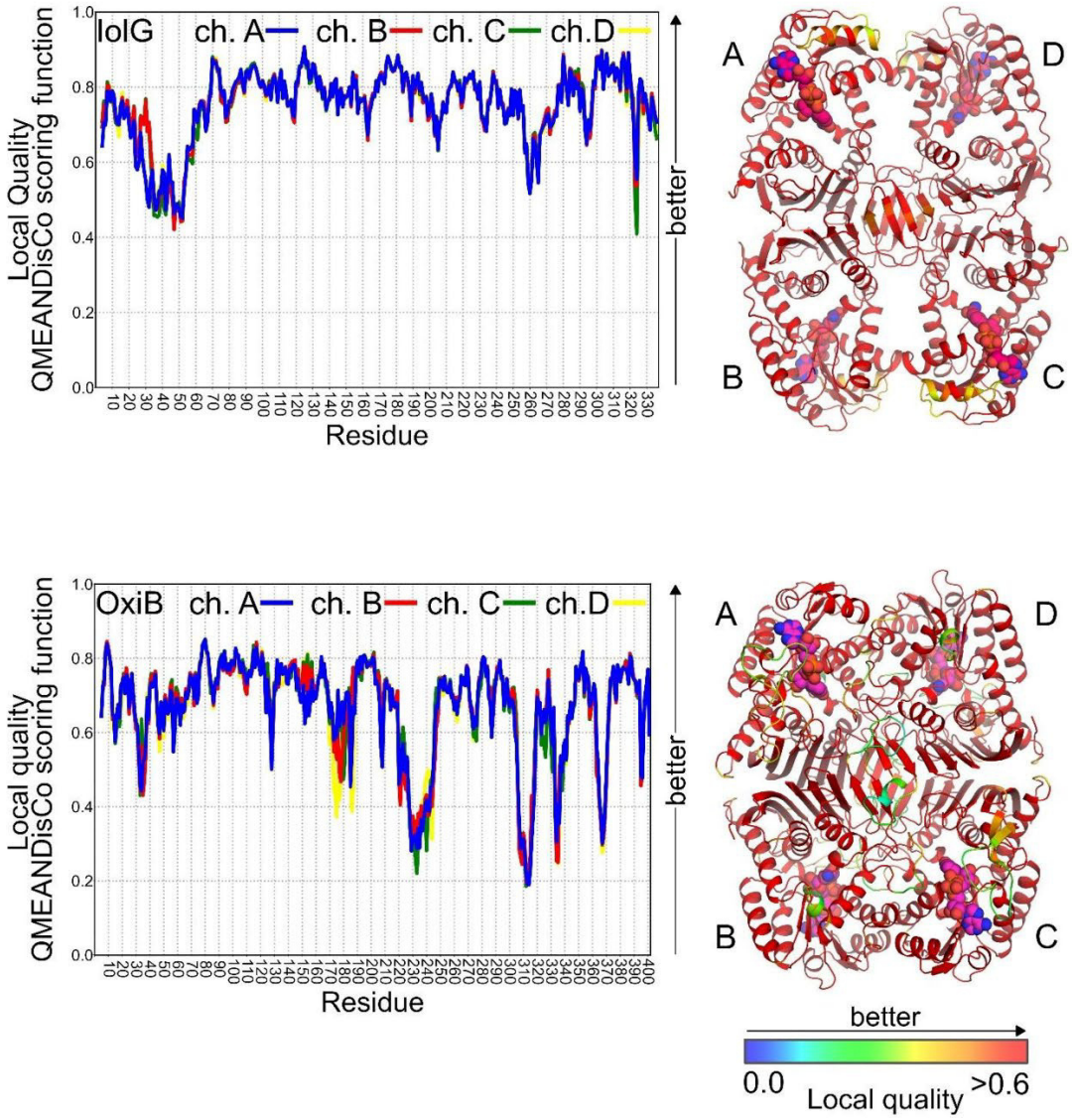

Fig. S6. Quality assessment of modeled IDHs. The per-residue model quality using the QMEANDisCo scoring function (10) is shown for each chain (ch. A, ch. B, ch. C, and ch. D) and mapped onto the modeled IDH structures. Values > 0.6 indicate a good quality. The cofactor positions are highlighted as spheres in magenta.

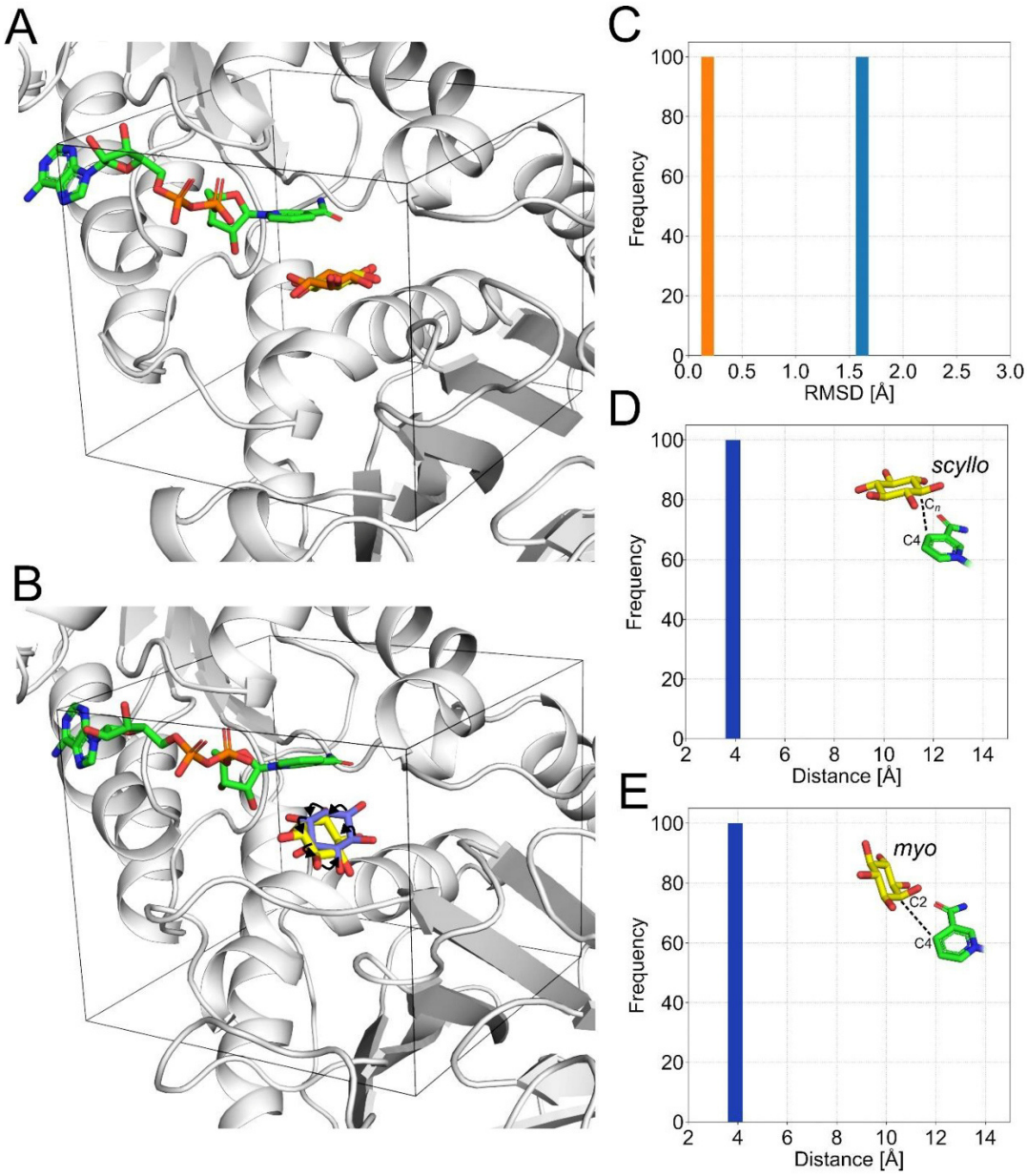

Fig. S7. Redocking of SI and MI. Redocking experiment of (A) SI into *L. casei* IDH2 (PDB id 4N54) and (B) MI into *L. casei* IDH1 (PDB id 4MIO). The SI and MI from the X-ray structures are shown in orange and blue, respectively. All docking poses are colored in yellow. The back box depicts the search space for finding docking poses. In panel B, the docked MI poses are slightly counter-clockwise rotated, indicated by black arrows. (C) Histogram of RMSD values of docked solutions versus the references SI (orange) and MI (blue). Distribution of distances between the reactive carbon of the docked (D) SI (mean 3.9 Å) or (E) MI (mean 4.1 Å) and the C4 carbon of the cofactor's nicotinamide group.

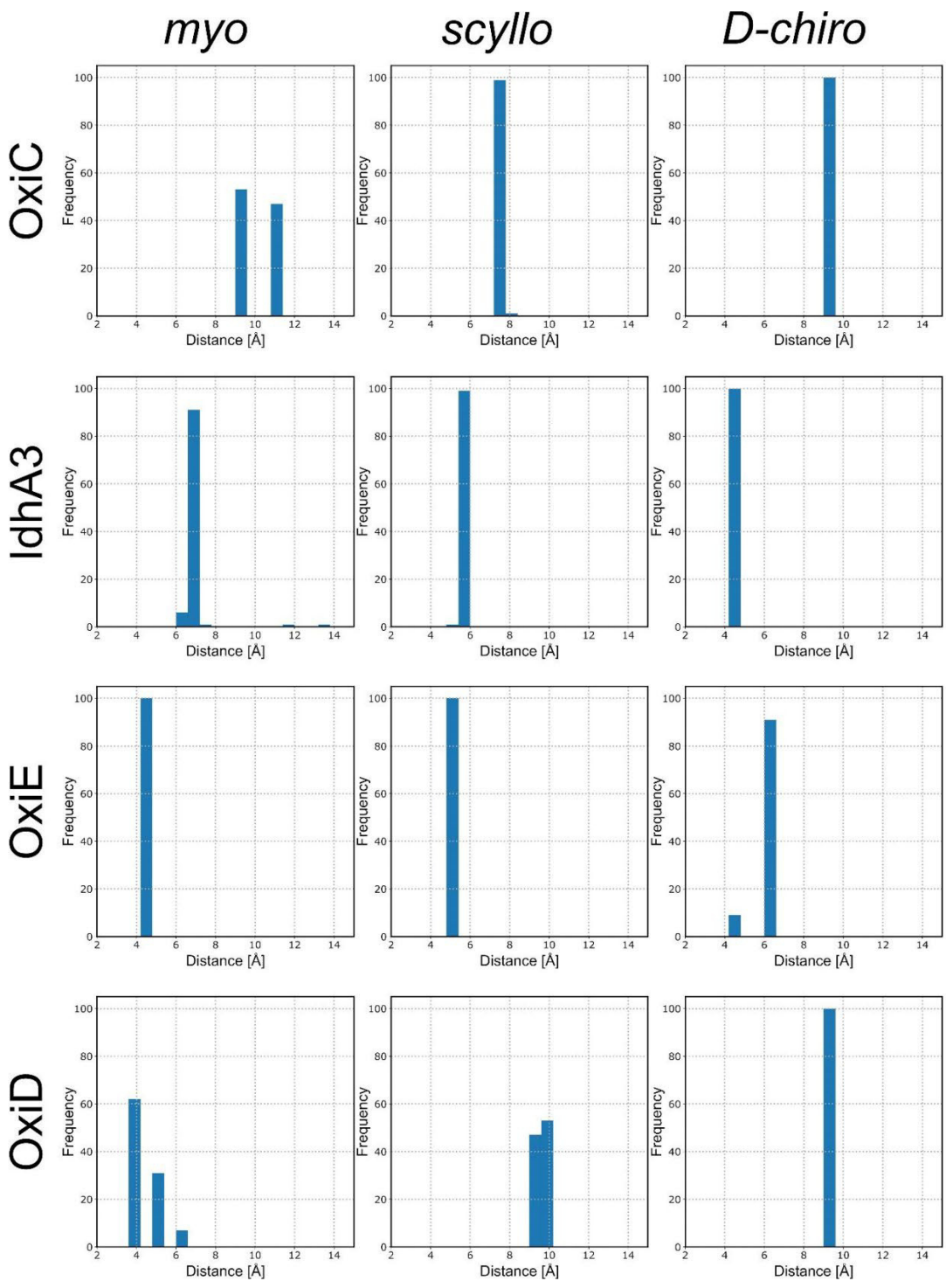

Continued next page

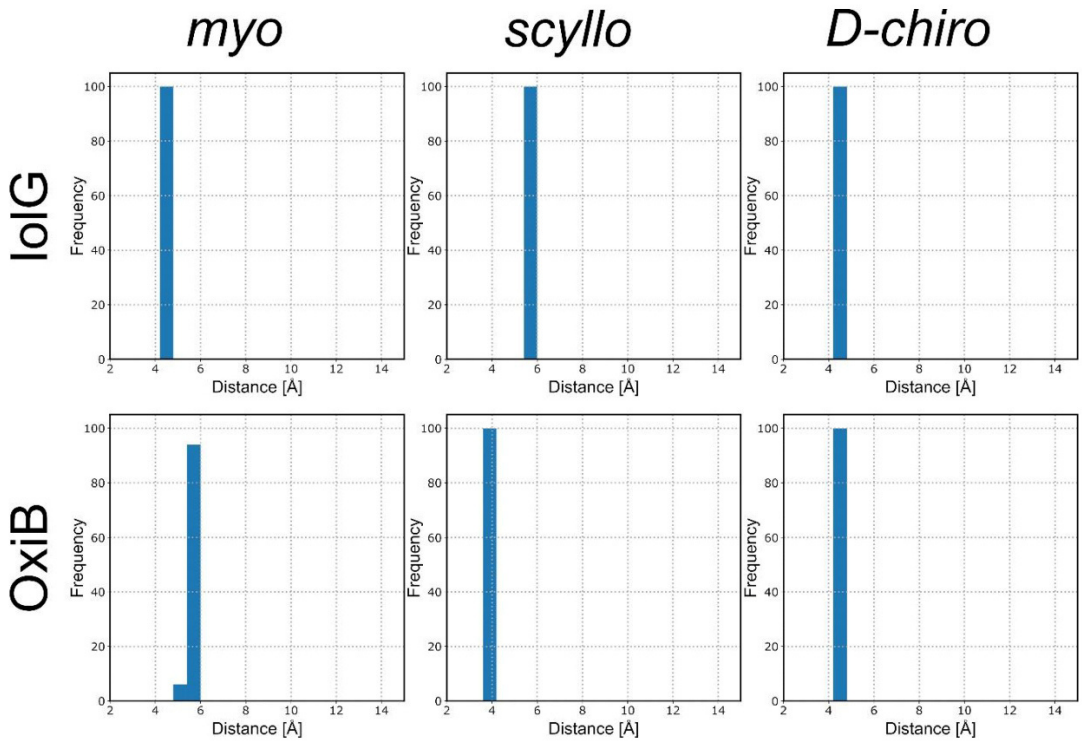

Fig. S8. Distribution of distances between the reactive carbon of the docked MI, SI, or DCI and the C4 carbon of the cofactors nicotinamide group.

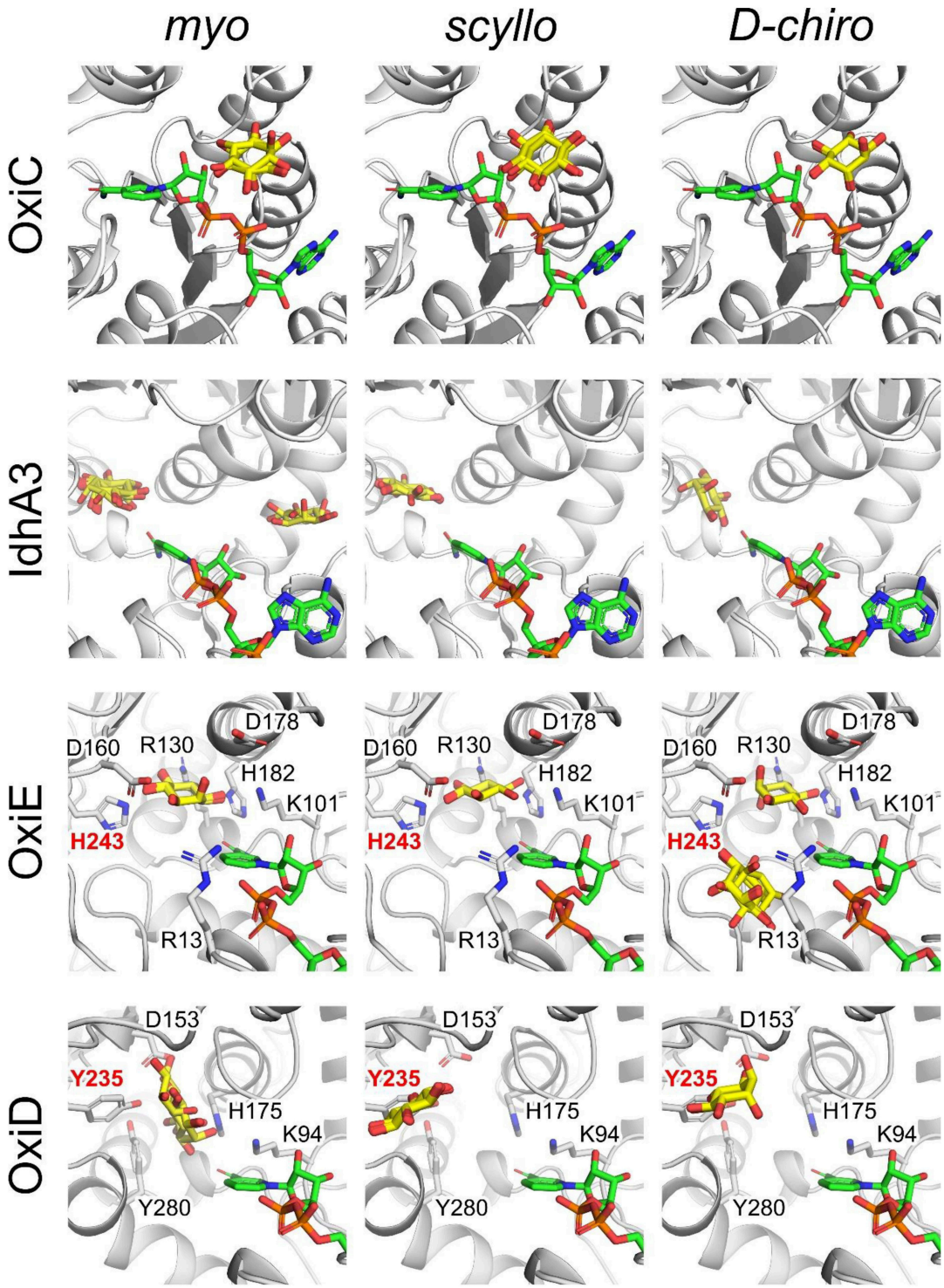

Continued next page

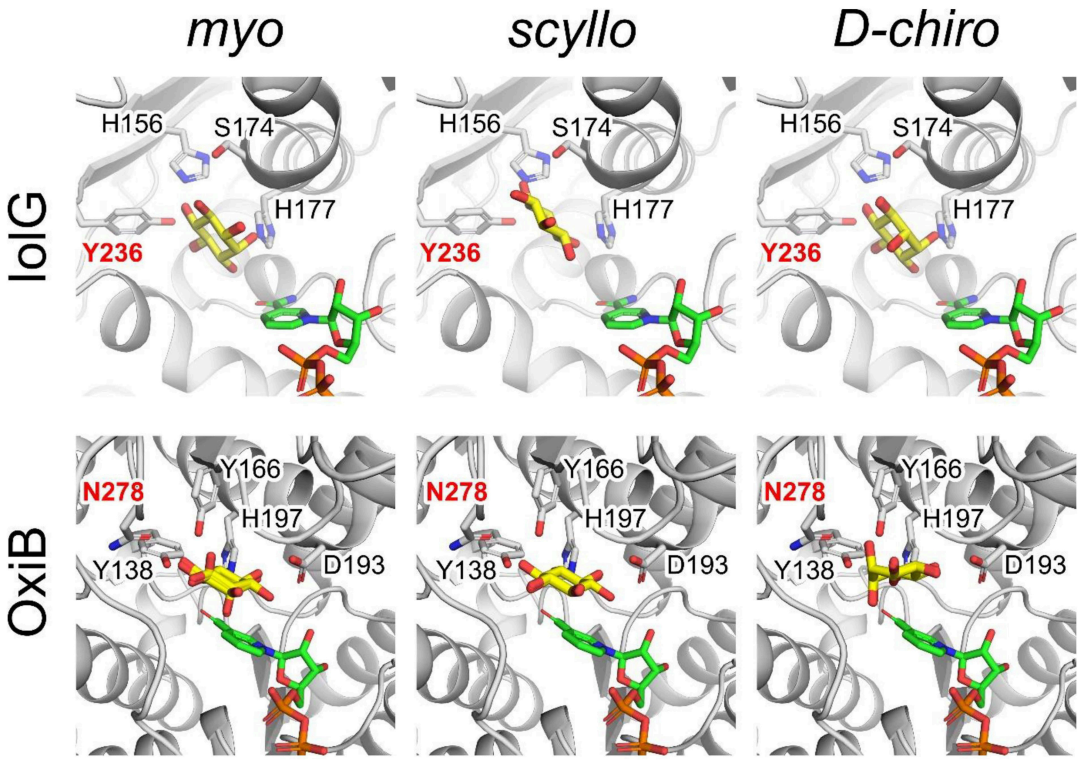

Fig. S9. Docked inositols into IDHs. Docking poses of MI, SI, and DCI into each IDH are shown in yellow, with the cofactor shown in green. If at least one valid docking result is found for the IDH, the residues that potentially form polar interactions with the docked inositol are shown as sticks. The predicted key interactions for IDH selectivity of the inositols (OxiE-H243, OxiD-Y235, IolG-Y236, OxiB-N278) derived from docking studies and the multiple sequence alignment shown (Fig. S5) are labeled in red.

REFERENCES

1. Ramaley R, Fujita Y, Freese E. 1979. Purification and properties of *Bacillus subtilis* inositol dehydrogenase. J Biol Chem 254:7684-7690.
2. Morinaga T, Ashida H, Yoshida K. 2010. Identification of two *scyllo*-inositol dehydrogenases in *Bacillus subtilis*. Microbiology 156:1538-1546.
3. Kang DM, Tanaka K, Takenaka S, Ishikawa S, Yoshida K. 2017. *Bacillus subtilis iolU* encodes an additional $NADP^+$-dependent *scyllo*-inositol dehydrogenase. Biosci Biotechnol Biochem 81:1026-1032.
4. Yoshida K, Sanbongi A, Murakami A, Suzuki H, Takenaka S, Takami H. 2012. Three inositol dehydrogenases involved in utilization and interconversion of inositol stereoisomers in a thermophile, *Geobacillus kaustophilus* HTA426. Microbiology 158:1942-1952.
5. Aamudalapalli HB, Bertwistle D, Palmer DRJ, Sanders DAR. 2018. *myo*-Inositol dehydrogenase and *scyllo*-inositol dehydrogenase from *Lactobacillus casei* BL23 bind their substrates in very different orientations. Biochim Biophys Acta 1866:1115-1124.
6. Rodionova IA, Leyn SA, Burkart MD, Boucher N, Noll KM, Osterman AL, Rodionov DA. 2013. Novel inositol catabolic pathway in *Thermotoga maritima*. Environ Microbiol 15:2254-2266.
7. Kohler PR, Zheng JY, Schoffers E, Rossbach S. 2010. Inositol catabolism, a key pathway in *Sinorhizobium meliloti* for competitive host nodulation. Appl Environ Microbiol 76:7972-7980.
8. Galbraith MP, Feng SF, Borneman J, Triplett EW, de Bruijn FJ, Rossbach S. 1998. A functional *myo*-inositol catabolism pathway is essential for rhizopine utilization by *Sinorhizobium meliloti*. Microbiology 144 2915-2924.
9. Fukano K, Ozawa K, Kokubu M, Shimizu T, Ito S, Sasaki Y, Nakamura A, Yajima S. 2018. Structural basis of L-glucose oxidation by *scyllo*-inositol dehydrogenase: Implications for a novel enzyme subfamily classification. PLoS One 13:e0198010.
10. Studer G, Rempfer C, Waterhouse AM, Gumienny R, Haas J, Schwede T. 2020. QMEANDisCo-distance constraints applied on model quality estimation. Bioinformatics 36:1765-1771.
11. Fasman GD. 2019. CRC Handbook of Biochemistry and Molecular Biology, 3rd edition ed. CRC Press, Taylor and Francis Group, Boca Raton.

2.3 Production of D-*chiro*-inositol with *Corynebacterium glutamicum* via two different synthesis routes

Ramp, P., Mack, C., Wirtz, A., Bott, M. (2022). – to be submitted

Author contributions

PR: Conceptualization, Methodology, Investigation, Writing Manuscript, Visualization

CM: Methodology, Investigation

AW: Methodology, Investigation

MB: Supervision, Writing – review & editing, Funding acquisition

Overall contribution: 80%

Production of D-*chiro*-inositol with *Corynebacterium glutamicum* via two different synthesis routes

Paul Ramp, Christina Mack, Astrid Wirtz, Michael Bott[#]

IBG-1: Biotechnology, Institute of Bio- and Geosciences, Forschungszentrum Jülich, Jülich, Germany

[#]Corresponding author: m.bott@fz-juelich.de

2.3.1 Abstract

D-*chiro*-inositol (DCI) is a promising drug candidate for treating insulin resistance and its associated diseases such as diabetes type 2 or polycystic ovary syndrome. Many bacteria can utilize DCI via a specific pathway as carbon and energy source. First, an inositol dehydrogenase (IDH) oxidizes DCI to the keto-intermediate 1-keto-D-*chiro*-inositol (1KDCI), and an inosose isomerase interconverts 1KDCI to 2-keto-*myo*-inositol (2KMI), which enters the main inositol catabolism. Both reactions are reversible. For the microbial cell factory *Corynebacterium glutamicum*, the IDHs that enable growth on DCI have been identified, but the inosose isomerase remains unknown. We therefore investigated the putative sugar phosphate isomerases that are located in the two gene clusters associated with inositol catabolism for their activity to interconvert 2KMI and 1KDCI. We identified Cg0212 as functional inosose isomerase and overproduction with the IDH IolG in a *C. glutamicum* mutant strain unable to degrade inositols led to the production of ~1.1 g/L DCI starting from 10 g/L MI. Production and complementation experiments revealed that *C. glutamicum*, besides Cg0212, possesses the inosose isomerase Cg2312 and at least one more unidentified inosose isomerase. In parallel, we established a novel synthetic production route for DCI starting from MI by utilizing the promiscuous activity of the two plant-derived NAD^+/NADPH-dependent D-ononitol and D-pinitol dehydrogenases MtOEPa and MtOEPb. Heterologous expression enabled an NAD^+/NADPH-driven, two-step process that produced ~1.6 g/L DCI from 10 g/L MI. Furthermore, the plasmids-based co-expression of the *MtOEPa* and *MtOEPb* genes with the endogenous *myo*-inositol-1-phosphate synthase (*ino1*) enabled direct production of 0.75 g/L DCI starting from 20 g/L glucose. By generating a novel, bicistronic expression vector containing two T7 promoters for *C. glutamicum* MB001(DE3), DCI production was increased by up to 70%, with a final titer of 1.2 g/L DCI starting from 20 g/L glucose (wt/vol). This demonstrates that *C. glutamicum* is an attractive host for the biotechnological production of D-*chiro*-inositol.

2.3.2 Introduction

D-*chiro*-inositol (DCI) is a cyclitol ($C_6H_{12}O_6$) and one of nine different isomers of inositol (*myo*-, *scyllo*-, *allo*-, *muco*-, *epi*-, *neo*-, D-*chiro*-, L-*chiro*-, and *cis*-inositol) (López-Gambero et al., 2020; Thomas et al., 2016). DCI is regarded as a therapeutic candidate for the treatment of metabolic illnesses linked to insulin resistance. Together with *myo*-inositol (MI), DCI regulates

several metabolic pathways and hormonal signaling in the human body and is involved in cell growth, survival, and reproduction (Chiofalo et al., 2017; Dinicola et al., 2014; Kachhawa et al., 2021; Vitale et al., 2021). As inositol phosphoglycans (IPGs), both MI and DCI (MI-IPG and DCI-IPG) function as second messengers involved in insulin signaling, with DCI-IPG being mainly involved in the regulation of glycogen synthesis (GS) and maintaining insulin sensitivity (Larner, 2002; Ortmeyer et al., 1993).

Insulin-resistant individuals, such as those with type 2 diabetes or women with polycystic ovary syndrome (PCOS), a diverse, multifaceted disorder characterized by ovarian dysfunction, infertility, hyperandrogenism, and name-giving polycystic ovaries, exhibit impaired synthesis of DCI-IPG (Homburg, 2008; Larner et al., 2010). Oral administration of DCI, both alone and in combination with MI, increased general insulin sensitivity in tissues of type 2 diabetes patients (Gambioli et al., 2021; Pintaudi et al., 2016) and induced ovulation in PCOS patients (Monastra et al., 2017; Ortmeyer et al., 1993).

The industrial preparation of DCI is currently achieved by removing the 3-*O*-methyl group of soybean-derived D-pinitol (DPIN) via chemical hydrolysis with a high concentration of hydrochloric or hydrobromic acid (Sanchez-Hidalgo et al., 2021). In recent years, an alternative biotechnological process for DCI was described. It is based on the fact that DCI was found in some microbial species, which can utilize inositols as single carbon and energy sources, such as *Bacillus subtilis*. In this species, MI and DCI are first taken up via specific transporters and then oxidized to 2-keto-*myo*-inositol (2KMI) and 1-keto-D-*chiro*-inositol (1KDCI), respectively, by the inositol dehydrogenase (IDH) IolG in a reversible reaction (Yoshida et al., 2006). The inosose isomerase IolI is then responsible for the reversible interconversion of 1KDCI to 2KMI, which then enters an inositol-specific catabolic pathway forming acetyl-CoA and dihydroxyacetone phosphate (Yoshida et al., 2006; Yoshida et al., 2008). IolI is a protein with a TIM barrel fold and structural similarity to both endonuclease IV and xylose isomerase (Yoshida et al., 2006). Enzymatic assays with purified IolI showed a reaction equilibrium with a molar ratio of 77:23 in favor of 2KMI. IolG is also able to reduce 1KDCI back to DCI with $NADH+H^+$. Thus, utilization of both IolG and IolI enables the production of DCI from MI (Yoshida et al., 2006). Using an engineered *B. subtilis* strain unable to degrade inositols and overexpressing IolG and IolI, production of DCI from MI with a yield of 6% was achieved (Yoshida et al., 2006).

Corynebacterium glutamicum is a soil-dwelling actinobacterium that is used as an industrial cell factory, in particular for large-scale production of L-glutamate and L-lysine (Becker et al.,

2018; Eggeling and Bott, 2015; Wendisch, 2020). In a recent study, we reported that *C. glutamicum* can grow not only with MI, but also with *scyllo*-inositol (SI) and DCI as single carbon and energy source, similar to *B. subtilis* (Ramp et al., 2022). We identified the IDHs IolG and OxiD catalyzing the initial oxidation of DCI, however, no IolI-type inosose isomerase that interconverts 1KDCI to 2KMI has been identified in *C. glutamicum* so far. In contrast to *B. subtilis*, *C. glutamicum* is not only able to degrade inositols, but also has the intrinsic capability to synthesize MI in two steps from glucose 6-phosphate, which makes it an attractive host for the production of inositols from cheap carbon sources. We recently demonstrated this potential by developing *C. glutamicum* strains that efficiently produce SI from glucose and sucrose (Ramp et al., 2021).

This study aimed for the engineering of *C. glutamicum* strains for the production of DCI. In that context, we searched for endogeneous isomerases catalyzing the conversion of 1KDCI to 2KMI to utilize them for DCI synthesis. We identified the inosose isomerases Cg0212, Cg2312 and Cg3390 in *C. glutamicum* that are able to catalyze this reaction. Overproduction of IolG together with Cg0212 in the chassis strain *C. glutamicum* MB001(DE3)Δ*IOL* unable to catabolize inositols allowed the production of DCI from MI with a yield of up to 11%. Importantly, we identified and implemented a novel alternative route for efficient production of DCI from MI which is based on the substrate promiscuity of two plant enzymes, the NAD^+-dependent D-ononitol dehydrogenase MtOEPa and the $NADP^+$-dependent D-pinitol dehydrogenase MtOEPb from *Medicago truncatula*. Using this pathway, also DCI production from glucose was achieved.

2.3.3 Materials and Methods

Bacterial strains, plasmids and growth conditions

All bacterial strains and plasmids used in this work are listed in Table 2.3.1. All cloning steps were performed with *Escherichia coli* DH5α as host. *E. coli* strains were cultivated at 37 °C on LB agar plates or in lysogeny broth (LB) (Bertani, 1951) with 50 µg/mL kanamycin when appropriate. For growth characterization, *C. glutamicum* was cultivated in a BioLector microcultivation system (m2p-labs, Baesweiler, Germany). Single colonies were transferred in BHI medium and cultivated for 8 h at 30°C as a first preculture. The second preculture containing defined CGXII medium (Keilhauer et al., 1993) with 0.03 g/L protocatechuic acid and 20 g/L glucose was inoculated with 10% of first preculture and cultivated for 16 h at 30°C.

Before inoculation of main cultures, cells were washed once with CGXII medium without a carbon source. BioLector cultivations were performed in 800 µL CGXII medium, which was supplemented with 1% (wt/vol) of the desired carbon source in 48-well FlowerPlates (m2p-labs, Baesweiler, Germany) at 1200 rpm at 30 °C. Growth in this system was measured online as scatterted light at 620 nm (Kensy et al., 2009). For protein production, *C. glutamicum* was cultivated in 200 mL BHI medium supplemented with 2% (wt/vol) glucose in 2 L baffled shake flasks at 100 rpm and 30°C. For production experiments, *C. glutamicum* was cultivated in 50 mL CGXII medium supplemented with 20 g/L glucose and for biotransformations with 10 g/L *myo*-inositol in 500 mL baffled shake flasks at 30°C and 130 rpm for 72 h. Where appropriate, 25 µg/mL kanamycin was added to the medium. Gene expression was induced by addition of isopropyl-β-D-thiogalactoside (IPTG) at the indicated concentrations. Bacterial growth was followed by measuring the optical density at 600 nm (OD_{600}) using an Ultrospec 2100 pro photometer (Biochrom).

Recombinant DNA work and construction of deletion mutants

All plasmids and oligonucleotides used in this study are listed in Table 2.3.1 and Table 2.3.S1, respectively. PCRs, DNA restrictions, and plasmid constructions were performed according to established protocols (Gibson et al., 2009; Green et al., 2012). DNA sequencing and oligonucleotide synthesis were performed by Eurofins Genomics (Ebersberg, Germany). Chemically competent *E. coli* cells were transformed according to an established protocol (Hanahan, 1983). *C. glutamicum* was transformed via electroporation as described previously (van der Rest et al., 1999). *C. glutamicum* MB001(DE3) deletion mutants were constructed via double homologous recombination as described previously (Niebisch and Bott, 2001) using the pK19mobsacB-derived plasmids. The chromosomal deletions were confirmed via colony-PCR using oligonucleotides annealing outside of the deleted region. For protein overproduction and purification genes were cloned into the recently described pPREx6 plasmid (Ramp et al., 2022) downstream of the T7 promoter and upstream of a Strep-Tag II sequence. For the construction of the pMKEx2-based expression plasmids, the corresponding target genes were cloned downstream of the *C. glutamicum* consensus ribosome binding site (RBS) via Gibson assembly. For construction of the bicistronic expression plasmid pMKEx2BiT7, we amplified the T7 promoter, the second multiple cloning site (MCS) and the corresponding terminator from pETDuet-1 using the oligonucleotides P62 and P63 and joined them with the pMKEx2 backbone amplified with the oligonucleotides P64xP65 and P66x67 (Table 2.3.S1) via Gibson

assembly. The DNA sequences of the *MtOEPa* and *MtOEPb* genes were codon-optimized for *C. glutamicum* and ordered as DNA strings from ThermoFisher Scientific.

Table 2.3.1. Bacterial strains and plasmids used in this study

Strain or plasmid	Relevant characteristics	Source or reference
Strains		
E. coli		
DH5α	F^- Φ80*dlac*Δ(*lacZ*)M15 Δ(*lacZYA-argF*) U169 *endA1 recA1 hsdR17* (r_K^- , m_K^+) *deoR thi-1 phoA supE44* λ^- *gyrA96 relA1*; strain used for cloning procedures	(Hanahan, 1983)
C. glutamicum		
MB001(DE3)	Derivative of the prophage-free strain MB001 with a chromosomally encoded *E. coli lacI* gene under control of its native promoter followed by the T7 RNA polymerase gene under control of the *lac*UV5 promoter.	(Kortmann et al., 2015)
MB001(DE3)Δ*iol1*Δ*iol2* (referred to as Δ*iol1*Δ*iol2*)	Derivative of MB001(DE3) in which both inositol clusters: iol1 cg0196-cg0212 and iol2 cg3389-cg3392 are deleted	(Ramp et al., 2021)
Δ*IOL*	Derivative of MB001(DE3)Δ*iol1*Δ*iol2* in which the putative inositol dehydrogenase cg2313 (*idhA3*) was deleted	This work
Δ*IOL* Δ*qsuB*	Derivative of Δ*IOL* in which qsuB is deleted	This work
Δ*IOL* Δcg2312	Derivative of Δ*IOL* in which cg2312 is deleted	This work
Δ*IOL* Δcg2716	Derivative of Δ*IOL* in which cg2716 is deleted	This work
Δ*IOL* Δcg2822	Derivative of Δ*IOL* in which cg2822 is deleted	This work
Δ*IOL* Δcg2917	Derivative of Δ*IOL* in which cg2917 is deleted	This work
ΔIDH	MB001(DE3) derivative with deletion of the genes *oxiC*-cg3390-*oxiD*-*oxiE* (cg3389-cg3392), *iolG* (cg0204), *iolW* (cg0207), *idhA3* (cg2313) and *oxiB* (cg0211)	(Ramp et al., 2022)
ΔIDHΔcg0212	ΔIDH derivative with deletion of the inosose isomerase genes cg0212	This work
ΔIDHΔIso	ΔIDHΔcg0212 derivative with deletion of the inosose isomerase gene cg2312	This work
Plasmids		
pK19mobsacB	Kan^R; plasmid for allelic exchange in *C. glutamicum*; (pK18 *ori*$V_{E.c.}$, *sacB*, *lacZ*α)	(Schäfer et al., 1994)
pK19mobsacB-Δcg2313	pK19mobsacB derivative with 1000 bp homologous flanks upstream and downstream of cg2313	This work
pK19mobsacB-Δcg0212	pK19mobsacB derivative with 1000 bp homologous flanks upstream and downstream of cg0212	This work
pK19mobsacB-Δcg2312-13	pK19mobsacB derivative with 1000 bp homologous flanks upstream and downstream of cg2312-2313	This work

pK19mobsacB-Δcg2716	pK19mobsacB derivative with 1000 bp homologous flanks upstream and downstream of cg2716	This work
pK19mobsacB-Δcg2822	pK19mobsacB derivative with 1000 bp homologous flanks upstream and downstream of cg2822	This work
pK19mobsacB-Δcg2917	pK19mobsacB derivative with 1000 bp homologous flanks upstream and downstream of cg2917	This work
pPREx6	Kan^R; pPREx2 derivative with P_{tac} exchanged for $P_{T7\text{-}lac}$ promoter	(Ramp et al., 2022)
pPREx6-IolH	Kan^R; pPREx6 derivative containing the *iolH* gene under control of P_{T7} and fused C-terminal to a Strep-tag II sequence	This work
pPREx6-Cg0212	Kan^R; pPREx6 derivative containing the cg0212 gene under control of P_{T7} and fused C-terminal to Strep-tag II sequence	This work
pPREx6-Cg3390	Kan^R; pPREx6 derivative containing the cg3390 gene under control of P_{T7} and fused C-terminal to Strep-tag II sequence	This work
pMKEx2	Kan^R; *E. coli-C. glutamicum* shuttle vector (*lacI*, P_{T7}, lacO1, pHM1519 ori_{Cg}; pACYC177 ori_{Ec}) for expression of target genes under control of the T7 promoter	(Kortmann et al., 2015)
pIolG	pMKEx2 derivative for overexpression of *iolG* (cg0204)	(Ramp et al., 2022)
pIolG-Cg0212	pMKEx2 derivative for overexpression of *iolG* (cg0204) and cg0212 in a synthetic operon	This work
pIolG-Cg2312	pMKEx2 derivative for overexpression of *iolG* (cg0204) and cg2312 in a synthetic operon	This work
pOEPa	pMKEx2 derivative for overexpression of MtOEPa (XM_003599277.2)	This work
pOEPb	pMKEx2 derivative for overexpression of MtOEPb (A0A396HGB9)	This work
pOEPa-b	pMKEx2 derivative for overexpression of MtOEPa and MtOEPb in a synthetic operon	This work
pOEPb-a	pMKEx2 derivative for overexpression of MtOEPb and MtOEPa in a synthetic operon	This work
pInoDCI	pMKEx2 derivative for overexpression of *ino1,* MtOEPa and MtOEPb in a synthetic operon	This work
pMKEx2-BiT7	pMKEx2-derivative containing two T7 promoters, lacOs, MCSs and T7 terminators in opposite direction	This work
pBiT7-InoDCI	pMKEx2-BiT7 containing *ino1* under control of T7-1 and MtOEPa and MtOEPb in a synthetic operon under control of T7-2	This work

Protein overproduction and purification

C. glutamicum MB001(DE3) was transformed with pPREx6-based expression plasmids for inositol dehydrogenase production and cultivated in 200 mL BHI medium supplemented with 20 g/L glucose. Gene overexpression was induced with 250 µM IPTG after 3 h and cells were harvested after 24 h of cultivation via centrifugation at 5,000 *g* for 20 min at 4 °C. Cell pellets

were washed and resuspended in 4 mL lysis buffer (100 mM KPO_4 pH 7.5, 150 mM NaCl, 1 mM $MgSO_4$) per g cell wet weight and lysed by five passages through a French Press at 124 MPa. The resulting cell extract was first centrifuged at 5,000 *g* and 4 °C for 20 min and the supernatant was then subjected to ultracentrifugation at 45,000 *g* and 4 °C for 1 h. The resulting supernatant was incubated with avidin (25 µg/mg protein) for 30 min on ice before performing purification on an Äkta pure protein purification system (Cytiva) via StrepTactin Sepharose affinity chromatography and subsequent size exclusion chromatography.

A StrepTrap HP 1 mL column (GE Healthcare) was equilibrated with binding buffer (100 mM KPO_4 pH 7.5, 150 mM NaCl, 1 mM $MgSO_4$) before loading the protein extract. The column was washed with 10 column volumes (CV) of binding buffer and remaining proteins were then eluted in six 0.5 ml fractions with elution buffer I (100 mM KPO_4 pH 7.5, 150 mM NaCl, 1 mM $MgSO_4$, 2.5 mM desthiobiotin). The protein-containing elution fractions were combined and concentrated by using a 10 kDa AMICON filter and centrifuging at 3,500 g and 4 °C to a final volume of 500 µL. The concentrated protein was then applied to a Superdex 200 Increase size exclusion chromatography column (GE Healthcare) that had been equilibrated with 2 CV of elution buffer II (100 mM KPO_4 pH 7.5, 1 mM $MgSO_4$). Protein was eluted with 1.5 CV of elution buffer II and collected in 2 mL fractions. The purity and the apparent molecular mass of the proteins after both purification steps were determined by 12% (wt/vol) SDS-PAGE according to standard procedures (Green et al., 2012). Protein concentrations were determined using the Bradford assay (Coomassie blue G-250) and measuring concentration-dependent blue coloration at 595 nm (Thermofisher Scientific).

In vitro interconversion studies

To analyze inososе isomerase activity *in vitro*, 50 µg of purified inososе isomerase was combined with 50 µg of purified IolG in 200 µL reaction buffer containing 50 mM KPO_4 pH 7.5, 1 mM $MgSO_4$, 0.1 mM $MnSO_4$, 5 mM NAD^+, and either 10 g/L MI or 10 g/L DCI. The reaction was incubated at 30°C for 16 h and stopped via heating at 85°C for 15 min. For inositol analysis, the samples were subjected to HPLC analysis.

Inositol analysis by HPLC

1 mL culture was centrifuged at 17,000 *g* for 20 min, the supernatant was filtered (0.2 µm syringe filter, Whatman™, GE Healthcare, Freiburg, Germany) and frozen at -20 °C until further analysis. Thawed samples were diluted with deionized water and used for HPLC analysis. A 5 µL sample was measured using an Agilent LC-1100 system (Agilent, Santa Clara, CA, USA) equipped with a Carbo-Pb Guard Catridge (Phenomenex, Aschaffenburg, Germany) and a Rezex RPM-Monosaccharide 300 × 7.8 mm column (Phenomenex, Aschaffenburg, Germany). Separation was performed at 85 °C with water as eluent at a flow rate of 0.6 mL/min. Sugar and sugar alcohols were detected with a refraction index detector operated at 35 °C.

2.3.4 Results and Discussion

Identification of enzymes with inososе isomerase activity in *C. glutamicum*

The inososе isomerase gene *iolI* of *B. subtilis* is part of the operon containing the conserved insositol catabolism genes. The genes encoding the conserved inositol catabolism in *C. glutamicum* are also organized as one operon but with different gene order and no *iolI* homolog. However, the two inositol clusters, *iol1* and *iol2,* contain additional genes that take part in inositol catabolism, as shown before (Ramp et al., 2022). They also contain three genes encoding putative sugar phosphate isomerases: IolH (Cg0205), Cg0212, and Cg3390 (Fig. 2.3.1).

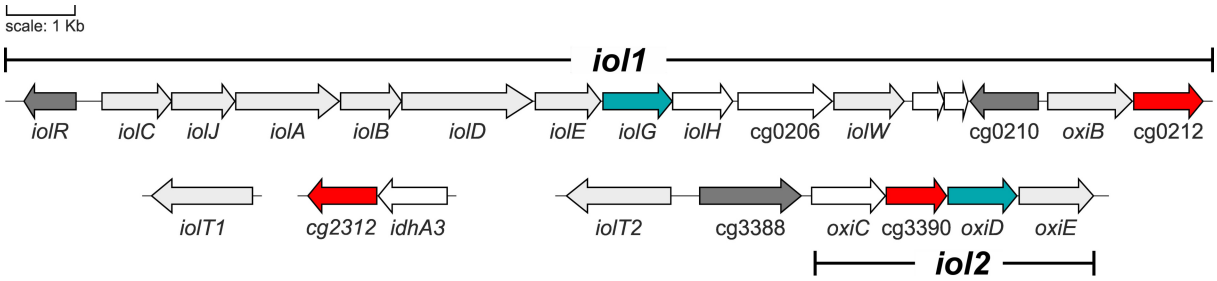

Fig. 2.3.1. **Genes related to inositol catabolism in *C. glutamicum.*** Genes shown in dark grey encode transcriptional regulators, genes in light grey have a known or predicted function, and genes in white have putative or unknown functions. The genes *iolG* and *oxiD* encoding IDHs with activity for DCI are shown in blue. Genes annotated as putative (sugar) phosphate isomerases (*iolH*, cg0212, cg3390) hypothesized to encode inososе isomerases are highlighted in red.

All three showed a sequence identity of 27-29% over a query cover of 20-54% to IolI of *B. subtilis*. *B. subtilis* also contains an IolH homolog that shows similarity to IolI, but no function has been described yet (Yoshida et al., 2006). Cg3390 was previously identified to be active on 2KMI, converting it to yet unknown, brown-colored compounds (Ramp et al., 2021). We hypothesized that one of these putative sugar phosphate isomerases has a similar function as IolI from *B. subtilis*.

To analyze if any of these putative isomerases enable interconversion of MI and DCI, we fused IolH, Cg0212, Cg3390 and the IDH IolG to a C-terminal Strep-Tag II and purified each enzyme after overproduction in *C. glutamicum* MB001(DE3) as described previously (Ramp et al., 2022). Each isomerase was tested *in vitro* for production of DCI or MI in the presence or absence of IolG with either MI or DCI as starting compound. No inositol interconversion was detected in all reaction mixtures containing only one enzyme and also in the reaction mixtures containing IolG and IolH, indicating that IolH does not catalyze the conversion of 2KMI to1KDCI. In contrast, when starting with MI, IolG in combination with Cg0212 led to the formation of 0.55 g/L DCI from 10 g/L MI, corresponding to a conversion rate of 5.5% (Fig. 2.3.2). When starting from 10 g/L DCI, this enzyme combination produced up to 3 g/L MI (30% conversion rate), indicating that this is the favored direction. In these reactions, the reduction of the keto-intermediate via IolG recovers NAD^+, which results in a cyclic reaction until the specific equilibrium is reached. In addition, the combination of IolG and Cg3390 enabled the conversion of MI to DCI, but in this case, only ~0.2 g/L DCI were formed from 10 g/L MI. In the opposite direction, nearly 1.0 g/L MI were synthesized from 10 g/L DCI, confirming this direction to be the favored one. For both reactions with IolG and Cg3390, much more substrate (7-8 g/L) disappeared than product was formed (Fig. 2.3.2) and the reaction mixture showed a brown coloration (data not shown). This effect was observed previously *in vivo* when IolG and Cg3390 were overproduced in the presence of MI (Ramp et al., 2021).

We assume that Cg3390 not only converts 2KMI to 1KDCI, but also to other unknown products that can be reduced irreversibly by IolG under regeneration of NAD^+. This shifts the concentration gradient so that more MI/DCI is processed as the new products leave the reaction cycle. For example, Cg3390 might catalyze the dehydration of 2KMI, leading to a diketo compound that IolG reduces. Such a reaction sequence would allow continued oxidation of MI by IolG. It is still unclear which compounds are formed and which are responsible for the brown coloration of the reaction mixture.

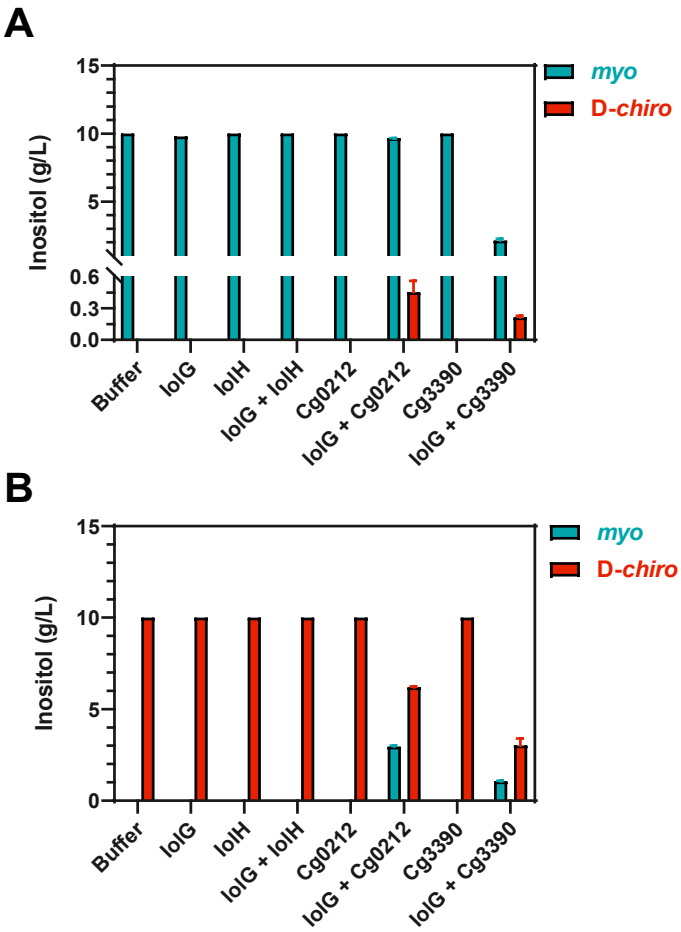

Fig. 2.3.2. *In vitro* enzymatic interconversion of DCI and MI with purified enzymes IolG, IolH, Cg0212 and Cg3390 starting from MI (A) or DCI (B). 50 µg purified protein each was mixed with MI or DCI in 200 µL reaction mixture and incubated at 30 °C for 24 h. Reaction was stopped by heating at 80°C for 15 min and inositol content was measured afterwards. Shown are inositol concentrations in g/L. Depicted are results from technical triplicates.

Establishment of a DCI production process

With Cg0212 identified as a functional isomerase enabling the conversion from MI to DCI, we aimed for a biotechnological production process with an engineered *C. glutamicum* strain that is unable to degrade inositols. We previously constructed *C. glutamicum* MB001(DE3)Δ*iol1*Δ*iol2* in which we deleted the gene clusters cg0196-cg0212 and cg3389-cg3392 (Fig. 2.3.1) (Ramp et al., 2021). We now additionally deleted the *idhA3* gene (cg2313), yielding the chassis strain *C. glutamicum* MB001(DE3)Δ*IOL*. For production of DCI, *iolG* and cg0212 were cloned as synthetic operon in the expression plasmid pMKEx2, which allows strong, inducible gene expression under the control of the T7 promoter. As controls, *iolG* and cg0212 were cloned separately in pMKEx2. The resulting plasmids pIolG-Cg212, pIolG and

pCg212 were introduced in *C. glutamicum* MB001(DE3)Δ*IOL*. A strain harboring pMKEx2 without insert served as an additional negative control.

All strains were cultivated in CGXII medium with 20 g/L glucose for biomass formation and 10 g/L MI as substrate for DCI synthesis at 30°C for 72 h. Overexpression of *iolG* and cg0212 led to the formation of ~ 1.1 g/L DCI from 10 g/L MI in 48 h, corresponding to a yield of ~11% (Fig. 2.3.3). To our surprise, overexpression of *iolG* alone also led to the accumulation of ~0.5 g/L DCI. As cg0212 and cg3390 as well as *iolH* were already deleted in *C. glutamicum* MB001(DE3)Δ*IOL*, this result hinted towards presence of yet another enzyme with inosose isomerase activity encoded in the genome of *C. glutamicum*.

A Blastp analysis using the amino acid sequence of IolI from *B.subtilis* as a template revealed the 3-dehydroshikimate dehydratase QsuB (cg0502) as closest homolog (21% identity, 51% query cover). To investigate if QsuB is responsible for DCI formation, we deleted the corresponding gene in *C. glutamicum* MB001(DE3)Δ*IOL* and analyzed the remaining DCI formation via overexpression of *iolG*. As negative control, we transformed *C. glutamicum* MB001(DE3)Δ*IOL* with the pMKEx2 empty vector. All strains were again cultivated in CGXII medium with 20 g/L glucose and 10 g/L MI at 30°C for 72 h. MI and DCI titers were measured at the end of the cultivation. To our surprise, the deletion of *qsuB* in a *C. glutamicum* MB001(DE3)Δ*IOL* had no effect on DCI production in comparison to the parental strain (Fig. 2.3.4). Both strains still produced up to 0.65 g/L DCI, indicating that QsuB is not the unknown inosose isomerase.

The InterPro database integrates predictive models or signatures representing protein domains, families and functional sites from multiple, diverse source databases (Hunter et al., 2009). This allows sorting a protein of interest into a protein family containing targets with similar domains and functional sites. IolI of *B. subtilis* is sorted into the Intepro xylose isomerase like superfamily (SSF51658). For *C. glutamicum* ATCC13032, a total of nine targets (Table 2.3.2) are classified in this xylose isomerase like superfamily. Among the identified proteins are the inositol dehydratase IolE, the mentioned isomerases IolH, Cg0212, Cg3390, and QsuB. The other identified proteins include the conserved, hypothetical protein Cg2917, the putative sugar phosphate isomerase Cg2822 and the two putative hydroxyl pyruvate isomerases Hyi (Cg2716) and Cg2312. It is noteworthy that cg2312 seems to be organized in an operon with cg2313, which encodes the putative inositol dehydrogenase IdhA3 (Ramp et al., 2022).

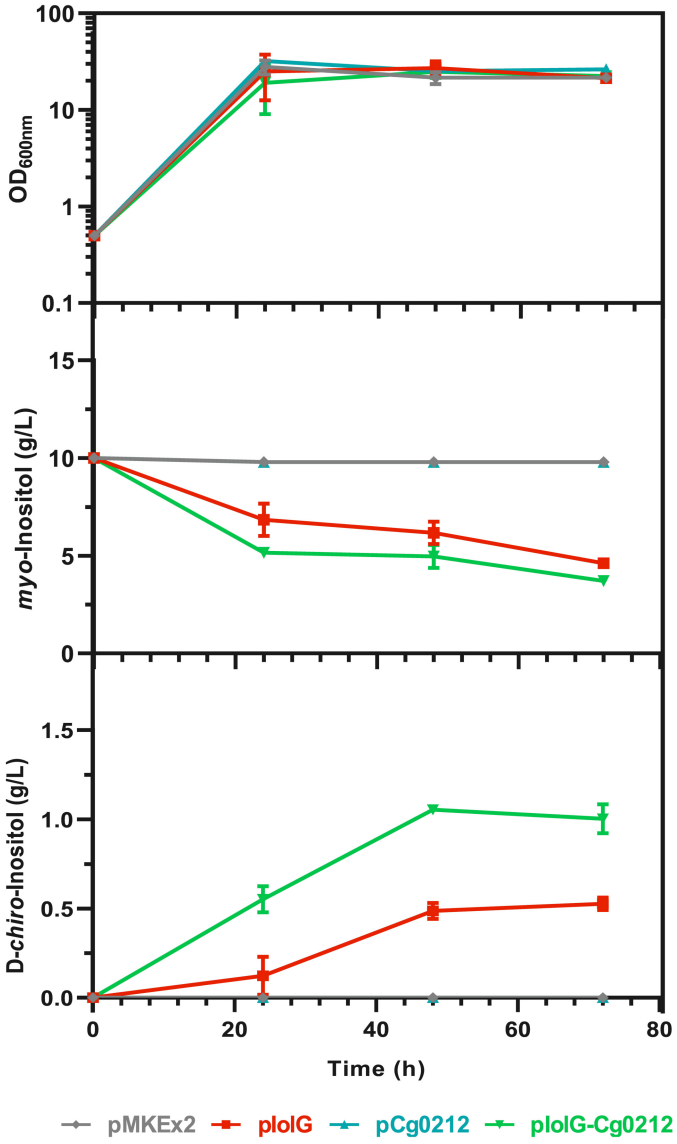

Fig. 2.3.3. Production of DCI from MI with *C. glutamicum* MB001(DE3)Δ*IOL* expressing IolG and Cg0212. Strains were cultivated in CGXII medium containing 20 g/L glucose and 10 g/L *myo*-inositol. Gene expression was induced by addition of 500µM IPTG at the cultivation start. Mean values of biological triplicates and standard deviations are shown.

We further focused on Cg2312, Cg2716, Cg2822 and Cg2917 since *iolE*, *iolH*, cg0212 and cg3390 are already deleted in *C. glutamicum* MB001(DE3)Δ*IOL* and *qsuB* deletion had no effect. We created individual deletion strains analogous to MB001(DE3)Δ*IOL*Δ*qsuB* and analyzed DCI production after 72h (Fig. 2.3.4). All strains reached the same final OD_{600} of ~30. Only the deletion of cg2312 led to a significantly decreased DCI titer of 0.37 g/L, while all other strains accumulated ~ 0.65 g/L DCI. However, because DCI formation was still observed in MB001(DE3)Δ*IOL*Δcg2312, at least one other inosose isomerases seems to be present.

Table 2.3.2. Xylose isomerase family proteins of *C. glutamicum* ATCC 13032 in the Interpro database.

Name	Locus tag	Accession number	Description
IolE	Cg0203	Q8NTY8	2-keto-*myo*-inositol dehydratase
IolH	Cg0205	Q8NTY6	sugar phosphate isomerases/epimerases
-	Cg0212	Q8NTX9	putative phosphate isomerase/epimerase
QsuB	Cg0502	Q8NT86	3-dehydroshikimate dehydratase
-	Cg2312	Q8NNS8	putative hydroxypyruvate isomerase
Hyi	Cg2716	Q8NMU3	hydroxypyruvate isomerase
-	Cg2822	Q8NML9	putative sugar phosphate isomerase
-	Cg2917	Q8NME4	conserved hypothetical protein
-	Cg3390	Q8NL87	putative sugar phosphate isomerase

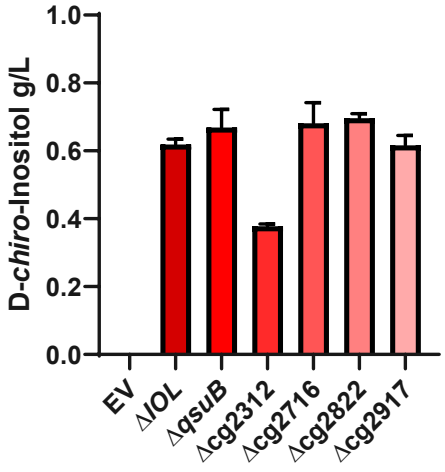

Fig. 2.3.4. DCI production by overexpression of *iolG* in *C. glutamicum* MB001(DE3)Δ*IOL* and derivatives in which *qsuB*, cg2312, cg2716, cg2822, or cg2917 was deleted. The strains were cultivated in CGXII medium containing 20 g/L glucose and 10 g/L *myo*-inositol for 72 h at 30°C. Gene expression was induced by addition of 500 µM IPTG at the start of the cultivation. Mean values of biological triplicates and standard deviations are shown.

To further test this hypothesis, we analyzed the growth on DCI of a *C. glutamicum* mutant, in which we deleted the identified inosose isomerases cg0212 and cg2312. We used the recently constructed mutant *C. glutamicum* MB001(DE3)ΔIDH, in which all seven IDHs were deleted as parental strain (Ramp et al., 2022). MB001(DE3)ΔIDH is unable to grow on DCI without complementary expression of a corresponding IDH, such as IolG. The resulting deletion strain

was named *C. glutamicum* MB001(DE3)ΔIDHΔIso and transformed with pMKEx2 plasmids containing *iolG* + cg0212 or cg2312. A strain transformed with pMKEx2-iolG served as control if growth can be restored without complementary expression of the identified inosose isomerases. As negative control the deletion strain was transformed with the plasmid pMKEx2-*eyfp*. *C. glutamicum* MB001(DE3) transformed with pMKEx2-*eyfp* served as positive control. Strains were cultivated in CGXII + 10 g/L DCI in a BioLector cultivation system at 30 °C for 72 h. Gene expression was induced in the overnight preculture cultivated in CGXII + 20 g/L glucose. Results are shown in Fig. 2.3.5.

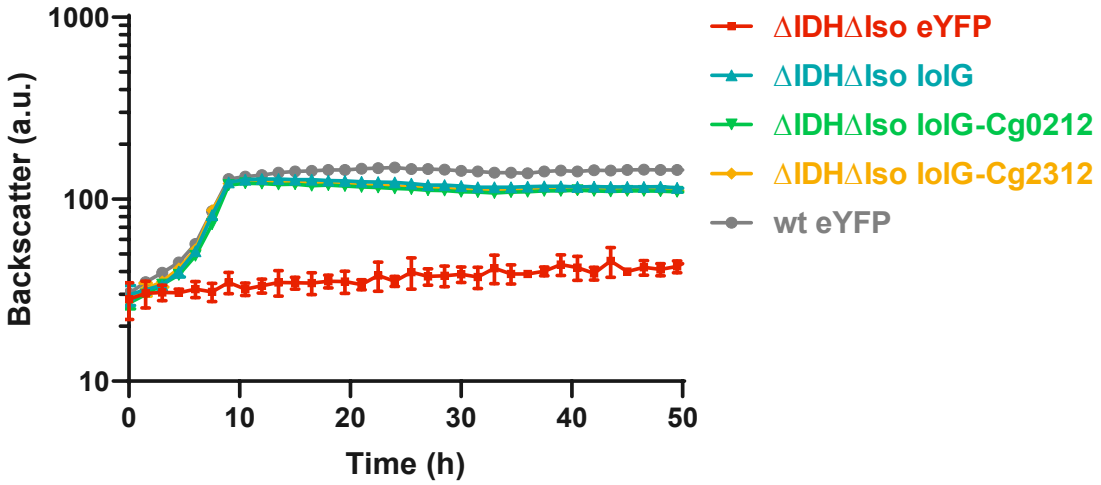

Fig. 2.3.5 Growth on DCI of *C. glutamicum* MB001(DE3)ΔIDHΔIso expressing the IDH *iolG* alone or in combination with the inosose isomerases or as negative control *eyfp* using the corresponding pMKEx2-based plasmids. *C. glutamicum* MB001(DE3) transformed with pMKEx2-eyfp was used as a positive control. The strains were cultivated in a BioLector system using CGXII minimal medium supplemented with DCI at 10 g/L. The cultures were incubated for 48 h at 30°C, 1200 rpm, and 85% humidity. Mean values and standard deviations of three biological replicates are shown. a.u. – arbitrary units.

As reported before, *C. glutamicum* MB001(DE3) (wt eYFP) grew on DCI, while *C. glutamicum* MB001(DE3)ΔIDHΔIso (ΔIDHΔIso eYFP) did not (Fig. 2.3.5). The expression of *iolG* alone was sufficient to restore growth to wild type level. Expression of cg0212 or cg2312 with *iolG* did not result in any difference to the strain expression *iolG* alone. This indicates the presence of another inosose isomerase, which interconverts 1KDCI to 2KMI. One possibility that cannot fully be excluded is that at least for growth, no additional inosose isomerase is necessary. *B. subtilis* was also found to grow solely on DCI and it possesses the inosose isomerase BsIolI, which interconverts 2KMI and 1KDCI. However, it was never analyzed if BsIolI is necessary

for growth on DCI. In addition, the inositol dehydratase IolE, which catalyzes the dehydration of 2KMI to yield 3D-(3,5/4)-trihydroxy-cyclohexane-1,2-dione (THcHDO) (Yoshida et al., 2004) for further degradation, was never analyzed for activity for other keto-inositol intermediates.

Developing a novel D-*chiro*-inositol production route in *C. glutamicum*

As described above, the strain *C. glutamicum* MB001(DE3)Δ*IOL* pIolG-Cg0212 enabled production of DCI from MI with a yield of 11%. However, this process is based on the unfavored backwards reaction of IolG reducing 1KDCI to DCI using NADH+H^+ and the reversible interconversion of 2KMI to 1KDCI by an isomerase with a reaction equilibrium in favor of 2KMI. Efficient DCI production with this strain therefore requires high concentrations of MI to drive the reaction in the direction of DCI and process regimes that allow *in situ* product removal, which might be difficult for two isomers such as MI and DCI. We therefore aimed to establish an alternative DCI production process that shifts the equilibrium in favor of DCI production.

In plants, DCI is mainly found as the 3-*O*-methylated derivative D-pinitol (DPIN) (3-*O*-methyl-D-*chiro*-inositol), which is synthesized from MI. MI is first methylated by an inositol methyl transferase (IMT) resulting in D-ononitol (ONO) (4-*O*-methyl-*myo*-inositol), which then is converted to D-pinitol. Recently, a two-step D-ononitol epimerization pathway was identified in *Medicago truncatula* (Pupel et al., 2019). In the first step, ONO is oxidized by the NAD^+-dependent dehydrogenase MtOEPa to 4-*O*-methyl-D-*myo*-1-inosoze. In the second step, the keto intermediate is reduced to DPIN by the NADPH-dependent D-pinitol dehydrogenase MtOEPb. As the only difference between ONO and MI and between DPIN and DCI is a single methyl group, we hypothesized that the two dehydrogenases MtOEPa and MtOEPb might also accept MI and D-*myo*-1-inosoze (synonym of 1KDCI) as substrates. Such a conversion would enable to drive the reaction towards DCI, as the cellular ratio of NAD^+/NADH (3.74 to 31.3) and $NADP^+$/NADPH (0.017 to 0.95) are in favor of NAD^+ and NADPH with absolute concentrations depending on the organism and growth conditions (Amador-Noguez et al., 2011; Andersen and von Meyenburg, 1977; Bennett et al., 2009; Spaans et al., 2015).

To test our hypothesis we cloned the *MtOEPa* and *MtOEPb* genes in synthetic operons with different gene orders (MtOEPa-b and MtOEPb-a) and individually in pMKEx2. The resulting plasmids were introduced into *C. glutamicum* MB001(DE3)Δ*IOL* and production of DCI from

MI was analyzed as described earlier. The expression of both dehydrogenases indeed enabled the formation of DCI (Fig. 2.3.6). Strain MB001(DE3)Δ*IOL* pOEPa-b accumulated up to 1.6 g/L DCI, whereas strain MB001(DE3)Δ*IOL* pOEPb-a formed only 0.5 g/L DCI starting from 10 g/L MI, showing that the gene order was relevant.

.

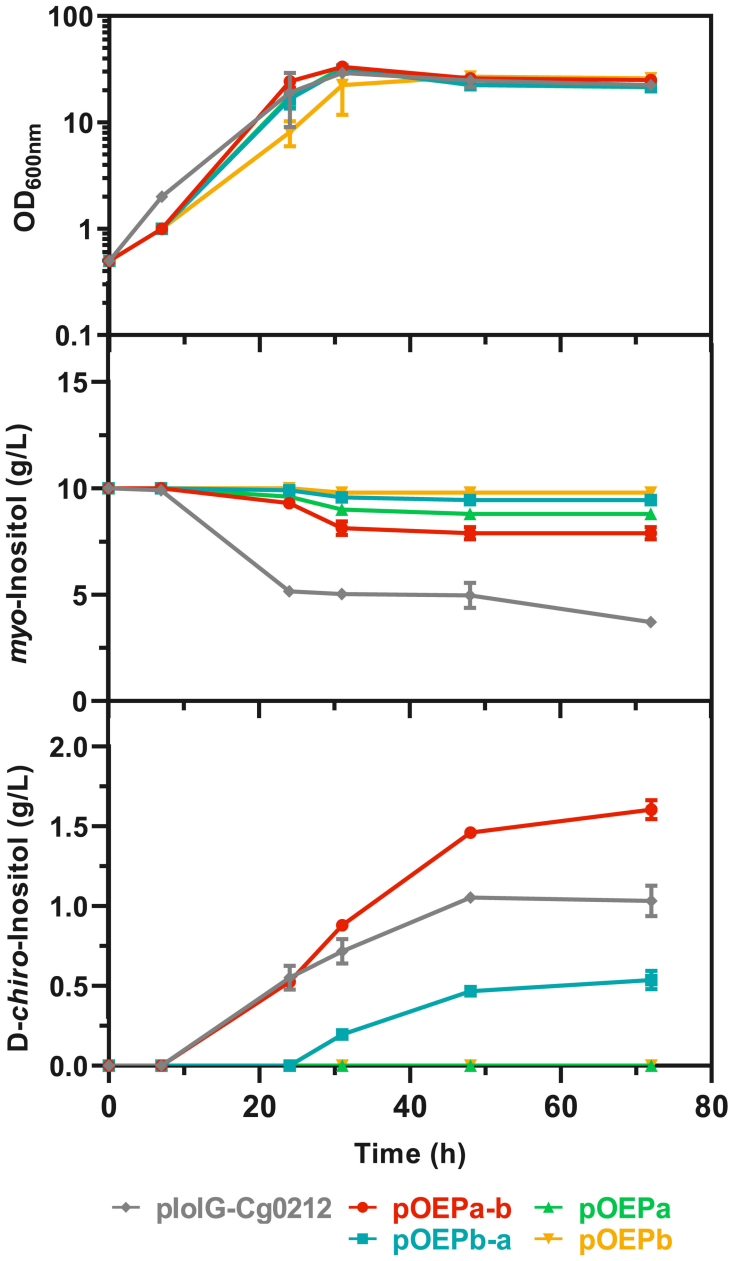

Fig. 2.3.6. Production of DCI from MI by expressing the two dehydrogenase genes *MtOEPa* and *MtOEPb* from the plant *M. trunculata* in *C. glutamicum* MB001(DE3)Δ*IOL*. The indicated strains were cultivated in CGXII medium containing 20 g/L glucose and 10 g/L *myo*-inositol. Gene expression was induced by addition of 500 µM IPTG at the start of the cultivation. Mean values of biological triplicates and standard deviations are shown.

C. glutamicum MB001(DE3)Δ*IOL* stills contains the inososе isomerases (Cg2312 + unknown) that interconvert 1KDCI and 2KMI, so we speculate that their presence hinder the reaction catalyzed by MtOEPa and MtOEPb. The production process using pOEPa-b will be repeated in a chassis strain in which all active inososе isomerases are deleted, once they are identified.

Production of DCI from glucose with *C. glutamicum*

With the use of the new two-step DCI production route based on MtOEPa and MtOEPb we also aimed for production of DCI from cheaper carbon sources like glucose. In a recent study we established production of SI from glucose and sucrose utilizing the innate ability of *C. glutamicum* to synthesize MI from glucose 6-phosphate via the *myo*-inositol-1-phosphate synthase Ino1 followed by dephosphorylation via an inositol monophosphatase (Chen et al., 2019). By overexpression of *ino1* together with the inositol dehydrogenase genes *iolG* and *iolW* production of SI from cheaper carbon sources was achieved (Ramp et al., 2021).

We cloned the *MtOEPa* and *MtOEPb* genes in a synthetic operon with *ino1* in pMKEx2 and introduced the resulting plasmid pInoDCI (Fig. 2.3.7A) in *C. glutamicum* MB001(DE3)Δ*IOL*. The strain was cultivated in CGXII medium with 20 g/L glucose for 72 h at 30°C in comparison to an empty vector containing strain. Gene expression was induced via supplementation of 500 µM IPTG after three hours. *C. glutamicum* MB001(DE3)Δ*IOL* pInoDCI grew similar to the empty vector control (Fig. 2.3.S1) and indeed accumulated up to 0.75 g/L DCI and 0.4 g/L MI after 72 h (Fig. 2.3.7B). The accumulation of MI hinted towards a limitation in the conversion of MI to DCI by MtOEPa and MtOEPb.

Gene order in synthetic operons resulting in polycistronic mRNAs encoding biochemical pathways is of relevance for optimally tuned gene expression. Translation initiation levels decrease with increasing distance to the transcriptional start (Lim et al., 2011). It is therefore likely to be assumed that expression, especially of the gene for MtOEPb, is insufficient for ideal DCI formation. To improve expression of the genes for MtOEPa and MtOEPb, but also keep a high expression level of *ino1* we constructed a new pMKEx2 expression plasmid allowing for bicistronic gene expression under the control of two T7 promoters. There are already multiple examples of bicistronic expression vectors for *C. glutamicum* (Gauttam et al., 2019; Goldbeck and Seibold, 2018; Liu et al., 2017), yet there is no plasmid containing two T7 promoter that would allow strong expression in *C. glutamicum* MB001(DE3). We amplified an expression cassette encoding the T7 promoter, a multiple cloning site including a ribosome binding site

plus a NdeI restriction site and a terminator from the bicistronic expression plasmid pET-DUET-1 and cloned this cassette in opposite direction to the original T7 promoter of pMKEx2, yielding the bicistronic expression plasmid pMKEx2-BiT7 (Fig. 2.3.7A).

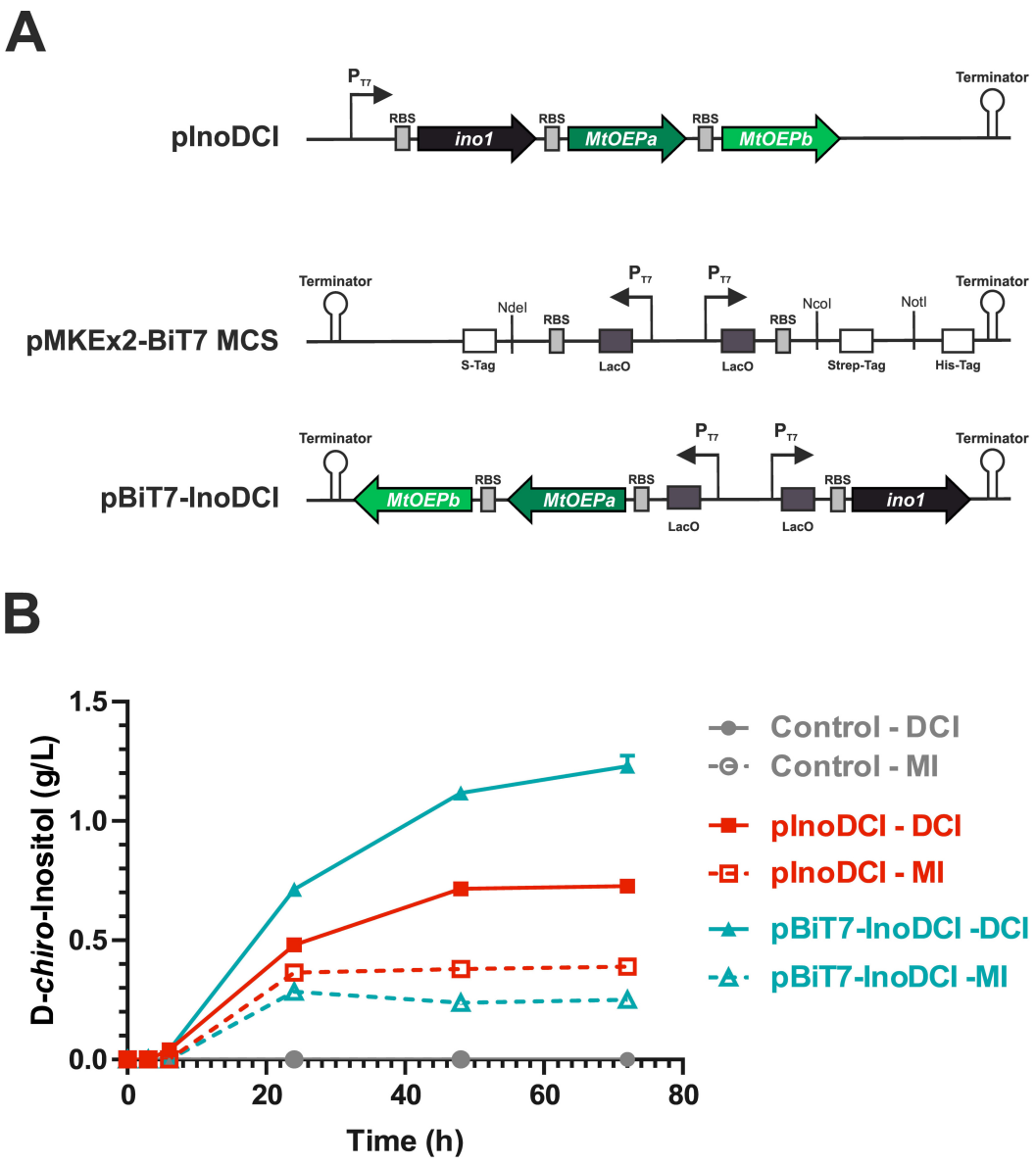

Fig. 2.3.7 Synthetic operons for the production of DCI starting from glucose. (A) Schematic overview of the expression cassettes of pInoDCI cloned in a single direction in pMKEx2 and the cloning sites in the newly constructed expression vector pMKEx2-BiT7 with the resulting bicistronic expression cassette of pBiT7-InoDCI. **(B)** Production of DCI and MI from glucose by expressing the dehydrogenase genes *MtOEPa* and *MtOEPb* plus *ino1* in two different expression cassettes in *C. glutamicum* MB001(DE3)Δ*IOL*. *C. glutamicum* MB001(DE3)Δ*IOL* containing pMKEx2 (Control) served as negative control. Strains were cultivated in CGXII medium containing 20 g/L glucose for 72h at 30°C. Gene expression was induced by addition of 500 µM IPTG after 3h of the cultivation start. Mean values of biological triplicates and standard deviations are shown.

We then cloned *ino1* under the control of the first and MtOEPa-b under the control of the second T7 promoter yielding the bicistronic plasmid pBiT7-InoDCI (Fig. 2.3.7A). The bicistronic expression of all genes did not affect growth (Fig. 2.3.S1) and led to an about 70% increase in DCI production with decreased accumulation of MI. At the end of the cultivation ~1.2 g/L DCI accumulated and 0.23 g/L MI (Fig. 2.3.7B). This indicates that functional expression of *MtOEPa* and *MtOEPb* is indeed one bottleneck in DCI production in *C. glutamicum*.

2.3.5 Conclusion and Outlook

We previously established *C. glutamicum* as a suitable host for the biotechnological production of SI, a promising drug candidate against Alzheimer's disease. In this study, we constructed *C. glutamicum* strains that enable the biotechnological production of another pharmacologically highly interesting inositol isomer: D-*chiro*-inositol. We identified the three inositol isomerases Cg0212, Cg2312 and Cg3390 in *C. glutamicum* that enable the interconversion of 2KMI to 1KDCI. Overexpression of cg0212 together with *iolG* led to DCI production from MI with yields of up to ~11%. Yet, *C. glutamicum* possesses at least one additional isomerase, which catalyzes the interconversion of 2KMI to 1KDCI, indicated by both, production and growth experiments. Further investigation will focus on identifying all residual putative inosose isomerases. Utilizing the promiscuous activity of the two D-ononitol and D-pinitol dehydrogenases MtOEPa and MtOEPb of the plant *M. trunculata*, we also established an alternative production route of DCI from MI and even glucose (Fig. 2.3.8). The final titer could be increased to 1.2 g/L DCI via bicistronic expression of *MtOEPa* and *MtOEPb* together with *ino1* from the novel generated *C. glutamicum* expression plasmid pMKE2-BiT7. Inositols become more and more of interest for pharmacological application, therefore cheap and efficient biotechnological production processes are highly desirable. With further engineering *C. glutamicum* has the potential to serve as a suitable host for the industrial production of MI, SI and DCI.

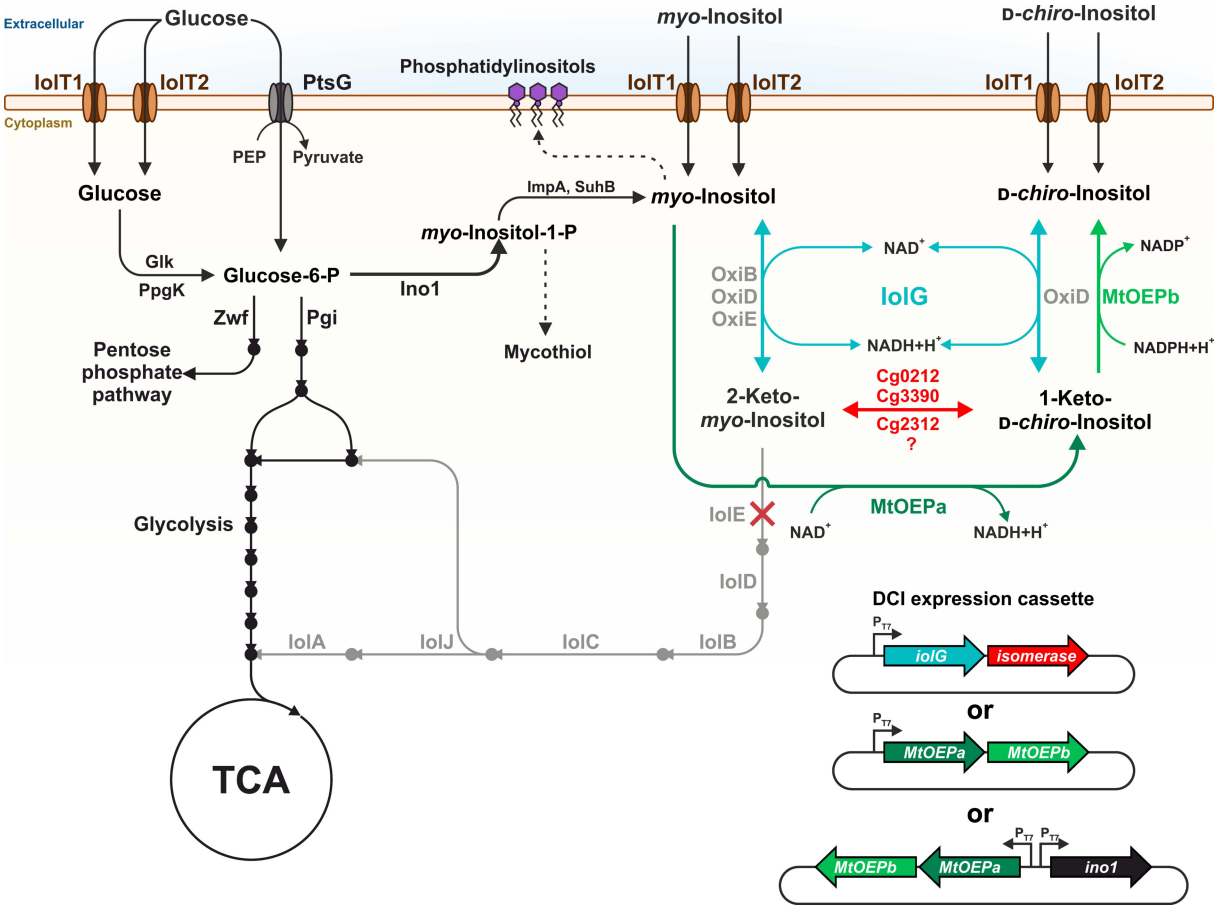

Fig. 2.3.8 Schematic overview of *myo*- (MI) and D-*chiro*-inositol (DCI) catabolism and engineered pathways for DCI production in *C. glutamicum* MB001(DE3)Δ*IOL*. Production of DCI from MI can either be achieved via IolG + inosose isomerase (blue + red arrows) or via the synthetic route consisting of *MtOEPa* + *MtOEPb* (green arrows). Conserved inositol catabolism (grey arrows and grey names) is deleted in *C. glutamicum* MB001(DE3)Δ*IOL*. 2-keto-*myo*-inositol cannot be degraded in the generated chassis strain (red cross at branch point). Reactions leading to cell constituents requiring L-*myo*-inositol-1-phosphate or *myo*-inositol for synthesis are indicated with dashed arrows.

2.3.6 Acknowledgements

This project was financially supported by the CLIB-Competence Center Biotechnology (CKB) funded by the European Regional Development Fund ERDF [grant number 34.EFRE-0300097] and by the German Federal Ministry of Education and Research (BMBF) [grant number 031B0918A], as part of the innovation lab „AutoBiotech“ within the project “BioökonomieREVIER”.

2.3.7 References

References given in chapter 2.3 are part of the reference list given for the general discussion.

Amador-Noguez, D., Brasg, I. A., Feng, X.-J., Roquet, N., Rabinowitz, J. D., 2011. Metabolome remodeling during the acidogenic-solventogenic transition in *Clostridium acetobutylicum*. Appl. Environ. Microbiol. 77**,** 7984-7997.

Andersen, K. B., von Meyenburg, K., 1977. Charges of nicotinamide adenine nucleotides and adenylate energy charge as regulatory parameters of the metabolism in *Escherichia coli*. J. Biol. Chem. 252**,** 4151-4156.

Becker, J., Rohles, C. M., Wittmann, C., 2018. Metabolically engineered *Corynebacterium glutamicum* for bio-based production of chemicals, fuels, materials, and healthcare products. Metab. Eng. 50**,** 122-141.

Bennett, B. D., Kimball, E. H., Gao, M., Osterhout, R., Van Dien, S. J., Rabinowitz, J. D., 2009. Absolute metabolite concentrations and implied enzyme active site occupancy in *Escherichia coli*. Nat. Chem. Biol. 5**,** 593-599.

Bertani, G., 1951. Studies on lysogenesis. The mode of phage liberation by lysogenic *Escherichia coli*. J. Bacteriol. 62**,** 293-300.

Chen, C., Chen, K., Su, T., Zhang, B., Li, G., Pan, J., Si, M., 2019. *Myo*-inositol-1-phosphate synthase (Ino-1) functions as a protection mechanism in *Corynebacterium glutamicum* under oxidative stress. Microbiol. Open 8**,** e00721.

Chiofalo, B., Laganà, A. S., Palmara, V., Granese, R., Corrado, G., Mancini, E., Vitale, S. G., Frangež, H. B., Vrtačnik-Bokal, E., Triolo, O., 2017. Fasting as possible complementary approach for polycystic ovary syndrome: Hope or hype? Med. Hypotheses 105**,** 1-3.

Dinicola, S., Chiu, T. T., Unfer, V., Carlomagno, G., Bizzarri, M., 2014. The rationale of the *myo*-inositol and D-*chiro*-inositol combined treatment for polycystic ovary syndrome. J. Clin. Pharmacol. 54**,** 1079-1092.

Eggeling, L., Bott, M., 2015. A giant market and a powerful metabolism: L-lysine provided by *Corynebacterium glutamicum*. Appl. Microbiol. Biotechnol. 99**,** 3387-3394.

Gambioli, R., Forte, G., Aragona, C., Bevilacqua, A., Bizzarri, M., Unfer, V., 2021. The use of D-*chiro*-Inositol in clinical practice. Eur. Rev. Med. Pharmacol. Sci. 25**,** 438-46.

Gauttam, R., Desiderato, C., Jung, L., Shah, A., Eikmanns, B. J., 2019. A step forward: Compatible and dual-inducible expression vectors for gene co-expression in *Corynebacterium glutamicum*. Plasmid 101**,** 20-27.

Gibson, D. G., Young, L., Chuang, R. Y., Venter, J. C., Hutchison, C. A., 3rd, Smith, H. O., 2009. Enzymatic assembly of DNA molecules up to several hundred kilobases. Nat. Methods 6**,** 343-345.

Goldbeck, O., Seibold, G. M., 2018. Construction of pOGOduet – an inducible, bicistronic vector for synthesis of recombinant proteins in *Corynebacterium glutamicum*. Plasmid. 95**,** 11-15.

Green, M. R., Hughes, H., Sambrook, J., MacCallum, P., 2012. Molecular cloning: a laboratory manual. Cold spring harbor laboratory press, Cold Spring Harbor, New York.

Hanahan, D., 1983. Studies on transformation of *Escherichia coli* with plasmids. J. Mol. Biol. 166**,** 557-580.

Homburg, R., 2008. Polycystic ovary syndrome. Best Pract. Res. Cl. Ga. 22**,** 261-274.

Hunter, S., Apweiler, R., Attwood, T. K., Bairoch, A., Bateman, A., Binns, D., Bork, P., Das, U., Daugherty, L., Duquenne, L., 2009. InterPro: the integrative protein signature database. Nucleic Acids Res. 37**,** 211-215.

Kachhawa, G., Senthil Kumar, K. V., Kulshrestha, V., Khadgawat, R., Mahey, R., Bhatla, N., 2021. Efficacy of *myo*-inositol and D-*chiro*-inositol combination on menstrual cycle

regulation and improving insulin resistance in young women with polycystic ovary syndrome: A randomized open-label study. Int. J. Gyncecol. Obstet. 158**,** 278-284.

Keilhauer, C., Eggeling, L., Sahm, H., 1993. Isoleucine synthesis in *Corynebacterium glutamicum*: molecular analysis of the *ilvB-ilvN-ilvC* operon. J. Bacteriol. 175**,** 5595-5603.

Kensy, F., Zang, E., Faulhammer, C., Tan, R. K., Büchs, J., 2009. Validation of a high-throughput fermentation system based on online monitoring of biomass and fluorescence in continuously shaken microtiter plates. Microb. Cell Fact. 8**,** 31.

Kortmann, M., Kuhl, V., Klaffl, S., Bott, M., 2015. A chromosomally encoded T7 RNA polymerase-dependent gene expression system for *Corynebacterium glutamicum*: construction and comparative evaluation at the single-cell level. Microb. Biotechnol. 8**,** 253-265.

Larner, J., 2002. D-*chiro*-inositol–its functional role in insulin action and its deficit in insulin resistance. Int. J. Exp. Diabetes Res. 3**,** 47-60.

Larner, J., Brautigan, D. L., Thorner, M. O., 2010. D-*chiro*-inositol glycans in insulin signaling and insulin resistance. Mol. Med. 16**,** 543-552.

Lim, H. N., Lee, Y., Hussein, R., 2011. Fundamental relationship between operon organization and gene expression. Proc. Natl. Acad. Sci. USA Proc. Natl. Acad. Sci. USA 108**,** 10626-10631.

Liu, X., Zhao, Z., Zhang, W., Sun, Y., Yang, Y., Bai, Z. J. E. i. l. s., 2017. Bicistronic expression strategy for high-level expression of recombinant proteins in *Corynebacterium glutamicum*. Eng. Life Sci. 17**,** 1118-1125.

López-Gambero, A. J., Sanjuan, C., Serrano-Castro, P. J., Suárez, J., Rodríguez de Fonseca, F., 2020. The biomedical uses of inositols: A nutraceutical approach to metabolic dysfunction in aging and neurodegenerative diseases. Biomedicines 8**,** 295.

Monastra, G., Unfer, V., Harrath, A. H., Bizzarri, M., 2017. Combining treatment with *myo*-inositol and D-*chiro*-inositol (40:1) is effective in restoring ovary function and metabolic balance in PCOS patients. Gynecol. Endocrinol. 33**,** 1-9.

Niebisch, A., Bott, M., 2001. Molecular analysis of the cytochrome bc_1-aa_3 branch of the *Corynebacterium glutamicum* respiratory chain containing an unusual diheme cytochrome c_1. Arch. Microbiol. 175**,** 282-294.

Ortmeyer, H. K., Bodkin, N., Lilley, K., Larner, J., Hansen, B. C., 1993. Chiroinositol deficiency and insulin resistance. I. Urinary excretion rate of chiroinositol is directly associated with insulin resistance in spontaneously diabetic rhesus monkeys. Endocrinology 132**,** 640-645.

Pintaudi, B., Di Vieste, G., Bonomo, M., 2016. The effectiveness of *myo*-inositol and D-*chiro*-inositol treatment in type 2 diabetes. Int. J. Endocrinol. 2016**,** 9132052.

Pupel, P., Szablińska-Piernik, J., Lahuta, L. B., 2019. Two-step D-ononitol epimerization pathway in *Medicago truncatula*. Plant J. 100**,** 237-250.

Ramp, P., Lehnert, A., Matamouros, S., Wirtz, A., Baumgart, M., Bott, M., 2021. Metabolic engineering of *Corynebacterium glutamicum* for production of *scyllo*-inositol, a drug candidate against Alzheimer's disease. Metab. Eng. 67**,** 173-185.

Ramp, P., Pfleger, C., Dittrich, J., Mack, C., Gohlke, H., Bott, M., 2022. Physiological, biochemical, and structural bioinformatic analysis of the multiple inositol dehydrogenases from *Corynebacterium glutamicum*. Microbiol. Spectr., e0195022.

Sanchez-Hidalgo, M., Leon-Gonzalez, A. J., Galvez-Peralta, M., Gonzalez-Mauraza, N. H., Martin-Cordero, C., 2021. D-pinitol: A cyclitol with versatile biological and pharmacological activities. Phytochem. Rev. 20**,** 211-224.

Schäfer, A., Tauch, A., Jäger, W., Kalinowski, J., Thierbach, G., Pühler, A., 1994. Small mobilizable multi-purpose cloning vectors derived from the *Escherichia coli* plasmids

pK18 and pK19: selection of defined deletions in the chromosome of *Corynebacterium glutamicum*. Gene 145**,** 69-73.

Spaans, S. K., Weusthuis, R. A., Van Der Oost, J., Kengen, S. W., 2015. NADPH-generating systems in bacteria and archaea. Front. Microbiol. 6**,** 742.

Thomas, M. P., Mills, S. J., Potter, B. V., 2016. The "other" inositols and their phosphates: synthesis, biology, and medicine (with recent advances in *myo*-inositol chemistry). Angew. Chem. Int. Ed. 55**,** 1614-1650.

van der Rest, M. E., Lange, C., Molenaar, D., 1999. A heat shock following electroporation induces highly efficient transformation of *Corynebacterium glutamicum* with xenogeneic plasmid DNA. Appl. Microbiol. Biotechnol. 52**,** 541-545.

Vitale, S. G., Corrado, F., Caruso, S., Di Benedetto, A., Giunta, L., Cianci, A., D'Anna, R., 2021. *Myo*-inositol supplementation to prevent gestational diabetes in overweight non-obese women: bioelectrical impedance analysis, metabolic aspects, obstetric and neonatal outcomes – a randomized and open-label, placebo-controlled clinical trial. Int. J. Food. Sci. Nutr. 72**,** 670-679.

Wendisch, V. F., 2020. Metabolic engineering advances and prospects for amino acid production. Metab. Eng. 58**,** 17-34.

Yoshida, K.-I., Yamaguchi, M., Morinaga, T., Ikeuchi, M., Kinehara, M., Ashida, H., 2006. Genetic modification of *Bacillus subtilis* for production of D-*chiro*-inositol, an investigational drug candidate for treatment of type 2 diabetes and polycystic ovary syndrome. Appl. Environ. Microbiol. 72**,** 1310-1315.

Yoshida, K.-I., Yamaguchi, M., Morinaga, T., Kinehara, M., Ikeuchi, M., Ashida, H., Fujita, Y., 2008. *Myo*-inositol catabolism in *Bacillus subtilis*. J. Biol. Chem. 283**,** 10415-10424.

Suppementary Information to "Production of D-*chiro*-inositol with *Corynebacterium glutamicum* via two different synthesis routes"

Table 2.3.S1. Oligonucleotides used in this study

Oligonucleotide name	Oligonucleotide sequence (5'□ 3')
pK19mobsacB plasmids	
P01_pK19Δcg2313_FW1	GAGGATCCCCGGGTACCGAGCTCGCCTCAAGCGGAACCTGAAG
P02_pK19Δcg2313_RV1	CTTGCTGAAAGCATCGAGG
P03_pK19Δcg2313_FW2	GTTAAACCTCGATGCTTTCAGCAAGGAGGGCAAGTTTGACTGAC
P04_pK19Δcg2313_RV2	CGTTGTAAAACGACGGCCAGTGAATTATGGTGGTCAAGCCGATG
P05_pK19Δcg0212_FW1	GCATGCCTGCAGGTCGACTCTAGAGTCGTGGTGGCTAACTTCCTG
P06_pK19Δcg0212_RV1	TTTAAGAAACCAGGGACTCTTCGAGGTTGTAGAGACCGAGTTTCATG
P07_pK19Δcg0212_FW2	CACCATGAAACTCGGTCTCTACAACCTCGAAGAGTCCCTGGTTTC
P08_pK19Δcg0212_RV2	GTTGTAAAACGACGGCCAGTGAATTAGATCCTTGGTCACCAGATC
P09_pK19Δcg2312-13_FW1	GAGGATCCCCGGGTACCGAGCTCGGAATCTGACTCCGAGCAG
P10_pK19Δcg2312-13_RV1	AAGTCAGCGTTCACGGTC
P11_pK19Δcg2312-1313_FW2	ATTTAGACCGTGAACGCTGACTTGAGGGCAAGTTTGACTGAC
P12_pK19Δcg2312-1313_RV2	CGTTGTAAAACGACGGCCAGTGAATTATGGTGGTCAAGCCGATG
P13_pK19Δcg2716_FW1	ATGCCTGCAGGTCGACTCTAGAGAGTCAGCCATGCATCTAC
P14_pK19Δcg2716_RV1	GGCAGCAAATCGAGACAAG
P15_pK19Δcg2716_FW2	TCTTATCTTGTCTCGATTTGCTGCCGGCTGGTTGGAGCTCTAG
P16_pK19Δcg2716_RV2	GTAAAACGACGGCCAGTGAATTACGATCACGTGGCGCTTC
P17_pK19Δcg2822_FW1	ATGCCTGCAGGTCGACTCTAGAGATAGATTGTTTAGGCCGTGAAAAGC
P18_pK19Δcg2822_RV1	AATTCCTGCGGCATCCAATTTGGC
P19_pK19Δcg2822_FW2	GCCAAATTGGATGCCGCAGGAATTAACGCCGAGTACAACTAAG
P20_pK19Δcg2822_RV2	GTAAAACGACGGCCAGTGAATTGTGTGAATTACTTTGCAACGC
P21_pK19Δcg2917_FW1	ATGCCTGCAGGTCGACTCTAGAGGAGGGTCCAGTGTTCTTG
P22_pK19Δcg2917_RV1	AACGATGGGGAAGTAGCC
P23_pK19Δcg2917_FW2	GAGAGGCTACTTCCCCATCGTTTGCGAGGCGCACTAGTTGATC
P24_pK19Δcg2917_RV2	GTAAAACGACGGCCAGTGAATTAAAGCATCGGAAACCGCAG
Recombination analysis	
P25_ΔCg2313_FW	GTTCCATCAAAGTCAATGC
P26_ΔCg2313_RV	GTGCGCCGTGTGATCAATG
P27_ΔQsuB_FW	CACTGGCGATGACCTTG
P28_ΔQsuB_RV	GAGACGTCGGTGTTGTG
P29_Δcg2312_FW	GGAATGGGCTGCGTTG
P30_Δcg2312_RV	GCAGAAGTTTCGGTGTG
P31_Δcg2716_FW	ATCCACCAATGCTGACAC
P32_Δcg2716_RV	AGGTTAGCGTCAGTGAC
P33_Δcg2822_FW	CAAGCTCCGGTTTCAGCG
P34_Δcg2822_RV	GTGTGAATTACTTTGCAACGC
P35_Δcg2917_FW	ATTTGCGCACGAAGGTGG
P36_Δcg2917_RV	CGCAATCGCACTGTCTG

pPREx6 plasmids	
P37_px6-IolH_FW	AGAAGGAGATATACATATGAACGTGGTTCGTATTG
P38_px6-IolH_FW	TGGGTGGGACCAGCTAGCTGCGTTTTCGATGAGTG
P39_px6-Cg0212_FW	TTAACTTTAAGAAGGAGATATACATATGAAACTCGGTCTCTAC
P40_px6-Cg0212_FW	CGAACTGTGGGTGGGACCAGCTAGCAGAAACCAGGGACTCTTC
P41_px6-Cg3390_FW	AGAAGGAGATATACATATGAAACCACAACTTATTG
P42_px6-Cg3390_FW	GGTGGGACCAGCTAGCGTTAGTGGAGGGGGCG
pMKEx2 plasmids	
P43_pCg0212_FW	CTTTAAGAAGGAGATATACCATGAAACTCGGTCTCTAC
P44_pCg0212_RV	GCACCAGAGCGAGCTCTGCGGCCGCTTAAGAAACCAGGGACTC
P45_pIolG-Cg0212_FW1	CTTTAAGAAGGAGATATACCATGAGCAAGAGCCTTCGCGTTGG
P46_pIolG-Cg0212_RV1	TGTCGCTCAGAGACCTGAGGTTAAGCGTAGAAATCTGGGCGAG
P47_pIolG-Cg0212_FW2	CCTCAGGTCTCTGAGCGACAGAAGGAGATATACCATGAAACTCGGTCTCTAC
P48_pIolG-Cg0212_RV2	GCACCAGAGCGAGCTCTGCGGCCGCTTAAGAAACCAGGGACTC
P49_pIolG-Cg2312_FW	CCTCAGGTCTCTGAGCGACAGAAGGAGATATACCATGACTTTTAAACTCGCAGC
P50_pIolG-Cg2312_RV	CCAGAGCGAGCTCTGCGGCCTTAGACCGTGAACGCTGAC
P51_pOEPa_FW	CCTCAGGTCTCTGAGCGACAGAAGGAGATATACCATGTCCAAGACCGTGTGC
P52_pOEPa_RV	TGGCACCAGAGCGAGCTCTGCGGCCTTACACCAGGCCACGGGACTTC
P53_pOEPb_FW	TTTAACTTTAAGAAGGAGATATACCATGGCAGGCAACAAGATCCC
P54_pOEPb_RV	TGGCACCAGAGCGAGCTCTGCGGCCTTACACGTCGCCATCCCAC
P55_pOEPa-b_FW	GCAGGTGCACAATGATACGATTACACCAGGCCACGGGAC
P56_pOEPa-b_RV	TCGTATCATTGTGCACCTGCGAAGGAGATATACCATGGCAGGCAACAAGATCCC
P57_pOEPb-a_FW	GCAGGTGCACAATGATACGATTACACGTCGCCATCCCACAGTTC
P58_pOEPb-a_RV	TCGTATCATTGTGCACCTGCGAAGGAGATATACCATGTCCAAGACCGTGTGCG
P59_pInoDCI_FW1	CTTTAAGAAGGAGATATACCATGAGCACGTCCACCATCAG
P60_pInoDCI_RV	ACATCGTTGAGTGGTCACCGTTACGCCTCGATGATGAATG
P61_pInoDCI_FW2	CGGTGACCACTCAACGATGTGAAGGAGATATACCATGTCCAAGACCGTG
P62_pMKEx2-BiT7_FW1	TCGGGCTCATGAGCGCTTGTTTCGGTAATCGTATTGTACACGGCCG
P63_pMKEx2-BiT7_FW2	CGGCCACGGGGCCTGCCACCATACATCCGGATATAGTTCCTCC
P64_pMKEx2-BiT7_FW3	CCGAAACAAGCGCTCATG
P65_pMKEx2-BiT7_RV1	TCGCAGACCGATACCAGGATCTTG
P66_pMKEx2-BiT7_RV2	TCACCGAGGCAGTTCCATAGGATGG
P67_pMKEx2-BiT7_RV3	GTATGGTGGCAGGCCCCGTG
P68_pBiT7-InoDCI_FW1	GCACCAGAGCGAGCTCTGCGGCCTTACGCCTCGATGATGAATG
P69_pBiT7-InoDCI_RV1	GTTAAGTATAAGAAGGAGATATACAATGTCCAAGACCGTGTGC
P70_pBiT7-InoDCI_RV2	CGATATCCAATTGAGATCTGCCATATTACACGTCGCCATCCCAC

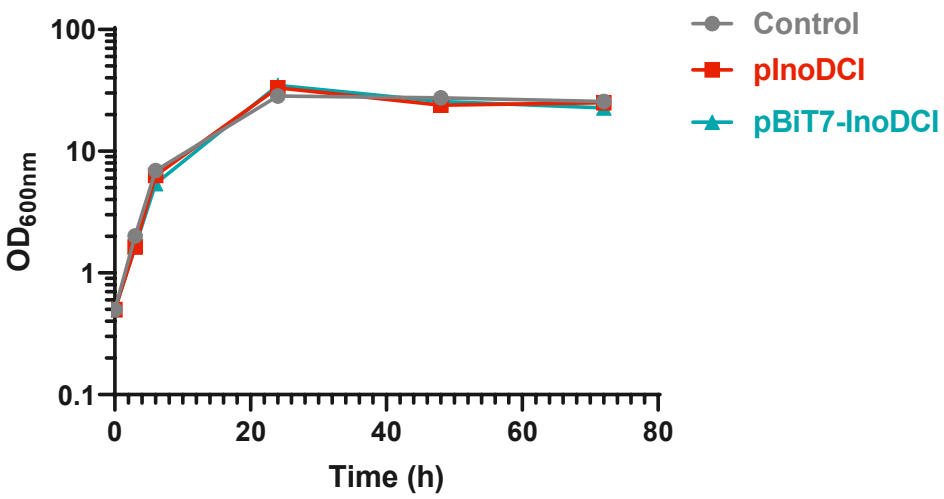

Fig. 2.3.S1 Growth of *C. glutamicum* MB001(DE3)Δ*IOL* transformed with pMKEx2 (Control), pInoDCI or the bicistronic expression plasmid pBiT7-InoDCI. Strains were cultivated in CGXII medium containing 20 g/L glucose for 72h at 30°C. Gene expression was induced by addition of 500µM IPTG after 3h of the cultivation start. Mean values of biological triplicates and standard deviations are shown.

3. Discussion

3.1 The complexity of the *C. glutamicum* inositol catabolism

The catabolism for MI is conserved throughout different microorganisms and has also been described in *C. glutamicum* (Krings et al., 2006). Over 20 genes and two gene clusters were identified that showed increased expression in the presence of MI, however, only the function of 10 of these genes was described so far. Through this thesis, we stepwise elucidated the function of nine more genes coding for enzymes that participate in the inositol catabolism of *C. glutamicum,* which turned out to be much more complex than previously described. We based our first studies on comparisons with the model organism *B. subtilis*, whose inositol catabolism and the corresponding enzymes have been intensively investigated over the last two decades (Kang et al., 2017a; Kang et al., 2017b; Michon et al., 2020; Morinaga et al., 2010a; Morinaga et al., 2010b; Yoshida et al., 1997; Yoshida et al., 1999; Yoshida et al., 2004; Yoshida et al., 2008; Yoshida et al., 2002). Using BlastP (Altschul et al., 1990; Altschul et al., 1997), we analyzed the genome of *C. glutamicum* for genes encoding homologs of the mIDH/sIDH enzymes of *B. subtilis* and identified the seven putative inositol dehydrogenases IolG, IolW, OxiB, OxiC, OxiD, OxiE, and IdhA3, which showed different sequence identities towards BsIolG, BsIolX, and BsIolW.

Other inositol-degrading bacteria possess up to four identified paralogous IDHs with overlapping substrate spectra (Aamudalapalli et al., 2018; Yoshida et al., 2012; Zhang et al., 2010). With seven IDH-encoding genes so far, *C. glutamicum* possesses the highest number of identified paralogs, which already hints toward the ability to utilize more inositols besides MI. In initial growth experiments, in which we cultivated *C. glutamicum* MB001(DE3) in CGXII minimal medium supplemented with MI, we observed that *C. glutamicum* naturally produces and degrades SI (Ramp et al., 2021; chapter 2.1). Further experiments revealed that *C. glutamicum* could grow with the inositols SI and DCI as single carbon and energy sources (Ramp et al., 2022; chapter 2.2). Unpublished follow-up experiments explained in detail in chapter 5.1 of the Appendix revealed that *C. glutamicum* could also grow on L-*chiro*-Inositol (LCI). Many other bacteria have been identified to grow on SI and DCI (Morinaga et al., 2010a; Morinaga et al., 2006; Yoshida et al., 2012), but to our knowledge, none has been reported to grow on LCI. The growth of *Sinorhizobium meliloti* on SI, DCI, LCI, *muco*-, and *allo*-inositol as sole carbon sources was analyzed. However, only growth on SI and DCI was detected (Kohler et al., 2010).

We found that both characterized inositol transporters, IolT1 and IolT2, facilitate uptake of all tested inositols MI, SI, DCI, and LCI (Ramp et al., 2022; chapter 2.2 and Appendix 5.1.) (Fig. 3.1). A Δ*iolT1*Δ*iolT2* double deletion mutant could not grow on the tested inositols, excluding that the putative inositol permease encoded by *iolP* (cg0206) participates in the uptake of MI, SI, DCI, or LCI. So far, only the inositol transporters of *B. subtilis* have been analyzed *in vivo* and *in vitro* for the transport of different inositols and sugars (Bettaney et al., 2013). In contrast to IolT1 and IolT2 of *C. glutamicum*, the three *B. subtilis* transporters IolT, IolF and YfiG showed different activities for tested inositols. IolT and YfiG mainly transported MI and DCI, while IolF only accepted DCI. SI was not analyzed in these experiments. *Allo*-, *epi*- and *muco*-inositol were not transported, while only YfiG was able to transport LCI. This suggests that *B. subtilis* might also be able to utilize LCI (Bettaney et al., 2013). IolT1 and IolT2 of *C. glutamicum* show a general broader substrate spectrum and were reported to transport also glucose, fructose, and xylose (Brüsseler et al., 2018; Lindner et al., 2011). Based on these facts, it is likely that IolT1 and IolT2 also facilitate the uptake of other inositols, like *allo*-, *epi*-, or *muco*-inositol and that *C. glutamicum* might be able to utilize them as single carbon and energy source.

3.2 Making sense of multiple inositol dehydrogenase activities

The initial step of inositol degradation is catalyzed by IDHs, which oxidize inositol with concomitant reduction of NAD^+ to $NADH+H^+$. In *B. subtilis*, IolG was identified to oxidize both MI and DCI to 2KMI and 1KDCI, respectively, while IolX was shown to be responsible for SI oxidation. As seven IDHs are encoded in the genome of *C. glutamicum,* we analyzed their function by expressing each of the corresponding genes individually in an IDH deletion strain lacking all seven IDH genes and testing the corresponding strain for growth on MI, SI, and DCI. These experiments revealed that the four IDHs IolG, OxiB, OxiD, and OxiE enabled growth on different inositols with overlapping activities for each substrate (Ramp et al., 2022; chapter 2.2). In the scope of additional experiments described in chapter 5.1 of the Appendix, we found that IolG, OxiB, and OxiD also enabled growth on LCI to different extents. To our surprise, we also observed that IdhA3 is able to recover growth of the ΔIDH strain on LCI almost to wt level. IdhA3 showed no activity for either MI, SI, or DCI. Therefore we report the first ever discovered L-*chiro*-IDH. For a better overview, the results of the complementation experiments of chapters 2.2 and Appendix 5.1 are summarized in Table 3.1 and Fig. 3.1.

In some cases, plasmid-based expression of single IDH genes was sufficient to regain wt-like growth. In the case of *oxiE*, plasmid-based expression enabled even faster growth on SI than observed for the wt, suggesting that genomic expression of *oxiE* is the bottleneck for growth on SI. OxiD showed the highest specific activity for MI of all IDHs in the enzyme kinetic studies (Ramp et al., 2022; chapter 2.2) and plasmid-based expression of *oxiD* enabled wt-like growth of the ΔIDH strain on MI and DCI. However, in previous studies, deletion of only *iolG* already resulted in a strong growth defect on MI (Krings et al., 2006). This suggests that transcriptional regulation of the operon cg3389-cg3392 in the *iol2* cluster limits the contribution of OxiD and OxiE to growth on inositols. The transcriptional regulation of inositol metabolism genes will be further discussed in chapter 3.4.

Table 3.1. Role of the indicated IDHs for growth on MI, DCI, LCI, and SI

Enzyme	Group[1]	Substrate	Growth[2]
IolG	(i)	*myo*-Inositol	++++
		D-*chiro*-Inositol	++++
		L-*chiro*-Inositol	+
		scyllo-Inositol	-
OxiD	(i)	*myo*-Inositol	++++
		D-*chiro*-Inositol	++++
		L-*chiro*-Inositol	++++
		scyllo-Inositol	-
OxiB	(ii)	*myo*-Inositol	+++
		D-*chiro*-Inositol	-
		L-*chiro*-Inositol	+
		scyllo-Inositol	++
OxiE	(ii)	*myo*-Inositol	++
		D-*chiro*-Inositol	-
		L-*chiro*-Inositol	-
		scyllo-Inositol	++++
IdhA3	(iv)	*myo*-Inositol	-
		D-*chiro*-Inositol	-
		L-*chiro*-Inositol	+++
		scyllo-Inositol	-

[1]Grouping as established in chapter 2.2, sorting IDHs in NAD^+-dependent mIDHs (i), NAD^+-dependent sIDHs (ii), NADPH-dependent sIDHs (iii), IDHs with no activity for any tested inositol (MI, SI, DCI) (iv).
[2]Growth of ΔIDH strain expressing the genes encoding the indicated IDHs, with "++++" indicating very good growth and "–"indicating no growth.

The analyzed IDHs showed many overlapping activities for the different inositols, but some explicitly distinguished between specific isomers. The distinction between the nine different inositol isomers is not simple, as they only differ in positioning one or two hydroxyl groups. Yet IDHs can discriminate between different inositols (Table 3.1). At the time the experiments reported in chapter 2.2 were performed, we noticed that the analyzed IDHs all accept MI as substrate, but distinguish between DCI and the all equatorial SI (Ramp et al., 2022). Based on this observation, we established a new grouping for IDHs that differs from the previous one (van Straaten et al., 2010). We defined the following four groups: (i) NAD^+-dependent IDHs known to have activity for MI and DCI; (ii) NAD^+-dependent IDHs known to have activity for MI and SI; (iii) $NADP^+$-dependent IDHs catalyzing the reduction of 2KMI to SI; (iv) IDHs with no activity for any tested inositol (Ramp et al., 2022; chapter 2.2). We placed IolG and OxiD in group (i), OxiB and OxiE in group (ii), and IolW in group (iii). OxiC and IdhA3 were placed in group (iv) as no activity for MI, SI or DCI was found. We searched in literature for IDHs that have activity for MI, SI, or DCI, sorted them into the corresponding groups and performed a sequence alignment to identify potential conserved sites that explain inositol selectivity. Over 10,000 amino acid sequences are present in the BRENDA enzyme database for the entry: “EC 1.1.1.18 - inositol 2-dehydrogenase”. However, only 13 other IDHs from six different bacterial species have been characterized for their activity for MI, SI, or DCI.

Furthermore, nearly no IDH has been tested for activity towards the other inositol isomers, ours included. The main reason, which is also true for our studies, is the difficult commercial availability of these isomers. Therefore, our IDH grouping is limited to the analysis of important features for acceptance of MI, SI, or DCI as substrates, but disregards features that might be relevant for acceptance of the other inositols. In our initial analysis, we found that IdhA3 has no activity for MI, SI, and DCI, but later discovered that the enzyme oxidizes LCI. Therefore, for a complete understanding of how IDHs select between inositols, the activity of more IDHs from different species need to be analyzed for all inositol isomers.

Despite the limitations of our analysis of IDHs, the amino acid sequence alignment revealed some conserved motifs and differences between the groups. We identified potential reasons why OxiC showed no activity for any tested inositols (incomplete NAD(P)H binding motif and catalytic triad), identified residues that separate NADPH-dependent IDHs from NAD^+-dependent IDHs, and residues that allow a prediction if an IDH accepts SI (Ramp et al., 2022; chapter 2.2). However, sequence alignments have their limitations. To better understand what

characteristics determine inositol selectivity, we also analyzed the binding of inositols to structural models of IDHs.

The solving of protein crystal structures can be a tedious task, but with the ever-advancing development of structure modeling software (Eswar et al., 2008; Kiefer et al., 2009), powerful algorithms (Dittrich et al., 2018; Morris et al., 1998; Steinegger et al., 2019), and the application of artificial intelligence (Jumper et al., 2021; Noé et al., 2020; Salehi and Burgueño, 2018), protein structures and interactions can be predicted with high reliability. In close collaboration with the research group of Prof. Holger Gohlke (Institute of Bio- and Geosciences 4: Bioinformatics, Forschungszentrum Jülich) we used such tools to perform molecular docking experiments on IDH structural models to predict the inositol acceptance of the tested IDHs and identify potential substrate binding sites. In 15 out of 18 cases, the correct IDH-inositol combinations were predicted. Also, the results of the docking experiments were in agreement with the conserved sites in motif V (Ramp et al., 2022; chapter 2.2, Fig. 4) that can be used to estimate the substrate preferences of IDHs.

The docking experiments correctly predicted no binding of MI, SI, and DCI to IdhA3. According to the structural model, we assumed the more exposed binding pocket of IdhA3 to be responsible for the lacking activity with these inositols. However, this assumption is questioned with the new finding that IdhA3 is active on LCI (Appendix 5.1). Our molecular docking pipeline offers an efficient tool to predict relatively accurate IDH-inositol interactions. Given enough computational resources, interaction studies of more IDHs with the other inositol isomers can be performed to identify potentially novel activities.

In some cases, solving a protein structure in complex with its cofactor and substrate is necessary, especially if nearly no comparable data exists about the protein of interest. Knowledge about inositol acceptance and reaction mechanisms of the catabolic NAD^+-dependent IDHs is accumulating (Aamudalapalli et al., 2018; van Straaten et al., 2010). However, little is known about the characteristics of NADPH-dependent IDHs and why they prefer to process the keto-inositol 2KMI. BsIolW, BsIolU, and CgIolW are the only NADPH-dependent IDHs identified and characterized, with the apo-protein crystal structure of BsIolW submitted to PDB (PDB: 3GDO). In the course of a 3-month fellowship granted by the Japan Society for the Promotion of Science (JSPS) in close collaboration with the research group of Prof. Makoto Nishiyama, Prof. Saori Kosono and Prof. Ayako Yoshida at the Agro-Biotechnology Research Center (AgTECH) at the University of Tokyo, Japan, we aimed to

solve the protein crystal structure of CgIolW in complex with NADPH and 2KMI. The experimental setup and the results are described and discussed in detail in chapter 5.2 of the Appendix.

We successfully solved the crystal structure of CgIolW as apo-form and report the first crystal structure with bound NADPH, however, we were unable to obtain a structure of the IolW-2KMI complex. We identified the binding sites for NADPH, which agreed with the sites found in other NAD(P)H-dependent IDHs (van Straaten et al., 2010; Zheng et al., 2013). These findings might also be combined with molecular docking experiments to determine the binding sites of 2KMI and the potential acceptance of other keto-intermediates.

3.3 Inososе isomerases – The missing link?

Inositol dehydrogenases have been the subject of many research studies dealing with enzymatic and structural analysis. They catalyze the initial step of inositol degradation: the NAD^+-dependent oxidation of inositols to a keto-intermediate. The first keto-intermediate discovered was 2KMI, which results from the oxidation of MI at the C2 or any C-atom in SI, which gave 2KMI the alternative name *scyllo*-inososе (Morinaga et al., 2010a; Yoshida et al., 2008). 2KMI then enters the residual degradation pathway via dehydration of the C1 by IolE, yielding THcDHO (Anderson and Magasanik, 1971; Berman and Magasanik, 1966b; Yoshida et al., 2004). Depending on the attacked C-atom of the inositol isomer, keto-intermediates deviating from 2KMI can be formed by IDHs.

DCI is oxidized by IolG at its C1 or C6 to yield 1KDCI (Yoshida et al., 2006). It is unknown whether 1KDCI or other keto-intermediates can also directly be processed by IolE for further degradation. Purified IolE from *B. subtilis* was only analyzed for activity for 2KMI *in vitro* (Yoshida et al., 2004). However, the identification of the inososе isomerase IolI, which catalyzes the interconversion of 1KDCI and 2KMI in the DCI-degrading *B. subtilis* suggests that 2KMI is the main substrate of IolE. Before this thesis BsIolI was the only inososе isomerase characterized so far (Yoshida et al., 2006). Genes encoding putative IolI homologs have been annotated in the genomes of *Lactobacillus rhamnosus* (Zhang et al., 2010)*, Erwinia toletana* (Caballo-Ponce et al., 2018), and some *Anaerostipes* species (Bui et al., 2021). We now add at least three more functional homologs (Cg0212, Cg2312, and Cg3390; Percent Identity Matrix provided in Table 3.2) to the list, with potentially more hidden in the genome of *C. glutamicum*. All three identified inososе isomerases enabled the interconversion of 1KDCI to 2KMI

(Fig. 3.1), but the mysterious activity of Cg3390 was not limited to that, as other yet unknown products were formed in addition to 2KMI (discussed in chapters 2.1 and 2.3).

Table 3.2. Percent identity matrix of inosose isomerases. Amino acid sequences alignments of IolI of *B. subtilis* and the inosose isomerases of *C. glutamicum* generated with ClustalOmega v1.2.4

Inosose Isomerase – Identity in %	IolI	Cg0212	Cg2312	Cg3390
IolI	100.00	20.87	21.94	21.08
Cg0212	20.87	100.00	16.45	24.12
Cg2312	21.94	16.45	100.00	22.16
Cg3390	21.08	24.12	22.16	100.00

The growth on LCI presumably also requires an inosose isomerase. Although the keto-intermediate formed by LCI oxidation is unknown, LCI cannot directly be converted to 2KMI or 1KDCI in one oxidation reaction. Based on the reaction mechanism of DCI oxidation by IolG, we speculate that LCI oxidation may result in 1-keto-L-*chiro*-Inositol (1KLCI) (Fig 3.1). However, the prediction of the formed keto-intermediate is uncertain, as other IDHs were identified that do not follow the mechanism of C1/C6 or C2 oxidation. For example, sIDH from *P. laeviglucosivorans* oxidized SI to 2KMI, however it acts on the C4 of MI resulting in the generation of *epi*-2-inosose (2-keto-*epi*-inositol) (Fukano et al., 2018). As described earlier, LcIDH2 simultaneously oxidizes MI at multiple sites (C1, C3, C5) resulting in a mixture of 70% *neo*-inosose (keto-*neo*-inositol), 20% 1D-*chiro*-inosose (1KDCI), and 10% 1L-*chiro*-inosose (1KLCI) (Ramos-Figueroa et al., 2020). This suggests that inositol degradation is far more complex than previously assumed and that inosose isomerases might play an important role in interconverting the various keto-intermediates so that they can enter the catabolic pathway. However, as mentioned above, it cannot be excluded that IolE is able to accept multiple keto-inositols.

In *C. glutamicum*, all identified inosose isomerases are encoded in small operons together with at least one IDH gene, like cg2312-*idhA3*, *oxiB*-cg0212, and *oxiC*-cg3390-*ociD*-*oxiE*. These IDH-isomerase modules might have different activities for different inositols and so contribute to the conserved MI catabolic pathway encoded in the larger *iolCJABDEGH* operon. None of these modules is directly regulated by IolR. Instead, they all possess either a LacI-type or an IclR-type repressor encoded upstream that might repress module gene expression as long as the

corresponding inositols are absent (Fig. 3.2). *C. glutamicum* probably has evolved such IDH-isomerase modules, in addition to the main inositol catabolic pathway, to be able to metabolize the various inositols found in soil (Turner et al., 2002), supporting its competitiveness with other microbes. The multiple IDH-isomerase modules might have evolved through operon duplication and further functional divergence (Fondi et al., 2009; Gevers et al., 2004). It might also have gained these modules via horizontal gene transfer, a common phenomenon in the evolution of novel catabolic pathways in bacteria (Juhas et al., 2009; Thomas and Nielsen, 2005).

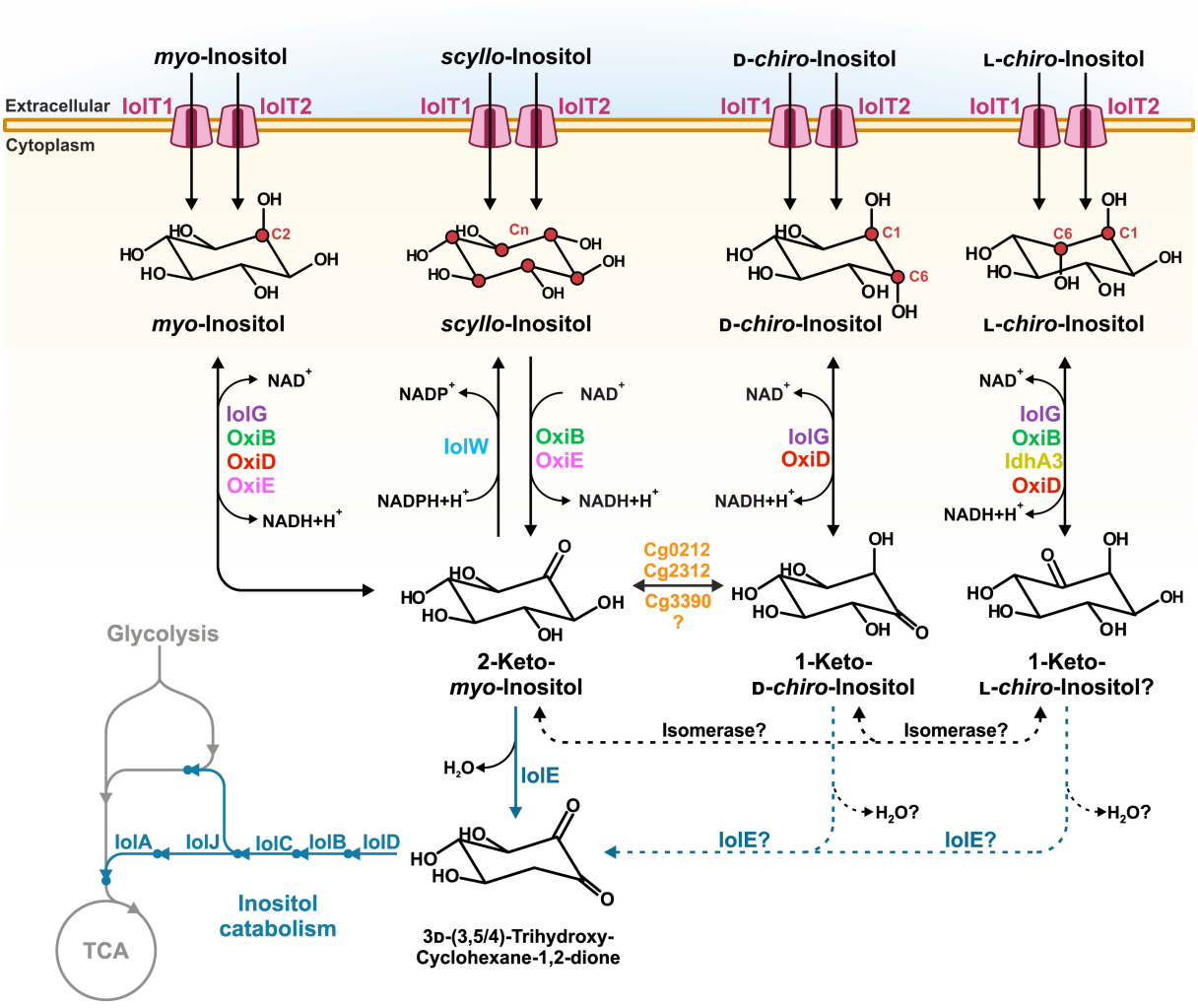

Fig. 3.1. Current model of the catabolism of *myo*-, *scyllo*-, D-*chiro*- and L-*chiro*-inositol in *C. glutamicum*. Catabolism starts with uptake of all inositols via the two specific secondary transporters IolT1 and IolT2. Each inositol is oxidized by specific NAD^+-dependent inositol dehydrogenases (IolG, OxiB, IdhA3, OxiD and OxiE) to corresponding keto-intermediates. *Myo*- and *scyllo*-inositol are oxidized to 2-keto-*myo*-inositol (2KMI), D-*chiro*-inositol is oxidized to 1-keto-D-*chiro*-inositol (1KDCI) and L-*chiro*-inositol is presumably oxidized to 1-keto-L-*chiro*-inositol (1KLCI). Known and hypothesized oxidized carbon atoms of each inositol are highlighted as a red circle. 2KMI enters the main catabolism by dehydration via IolE to yield 3D-(3,5/4)-trihydroxy-cyclohexane-1,2-dione, which is further degraded following the conserved pathway shown in Fig. 1.4. 1KDCI and 2KMI are interconverted by the inosose isomerases Cg0212, Cg2312, Cg3390 and at least one unknown enzyme. Hypothesized 1KLCI is presumably isomerized to 1KDCI or 2KMI by an unknown inosose isomerase (dashed arrows). IolE is hypothesized to accept other keto-inositol intermediates for further degradation (dashed arrows).

3.4 Regulation of the inositol metabolism in *C. glutamicum*

In *C. glutamicum*, inositol catabolism is regulated by the GntR-type regulator IolR, which represses the expression of the *iolCABDEGHPW* operon, the gene encoding the putative LacI-family transcriptional regulator Cg0210 preceding *oxiB*, and *iolT1* (Fig. 3.2). In *B. subtilis,* the functional equivalent IolR belongs to the DeoR family of transcriptional regulators and derepression of its target genes is triggered by binding of the inositol degradation intermediate DKGP (Yoshida et al., 2008). In view of the strong conservation of the whole inositol degradation pathway, DKGP might also serve as ligand of IolR of *C. glutamicum*, although the protein shows only 21% sequence identity to IolR of *B. subtilis* (Fig. 3.2). As *C. glutamicum* can utilize multiple inositols, it makes sense that IolR is regulated by a common intermediate. Members of the DeoR family of bacterial transcription repressors are known to interact with phosphorylated sugars as inducer (Engels and Wendisch, 2007; van Rooijen and de Vos, 1990). DKGP may be more distinguishable than the other intermediates as it is a specific and the first phosphorylated intermediate in the inositol catabolic pathway.

The *cg3389-cg3392* operon and the IDH genes *idhA3* and *oxiB* are not regulated by IolR. However, other transcriptional regulators are known or assumed to control expression of these genes. Both *idhA3* and *oxiB* are preceded in the opposite direction by genes for LacI-type regulators, which might repress these IDH genes (Fig. 3.2). The operon *cg3389-cg3392* is known to be repressed by the LacI-type transcriptional regulator IpsA. Deletion of the *ipsA* gene caused a four-fold increased expression (Baumgart et al., 2013). IpsA is a major regulator of MI synthesis in *C. glutamicum* and its activity is inhibited by MI when present at sufficient concentrations in the cell (Baumgart et al., 2013). As expression of the genes *cg3389-cg3392* was upregulated up to 20-fold in the wt when cultivated with MI compared to glucose as sole carbon source, additional regulators are probably involved in the control of this operon. A likely candidate is the IclR-family transcriptional regulator Cg3388 encoded immediately upstream of the operon in the same direction. In a recent study, unrelated to inositol metabolism, Cg3388 was shown to bind to the intergenic region between its own gene and the *iolT2-rhcM2D2* operon, repressing its expression. 1,2,4-trihydroxybenzene, hydroquinone, and indole inhibited the DNA-binding capacity of Cg3388 as effector molecules (Walter et al., 2020) . As all these compounds contain benzol-ring structures, which share structural similarity to the cyclohexane ring motif of inositols, also inositol isomers might directly inhibit DNA-binding of Cg3388 and thereby derepress the *cg3389-cg3392* operon.

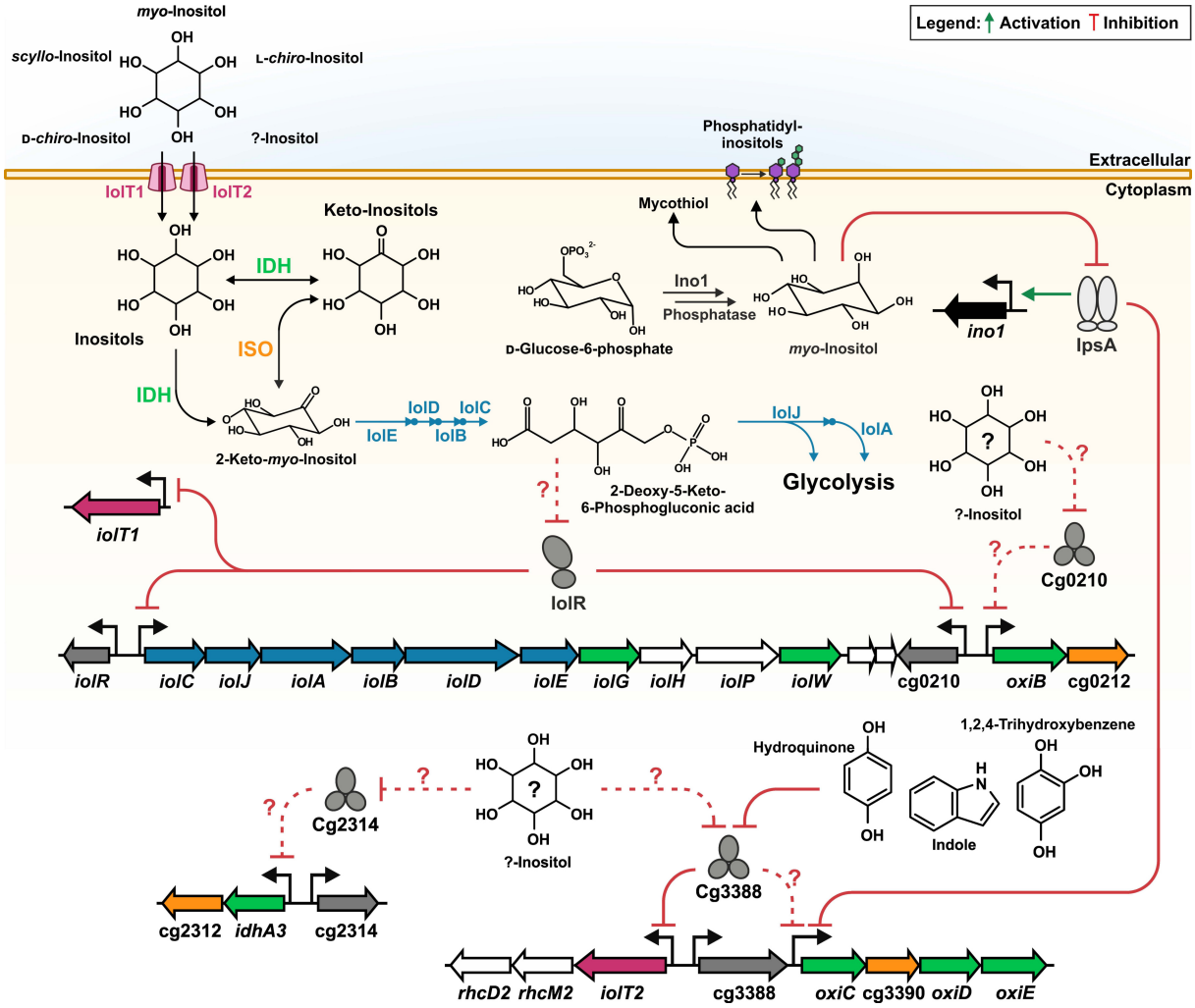

Fig. 3.2. Schematic model of inositol metabolism regulation in *C. glutamicum*. Inositols are taken up by the specific inositol transporters IolT1 and IolT2. Inositols are oxidized by inositol dehydrogenases (IDH, encoding genes highlighted in green) to keto-inositols, e.g. 2-keto-*myo*-inositol (2KMI). Keto-inositols are interconverted by inosose isomerases (ISO), encoded by genes highlighted in orange. 2KMI enters the conserved pathway shown in Fig. 1.4. Genes encoding the inositol degrading enzymes (IolEDBCJA, highlighted in blue), the transporter IolT1 (highlighted in pink) and the LacI-type regulator Cg0210 are repressed by the GntR-type regulator IolR. Accumulating 2-deoxy-5-keto-6-phosphogluconic acid (DKGP) in the inositol degradation pathway presumably binds to IolR causing dissociation from its operator and induction of gene expression. Synthesis of *myo*-inositol (MI) starting from D-glucose-6-phosphate is regulated via a negative feedback loop. Binding of MI to the transcriptional regulator IpsA inactivates its function as repressor for the *oxiC*-cg3390-*oxiDE* operon and as activator for *ino1*. Binding of the IclR-type regulator Cg3388 to hydroquinone, indole or 1,2,4-trihydroxybenzene causes dissociation from its operator, inducing gene expression of the *iolT2-rhcM2D2* operon. Cg3388 is hypothesized to control gene expression of the *oxiC*-cg3390-*oxiDE* operon via binding to an unknown inositol compound. LacI-type regulators Cg0210 and Cg2314 are speculated to control gene expression of adjacent IDH-ISO operons, also via binding to an unknown inositol compound. Bold arrows show experimentally proven reactions, dashed arrows indicate hypothesized interactions.

3.5 *C. glutamicum* as a suitable host for production of rare inositols

We unveiled the profound versatility of the inositol metabolism of *C. glutamicum* and used this knowledge to develop biotechnological processes for producing rare inositols. As the demand for efficient, sustainable production processes of rare inositol isomers is increasing, one major goal of this thesis was to establish *C. glutamicum* as a novel production host.

The first task was to develop a *C. glutamicum* chassis strain that is unable to degrade inositols. This initially required the deletion of gene clusters *iol1* and *iol2*, as they both encode IDHs that are active on MI or SI (Ramp et al., 2021; chapter 2.1). The resulting strain named MB001(DE3)Δ*iol1*Δ*iol2* showed no degradation of MI or SI anymore. The studies elaborated in chapters 2.3 and 5.1 now indicate that more deletions might be beneficial for a suitable chassis strain. Although not active for MI, DCI or SI, IdhA3 was proven to oxidize LCI. Furthermore, six putative and proven inosose isomerases were identified of which Cg0212, Cg2312 and Cg3390 interconvert 1KDCI and 2KMI, while Cg2716, Cg2822 and Cg2917 might still show activity for other keto-intermediates. Interconversion of keto-inositols might interfere with inositol biotransformation and IdhA3 might be active for inositols whose production will be aimed for in the future. To generate a clean chassis strain for the production of any inositol, the genes encoding the inosose isomerases and *idhA3* should be also be deleted.

On the other side, the large number of IDHs and inosose isomerases and their reversible activities to interconvert inositols make *C. glutamicum* an attractive host for the production of inositols. Overproduction of IolG and Cg0212 successfully led to the production of DCI from MI (Fig. 3.3A), demonstrating *C. glutamicum's* innate ability to synthesize rare inositols. The identification of IdhA3 as an LCI-IDH and its potential corresponding isomerase Cg2312 might offer a similar, novel tool for the production of LCI starting from MI.

Inositol production processes utilizing IDH-isomerase combinations have been employed before (Yoshida et al., 2006), but they have the same disadvantage as other processes based on reversible isomerase/epimerase reactions: they are dependent on the reaction equilibrium ratio, which can often lie on the side of the substrate (Fang et al., 2018; Mu et al., 2015). For the inosose isomerases IolI of *B. subtilis* and Cg0212 the reaction equilibrium mainly resides on the side of 2KMI (77:23 for 2KMI:1KDCI) (Yoshida et al., 2006), which is in favor of their physiological function. To reach economic product yields with such reactions, often extremely high concentration of substrate needs to be applied (>100 g/L). A possibility to push the reaction in the direction of the product is to perform in situ product removal (ISPR) (Dafoe and Daugulis,

2014). This comes with higher demand for efficient downstream processing and chromatographic methods. Especially for inositol isomers, efficient separation is difficult as they differ only slightly from each other. In addition, production processes based on IDH-isomerase combinations, like those established for DCI, have the disadvantage of relying on the same enzyme to react in both directions (Yoshida et al., 2006).

More efficient processes for the interconversion of inositols are desirable, whose driving force towards the product is not only based on the simple concentration gradient. Reactions based on NADPH-driven processes provide a promising alternative. The phosphate group of NADPH modifies the cofactor's structure, allowing enzymes to have different specificities for NADH/NAD^+ and NADPH/$NADP^+$. This enables two redox systems to function in tandem as driving forces for catabolic (NAD^+-driven) and anabolic (NADPH-driven) processes, as the cellular ratio of NAD^+/NADH and $NADP^+$/NADPH are in favor of NAD^+ and NADPH (Amador-Noguez et al., 2011; Andersen and von Meyenburg, 1977; Bennett et al., 2009; Spaans et al., 2015). *C. glutamicum* is already equipped with such a system for inositol synthesis, as it possesses the NADPH-dependent sIDH IolW. The overproduction of IolW together with IolG enabled biotransformation of MI to SI (Fig. 3.3B) with accumulating 2KMI in CGXII minimal medium with titers of 4.4 g/L SI and 2.7 g/L 2KMI after 48 h (Ramp et al., 2021; chapter 2.1). In earlier studies, a similar setup enabled complete conversion of 10 g/L MI to 10 g/L SI in *B. subtilis* when cultivated in rich medium (Tanaka et al., 2013). Comparing these results to our findings, we concluded that the main bottleneck for the reaction catalyzed by IolG and IolW was not the reaction equilibrium of the substrate and product but the availability of NADPH.

NADPH is essential for growth, as it is required for biomass formation, such as amino acid biosynthesis. The stoichiometric demand of *C. glutamicum* growing on glucose and fructose is approximately 11.5-15.5 mmol NADPH/g biomass (Kiefer et al., 2004; Marx et al., 1999). *C. glutamicum* maintains its NADPH supply mainly via the pentose phosphate pathway (PPP) and the tricarboxylic acid cycle (Dominguez et al., 1998; Kiefer et al., 2004). About 50% of the provided NADPH was consumed by the glutamate dehydrogenase reaction, which functions mainly as donor of its amino group via transamination to cell mass synthesis and to a lesser extent, to provide glutamate and the other amino acids of the glutamate family for protein synthesis (Marx et al., 1999). Addition of rich medium to our SI production process enabled also a 100% conversion rate of MI to SI (Ramp et al., 2021; chapter 2.1), as described before (Tanaka et al., 2013). So by providing amino acids via cultivation in rich medium, less NADPH is required for *de novo* amino acid synthesis and therefore becomes available for the production

of SI. However, using rich medium drastically increases the cost and demand for cultivation and downstream processing. Therefore, metabolic engineering for increased NADPH supply is more desirable.

There are many strategies reported to increase the NADPH supply in *C. glutamicum*. One major approach is to release the negative feedback inhibition of the glucose-6-phosphate dehydrogenase Zwf and 6-phosphogluconate dehydrogenase Gnd, enabling a higher flux through the pentose phosphate pathway and therefore increased NADPH synthesis (Becker et al., 2007; Ohnishi et al., 2005). This approach can be combined by actively redirecting the flux through the pentose phosphate pathway by downregulation of the activity of the phosphoglucoisomerase Pgi, which catalyzes the interconversion of G6P to fructose-6-phophate, the initial reaction of the glycolysis (Bartek et al., 2010). Other strategies are based on introducing heterologous NADPH synthesis systems, like the cytosolic or membrane-bound transhydrogenases from *E. coli* (Kabus et al., 2007; Milke et al., 2020). Transhydrogenases interconvert NADH and NADPH, which would especially benefit the biotransformation of MI to SI, as IolG builds up NADH. Such a cycle reaction was attempted in *B. subtilis* to improve the production of SI from MI. The overexpression of the membrane-integral nicotinamide nucleotide transhydrogenase PntAB gene from *E. coli* in *B. subtilis* lead to slightly increased production of SI from MI (Tanaka et al., 2017). Another strategy is to replace the endogenous NAD-dependent glyceraldehyde-3-phosphate dehydrogenase (GapA) with a heterologous, nonphosphorylating NADP-dependent glyceraldehyde-3-phosphate dehydrogenase (GapN) (Takeno et al., 2016).

There is much room for improvement via metabolic engineering in *C. glutamicum* to improve the production of SI from MI in minimal medium. Yet, *C. glutamicum* has another advantage that underlines its potential as an efficient inositol production host. As *C. glutamicum* naturally synthesizes MI from G6P, production costs can be strongly reduced by the use of cheaper carbon sources. The inositol biosynthesis in *C. glutamicum* is tightly regulated by the MI-dependent transcriptional activator IpsA, which dissociates from the promoter region of the *myo*-inositol-1-phosphate synthase gene *ino1* after binding excessive MI (Baumgart et al., 2013). Combined overexpression of *ino1* with the monophosphatase gene *impA* and the IDH genes *iolG* and *iolW* successfully lead to the production of SI directly from glucose and sucrose (Fig. 3.3C) (Ramp et al., 2021; chapter 2.1).

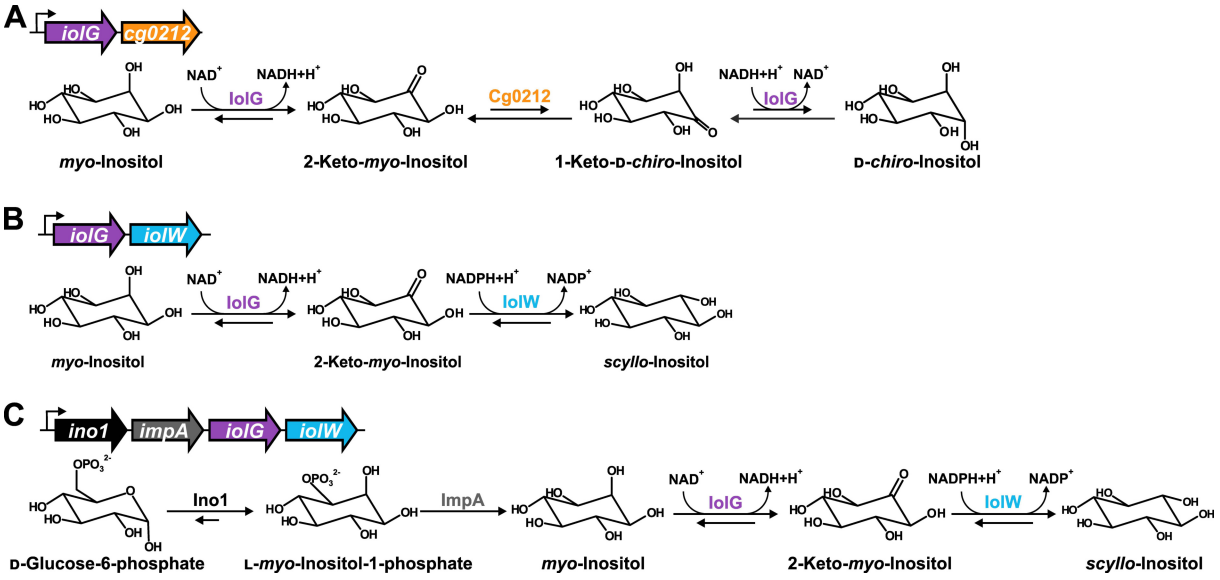

Fig. 3.3. Biosynthesis pathways utilizing inositol genes of *C. glutamicum* for the production of D-*chiro*- and *scyllo*-inositol. Shown are the generated expression cassettes and schematic reactions for the production of D-*chiro*-inositol starting from *myo*-inositol (MI) **(A)**, *scyllo*-inositol (SI) from MI **(B)** and SI from glucose-6-phosphate **(C)** with the *C. glutamicum* chassis strains MB001(DE3)Δ*iol1*Δ*iol2* and MB001(DE3)Δ*IOL*.

Surprisingly, the production of SI from 20 g/L sucrose reached higher titers (4.4 g/L) than from 20 g/L glucose (1.8 g/L), although only 10 g/L G6P are formed from 20 g/L sucrose. One possible explanation could be the promiscuous activity of IolG. BsIolG was shown to oxidize glucose to gluconate (Ramaley et al., 1979). This might occur in our production process, where free glucose is taken up by IolT1 and IolT2 and oxidized by highly overproduced IolG to gluconate, which cannot enter inositol synthesis anymore. Sucrose is taken up by PtsS of the PTS as sucrose-6-phosphate and hydrolyzed by ScrB to yield free fructose and G6P, for which IolG might not be active.

Biosynthesis of inositols starting directly from G6P competes with the first reactions of the central carbon metabolism in *C. glutamicum*. Ino1 has a reported K_m of 12 mM for G6P and a k_{cat} of 0.04 s^{-1} (Chen et al., 2019). It is therefore likely outperformed by the phosphoglucoisomerase Pgi (kinetics for G6P: *E coli* Pgi: K_m 0.28 mM, k_{cat} 212.21 s^{-1}; *M. tuberculosis* Pgi: K_m 0.27 mM, k_{cat} 617.43 s^{-1}) (Gao et al., 2005; Mathur and Garg, 2007) and glucose 6-phosphate dehydrogenase Zwf of *C. glutamicum*, which has a K_m value of 0.17 mM for G6P and a k_{cat} of 144.65 s^{-1} (Moritz et al., 2000). A reason for the slow activity of Ino1 could be that the catalytic mechanism starts with the open form of G6P, which makes up only 0.4% of the total sugar concentration in an aqueous solution (Ramos-Figueroa and Palmer, 2022).

Increasing the supply of G6P and redirecting carbon flux towards inositol biosynthesis is an applicable strategy to increase titers. However, simple deletion of e.g. *pgi* or *pfkA*, the gene encoding the phosphofructokinase PfkA catalyzing the phosphorylation of fructose-6-phosphate to fructose-1,6-bisphosphate comes with tremendous growth defects for *C. glutamicum* (Lindner et al., 2013; Siedler et al., 2013), which results in slower biomass formation and lower space-time yield. To overcome these obstacles, dynamic regulation strategies offer an alternative, in which flux through glycolysis is switched off and directed towards inositol synthesis after biomass formation. Such genetic circuits have been developed for MI and glucarate production in *E. coli* (Brockman and Prather, 2015; Reizman et al., 2015). In a particular case, the glycolysis controlling genes *pgi* and *pfkA* were expressed from a promoter controlled by a specific heterologous transcription factor, which activates gene expression in absence of its inductor. Accumulation of the inductor produced by another heterologous synthase leads to disruption of transcription factor binding and deactivates gene expression. Varying the expression level of the synthase, leads to different inductor accumulation rates, which allows downregulation of the controlled genes at variable times and cell densities over the course of cultivation (Gupta et al., 2017). For *C. glutamicum*, a similar system based on the VanR/P_{vanABK} regulatory system has been developed. The activity of the transcriptional repressor VanR is modulated by the inductor molecules ferulic acid, vanillin or vanillic acid, which are co-metabolized with D-glucose (Siebert et al., 2021). External addition of different concentrations of these inductor molecules enables dynamic regulation of genes expressed under the control of the VanR/P_{vanABK} system over the time of cultivation. Expression of *pgi* or *pfkA* in *C. glutamicum* controlled by the P_{vanABK} promoter would allow dynamic regulation of the G6P fluxed between the glycolytic pathway and the inositol synthesis pathway.

3.6 Novel synthesis routes and prospects for the production of other inositols

The inositol catabolism of *C. glutamicum* and other bacteria still has unknown reactions that can potentially be used for biotechnological production processes. The use of IolG and IolW proved to be an ideal production process for interconversion of MI to SI. However, IolW of *B. subtilis* and *C. glutamicum* are the only NADPH-dependent IDHs found so far. For the production of other inositol isomers, NADPH-dependent IDHs reducing other inositol keto-compounds like 1KDCI or *neo*-keto-inositol are desirable. One possibility could be the rational

engineering of NAD^+-dependent IDHs known to reduce other keto-intermediates, like IolG, to accept NADPH as cofactor. Such an approach has already been reported (Zheng et al., 2013). By altering the 2'-phosphate recognition site, BsIolG accepted $NADP^+$ as cofactor for oxidation of MI. Switching the preference for NAD^+/NADPH in oxidoreductases is an attractive strategy for the engineering of biocatalysts or metabolic pathways. However, the change of cofactor selectivity often leads to decreased catalytic activity (Chánique and Parra, 2018), which was also the case for BsIolG (Zheng et al., 2013). In addition, the reduction of keto-inositols by the modified IolG using NADPH has not been analyzed. Therefore it is of great interest to understand the structural features of IolW that determine its preference toward 2KMI. Our insights gained from the crystal structure analysis of CgIolW might be used to efficiently alter the cofactor specificity of NAD^+-dependent IDHs to accept NADPH or even engineer IolW to accept other keto-intermediates. Interchanging and combination of the NAD^+/NADPH-binding N-terminal-domain and the substrate-binding C-terminal domain of IDHs (discussed in more detail in chapter 5.3 of the Appendix) might enable the design of new biocatalysts.

The bacterial inositol catabolism is not the only source from which useful new biocatalysts can be derived. IDHs are found in other metabolic pathways in bacteria and even plants. In some *Streptomyces* species, IDHs are involved in the biosynthesis of aminoglycoside antibiotics including inositols (Kudo and Eguchi, 2009; Kudo and Eguchi, 2022). For example, the IDH Hyg17 from *Streptomyces hygroscopicus* NRRL 2388 oxidizes MI directly to *neo*-keto-inositol, which is further processed to be incorporated in hygromycin A (Palaniappan et al., 2009). Plant-derived examples include the two elaborated dehydrogenases MtOEPa and MtOEPb from *Medicago truncatula* (chapter 2.3). Alongside methyl-inositol epimerases, they catalyze the isomerization of the *O*-methylated inositol isomers D-ononitol to D-pinitol (Fig. 3.4A). So far, they are the only NAD^+/NADPH-dependent IDHs found in plants that catalyze this reaction. The identification of other *O*-methylated isomers like quebrachitol (2-*O*-methyl-L-*chiro*-inositol) or brahol (5-*O*-methyl-*allo*-inositol) (Ahmad et al., 1998; Siracusa et al., 2022) hints at the existence of other IDHs that could be used for the production of inositol isomers (e.g. L-*chiro*-inositol or *allo*-inositol). These IDHs accept slightly different inositols and catalyze different reactions, but the promiscuous activity of these enzymes makes them attractive. We could prove that by employing MtOEPa and MtOEPb for the novel synthesis route to produce DCI from MI and G6P (Fig. 3.4B and C). These enzymes have no structural identity to any bacterial IDH or share similar characteristics as they are predicted to have

deviating catalytic centers (Pupel et al., 2019). Yet they also oxidize and reduce unmethylated inositols similar to bacterial IDHs.

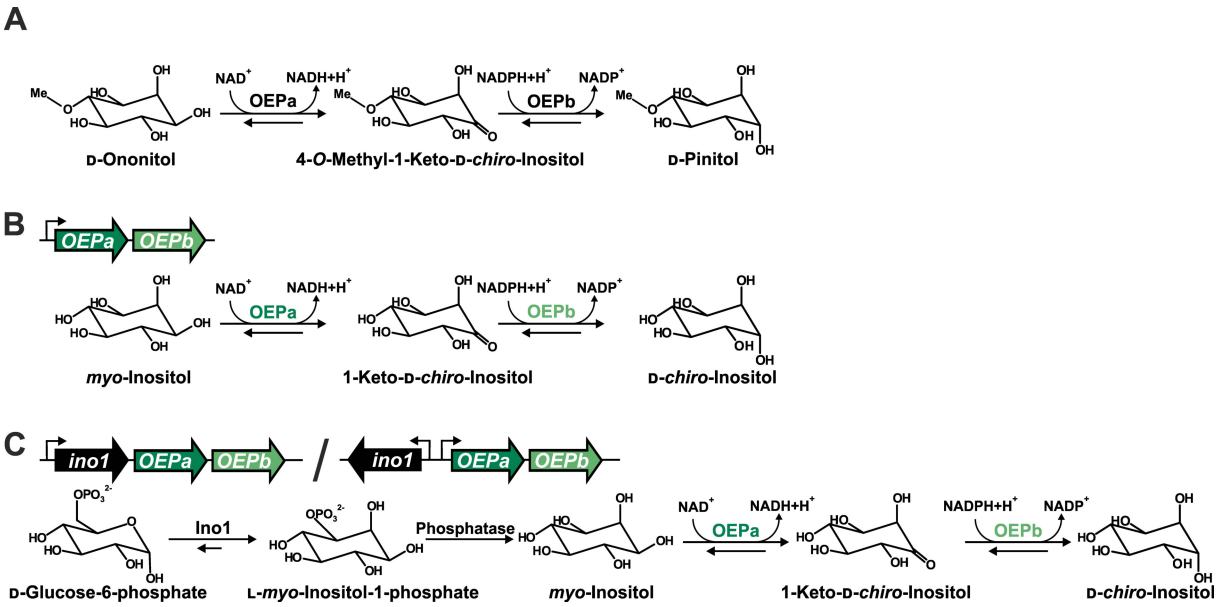

Fig. 3.4. Biosynthesis pathways utilizing the plant-derived inositol dehydrogenase genes MtOEPa and MtOEPb for the production of D-*chiro*-Inositol. Shown are the natural NAD(P)H dependent isomerization of D-ononitol to D-pinitol catalyzed by MtOEPa (OEPa) and MtOEPb (OEPb) in *Medicago truncatula* **(A)**, the generated expression cassettes and schematic reactions for the production of D-*chiro*-inositol starting from *myo*-inositol **(B)** and from glucose-6-phosphate **(C)** with the *C. glutamicum* chassis strain MB001(DE3)Δ*IOL* .

The production process for DCI from MI was much less efficient than the production of SI by IolG/IolW. This was mainly because this process relies on the unspecific side activity of these enzymes, which already have low specific activities for their preferred substrate (11.60-54.36 pmol min^{-1}) (Pupel et al., 2019). A powerful tool to increase their activity for unmethylated inositols would be growth-based adaptive laboratory evolution (Dragosits and Mattanovich, 2013; Portnoy et al., 2011). As we expect MtOEPa to oxidize MI to 1KDCI, the expression of the *MtOEPa* gene in *C. glutamicum* MB001(DE3)ΔIDH (Ramp et al., 2022; chapter 2.2) is assumed to complement growth. By screening for growth and isolation of clones showing higher fitness, the activity of MtOEPa might be improved. Combining the identification of novel IDHs with ALE and rational protein engineering might enable the development of new biocatalysts for the production of the other inositol isomers.

3.7 Conclusion

The studies summarized in this thesis contribute to the overall understanding of the inositol catabolism of *C. glutamicum* and demonstrate the potential of this microbial cell factory as a suitable host for the production of rare inositols (Fig. 3.5). At the beginning, more than 12 genes encoded in the two *iol1* and *iol2* clusters of *C. glutamicum* had an unknown function. Throughout this thesis, we revealed the activities of five IDHs and two inosose isomerases that lay hidden in these uncharacterized parts. In addition, another IDH and a further inosose isomerase were identified elsewhere in the genome. These nine newly characterized genes and their corresponding enzymes have profound functions for the degradation of multiple inositols in the versatile inositol catabolism of *C. glutamicum*, proving it as one of the best genetically equipped microorganisms for scavenging inositols from soil. Combining physiological, biochemical, structural, and bioinformatics analysis of IDHs, we elucidated characteristics that explain their selectivity towards inositols and catalytic preferences. As research on inosose isomerases is nearly nonexistent, identifying multiple inosose isomerases in *C. glutamicum* and analyzing their function in the interconversion of keto-inositols paves the way to better understand their contribution to inositol degradation.

We transferred the gained fundamental knowledge of the inositol catabolism of *C. glutamicum* to establish efficient biotechnological processes for the production of rare inositols. Deleting all inositol catabolism-associated genes identified enabled the generation of suitable *C. glutamicum* chassis strains. By reengineering parts of the inositol metabolism of *C. glutamicum*, we achieved the production of *myo*-inositol and of the pharmaceutical relevant inositol isomers *scyllo*-inositol and D-*chiro*-inositol. We established a novel biosynthesis route for D-*chiro*-inositol by heterologous expression of plant-derived IDHs, showing that much potential for inositol production processes is hidden in alternative inositol pathways. The findings summarized in this thesis lay the groundwork for further engineering of *C. glutamicum* and inositol dehydrogenases towards efficient and industrial relevant processes for the sustainable production of inositols.

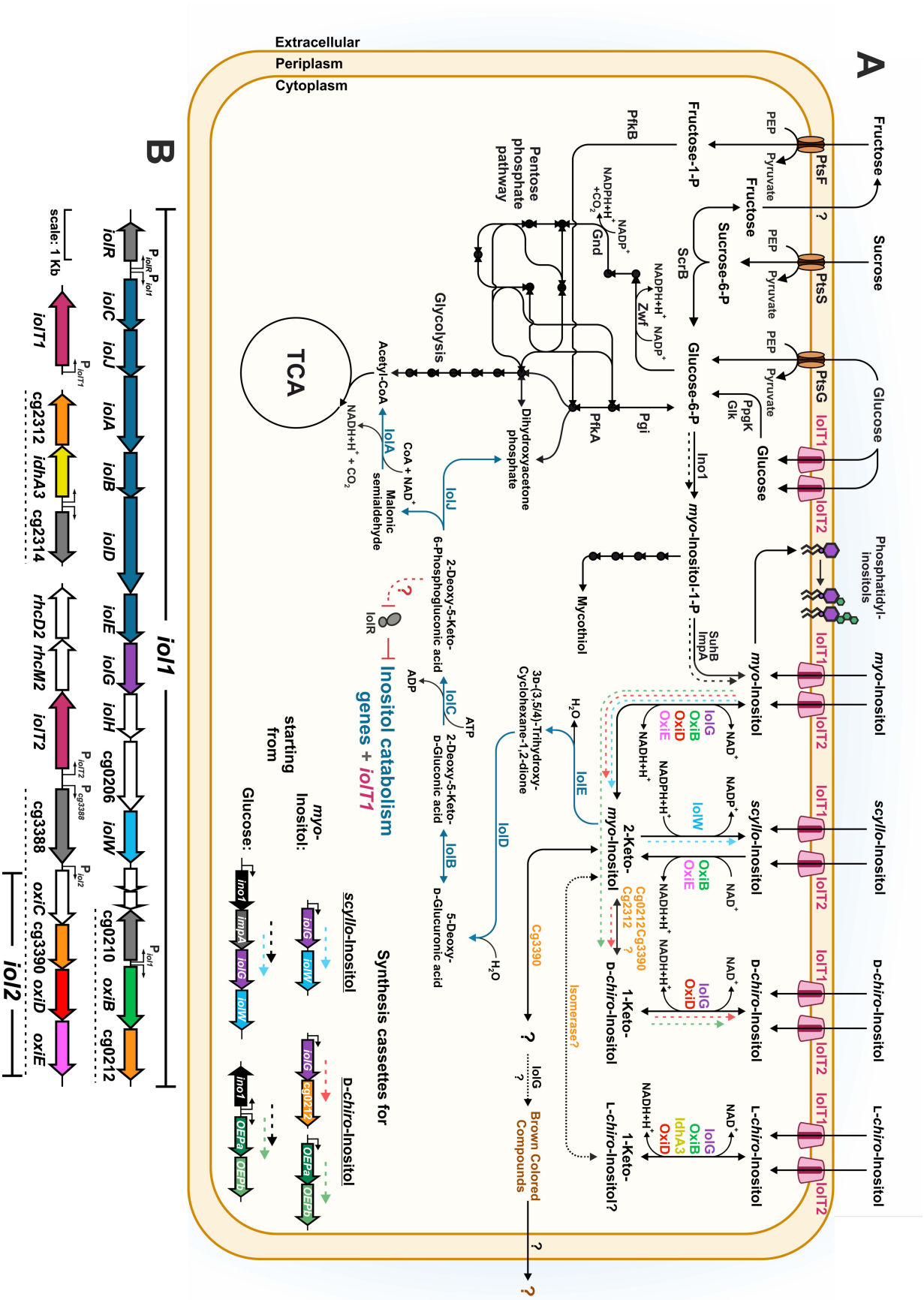
A
Extracellular
Periplasm
Cytoplasm
Fructose
Sucrose
Glucose
PtsF
PtsS
PtsG
IolT1
IolT2
PEP
Pyruvate
PpgK
Glk
Fructose-1-P
Fructose-6-P
Sucrose-6-P
ScrB
PfkB
PfkA
Pgi
Zwf
Gnd
NADPH+H+ NADP+
NADPH+H+ +CO2 NADP+
Pentose phosphate pathway
Glycolysis
TCA
Acetyl-CoA
CoA + NAD+
NADH+H+ + CO2
IolA
Malonic semialdehyde
IolJ
Dihydroxyacetone phosphate
Ino1
myo-Inositol-1-P
SuhB ImpA
Mycothiol
Phosphatidyl-inositols
myo-Inositol
scyllo-Inositol
D-chiro-Inositol
L-chiro-Inositol
IolG
OxiB
OxiD
OxiE
IolW
IdhA3
NAD+
NADH+H+
NADPH+H+
NADP+
2-Keto-myo-Inositol
1-Keto-D-chiro-Inositol
1-Keto-L-chiro-Inositol?
Cg0212 Cg3390 Cg2312 ?
Isomerase?
IolE
H2O
3D-(3,5/4)-Trihydroxy-Cyclohexane-1,2-dione
IolD
Cg3390
IolG ?
? ?
Brown Colored Compounds
2-Deoxy-5-Keto-6-Phosphogluconic acid
ADP
IolC
ATP
2-Deoxy-5-Keto-D-Gluconic acid
IolB
5-Deoxy-D-Glucuronic acid
IolR
Inositol catabolism genes + iol/T1
Synthesis cassettes for
scyllo-Inositol
D-chiro-Inositol
myo-Inositol:
Glucose:
starting from
ino1
impA
OEPa
OEPb
B
iol1
iol2
scale: 1 Kb
iolR
iolC
iolJ
iolA
iolB
iolD
iolE
iolG
iolH
iolW
iolT1
iolT2
cg0206
cg0210
oxiB
cg0212
cg2312
idhA3
cg2314
rhcD2
rhcM2
cg3388
oxiC
cg3390
oxiD
oxiE

Fig. 3.5. Schematic summary of elucidated inositol metabolism, generated synthesis cassettes (A) and organization of identified and characterized inositol genes (B) in *Corynebacterium glutamicum*.

C. glutamicum takes up *myo*-, *scyllo*-, D-*chiro*-, and L-*chiro*-inositol via the two specific inositol transporters IolT1 and IolT2. In the cytoplasm, inositols are oxidized by diverse NAD^+-dependent inositol dehydrogenases (IolG, OxiB, IdhA3, OxiD, OxiE) to yield 2-keto-*myo*-inositol (2KMI) or other keto-intermediates (1-keto-D-*chiro*- or hypothesized 1-keto-L-*chiro*-inositol; 1KDCI and 1KLCI). Inosose isomerases encoded by cg0212, cg2312, cg3390 and yet unidentified genes interconvert 2KMI and 1KDCI, 1KLCI is believed to be converted to 2KMI via an inosose isomerase. Cg3390 also interconverts 2KMI to other, unknown products, which exhibit brown coloration after further reactions. 2KMI enters the inositol degradation pathway encoded by the *iolCJABDE* operon, where it is converted to intermediates of central metabolism, dihydroxyacetone phosphate, acetyl-CoA, and CO_2. 2KMI is also naturally reduced by the NADPH dependent IDH IolW to yield *scyllo*-inositol. Expression of the *iolCJABDEGH* operon and *iolT1* is regulated via the transcriptional repressor IolR. IolR of *C. glutamicum* is believed to bind accumulating 2-deoxy-5-keto-6-phosphogluconic acid (DKGP) causing dissociation from its operator and thus induction of gene expression. L-*myo*-inositol-1-phosphate (MIP1) is synthesized from D-glucose-6-phosphate (G6P) by Ino1. Together with UDP-GlcNAc and L-cysteine it is one of the precursors for the dominant thiol mycothiol. MIP1 is dephosphorylated to free MI via the inositol phosphatases ImpA and SuhB. Free MI is linked to cytidine diphosphate diacylglycerol to generate phosphatidylinositol, which can be converted to more complex inositol-containing lipids. Overexpression of *C. glutamicums* own IDHs (*iolG* and *iolW*) and inosose isomerase cg0212 in an inositol catabolism deficient strain enables production of D-*chiro*-Inositol (red dashed arrows) and *scyllo*-inositol (blue dashed arrows) from *myo*-inositol. Heterologous overexpression of the NAD(P)H-dependent IDHs from *Medicago truncatula* (OEPa and OPEb) enables an alternative biosynthesis route to produce D-*chiro*-inositol from *myo*-inositol (green dashed arrows). Additional overexpression of *ino1* (and *impA*) enables production of inositols from G6P (black arrows + colored arrows). Glucose is either taken up by the phosphotransferase system PtsG followed by phosphoenol pyruvate (PEP) dependent phosphorylation or via IolT1 and IolT2 and subsequent phosphorylation by the glucosekinases Glk and Ppgk. *C. glutamicum* can also utilize sucrose via uptake by the phosphotransferase system PtsS, PEP-dependent phosphorylation and hydrolyzation by the sucrose-6-phosphate hydrolase ScrB to yield G6P and fructose. Fructose is exported via an unknown transporter and taken up by the fructose phosphotransferase system PtsF resulting in fructose-1-phosphate. The phosphofructokinase PfkB converts fructose-1-phopshate to fructose-1,6-bisphosphate which enters the glycolysis. G6P also enters glycolysis after isomerization to fructose-6-phosphate by the phosphorglucoisomerase Pgi and phosphorylation to fructose-1,6-bisphosphate by the phosphofructokinase PfkA. G6P also enters the pentose phosphate pathway after step-wise $NADP^+$-dependent oxidation by the glucose-6-phosphate dehydrogenase Zwf and 6-phosphogluconate dehydrogenase Gnd. Colors of genes in **(B)** resemble colors of protein names in **(A)**. Colors of arrows in **(A)** do not correspond to genes in **(B)**. Putative genes or genes not being part of inositol metabolism are depicted in white. Dashed lines in **(B)** show putative IDH-isomerase modules.

4. References

Aamudalapalli, H. B., Bertwistle, D., Palmer, D. R., Sanders, D. A., 2018. *Myo*-inositol dehydrogenase and *scyllo*-inositol dehydrogenase from *Lactobacillus casei* BL23 bind their substrates in very different orientations. BBA-Proteins Proteom 1866, 1115-1124.

Ahlert, J., Distler, J., Mansouri, K., Piepersberg, W., 1997. Identification of *stsC*, the gene encoding the L-glutamine:*scyllo*-inososе aminotransferase from streptomycin-producing Streptomycetes. Arch. Microbiol. 168, 102-113.

Ahmad, V. U., Ali, Z., Ali, M. S., Zahid, M., Tareen, R. B., 1998. Brahol: A new derivative of *allo*-inositol from *Stocksia brahuica*. Nat. Prod. Sci. 4, 170-173.

Al-Suod, H., Ligor, M., Rațiu, I.-A., Rafińska, K., Górecki, R., Buszewski, B., 2017. A window on cyclitols: Characterization and analytics of inositols. Phytochem. Lett. 20, 507-519.

Al Mughram, M. H., Catalano, C., Bowry, J. P., Safo, M. K., Scarsdale, J. N., Kellogg, G. E., 2021. 3D interaction homology: hydropathic analyses of the "π–cation" and "π–π" interaction motifs in phenylalanine, tyrosine, and tryptophan residues. J. Chem. Inf. Model. 61, 2937-2956.

Alberts, B., Bray, D., Hopkin, K., Johnson, A. D., Lewis, J., Raff, M., Roberts, K., Walter, P., 2015. Cell signaling in essential cell biology. Garland Science, New York, NY, USA, pp. 525-555.

Altschul, S. F., Gish, W., Miller, W., Myers, E. W., Lipman, D. J., 1990. Basic local alignment search tool. J. Mol. Biol. 215, 403-410.

Altschul, S. F., Madden, T. L., Schäffer, A. A., Zhang, J., Zhang, Z., Miller, W., Lipman, D. J., 1997. Gapped BLAST and PSI-BLAST: a new generation of protein database search programs. Nucleic Acids Res. 25, 3389-3402.

Amador-Noguez, D., Brasg, I. A., Feng, X.-J., Roquet, N., Rabinowitz, J. D., 2011. Metabolome remodeling during the acidogenic-solventogenic transition in *Clostridium acetobutylicum*. Appl. Environ. Microbiol. 77, 7984-7997.

Andersen, K. B., von Meyenburg, K., 1977. Charges of nicotinamide adenine nucleotides and adenylate energy charge as regulatory parameters of the metabolism in *Escherichia coli*. J. Biol. Chem. 252, 4151-4156.

Anderson, W. A., Magasanik, B., 1971. The pathway of *myo*-inositol degradation in *Aerobacter aerogenes*. Conversion of 2-deoxy-5-keto-D-gluconic acid to glycolytic intermediates. J. Biol. Chem. 246, 5662-5675.

Arndt, A., Auchter, M., Ishige, T., Wendisch, V. F., Eikmanns, B., 2008. Ethanol catabolism in *Corynebacterium glutamicum*. Microb. Physiol. 15, 222-233.

Arner, R. J., Prabhu, K. S., Reddy, C. C., 2004. Molecular cloning, expression, and characterization of *myo*-inositol oxygenase from mouse, rat, and human kidney. Biochem. Biophys. Res. Commun. 324, 1386-1392.

Arner, R. J., Prabhu, K. S., Thompson, J. T., Hildenbrandt, G. R., Liken, A. D., Reddy, C., 2001. *myo*-Inositol oxygenase: molecular cloning and expression of a unique enzyme that oxidizes *myo*-inositol and D-*chiro*-inositol. Biochem. J 360, 313-320.

Ashrafian, H., Zadeh, E. H., Khan, R. H., 2021. Review on Alzheimer's disease: inhibition of amyloid beta and tau tangle formation. Int. J. Biol. Macromol. 167, 382-394.

Asplin, I., Galasko, G., Larner, J., 1993. *chiro*-inositol deficiency and insulin resistance: a comparison of the *chiro*-inositol- and the *myo*-inositol-containing insulin mediators isolated from urine, hemodialysate, and muscle of control and type II diabetic subjects. Proc. Natl. Acad. Sci. USA 90, 5924-5928.

Bachhawat, N., Mande, S. C., 1999. Identification of the INO1 gene of *Mycobacterium tuberculosis* H37Rv reveals a novel class of inositol-1-phosphate synthase enzyme. J. Mol. Biol. 291, 531-536.

Balla, T., 2013. Phosphoinositides: tiny lipids with giant impact on cell regulation. Physiol. Rev. 93, 1019-1137.

Baritugo, K.-A., Kim, H. T., David, Y., Choi, J.-i., Hong, S. H., Jeong, K. J., Choi, J. H., Joo, J. C., Park, S. J., 2018. Metabolic engineering of *Corynebacterium glutamicum* for fermentative production of chemicals in biorefinery. Appl. Microbiol. Biotechnol. 102, 3915-3937.

Bartek, T., Blombach, B., Zönnchen, E., Makus, P., Lang, S., Eikmanns, B. J., Oldiges, M., 2010. Importance of NADPH supply for improved L-valine formation in *Corynebacterium glutamicum*. Biotechnol. Progr. 26, 361-371.

Bature, F., Guinn, B.-A., Pang, D., Pappas, Y., 2017. Signs and symptoms preceding the diagnosis of Alzheimer's disease: a systematic scoping review of literature from 1937 to 2016. BMJ Open 7, e015746.

Baumgart, M., Luder, K., Grover, S., Gätgens, C., Besra, G. S., Frunzke, J., 2013. IpsA, a novel LacI-type regulator, is required for inositol-derived lipid formation in *Corynebacteria* and *Mycobacteria*. BMC Biol. 11, 122.

Becker, J., Klopprogge, C., Herold, A., Zelder, O., Bolten, C. J., Wittmann, C., 2007. Metabolic flux engineering of L-lysine production in *Corynebacterium glutamicum*—overexpression and modification of G6P dehydrogenase. J. Biotechnol. 132, 99-109.

Becker, J., Rohles, C. M., Wittmann, C., 2018. Metabolically engineered *Corynebacterium glutamicum* for bio-based production of chemicals, fuels, materials, and healthcare products. Metab. Eng. 50, 122-141.

Becker, J., Wittmann, C., 2016. Industrial microorganisms: *Corynebacterium glutamicum*. Industrial Biotechnology: Microorganisms. Wiley Online Library, pp. 183-220.

Becker, J., Zelder, O., Häfner, S., Schröder, H., Wittmann, C., 2011. From zero to hero-design-based systems metabolic engineering of *Corynebacterium glutamicum* for L-lysine production. Metab. Eng. 13, 159-168.

Bellamacina, C. R., 1996. The nicotinamide dinucleotide binding motif: a comparison of nucleotide binding proteins. FASEB J. 10, 1257-1269.

Bendt, A. K., Burkovski, A., Schaffer, S., Bott, M., Farwick, M., Hermann, T., 2003. Towards a phosphoproteome map of *Corynebacterium glutamicum*. Proteomics 3, 1637-1646.

Bennett, B. D., Kimball, E. H., Gao, M., Osterhout, R., Van Dien, S. J., Rabinowitz, J. D., 2009. Absolute metabolite concentrations and implied enzyme active site occupancy in *Escherichia coli*. Nat. Chem. Biol. 5, 593-599.

Benvenga, S., Feldt-Rasmussen, U., Bonofiglio, D., Asamoah, E., 2019. Nutraceutical supplements in the thyroid setting: health benefits beyond basic nutrition. Nutrients 11, 2214.

Berman, T., Magasanik, B., 1966a. The pathway of *myo*-inositol degradation in *Aerobacter aerogenes*. Dehydrogenation and dehydration. J. Biol. Chem. 241, 800-806.

Berman, T., Magasanik, B., 1966b. The pathway of *myo*-inositol degradation in *Aerobacter aerogenes*. Ring scission. J. Biol. Chem. 241, 807-813.

Berry, G. T., Mallee, J. J., Kwon, H. M., Rim, J. S., Mulla, W. R., Muenke, M., Spinner, N. B., 1995. The human osmoregulatory Na+/*myo*-inositol cotransporter gene (SLC5A3): molecular cloning and localization to chromosome 21. Genomics 25, 507-513.

Bertani, G., 1951. Studies on lysogenesis. The mode of phage liberation by lysogenic *Escherichia coli*. J. Bacteriol. 62, 293-300.

Bettaney, K. E., Sukumar, P., Hussain, R., Siligardi, G., Henderson, P. J., Patching, S. G., 2013. A systematic approach to the amplified expression, functional characterization and purification of inositol transporters from *Bacillus subtilis*. Mol. Membr. Biol. 30, 3-14.

Binder, S., Schendzielorz, G., Stäbler, N., Krumbach, K., Hoffmann, K., Bott, M., Eggeling, L., 2012. A high-throughput approach to identify genomic variants of bacterial metabolite producers at the single-cell level. Genome Biol. 13, R40.

Bizzarri, M., Carlomagno, G., 2014. Inositol: history of an effective therapy for polycystic ovary syndrome. Eur. Rev. Med. Pharmacol. Sci. 18, 1896-1903.

Bizzarri, M., Fuso, A., Dinicola, S., Cucina, A., Bevilacqua, A., 2016. Pharmacodynamics and pharmacokinetics of inositol(s) in health and disease. Expert Opin. Drug Metab. Toxicol. 12, 1181-1196.

Blombach, B., Seibold, G. M., 2010. Carbohydrate metabolism in *Corynebacterium glutamicum* and applications for the metabolic engineering of L-lysine production strains. Appl. Microbiol. Biotechnol. 86, 1313-1322.

Blunsom, N. J., Cockcroft, S., 2020a. CDP-diacylglycerol synthases (CDS): gateway to phosphatidylinositol and cardiolipin synthesis. Front. Cell Dev. Biol. 8, 63.

Blunsom, N. J., Cockcroft, S., 2020b. Phosphatidylinositol synthesis at the endoplasmic reticulum. Biochim. Biophys. Acta, Mol. Cell. Biol. Lipids 1865, 158471.

Bott, M., Eggeling, L., 2017. Amino acid fermentation. In: Thomas Scheper, R. U., (Ed.), Advances in Biochemical Engineering/Biotechnology. vol. 159. Springer, pp. 227-254.

Bottoms, C. A., Smith, P. E., Tanner, J. J., 2002. A structurally conserved water molecule in Rossmann dinucleotide-binding domains. Protein Sci. 11, 2125-2137.

Boucher, J., Kleinridders, A., Kahn, C. R., 2014. Insulin receptor signaling in normal and insulin-resistant states. Cold Spring Harbor Perspect. Biol. 6, a009191.

Brockman, I. M., Prather, K. L., 2015. Dynamic knockdown of *E. coli* central metabolism for redirecting fluxes of primary metabolites. Metab. Eng. 28, 104-113.

Brüsseler, C., Radek, A., Tenhaef, N., Krumbach, K., Noack, S., Marienhagen, J., 2018. The *myo*-inositol/proton symporter IolT1 contributes to D-xylose uptake in *Corynebacterium glutamicum*. Bioresource. Technol. 249, 953-961.

Buehner, M., Ford, G. C., Moras, D., Olsen, K. W., Rossmann, M. G., 1974. Three-dimensional structure of D-glyceraldehyde-3-phosphate dehydrogenase. J. Mol. Biol. 90, 25-49.

Bui, T. P. N., Mannerås-Holm, L., Puschmann, R., Wu, H., Troise, A. D., Nijsse, B., Boeren, S., Bäckhed, F., Fiedler, D., deVos, W. M., 2021. Conversion of dietary inositol into propionate and acetate by commensal *Anaerostipes* associates with host health. Nat. Comm. 12, 4798.

Buré, C., Cacas, J.-L., Mongrand, S., Schmitter, J.-M., 2014. Characterization of glycosyl inositol phosphoryl ceramides from plants and fungi by mass spectrometry. Anal. Bioanal. Chem. 406, 995-1010.

Caballo-Ponce, E., Meng, X., Uzelac, G., Halliday, N., Cámara, M., Licastro, D., Silva, D. P. d., Ramos, C., Venturi, V., 2018. Quorum Sensing in *Pseudomonas savastanoi* pv. *savastanoi* and *Erwinia toletana*: Role in Virulence and Interspecies Interactions in the Olive Knot. Appl. Environ. Microbiol. 84, e00950-18.

Caputo, M., Bona, E., Leone, I., Samà, M., Nuzzo, A., Ferrero, A., Aimaretti, G., Marzullo, P., Prodam, F., 2020. Inositols and metabolic disorders: From farm to bedside. J. Trat. Complem. Med. 10, 252-259.

Carugo, O., Argos, P., 1997. NADP-dependent enzymes. II: Evolution of the mono-and dinucleotide binding domains. Proteins 28, 29-40.

Chang, H.-H., Chao, H.-N., Walker, C. S., Choong, S.-Y., Phillips, A., Loomes, K. M., 2015. Renal depletion of *myo*-inositol is associated with its increased degradation in animal models of metabolic disease. Am. J. Physiol Renal Physiol. 309, F755-F763.

Chánique, A. M., Parra, L. P., 2018. Protein engineering for nicotinamide coenzyme specificity in oxidoreductases: attempts and challenges. Front. Microbiol. 9, 194.

Chartier-Harlin, M. C., Crawford, F., Houlden, H., Warren, A., Hughes, D., Fidani, L., Goate, A., Rossor, M., Roques, P., Hardy, J., 1991. Early-onset Alzheimer's disease caused by mutations at codon 717 of the beta-amyloid precursor protein gene. Nature 353, 844-846.

Chatterjee, D., Khoo, K.-H., 1998. Mycobacterial lipoarabinomannan: an extraordinary lipoheteroglycan with profound physiological effects. Glycobiol. 8, 113-120.

Chayen, N. E., Saridakis, E., 2008. Protein crystallization: from purified protein to diffraction-quality crystal. Nat. Methods. 5, 147-153.

Cheatham, B., Vlahos, C. J., Cheatham, L., Wang, L., Blenis, J., Kahn, C. R. J. M., 1994. Phosphatidylinositol 3-kinase activation is required for insulin stimulation of pp70 S6 kinase, DNA synthesis, and glucose transporter translocation. Mol. Cell. Biol. 14, 4902-4911.

Chen, C., Chen, K., Su, T., Zhang, B., Li, G., Pan, J., Si, M., 2019. *Myo*-inositol-1-phosphate synthase (Ino-1) functions as a protection mechanism in *Corynebacterium glutamicum* under oxidative stress. Microbiol. Open 8, e00721.

Cheng, K., Zheng, W., Chen, H., Zhang, Y.-H. P. J., 2019. Upgrade of wood sugar D-xylose to a value-added nutraceutical by in vitro metabolic engineering. Metab. Eng. 52, 1-8.

Chiofalo, B., Laganà, A. S., Palmara, V., Granese, R., Corrado, G., Mancini, E., Vitale, S. G., Frangež, H. B., Vrtačnik-Bokal, E., Triolo, O., 2017. Fasting as possible complementary approach for polycystic ovary syndrome: Hope or hype? Med. Hypotheses 105, 1-3.

Chukwuma, C. I., Ibrahim, M. A., Islam, M., 2016. *Myo*-inositol inhibits intestinal glucose absorption and promotes muscle glucose uptake: A dual approach study. J. Physiol. Biochem. 72, 791-801.

Claes, W. A., Pühler, A., Kalinowski, J., 2002. Identification of two *prpDBC* gene clusters in *Corynebacterium glutamicum* and their involvement in propionate degradation via the 2-methylcitrate cycle. J. Bacteriol. 184, 2728-2739.

Clements Jr, R. S., Diethelm, A. G., 1979. The metabolism of *myo*-inositol by the human kidney. J. Lab. Clin. Med. 93, 210-219.

Coady, M. J., Wallendorff, B., Gagnon, D. G., Lapointe, J.-Y., 2002. Identification of a novel Na^+/*myo*-inositol cotransporter. J. Biol. Chem. 277, 35219-35224.

Cosgrove, D. J., Irving, G., 1980. Inositol phosphates: their chemistry, biochemistry, and physiology. Elsevier Science & Technology, Amsterdam.

Cui, W., Ma, A., Farhadi, A., Saqib, H. S. A., Liu, S., Chen, H., Ma, H., 2022. How *myo*-inositol improves the physiological functions of aquatic animals: A review. Aquaculture 553:738118, 738118.

D'Oria, R., Laviola, L., Giorgino, F., Unfer, V., Bettocchi, S., Scioscia, M., 2017. PKB/Akt and MAPK/ERK phosphorylation is highly induced by inositols: Novel potential insights in endothelial dysfunction in preeclampsia. Pregnancy Hypertens 10, 107-112.

Dafoe, J. T., Daugulis, A. J., 2014. In situ product removal in fermentation systems: improved process performance and rational extractant selection. Biotechnol. Lett. 36, 443-460.

De Strooper, B., 2003. Aph-1, Pen-2, and nicastrin with presenilin generate an active γ-secretase complex. Neuron 38, 9-12.

DeKosky, D. S. T., Harbaugh, R. E., Schmitt, F. A., Bakay, R. A., Chui, H. C., Knopman, D. S., Reeder, T. M., Shetter, A. G., Senter, H. J., Markesbery, W. R., 1992. Cortical biopsy in Alzheimer's disease: diagnostic accuracy and neurochemical, neuropathological, and cognitive correlations. Ann. Neurol. 32, 625-632.

Deshpande, A. D., Harris-Hayes, M., Schootman, M., 2008. Epidemiology of diabetes and diabetes-related complications. Phys. Ther. 88, 1254-1264.

Di Paolo, G., De Camilli, P., 2006. Phosphoinositides in cell regulation and membrane dynamics. Nature 443, 651-657.

Dinicola, S., Chiu, T. T., Unfer, V., Carlomagno, G., Bizzarri, M., 2014. The rationale of the *myo*-inositol and D-*chiro*-inositol combined treatment for polycystic ovary syndrome. J. Clin. Pharmacol. 54, 1079-1092.

Dinicola, S., Minini, M., Unfer, V., Verna, R., Cucina, A., Bizzarri, M., 2017. Nutritional and acquired deficiencies in inositol bioavailability. Correlations with metabolic disorders. Int. J. Mol. Sci. 18, 2187.

Dittrich, J., Schmidt, D., Pfleger, C., Gohlke, H., 2018. Converging a knowledge-based scoring function: DrugScore2018. J. Chem. Inf. Model. 59, 509-521.

Dominguez, H., Rollin, C., Guyonvarch, A., Guerquin-Kern, J. L., Cocaign-Bousquet, M., Lindley, N. D., 1998. Carbon-flux distribution in the central metabolic pathways of *Corynebacterium glutamicum* during growth on fructose. Eur. J. Biochem. 254, 96-102.

Dragosits, M., Mattanovich, D., 2013. Adaptive laboratory evolution – principles and applications for biotechnology. Microb. Cell. Fact. 12, 64.

Eggeling, L., Bott, M., 2005. Handbook of *Corynebacterium glutamicum*. CRC press, Boca Raton, USA.

Eggeling, L., Bott, M., 2015. A giant market and a powerful metabolism: L-lysine provided by *Corynebacterium glutamicum*. Appl. Microbiol. Biotechnol. 99, 3387-3394.

Eisenhaber, B., Maurer-Stroh, S., Novatchkova, M., Schneider, G., Eisenhaber, F., 2003. Enzymes and auxiliary factors for GPI lipid anchor biosynthesis and post-translational transfer to proteins. Bioessays 25, 367-385.

Emsley, P., Lohkamp, B., Scott, W. G., Cowtan, K., 2010. Features and development of Coot. Acta Crystallogr. D. 66, 486-501.

Engels, V., Wendisch, V. F., 2007. The DeoR-type regulator SugR represses expression of *ptsG* in *Corynebacterium glutamicum*. J. Bacteriol. 189, 2955-2966.

Eswar, N., Eramian, D., Webb, B., Shen, M.-Y., Sali, A., 2008. Protein structure modeling with MODELLER. Structural proteomics. Springer, pp. 145-159.

Evans, P. R., Murshudov, G. N., 2013. How good are my data and what is the resolution? Acta Crystallogr. D. 69, 1204-1214.

Fagone, P., Jackowski, S., 2009. Membrane phospholipid synthesis and endoplasmic reticulum function. J. Lipid Res 50, S311-S316.

Fang, Z., Zhang, W., Zhang, T., Guang, C., Mu, W., 2018. Isomerases and epimerases for biotransformation of pentoses. Appl. Microbiol. Biotechnol. 102, 7283-7292.

Fenili, D., Brown, M., Rappaport, R., McLaurin, J., 2007. Properties of *scyllo*–inositol as a therapeutic treatment of AD-like pathology. J. Mol. Med. 85, 603-611.

Ferguson, M., 1999. The structure, biosynthesis and functions of glycosylphosphatidylinositol anchors, and the contributions of trypanosome research. J. Cell Sci. 112, 2799-2809.

Follmann, M., Ochrombel, I., Krämer, R., Trötschel, C., Poetsch, A., Rückert, C., Hüser, A., Persicke, M., Seiferling, D., Kalinowski, J., 2009. Functional genomics of pH homeostasis in *Corynebacterium glutamicum* revealed novel links between pH response, oxidative stress, iron homeostasis and methionine synthesis. BMC Genomics 10, 621.

Fondi, M., Emiliani, G., Fani, R., 2009. Origin and evolution of operons and metabolic pathways. Res. Microbiol. 160, 502-512.

Freudl, R., 2017. Beyond amino acids: use of the *Corynebacterium glutamicum* cell factory for the secretion of heterologous proteins. J. Biotechnol. 258, 101-109.

Fry, J., Wood, M., Poole, P. S., 2001. Investigation of *myo*-inositol catabolism in *Rhizobium leguminosarum* bv. *viciae* and its effect on nodulation competitiveness. Mol. Plant Microbe Interact. 14, 1016-1025.

Fujisawa, T., Fujinaga, S., Atomi, H., 2017. An *in vitro* enzyme system for the production of *myo*-inositol from starch. Appl. Environ. Microbiol. 83, e00550-17.

Fukano, K., Ozawa, K., Kokubu, M., Shimizu, T., Ito, S., Sasaki, Y., Nakamura, A., Yajima, S., 2018. Structural basis of L-glucose oxidation by *scyllo*-inositol dehydrogenase: Implications for a novel enzyme subfamily classification. PLoS One 13, e0198010.

Gambioli, R., Forte, G., Aragona, C., Bevilacqua, A., Bizzarri, M., Unfer, V., 2021. The use of D-*chiro*-Inositol in clinical practice. Eur. Rev. Med. Pharmacol. Sci. 25, 438-446.

Gao, H., Chen, Y., Leary, J. A., 2005. Kinetic measurements of phosphoglucose isomerase and phosphomannose isomerase by direct analysis of phosphorylated aldose–ketose isomers using tandem mass spectrometry. Int. J. Mass Spectrom. 240, 291-299.

Gardocki, M. E., Jani, N., Lopes, J. M. J. B. e. B. A.-M., 2005. Phosphatidylinositol biosynthesis: biochemistry and regulation. Biochim. Biophys. Acta, Mol. Cell. Biol. Lipids 1735, 89-100.

Gauttam, R., Desiderato, C., Jung, L., Shah, A., Eikmanns, B. J., 2019. A step forward: Compatible and dual-inducible expression vectors for gene co-expression in *Corynebacterium glutamicum*. Plasmid 101, 20-27.

Gerke, J., 2015. Phytate (inositol hexakisphosphate) in soil and phosphate acquisition from inositol phosphates by higher plants. A review. Plants 4, 253-266.

Gerstmeir, R., Wendisch, V. F., Schnicke, S., Ruan, H., Farwick, M., Reinscheid, D., Eikmanns, B., 2003. Acetate metabolism and its regulation in *Corynebacterium glutamicum*. J. Biotechnol. 104, 99-122.

Gevers, D., Vandepoele, K., Simillion, C., Van de Peer, Y., 2004. Gene duplication and biased functional retention of paralogs in bacterial genomes. Trends. Microbiol. 12, 148-154.

Gibson, D. G., Young, L., Chuang, R. Y., Venter, J. C., Hutchison, C. A., 3rd, Smith, H. O., 2009. Enzymatic assembly of DNA molecules up to several hundred kilobases. Nat. Methods 6, 343-345.

Goldbeck, O., Seibold, G. M., 2018. Construction of pOGOduet–an inducible, bicistronic vector for synthesis of recombinant proteins in *Corynebacterium glutamicum*. Plasmid 95, 11-15.

Goodhart, R. S., Shils, M. E., 1980. Modern nutrition in health and disease. Lea & Febiger, Philadelphia, USA.

Green, M. R., Hughes, H., Sambrook, J., MacCallum, P., 2012. Molecular cloning: a laboratory manual. Cold Spring Harbor Laboratory Press, Cold Spring Harbor, New York.

Griffin, W., Stanley, L., Ling, C., White, L., MacLeod, V., Perrot, L., White 3rd, C., Araoz, C., 1989. Brain interleukin 1 and S-100 immunoreactivity are elevated in Down syndrome and Alzheimer disease. Proc. Natl. Acad. Sci. USA 86, 7611-7615.

Guo, Y., Gong, W., Wang, L., Guo, J., Jin, G., Gu, G., Guo, Z., 2018. Characterization and biochemical investigation of the potential inositol monophosphate phosphatase involved in bacterial mycothiol biosynthesis. J. Carbohydr. Chem. 37, 507-521.

Gupta, A., Reizman, I. M. B., Reisch, C. R., Prather, K. L., 2017. Dynamic regulation of metabolic flux in engineered bacteria using a pathway-independent quorum-sensing circuit. Nat. Biotechnol. 35, 273-279.

Hanahan, D., 1983. Studies on transformation of *Escherichia coli* with plasmids. J. Mol. Biol. 166, 557-580.

Hansen, C. A., Dean, A. B., Draths, K., Frost, J., 1999. Synthesis of 1, 2, 3, 4-tetrahydroxybenzene from D-glucose: exploiting *myo*-inositol as a precursor to aromatic chemicals. JACS 121, 3799-3800.

Heimark, D., McAllister, J., Larner, J., 2013. Decreased *myo*-inositol to *chiro*-inositol (M/C) ratios and increased M/C epimerase activity in PCOS theca cells demonstrate increased insulin sensitivity compared to controls. Endocr. J. 61, 111-117.

Henke, N. A., Wichmann, J., Baier, T., Frohwitter, J., Lauersen, K. J., Risse, J. M., Peters-Wendisch, P., Kruse, O., Wendisch, V. F., 2018. Patchoulol production with metabolically engineered *Corynebacterium glutamicum*. Genes 9, 219.

Hipps, P. P., Ackermann, K. E., Sherman, W. R., 1982. Inositol epimerase-Inosose reductase from bovine brain. Method. Enzymol. 89, 593-598.

Hipps, P. P., Sehgal, R. K., Holland, W. H., Sherman, W. R., 1973. Identification and partial characterization of inositol:NAD^+ epimerase and inosose: NAD(P)H reductase from the fat body of the American cockroach, *Periplaneta americana*. Biochem. 12, 4705-4712.

Holmes, C., Lovestone, S., 2002. The clinical phenotype of familial and sporadic late onset Alzheimer's disease. Int. J. Geriatr. Psych. 17, 146-149.

Holub, B. J., 1986. Metabolism and function of *myo*-inositol and inositol phospholipids. Annu. Rev. Nutr. 6, 563-597.

Homburg, R., 2008. Polycystic ovary syndrome. Best Pract. Res. Cl. Ga. 22, 261-274.

Howard Jr, C. F., Anderson, L., 1967. Metabolism of *myo*-inositol in animals: II. Complete catabolism of *myo*-inositol-^{14}C by rat kidney slices. Arch. Biochem. Biophys. 118, 332-339.

Huber, K., 2016. Cellular *myo*-inositol metabolism. In: Walk, C. L., Kühn, I., Stein, H. H., Kidd, M. T., Rodehutscord, M., (Ed.), Phytate destruction-consequences for precision animal nutrition. vol. 1. Wageningen Academic Publishers, pp. 53-60.

Hunter, S., Apweiler, R., Attwood, T. K., Bairoch, A., Bateman, A., Binns, D., Bork, P., Das, U., Daugherty, L., Duquenne, L., 2009. InterPro: the integrative protein signature database. Nucleic Acids Res. 37, 211-215.

Hüser, A. T., Becker, A., Brune, I., Dondrup, M., Kalinowski, J., Plassmeier, J., Pühler, A., Wiegräbe, I., Tauch, A., 2003. Development of a *Corynebacterium glutamicum* DNA microarray and validation by genome-wide expression profiling during growth with propionate as carbon source. J. Biotechnol. 106, 269-286.

Hüser, A. T., Chassagnole, C., Lindley, N. D., Merkamm, M., Guyonvarch, A., Elišáková, V., Pátek, M., Kalinowski, J. r., Brune, I., Pühler, A., 2005. Rational design of a *Corynebacterium glutamicum* pantothenate production strain and its characterization by metabolic flux analysis and genome-wide transcriptional profiling. Appl. Environ. Microbiol. 71, 3255-3268.

Ikeda, M., Nakagawa, S., 2003. The *Corynebacterium glutamicum* genome: features and impacts on biotechnological processes. Appl. Microbiol. Biotechnol. 62, 99-109.

Inui, M., Kawaguchi, H., Murakami, S., Vertès, A. A., Yukawa, H., 2004. Metabolic engineering of *Corynebacterium glutamicum* for fuel ethanol production under oxygen-deprivation conditions. Microb. Physiol. 8, 243-254.

Jackson, M., Crick, D. C., Brennan, P. J., 2000. Phosphatidylinositol is an essential phospholipid of *mycobacteria*. J. Biol. Chem. 275, 30092-30099.

Jeon, Y., Aja, S., Ronnett, G. V., Kim, E.-K., 2016. D-*chiro*-inositol glycan reduces food intake by regulating hypothalamic neuropeptide expression via AKT-FoxO1 pathway. Biochem. Biophys. Res. Commun. 470, 818-823.

Jiang, Y., Qian, F., Yang, J., Liu, Y., Dong, F., Xu, C., Sun, B., Chen, B., Xu, X., Li, Y., 2017. CRISPR-Cpf1 assisted genome editing of *Corynebacterium glutamicum*. Nat. Comm. 8, 15179.

Juhas, M., Van Der Meer, J. R., Gaillard, M., Harding, R. M., Hood, D. W., Crook, D. W., 2009. Genomic islands: tools of bacterial horizontal gene transfer and evolution. FEMS Microbiol. Rev. 33, 376-393.

Jumper, J., Evans, R., Pritzel, A., Green, T., Figurnov, M., Ronneberger, O., Tunyasuvunakool, K., Bates, R., Žídek, A., Potapenko, A., Bridgland, A., Meyer, C., Kohl, S. A. A., Ballard, A. J., Cowie, A., Romera-Paredes, B., Nikolov, S., Jain, R., Adler, J., Back, T.,

Petersen, S., Reiman, D., Clancy, E., Zielinski, M., Steinegger, M., Pacholska, M., Berghammer, T., Bodenstein, S., Silver, D., Vinyals, O., Senior, A. W., Kavukcuoglu, K., Kohli, P., Hassabis, D., 2021. Highly accurate protein structure prediction with AlphaFold. Nature 596, 583-589.

Kabsch, W., 2010. XDS. Acta Crystallogr. D. 66, 125-132.

Kabus, A., Georgi, T., Wendisch, V. F., Bott, M., 2007. Expression of the *Escherichia coli pntAB* genes encoding a membrane-bound transhydrogenase in *Corynebacterium glutamicum* improves L-lysine formation. Appl. Environ. Microbiol. 75, 47-53.

Kachhawa, G., Senthil Kumar, K. V., Kulshrestha, V., Khadgawat, R., Mahey, R., Bhatla, N., 2021. Efficacy of *myo*-inositol and D-*chiro*-inositol combination on menstrual cycle regulation and improving insulin resistance in young women with polycystic ovary syndrome: A randomized open-label study. Int. J. Gyncecol. Obstet. 158, 278-284.

Kadamur, G., Ross, E. M., 2013. Mammalian phospholipase C. Annu. Rev. Physiol. 75, 127-154.

Kalinowski, J., Bathe, B., Bartels, D., Bischoff, N., Bott, M., Burkovski, A., Dusch, N., Eggeling, L., Eikmanns, B. J., Gaigalat, L., 2003. The complete *Corynebacterium glutamicum* ATCC 13032 genome sequence and its impact on the production of L-aspartate-derived amino acids and vitamins. J. Biotechnol. 104, 5-25.

Kamiński, K., Ludwiczak, J., Jasiński, M., Bukala, A., Madaj, R., Szczepaniak, K., Dunin-Horkawicz, S., 2022. Rossmann-toolbox: a deep learning-based protocol for the prediction and design of cofactor specificity in Rossmann fold proteins. Brief. Bioinform. 23, bbab371.

Kang, D.-M., Michon, C., Morinaga, T., Tanaka, K., Takenaka, S., Ishikawa, S., Yoshida, K.-I., 2017a. *Bacillus subtilis* IolQ (DegA) is a transcriptional repressor of *iolX* encoding NAD+-dependent *scyllo*-inositol dehydrogenase. BMC Microbiol. 17, 154.

Kang, D.-M., Tanaka, K., Takenaka, S., Ishikawa, S., Yoshida, K.-I., 2017b. B*acillus subtilis* iolU encodes an additional NADP+-dependent *scyllo*-inositol dehydrogenase. Biosci. Biotech. Bioch. 81, 1026-1032.

Kasuga, K., Sasaki, A., Matsuo, T., Yamamoto, C., Minato, Y., Kuwahara, N., Fujii, C., Kobayashi, M., Agematu, H., Tamura, T., 2017. Heterologous production of kasugamycin, an aminoglycoside antibiotic from *Streptomyces kasugaensis*, in *Streptomyces lividans* and *Rhodococcus erythropolis* L-88 by constitutive expression of the biosynthetic gene cluster. Appl. Microbiol. Biotechnol. 101, 4259-4268.

Keilhauer, C., Eggeling, L., Sahm, H., 1993. Isoleucine synthesis in *Corynebacterium glutamicum*: molecular analysis of the *ilvB-ilvN-ilvC* operon. J. Bacteriol. 175, 5595-5603.

Kensy, F., Zang, E., Faulhammer, C., Tan, R. K., Büchs, J., 2009. Validation of a high-throughput fermentation system based on online monitoring of biomass and fluorescence in continuously shaken microtiter plates. Microb. Cell Fact. 8, 31.

Kessler, A., Müller, G., Wied, S., Crecelius, A., Eckel, J., 1998. Signalling pathways of an insulin-mimetic phosphoinositolglycan–peptide in muscle and adipose tissue. Biochem. J. 330, 277-286.

Kiani, A., Paolacci, S., Calogero, A., Cannarella, R., Di Renzo, G., Gerli, S., Della Morte, C., Busetto, G., De Berardinis, E., Giudice, D., 2021. From *Myo*-inositol to D-*chiro*-inositol molecular pathways. J. Eur. Rev. Med. Pharmacol. Sci. 25, 2390-2402.

Kiefer, F., Arnold, K., Künzli, M., Bordoli, L., Schwede, T., 2009. The SWISS-MODEL repository and associated resources. Nucleic Acids Res. 37, 387-392.

Kiefer, P., Heinzle, E., Wittmann, C. J. J. o. I. M., Biotechnology, 2002. Influence of glucose, fructose and sucrose as carbon sources on kinetics and stoichiometry of lysine production by *Corynebacterium glutamicum*. 28, 338-343.

Kiefer, P., Heinzle, E., Zelder, O., Wittmann, C., 2004. Comparative metabolic flux analysis of lysine-producing *Corynebacterium glutamicum* cultured on glucose or fructose. Appl. Environ. Microbiol. 70, 229-239.

Kingston, R. L., Scopes, R. K., Baker, E. N., 1996. The structure of glucose-fructose oxidoreductase from *Zymomonas mobilis*: an osmoprotective periplasmic enzyme containing non-dissociable NADP. Structure 4, 1413-1428.

Kinnard, R. L., Narasimhan, B., Pliskamatyshak, G., Murthy, P. P., 1995. Characterization of *scyllo*-inositol-containing phosphatidylinositol in plant cells. Biochem. Bioph. Res. Co. 210, 549-555.

Kinoshita, S., Udaka, S., Shimono, M., 1957. Studies on the amino acid fermentation. Part 1. Production of L-glutamic acid by various microorganisms. J. Gen. Appl. Microbiol. 50, 331-43.

Koch, A., Mizrahi, V., 2018. *Mycobacterium tuberculosis*. Trends Microbiol 26, 555-556.

Kohler, P. R., Rossbach, S., 2013. Bacterial inositol catabolism - A sweet ride into the host. In: Bruijn, F. J. d., (Ed.), Molecular Microbial Ecology of the Rhizosphere. vol. 1. John Wiley & Sons, Ltd, pp. 1163-1171.

Kohler, P. R., Zheng, J. Y., Schoffers, E., Rossbach, S., 2010. Inositol catabolism, a key pathway in *Sinorhizobium meliloti* for competitive host nodulation. Appl. Environ. Microbiol. 76, 7972-80.

Kortmann, M., Kuhl, V., Klaffl, S., Bott, M., 2015. A chromosomally encoded T7 RNA polymerase-dependent gene expression system for *Corynebacterium glutamicum*: Construction and comparative evaluation at the single-cell level. Microb. Biotechnol. 8, 253–265.

Krause, F. S., Blombach, B., Eikmanns, B. J., 2010. Metabolic engineering of *Corynebacterium glutamicum* for 2-ketoisovalerate production. Appl. Environ. Microbiol. 76, 8053-8061.

Krings, E., Krumbach, K., Bathe, B., Kelle, R., Wendisch, V. F., Sahm, H., Eggeling, L., 2006. Characterization of *myo*-inositol utilization by *Corynebacterium glutamicum*: the stimulon, identification of transporters, and influence on L-lysine formation. J. Bacteriol. 188, 8054-8061.

Kudo, F., Eguchi, T., 2009. Biosynthetic genes for aminoglycoside antibiotics. J. Antibiot. 62, 471-481.

Kudo, F., Eguchi, T., 2022. Biosynthesis of cyclitols. Nat. Prod. Rep. 39, 1622-1642.

Kulis-Horn, R. K., Rückert, C., Kalinowski, J., Persicke, M., 2017. Sequence-based identification of inositol monophosphatase-like histidinol-phosphate phosphatases (HisN) in *Corynebacterium glutamicum*, *Actinobacteria*, and beyond. BMC Microbiol. 17, 161.

L'Annunziata, M. F., Turner, B., Richardson, A., Mullaney, E., 2007. Origins and biochemical transformations of inositol stereoisomers and their phosphorylated derivatives in soil. In: Turner, B. R., AE; Mullaney, EJ, (Ed.), Inositol phosphates: linking agriculture the environment. Paperbackshop UK, pp. 41-60.

Lamichhane, J., Jha, A. K., Singh, B., Pandey, R. P., Sohng, J. K., 2014. Heterologous production of spectinomycin in *Streptomyces venezuelae* by exploiting the dTDP-D-desosamine pathway. J. Biotechnol. 174, 57-63.

Larner, J., 2002. D-*chiro*-inositol–its functional role in insulin action and its deficit in insulin resistance. Int. J. Exp. Diabetes Res. 3, 47-60.

Larner, J., Brautigan, D. L., Thorner, M. O., 2010. D-*chiro*-inositol glycans in insulin signaling and insulin resistance. Mol. Med. 16, 543-552.

Laslo, T., von Zaluskowski, P., Gabris, C., Lodd, E., Rückert, C., Dangel, P., Kalinowski, J., Auchter, M., Seibold, G., Eikmanns, B. J., 2012. Arabitol metabolism of *Corynebacterium glutamicum* and its regulation by AtlR. J. Bacteriol. 194, 941-955.

Lee, J.-Y., Na, Y.-A., Kim, E., Lee, H.-S., Kim, P., 2016. The actinobacterium *Corynebacterium glutamicum*, an industrial workhorse. J. Microbiol. Biotechnol. 26, 807–822.

Lewin, L. M., Yannai, Y., Sulimovici, S., Kraicer, P., 1976. Studies on the metabolic role of *myo*-inositol. Distribution of radioactive *myo*-inositol in the male rat. Biochem. J. 156, 375-380.

Li, Y., Han, P., Wang, J., Shi, T., You, C., 2021. Production of *myo*-inositol: Recent advance and prospective. Biotechnol. Appl. Bioc. 69, 1101-1111.

Li, Y., Liu, S., You, C. J. B. J., 2020. Permeabilized *Escherichia coli* whole cells containing co-expressed two thermophilic enzymes facilitate the synthesis of *scyllo*-inositol from *myo*-inositol. Biotechnol. J. 15, 1900191.

Lim, H. N., Lee, Y., Hussein, R., 2011. Fundamental relationship between operon organization and gene expression. Proc. Natl. Acad. Sci. USA 108, 10626-10631.

Lindner, S. N., Petrov, D. P., Hagmann, C. T., Henrich, A., Kramer, R., Eikmanns, B. J., Wendisch, V. F., Seibold, G. M., 2013. Phosphotransferase system-mediated glucose uptake is repressed in phosphoglucoisomerase-deficient *Corynebacterium glutamicum* strains. Appl. Environ. Microbiol. 79, 2588-2595.

Lindner, S. N., Seibold, G. M., Henrich, A., Krämer, R., Wendisch, V. F., 2011. Phosphotransferase system-independent glucose utilization in *Corynebacterium glutamicum* by inositol permeases and glucokinases. Appl. Environ. Microbiol. 77, 3571-3581.

Liu, X., Zhao, Z., Zhang, W., Sun, Y., Yang, Y., Bai, Z. J. E. i. l. s., 2017. Bicistronic expression strategy for high-level expression of recombinant proteins in *Corynebacterium glutamicum*. Eng. Life Sci. 17, 1118-1125.

Liu, Y.-B., Long, M.-X., Yin, Y.-J., Si, M.-R., Zhang, L., Lu, Z.-Q., Wang, Y., Shen, X.-H., 2013. Physiological roles of mycothiol in detoxification and tolerance to multiple poisonous chemicals in *Corynebacterium glutamicum*. Arch. Microbiol. 195, 419-429.

Liu, Y., Gong, X., Wang, C., Du, G., Chen, J., Kang, Z., 2016. Production of glucaric acid from *myo*-inositol in engineered *Pichia pastoris*. Enzyme Microb. Technol. 91, 8-16.

Lizcano, J. M., Alessi, D. R., 2002. The insulin signalling pathway. Curr. Biol. 12, 236-238.

Loewus, F. A., Kelly, S., 1962. Conversion of glucose to inositol in parsley leaves. Biochem. Biophys. Res. Commun. 7, 204-208.

Loewus, F. A., Murthy, P. P. N., 2000. *myo*-Inositol metabolism in plants. Plant Sci. 150, 1-19.

López-Gambero, A. J., Sanjuan, C., Serrano-Castro, P. J., Suárez, J., Rodríguez de Fonseca, F., 2020. The biomedical uses of inositols: A nutraceutical approach to metabolic dysfunction in aging and neurodegenerative diseases. Biomedicines 8, 295.

Lu, Y., Wang, L., Teng, F., Zhang, J., Hu, M., Tao, Y., 2018. Production of *myo*-inositol from glucose by a novel trienzymatic cascade of polyphosphate glucokinase, inositol 1-phosphate synthase and inositol monophosphatase. Enzyme Microb. Technol. 112, 1-5.

Magasanik, B., 1953. The pathway of inositol dissimilation in *Aerobacter aerogenes*. J. Biol. Chem. 205, 1019-1026.

Mahr, R., Gätgens, C., Gätgens, J., Polen, T., Kalinowski, J., Frunzke, J., 2015. Biosensor-driven adaptive laboratory evolution of L-valine production in *Corynebacterium glutamicum*. Metab. Eng. 32, 184-194.

Majumder, A. L., Biswas, B., 2006. Biology of inositols and phosphoinositides. Springer Science & Business Media, New York, USA.

Manske, C., Schell, U., Hilbi, H., 2016. Metabolism of *myo*-inositol by *Legionella pneumophila* promotes infection of amoebae and macrophages. Appl. Environ. Microbiol. 82, 5000-5014.

Marchesini, G., Brizi, M., Morselli-Labate, A. M., Bianchi, G., Bugianesi, E., McCullough, A. J., Forlani, G., Melchionda, N., 1999. Association of nonalcoholic fatty liver disease with insulin resistance. Am. J. Med. 107, 450-455.

Marx, A., Eikmanns, B. J., Sahm, H., de Graaf, A. A., Eggeling, L., 1999. Response of the central metabolism in *Corynebacterium glutamicum* to the use of an NADH-dependent glutamate dehydrogenase. Metab. Eng. 1, 35-48.

Mathur, D., Garg, L. C., 2007. Functional phosphoglucose isomerase from *Mycobacterium tuberculosis* H37Rv: rapid purification with high yield and purity. Protein Expression Purif. 52, 373-378.

McCoy, A. J., Grosse-Kunstleve, R. W., Adams, P. D., Winn, M. D., Storoni, L. C., Read, R. J., 2007. Phaser crystallographic software. J. Appl. Crystallogr. 40, 658-674.

McLaurin, J., Golomb, R., Jurewicz, A., Antel, J. P., Fraser, P. E., 2000. Inositol stereoisomers stabilize an oligomeric aggregate of Alzheimer amyloid β peptide and inhibit Aβ-induced toxicity. J. Biol. Chem. 275, 18495-18502.

Mears, D., 2004. Regulation of insulin secretion in islets of Langerhans by Ca^{2+} channels. J. Membr. Biol. 200, 57-66.

Meng, D., Wei, X., Zhang, Y.-H. P. J., Zhu, Z., You, C., Ma, Y., 2018. Stoichiometric conversion of cellulosic biomass by *in vitro* synthetic enzymatic biosystems for biomanufacturing. ACS Catal. 8, 9550-9559.

Michell, R. H., 2008. Inositol derivatives: evolution and functions. Nat. Rev. Mol. Cell. Biol. 9, 151-161.

Michell, R. H., 2018. Do inositol supplements enhance phosphatidylinositol supply and thus support endoplasmic reticulum function? Br. J. Nutr. 120, 301-316.

Michon, C., Kang, C. M., Karpenko, S., Tanaka, K., Ishikawa, S., Yoshida, K.-I., 2020. A bacterial cell factory converting glucose into *scyllo*-inositol, a therapeutic agent for Alzheimer's disease. Comm. Biol. 3, 93.

Milke, L., Mutz, M., Marienhagen, J., 2020. Synthesis of the character impact compound raspberry ketone and additional flavoring phenylbutanoids of biotechnological interest with *Corynebacterium glutamicum*. Microb. Cell. Fact. 19, 1-12.

Mishra, A. K., Driessen, N. N., Appelmelk, B. J., Besra, G. S., 2011. Lipoarabinomannan and related glycoconjugates: structure, biogenesis and role in *Mycobacterium tuberculosis* physiology and host–pathogen interaction. FEMS Microbiol. Rev. 35, 1126-1157.

Monastra, G., Unfer, V., Harrath, A. H., Bizzarri, M., 2017. Combining treatment with *myo*-inositol and D-*chiro*-inositol (40: 1) is effective in restoring ovary function and metabolic balance in PCOS patients. Gynecol. Endocrinol. 33, 1-9.

Morinaga, T., Ashida, H., Yoshida, K.-I., 2010a. Identification of two *scyllo*-inositol dehydrogenases in *Bacillus subtilis*. Microbiology 156, 1538-1546.

Morinaga, T., Matsuse, T., Ashida, H., Yoshida, K.-I., 2010b. Differential substrate specificity of two inositol transporters of *Bacillus subtilis*. Biosci. Biotech. Bioch. 74, 1312-1314.

Morinaga, T., Yamaguchi, M., Makino, Y., Nanamiya, H., Takahashi, K., Yoshikawa, H., Kawamura, F., Ashida, H., Yoshida, K.-I., 2006. Functional *myo*-inositol catabolic genes of *Bacillus subtilis* Natto are involved in depletion of pinitol in Natto (fermented soybean). Biosci. Biotechnol. Biochem. 70, 1913-1920.

Morita, Y. S., Fukuda, T., Sena, C. B., Yamaryo-Botte, Y., McConville, M. J., Kinoshita, T., 2011. Inositol lipid metabolism in *mycobacteria*: biosynthesis and regulatory mechanisms. BBA -Gen. Subjects 1810, 630-641.

Moritz, B., Striegel, K., de Graaf, A. A., Sahm, H., 2000. Kinetic properties of the glucose-6-phosphate and 6-phosphogluconate dehydrogenases from *Corynebacterium glutamicum* and their application for predicting pentose phosphate pathway flux *in vivo*. Eur. J. Biochem. 267, 3442-3452.

Morris, G. M., Goodsell, D. S., Halliday, R. S., Huey, R., Hart, W. E., Belew, R. K., Olson, A. J., 1998. Automated docking using a Lamarckian genetic algorithm and an empirical binding free energy function. J. Comput. Chem. 19, 1639-1662.

Mu, W., Yu, L., Zhang, W., Zhang, T., Jiang, B., 2015. Isomerases for biotransformation of D-hexoses. Appl. Microbiol. Biotechnol. 99, 6571-6584.

Murphy, J. R., 1996. *Corynebacterium diphtheriae*. In: Baron, S., (Ed.), Medical Microbiology. vol. 4. University of Texas Medical Branch at Galveston, Galveston, USA.

Murshudov, G. N., Skubák, P., Lebedev, A. A., Pannu, N. S., Steiner, R. A., Nicholls, R. A., Winn, M. D., Long, F., Vagin, A. A., 2011. REFMAC5 for the refinement of macromolecular crystal structures. Acta Crystallogr. D. 67, 355-367.

Mustafi, N., Grünberger, A., Kohlheyer, D., Bott, M., Frunzke, J., 2012. The development and application of a single-cell biosensor for the detection of L-methionine and branched-chain amino acids. Metab. Eng. 14, 449-457.

Nakamura, Y., Fukami, K., 2017. Regulation and physiological functions of mammalian phospholipase C. J. Biochem. 161, 315-321.

Newton, G. L., Buchmeier, N., Fahey, R. C., 2008. Biosynthesis and functions of mycothiol, the unique protective thiol of *Actinobacteria*. Microb. Mol. Biol. Rev. 72, 471-494.

Nguyen, A. Q., Schneider, J., Reddy, G. K., Wendisch, V. F., 2015. Fermentative production of the diamine putrescine: system metabolic engineering of *Corynebacterium glutamicum*. Metabolites 5, 211-231.

Niebisch, A., Bott, M., 2001. Molecular analysis of the cytochrome bc_1-aa_3 branch of the *Corynebacterium glutamicum* respiratory chain containing an unusual diheme cytochrome c_1. Arch. Microbiol. 175, 282-294.

Nigou, J., Besra, G. S., 2002. Characterization and regulation of inositol monophosphatase activity in *Mycobacterium smegmatis*. Biochem. J. 361, 385-390.

Noé, F., De Fabritiis, G., Clementi, C., 2020. Machine learning for protein folding and dynamics. Curr. opin. Struct. Biol. 60, 77-84.

Ohnishi, J., Katahira, R., Mitsuhashi, S., Kakita, S., Ikeda, M., 2005. A novel *gnd* mutation leading to increased L-lysine production in *Corynebacterium glutamicum*. FEMS Microbiol. Lett. 242, 265-74.

Okino, S., Inui, M., Yukawa, H., 2005. Production of organic acids by *Corynebacterium glutamicum* under oxygen deprivation. Appl. Microbiol. Biotechnol. 68, 475-480.

Okino, S., Noburyu, R., Suda, M., Jojima, T., Inui, M., Yukawa, H., 2008. An efficient succinic acid production process in a metabolically engineered *Corynebacterium glutamicum* strain. Appl. Microbiol. Biotechnol. 81, 459–464.

Omura, K., Swern, D., 1978. Oxidation of alcohols by "activated" dimethyl sulfoxide. A preparative, steric and mechanistic study. Tetrahedron 34, 1651-1660.

Ortmeyer, H. K., Bodkin, N., Lilley, K., Larner, J., Hansen, B. C., 1993. Chiroinositol deficiency and insulin resistance. I. Urinary excretion rate of chiroinositol is directly associated with insulin resistance in spontaneously diabetic rhesus monkeys. Endocrinology 132, 640-645.

Owczarczyk-Saczonek, A., Lahuta, L. B., Ligor, M., Placek, W., Górecki, R. J., Buszewski, B., 2018. The healing-promoting properties of selected cyclitols - A review. Nutrients 10, 1891.

Özturan, A., Arslan, S., Kocaadam, B., Elibol, E., İmamoğlu, İ., Karadağ, M. G., 2019. Effect of inositol and its derivatives on diabetes: a systematic review. Crit. Rev. Food Sci. Nutr. 59, 1124-1136.

Pace, C. J., Gao, J., 2013. Exploring and exploiting polar–π interactions with fluorinated aromatic amino acids. Acc. Chem. Res. 46, 907-915.

Palaniappan, N., Dhote, V., Ayers, S., Starosta, A. L., Wilson, D. N., Reynolds, K. A., 2009. Biosynthesis of the aminocyclitol subunit of hygromycin A in *Streptomyces hygroscopicus* NRRL 2388. Chem. Biol. 16, 1180-1189.

Parys, J. B., De Smedt, H., 2012. Inositol 1,4,5-trisphosphate and its receptors. Adv. Exp. Med. Biol. 740, 255-279.

Paulick, M. G., Bertozzi, C. R., 2008. The glycosylphosphatidylinositol anchor: a complex membrane-anchoring structure for proteins. Biochem. 47, 6991-7000.

Petersen, K. F., Oral, E. A., Dufour, S., Befroy, D., Ariyan, C., Yu, C., Cline, G. W., DePaoli, A. M., Taylor, S. I., Gorden, P., 2002. Leptin reverses insulin resistance and hepatic steatosis in patients with severe lipodystrophy. J. Clin. Invest. 109, 1345-1350.

Petersen, M. C., Shulman, G. I., 2018. Mechanisms of insulin action and insulin resistance. Physiol. Rev. 98, 2133-2223.

Pettersen, E. F., Goddard, T. D., Huang, C. C., Meng, E. C., Couch, G. S., Croll, T. I., Morris, J. H., Ferrin, T. E., 2021. UCSF ChimeraX: Structure visualization for researchers, educators, and developers. Protein Sci. 30, 70-82.

Pintaudi, B., Di Vieste, G., Bonomo, M., 2016. The effectiveness of *myo*-inositol and D-*chiro*-inositol treatment in type 2 diabetes. Int. J. Endocrinol. 2016, 9132052.

Polen, T., Wendisch, V. F., 2004. Genome wide expression analysis in amino acid-producing bacteria using DNA microarrays. Appl. Biochem. Biotechnol. 118, 215-232.

Portnoy, V. A., Bezdan, D., Zengler, K., 2011. Adaptive laboratory evolution - harnessing the power of biology for metabolic engineering. Curr. Opin. Biotechnol. 22, 590-594.

Prince, M., Bryce, R., Albanese, E., Wimo, A., Ribeiro, W., Ferri, C. P., 2013. The global prevalence of dementia: A systematic review and metaanalysis. Alzheimer's & Dementia 9, 63-75.

Pulina, M. V., Hopkins, M., Haroutunian, V., Greengard, P., Bustos, V., 2019. C99 selectively accumulates in vulnerable neurons in Alzheimer's disease. Alzheimers Dement. 16, 273-282.

Pupel, P., Szablińska-Piernik, J., Lahuta, L. B., 2019. Two-step d-ononitol epimerization pathway in *Medicago truncatula*. Plant J. 100, 237-250.

Ramaley, R., Fujita, Y., Freese, E., 1979. Purification and properties of *Bacillus subtilis* inositol dehydrogenase. J. Biol. Chem. 254, 7684-7690.

Ramos-Figueroa, J. S., Aamudalapalli, H. B., Jagdhane, R. C., Smith, J., Palmer, D. R. J., 2020. Preparation and application of ^{13}C-Labeled *myo*-inositol to identify new catabolic products in inositol metabolism in *Lactobacillus casei*. Biochem. 59, 2974-2985.

Ramos-Figueroa, J. S., Palmer, D. R. J., 2022. Phosphonate and α-fluorophosphonate analogues of D-glucose-6-phosphate as active-site probes of 1L-*myo*-inositol 1-phosphate synthase. Biochemistry 61, 868-878.

Ramp, P., Lehnert, A., Matamouros, S., Wirtz, A., Baumgart, M., Bott, M., 2021. Metabolic engineering of *Corynebacterium glutamicum* for production of *scyllo*-inositol, a drug candidate against Alzheimer's disease. Metab. Eng. 67, 173-185.

Ramp, P., Pfleger, C., Dittrich, J., Mack, C., Gohlke, H., Bott, M., 2022. Physiological, biochemical, and structural bioinformatic analysis of the multiple inositol dehydrogenases from *Corynebacterium glutamicum*. Microbiol. Spectr., e0195022.

Rasmussen, S. K., Ingvardsen, C. R., Torp, A. M., 2010. Mutations in genes controlling the biosynthesis and accumulation of inositol phosphates in seeds. Biochem. Soc. Trans. 38, 689-694.

Regidor, P.-A., Schindler, A. E., 2016. *Myo*-inositol as a safe and alternative approach in the treatment of infertile PCOS women: a German observational study. Int. J. Endocrinol. 2016, 9537632.

Reizman, I. M. B., Stenger, A. R., Reisch, C. R., Gupta, A., Connors, N. C., Prather, K. L., 2015. Improvement of glucaric acid production in *E. coli* via dynamic control of metabolic fluxes. Metab. Eng. Comm. 2, 109-116.

Rossmann, M. G., Moras, D., Olsen, K. W., 1974. Chemical and biological evolution of a nucleotide-binding protein. Nature 250, 194-199.

Salehi, A., Delcroix, J. D., Swaab, D. F., 2004. Alzheimer's disease and NGF signaling. J. Neural Transm. 111, 323-345.

Salehi, H., Burgueño, R., 2018. Emerging artificial intelligence methods in structural engineering. Eng. Struct. 171, 170-189.

Salloway, S., Sperling, R., Keren, R., Porsteinsson, A. P., van Dyck, C. H., Tariot, P. N., Gilman, S., Arnold, D., Abushakra, S., Hernandez, C., Crans, G., Liang, E., Quinn, G., Bairu, M., Pastrak, A., Cedarbaum, J. M., 2011. A phase 2 randomized trial of ELND005, *scyllo*-inositol, in mild to moderate Alzheimer disease. Neurology 77, 1253-1262.

Saltiel, A. R., Cuatrecasas, P., 1986. Insulin stimulates the generation from hepatic plasma membranes of modulators derived from an inositol glycolipid. Proc. Natl. Acad. Sci. USA 83, 5793-5797.

Saltiel, A. R., Siegel, M. I., Jacobs, S., Cuatrecasas, P., 1982. Putative mediators of insulin action: regulation of pyruvate dehydrogenase and adenylate cyclase activities. Proc. Natl. Acad. Sci. USA 79, 3513-3517.

Sanchez-Hidalgo, M., Leon-Gonzalez, A. J., Galvez-Peralta, M., Gonzalez-Mauraza, N. H., Martin-Cordero, C., 2021. D-Pinitol: A cyclitol with versatile biological and pharmacological activities. Phytochem. Rev. 20, 211-224.

Sangal, V., Hoskisson, P. A., 2016. Evolution, epidemiology and diversity of *Corynebacterium diphtheriae*: new perspectives on an old foe. Infect. Genet. Evol. 43, 364-370.

Sarmah, M. P., Shashidhar, M. S., 2003. Sulfonate protecting groups.: Improved synthesis of *scyllo*-inositol and its orthoformate from *myo*-inositol. Carbohydr. Res. 338, 999-1001.

Schäfer, A., Tauch, A., Jäger, W., Kalinowski, J., Thierbach, G., Pühler, A., 1994. Small mobilizable multi-purpose cloning vectors derived from the *Escherichia coli* plasmids pK18 and pK19: selection of defined deletions in the chromosome of *Corynebacterium glutamicum*. Gene 145, 69-73.

Schaffer, S., Weil, B., Nguyen, V. D., Dongmann, G., Günther, K., Nickolaus, M., Hermann, T., Bott, M., 2001. A high-resolution reference map for cytoplasmic and membrane-associated proteins of *Corynebacterium glutamicum*. Electrophoresis 22, 4404-4422.

Scherer, J., 1850. Ueber eine neue, aus dem Muskelfleische gewonnene Zuckerart. Liebigs Ann. Chem. 73, 322-328.

Schneider, S., 2015. Inositol transport proteins. FEBS Lett. 589, 1049-1058.

Seubert, P., Oltersdorf, T., Lee, M. G., Barbour, R., Blomquist, C., Davis, D. L., Bryant, K., Fritz, L. C., Galasko, D., Thal, L. J., Lieberburg, I., Schenk, D. B., 1993. Secretion of β-amyloid precursor protein cleaved at the amino terminus of the β-amyloid peptide. Nature 361, 260-263.

Shimizu, T., Takaya, N., Nakamura, A., 2012. An L-glucose catabolic pathway in *Paracoccus* species 43P. J. Biol. Chem. 287, 40448-40456.

Siebert, D., Altenbuchner, J., Blombach, B., 2021. A timed off-switch for dynamic control of gene expression in *Corynebacterium glutamicum*. Front. Bioeng. Biotechnol., 649.

Siedler, S., Lindner, S. N., Bringer, S., Wendisch, V. F., Bott, M., 2013. Reductive whole-cell biotransformation with *Corynebacterium glutamicum*: improvement of NADPH generation from glucose by a cyclized pentose phosphate pathway using *pfkA* and *gapA* deletion mutants. Appl. Microbiol. Biotechnol. 97, 143-152.

Sigurdsson, E. M., Knudsen, E., Asuni, A., Fitzer-Attas, C., Sage, D., Quartermain, D., Goni, F., Frangione, B., Wisniewski, T., 2004. An attenuated immune response is sufficient to enhance cognition in an Alzheimer's disease mouse model immunized with amyloid-β derivatives. J. Neurosci. 24, 6277-6282.

Siracusa, L., Napoli, E., Ruberto, G., 2022. Novel chemical and biological insights of inositol derivatives in mediterranean plants. Molecules 27, 1525.

Spaans, S. K., Weusthuis, R. A., Van Der Oost, J., Kengen, S. W., 2015. NADPH-generating systems in bacteria and archaea. Front. Microbiol. 6, 742.

Stansen, C., Uy, D., Delaunay, S., Eggeling, L., Goergen, J.-L., Wendisch, V. F., 2005. Characterization of a *Corynebacterium glutamicum* lactate utilization operon induced during temperature-triggered glutamate production. Appl. Environ. Microbiol. 71, 5920-5928.

Steinegger, M., Meier, M., Mirdita, M., Vöhringer, H., Haunsberger, S. J., Söding, J., 2019. HH-suite3 for fast remote homology detection and deep protein annotation. BMC Bioinf. 20, 473.

Stella, R. G., Wiechert, J., Noack, S., Frunzke, J., 2019. Evolutionary engineering of *Corynebacterium glutamicum*. Biotechnol. J. 14, 1800444.

Stieglitz, K. A., Roberts, M. F., Li, W., Stec, B., 2007. Crystal structure of the tetrameric inositol 1-phosphate phosphatase (TM1415) from the hyperthermophile, *Thermotoga maritima*. FEBS J. 274, 2461-2469.

Stieglitz, K. A., Yang, H., Roberts, M. F., Stec, B., 2005. Reaching for mechanistic consensus across life kingdoms: structure and insights into catalysis of the *myo*-inositol-1-phosphate synthase (mIPS) from *Archaeoglobus fulgidus*. Biochem 44, 213-224.

Sureshan, K. M., Murakami, T., Watanabe, Y., 2009. Total syntheses of cyclitol based natural products from *myo*-inositol: brahol and pinpollitol. Tetrahedron 65, 3998-4006.

Suzuki, M., Tanaka, K., Kuwano, M., Yoshida, K. T., 2007. Expression pattern of inositol phosphate-related enzymes in rice (*Oryza sativa L.*): implications for the phytic acid biosynthetic pathway. Gene 405, 55-64.

Taberman, H., Parkkinen, T., Rouvinen, J., 2016. Structural and functional features of the NAD (P) dependent Gfo/Idh/MocA protein family oxidoreductases. Protein Sci. 25, 778-786.

Takami, M., Nagashima, Y., Sano, Y., Ishihara, S., Morishima-Kawashima, M., Funamoto, S., Ihara, Y., 2009. γ-secretase: successive tripeptide and tetrapeptide release from the transmembrane domain of β-carboxyl terminal fragment. J. Neurosci. 29, 13042-13052.

Takeno, S., Hori, K., Ohtani, S., Mimura, A., Mitsuhashi, S., Ikeda, M., 2016. L-Lysine production independent of the oxidative pentose phosphate pathway by *Corynebacterium glutamicum* with the *Streptococcus mutans gapN* gene. Metab. Eng. 37, 1-10.

Tanaka, K., Natsume, A., Ishikawa, S., Takenaka, S., Yoshida, K.-I., 2017. A new-generation of *Bacillus subtilis* cell factory for further elevated *scyllo*-inositol production. Microb. Cell Fact. 16, 67.

Tanaka, K., Tajima, S., Takenaka, S., Yoshida, K.-I., 2013. An improved *Bacillus subtilis* cell factory for producing *scyllo*-inositol, a promising therapeutic agent for Alzheimer's disease. Microb. Cell Fact. 12, 124.

Tang, E., Shen, X., Wang, J., Sun, X., Yuan, Q., 2020. Synergetic utilization of glucose and glycerol for efficient *myo*-inositol biosynthesis. Biotech. Bioeng. 117, 1247-1252.

Tariot, P., Lyketsos, C., Crans, G., Cedarbaum, J., Hernandez, C., Abushakra, S., 2012. The effects of ELND005 (*scyllo*-Inositol) on emergence of neuropsychiatric symptoms (NPS) in mild/moderate Alzheimer's Disease: Results from a 78-week phase 2 study (P04.215). Neurology 78, P04.215.

Tartaglio, V., Rennie, E. A., Cahoon, R., Wang, G., Baidoo, E., Mortimer, J. C., Cahoon, E. B., Scheller, H. V., 2017. Glycosylation of inositol phosphorylceramide sphingolipids is required for normal growth and reproduction in *Arabidopsis*. Plant J. 89, 278-290.

Taylor, C. W., Machaca, K., 2019. IP3 receptors and store-operated Ca^{2+} entry: a license to fill. Curr. Opin. Cell Biol. 57, 1-7.

Thomas, C. M., Nielsen, K. M., 2005. Mechanisms of, and barriers to, horizontal gene transfer between bacteria. Nat. Rev. Microbiol. 3, 711-721.

Thomas, M. P., Mills, S. J., Potter, B. V., 2016. The "other" inositols and their phosphates: synthesis, biology, and medicine (with recent advances in *myo*-inositol chemistry). Angew. Chem. Int. Ed. 55, 1614-1650.

Tolias, K. F., Cantley, L. C., 1999. Pathways for phosphoinositide synthesis. Chem. Phys. Lipids. 98, 69-77.

Townsend, M., Cleary, J. P., Mehta, T., Hofmeister, J., Lesne, S., O'Hare, E., Walsh, D. M., Selkoe, D. J., 2006. Orally available compound prevents deficits in memory caused by the Alzheimer amyloid-β oligomers. Ann. Neurol. 60, 668-676.

Tsui, M. M., York, J. D., 2010. Roles of inositol phosphates and inositol pyrophosphates in development, cell signaling and nuclear processes. Adv. Enzyme Regul. 50, 324.

Turner, B., Papházy, M., Haygarth, P., McKelvie, I., Inositol phosphates in the environment Vol. 357. Philos. T. Roy. Soc. B, 2002, pp. 449–469.

Uldry, M., Ibberson, M., Horisberger, J.-D., Chatton, J.-Y., Riederer, B. M., Thorens, B., 2001. Identification of a mammalian H^+-*myo*-inositol symporter expressed predominantly in the brain. EMBO J. 20, 4467-4477.

Unfer, V., Carlomagno, G., Papaleo, E., Vailati, S., Candiani, M., Baillargeon, J.-P., 2014. Hyperinsulinemia alters *myo*-inositol to D-*chiro*-inositol ratio in the follicular fluid of patients with PCOS. Reprod. Sci. 21, 854-858.

Vallino, J. J., Stephanopoulos, G., 1994. Carbon flux distributions at the glucose-6-phosphate branch point in *Corynebacterium glutamicum* during lysine overproduction. Biotechnol. Progr. 10, 327-334.

Van Cauwenberghe, C., Vandendriessche, C., Libert, C., Vandenbroucke, R. E., 2016. Caloric restriction: beneficial effects on brain aging and Alzheimer's disease. Mamm. Genome 27, 300-319.

van der Rest, M. E., Lange, C., Molenaar, D., 1999. A heat shock following electroporation induces highly efficient transformation of *Corynebacterium glutamicum* with xenogeneic plasmid DNA. Appl. Microbiol. Biotechnol. 52, 541-545.

van Rooijen, R. J., de Vos, W. M., 1990. Molecular cloning, transcriptional analysis, and nucleotide sequence of *lacR*, a gene encoding the repressor of the lactose phosphotransferase system of *Lactococcus lactis*. J. Biol. Chem. 265, 18499-18503.

van Straaten, K. E., Zheng, H., Palmer, D. R., Sanders, D. A., 2010. Structural investigation of *myo*-inositol dehydrogenase from *Bacillus subtilis*: implications for catalytic mechanism and inositol dehydrogenase subfamily classification. Biochem. J. 432, 237-247.

Vance, J. E., 2015. Phospholipid synthesis and transport in mammalian cells. Traffic 16, 1-18.

Veevers, R., Hayward, S., 2019. Methodological improvements for the analysis of domain movements in large biomolecular complexes. Biophys. Physicobiol. 16, 328-336.

Vercellone, A., Nigou, J., Puzo, G., 1998. Relationships between the structure and the roles of lipoarabinomannans and related glycoconjugates in tuberculosis pathogenesis. Front. Biosci. 3, e149-163.

Vetting, M. W., Frantom, P. A., Blanchard, J. S., 2008. Structural and enzymatic analysis of MshA from *Corynebacterium glutamicum*: substrate-assisted catalysis. J. Biol. Chem. 283, 15834-15844.

Vilchèze, C., Av-Gay, Y., Attarian, R., Liu, Z., Hazbón, M. H., Colangeli, R., Chen, B., Liu, W., Alland, D., Sacchettini, J. C., 2008. Mycothiol biosynthesis is essential for ethionamide susceptibility in *Mycobacterium tuberculosis*. Mol. Microbiol. 69, 1316-1329.

Vitale, S. G., Corrado, F., Caruso, S., Di Benedetto, A., Giunta, L., Cianci, A., D'Anna, R., 2021. *Myo*-inositol supplementation to prevent gestational diabetes in overweight non-obese women: bioelectrical impedance analysis, metabolic aspects, obstetric and neonatal outcomes – a randomized and open-label, placebo-controlled clinical trial. Int. J. Food. Sci. Nutr. 72, 670-679.

Wakelam, M. J., Michell, R. H., Evolution of the diverse biological roles of inositols. Biochemical Society Symposia, Vol. 74. Portland Press, 2007, pp. 223-246.

Walter, T., Veldmann, K. H., Götker, S., Busche, T., Rückert, C., Kashkooli, A. B., Paulus, J., Cankar, K., Wendisch, V. F., 2020. Physiological response of *Corynebacterium glutamicum* to indole. Microorganisms 8, 1945.

Wang, Q., Zhang, J., Al Makishah, N. H., Sun, X., Wen, Z., Jiang, Y., Yang, S., 2021. Advances and perspectives for genome editing tools of *Corynebacterium glutamicum*. Front. Microbiol. 12, 654058.

Wang, W., Xie, Y., Liu, L., King, G. J., White, P., Ding, G., Wang, S., Cai, H., Wang, C., Xu, F., 2022. Genetic control of seed phytate accumulation and the development of low-phytate crops: A review and perspective. J. Agric. Food. Chem. 70, 3375-3390.

Weber, T., Welzel, K., Pelzer, S., Vente, A., Wohlleben, W., 2003. Exploiting the genetic potential of polyketide producing *Streptomycetes*. J. Biotechnol. 106, 221-32.

Wendisch, V. F., 2020. Metabolic engineering advances and prospects for amino acid production. Metab. Eng 58, 17-34.

Wendisch, V. F., Bott, M., Kalinowski, J., Oldiges, M., Wiechert, W., 2006. Emerging *Corynebacterium glutamicum* systems biology. J. Biotechnol. 124, 74-92.

Wendisch, V. F., Eberhardt, D., Herbst, M., Vold Korgaard Jensen, J., 2014. Biotechnological production of amino acids and nucleotides. Biotechnological production of natural ingredients for food industry. Bentham Science eBooks, pp. 60-163.

Werpy, T., Petersen, G., Top value added chemicals from biomass: volume I-results of screening for potential candidates from sugars and synthesis gas. National Renewable Energy Lab., Golden, CO (US), 2004.

Wheatcroft, S., Williams, I., Shah, A., Kearney, M., 2003. Pathophysiological implications of insulin resistance on vascular endothelial function. Diabetic Med. 20, 255-268.

White, M. J., Hirsch, J., Henry, S., 1991. The *OPI1* gene of *Saccharomyces cerevisiae,* a negative regulator of phospholipid biosynthesis, encodes a protein containing polyglutamine tracts and a leucine zipper. J. Biol. Chem. 266, 863-872.

Wilcox, G., 2005. Insulin and insulin resistance. Cln. Biochem. Rev. 26, 19.

Wolf, S., Becker, J., Tsuge, Y., Kawaguchi, H., Kondo, A., Marienhagen, J., Bott, M., Wendisch, V. F., Wittmann, C., 2021. Advances in metabolic engineering of *Corynebacterium glutamicum* to produce high-value active ingredients for food, feed, human health, and well-being. Essays Biochem. 65, 197-212.

Yamamoto, S., Suda, M., Niimi, S., Inui, M., Yukawa, H., 2013. Strain optimization for efficient isobutanol production using *Corynebacterium glutamicum* under oxygen deprivation. Biotechnol. Bioeng. 110, 2938-2948.

Yamaoka, M., Osawa, S., Morinaga, T., Takenaka, S., Yoshida, K.-I., 2011. A cell factory of *Bacillus subtilis* engineered for the simple bioconversion of *myo*-inositol to *scyllo*-inositol, a potential therapeutic agent for Alzheimer's disease. Microb. Cell. Fact. 10, 69.

Yan, R., Bienkowski, M. J., Shuck, M. E., Miao, H., Tory, M. C., Pauley, A. M., Brashier, J. R., Stratman, N. C., Mathews, W. R., Buhl, A. E., Carter, D. B., Tomasselli, A. G., Parodi, L. A., Heinrikson, R. L., Gurney, M. E., 1999. Membrane-anchored aspartyl protease with Alzheimer's disease β-secretase activity. Nature 402, 533-537.

Yap, A., Nishiumi, S., Yoshida, K.-I., Ashida, H., 2007. Rat L6 myotubes as an *in vitro* model system to study GLUT4-dependent glucose uptake stimulated by inositol derivatives. Cytotechnol. 55, 103-108.

Yi, M., Yang, L., Ma, J., Liu, H., He, M., Hu, C., Yu, P., 2020. Biosynthesis of *myo*-inositol in *Escherichia coli* by engineering *myo*-inositol-1-phosphate pathway. Biochem. Eng. J. 164, 107792.

Yoshida, K.-I., Aoyama, D., Ishio, I., Shibayama, T., Fujita, Y., 1997. Organization and transcription of the *myo*-inositol operon, iol, of *Bacillus subtilis*. J. Bacteriol. 179, 4591-4598.

Yoshida, K.-I., Sanbongi, A., Murakami, A., Suzuki, H., Takenaka, S., Takami, H., 2012. Three inositol dehydrogenases involved in utilization and interconversion of inositol stereoisomers in a thermophile, *Geobacillus kaustophilus* HTA426. Microbiology 158, 1942-1952.

Yoshida, K.-I., Shibayama, T., Aoyama, D., Fujita, Y., 1999. Interaction of a repressor and its binding sites for regulation of the *Bacillus subtilis iol* divergon. J. Mol. Biol. 285, 917-929.

Yoshida, K.-I., Yamaguchi, M., Ikeda, H., Omae, K., Tsurusaki, K.-i., Fujita, Y., 2004. The fifth gene of the *iol* operon of *Bacillus subtilis*, *iolE*, encodes 2-keto-*myo*-inositol dehydratase. Microbiology 150, 571-580.

Yoshida, K.-I., Yamaguchi, M., Morinaga, T., Ikeuchi, M., Kinehara, M., Ashida, H., 2006. Genetic modification of *Bacillus subtilis* for production of D-*chiro*-inositol, an investigational drug candidate for treatment of type 2 diabetes and polycystic ovary syndrome. Appl. Environ. Microbiol. 72, 1310-1315.

Yoshida, K.-I., Yamaguchi, M., Morinaga, T., Kinehara, M., Ikeuchi, M., Ashida, H., Fujita, Y., 2008. *Myo*-inositol catabolism in *Bacillus subtilis*. J. Biol. Chem. 283, 10415-10424.

Yoshida, K.-I., Yamamoto, Y., Omae, K., Yamamoto, M., Fujita, Y., 2002. Identification of two *myo*-inositol transporter genes of *Bacillus subtilis*. J. Bacteriol. 184, 983-991.

You, R., Wang, L., Shi, C., Chen, H., Zhang, S., Hu, M., Tao, Y., 2020. Efficient production of *myo*-inositol in *Escherichia coli* through metabolic engineering. Microb. Cell. Fact. 19, 109.

Zhang, W. Y., Sun, Z. H., Yu, D. L., Airideng, C., Chen, W., Meng, H., Zhang, H. P., 2010. Comparative analysis of *iol* clusters in *Lactobacillus casei* strains. World J. Microbiol. Biotechnol. 26, 1949-1955.

Zheng, H., Bertwistle, D., Sanders, D. A., Palmer, D. R., 2013. Converting NAD-specific inositol dehydrogenase to an efficient NADP-selective catalyst, with a surprising twist. Biochem 52, 5876-5883.

Zhou, L.-B., Zeng, A.-P., 2015. Engineering a lysine-ON riboswitch for metabolic control of lysine production in *Corynebacterium glutamicum*. ACS Synth. Biol. 4, 1335-1340.

5. Appendix

5.1 L-*chiro*-inositol metabolism in *C. glutamicum*

5.1.1 Background

The research on bacterial inositol metabolism mainly concerns the inositol isomers MI, DCI and SI. One can only speculate why the other isomers have mostly been neglected. Possible explanations are the difficult commercial availability of other inositol isomers. MI is a relatively cheap compound and although DCI and SI are much more expensive, multiple production processes have been developed. In addition, MI, DCI, and SI have been reported to have pharmacological activities, which makes them particularly interesting. Many bacteria can degrade and interconvert MI, DCI, and SI, yet no microbial growth or a corresponding pathway was confirmed for any other inositol isomer. However, with *neo*-inositol found in soil (Turner et al., 2002) and IDHs identified that generate L-*chiro*- and *neo*-inosose (Ramos-Figueroa et al., 2020), there should be microorganisms that can utilize and generate other isomers besides MI, DCI, or SI.

We identified seven IDHs in *C. glutamicum* with overlapping activities for MI, DCI, and SI and multiple inosose isomerases that interconvert 2KMI and 1KDCI. Still, the function of IdhA3 and OxiC remains unknown. Given the multiple paralogous enzymes responsible for degradation of inositols, we speculate that *C. glutamicum* can take up, degrade, and ultimately grow on more inositol isomers. The next inositol isomer which was commercially available for us in sufficient amounts was L-*chiro*-Inositol (LCI). We therefore investigated the ability of *C. glutamicum* to utilize L-*chiro*-inositol as single carbon and energy source.

5.1.2 Results and Discussion

The experimental setup to investigate growth on LCI was similar to the transporter analysis and complementation experiments described in chapter 2.2. The IDH deficient strain *C. glutamicum* MB001(DE3)ΔIDH was transformed with pMKEx2-based expression plasmids encoding one of the seven IDHs and tested for growth on L-*chiro*-inositol in the BioLector system. As controls, the parent strain *C. glutamicum* MB001(DE3) and the ΔIDH strain were transformed with pMKEx2-eyfp. Target gene expression was induced by adding 20 µM IPTG to the second,

overnight preculture and the main culture to enable an immediate start of growth in CGXII minimal medium supplemented with 1% (wt/vol) LCI.

Indeed, *C. glutamicum* MB001(DE3) was able to grow on LCI with a growth rate comparable to growth on MI (0.42 h^{-1}) (Fig. 5.1A). The transporter studies showed the same profile as for the other inositols. Both transporters IolT1 and IolT2 contribute to uptake of LCI, with no additional transporter enabling growth, as the strain Δ*iolT1*Δ*iolT2* was unable to grow on LCI. IolT1 seems to be the main transporter as strain Δ*iolT1* showed a slightly slower growth rate (0.39 h^{-1}) and lower final backscatter than the strain Δ*iolT2* (0.42 h^{-1}) (Fig. 5.1).

The strain ΔIDH (pMKEx2-*eyfp*) was unable to grow on LCI, proving that no additional gene enabling LCI utilization is present (Fig. 5.1B). Four IDHs complemented growth on LCI to different degrees, IolG, OxiB, OxiD, and to our surprise IdhA3, which was not active on MI, DCI, or SI in previous experiments. Expression of *iolG* and *oxiB* enabled very slow growth on LCI with rates of 0.03 h^{-1} and 0.08 h^{-1}, respectively, while expression of *oxiD* and *idhA3* complemented growth of the ΔIDH strain comparable to the positive control with rates of 0.41 h^{-1} and 0.36 h^{-1}, respectively.

This experiment showed the first difference in stereoselectivity and activity between OxiD and IolG, which possess comparable activities for MI and DCI (Ramp et al, 2022; chapter 2.2). In addition, OxiB, which was identified as a sIDH, was active on LCI, while OxiE did not rescue growth. The biggest difference to all previous experiments was the activity of IdhA3. IdhA3 differs from all other IDHs of *C. glutamicum* in the catalytic triad, in which it contains a Glu residue instead of a conserved Asp residue (Ramp et al, 2022; chapter 2.2 Fig. S5). As the docking experiments clearly showed no binding of MI, DCI, and SI, we speculated that this exchange might be responsible for the lacking activity on these substrates. The observation that IdhA3 was active on LCI shows that the exchange of the Asp residue against Glu does not diminish enzymatic activity and, in addition, that this Glu residue is not a specific requirement for LCI oxidation, as OxiD contains the canonical Asp residue and allows even better growth on LCI than IdhA3.

Further investigations will deal with the identification of LCI binding sites in IdhA3 via molecular docking experiments. In addition, the resulting keto-intermediate resulting from LCI oxidation needs to be identified. As DCI is oxidized at the C1 to 1KDCI, we hypothesize that LCI is processed in a similar way to yield 1-keto-L-*chiro*-inositol (1KLCI). Following this hypothesis, an inosose isomerase activity is presumably required for the interconversion of

1KLCI to 2KMI. Given the genomic organization of *idhA3* in a putative operon with the identified inosose isomerase Cg2312, we speculate that both genes act as a module for LCI utilization.

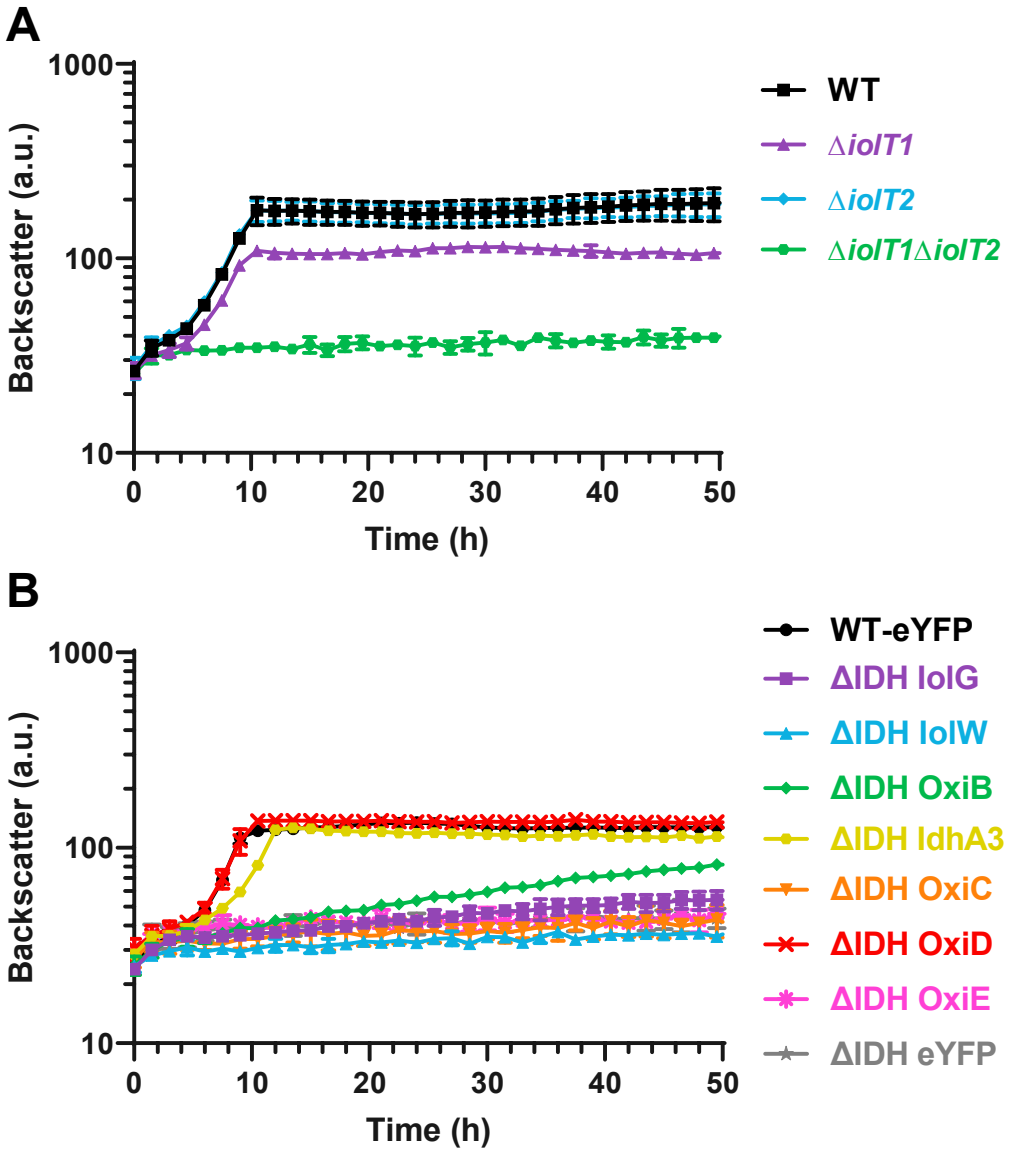

Fig. 5.1. Growth of *C. glutamicum* on L-*chiro*-inositol. (A) Growth of *C. glutamicum* MB001(DE3) (wt) and different iolT1/iolT2 deletion strains. **(B)** Growth of *C. glutamicum* MB001(DE3)ΔIDH expressing one of the seven IDH genes or as negative control *eyfp* using the corresponding pMKEx2-based plasmids. *C. glutamicum* MB001(DE3) transformed with pMKEx2-eyfp was used as a positive control. The strains were cultivated in a BioLector cultivation system for 48 h at 30°C, 1200 rpm, and 85% humidity in CGXII minimal medium supplemented with 10 g/L of LCI. Mean values and standard deviations of three biological replicates are shown.

5.2 Structure elucidation of the *scyllo*-inositol dehydrogenase IolW

5.2.1 Background

The sIDH IolW in *C. glutamicum* is the only IDH that uses NADPH as cofactor and catalyzes the reduction of the inositol keto-intermediate 2KMI to SI. In contrast, all other IDHs identified in *C. glutamicum* use NAD^+ to oxidize inositols for their subsequent degradation. Only two other enzymes with the same characteristics as IolW of *C. glutamicum* have been identified, namely the homologous proteins IolW and IolU of *B. subtilis*. The physiological benefit of SI production for *C. glutamicum* and *B. subtilis* is unknown, one might consider this reaction as a possibility to reoxidize excess NADPH. Using IolW in combination with the mIDH IolG enabled the development of efficient biotechnological production processes for SI. The advantage of these processes lies in the different cofactor specificities of IolG (NAD^+) and IolW (NADPH), which favors the conversion from MI to SI due to high cellular NAD^+/NADH and NADPH/$NADP^+$ ratios. This type of conversion would also be beneficial for the biotechnological production of other inositol isomers. However, no bacterial NADPH-dependent IDH that is active on other inositol keto-compounds, like e.g. 1KDCI, has been identified so far.

Understanding the structural characteristics of IDHs, which allow them not only to distinguish between different inositols, but also between cofactors and their oxidized or reduced state, might be helpful for the development of new biocatalysts for the production of other inositols. The crystal structure of BsIolW has been solved previously, but without bound substrate or cofactor. Therefore, we aimed for the elucidation the crystal structure of CgIolW in complex with its cofactor NADPH and potentially the substrate 2KMI. These experiments were performed as part of a 3-month scholarship granted by the Japan Society for the Promotion of Science (JSPS) in close collaboration with Prof. Makoto Nishiyama, Prof. Saori Kosono, and Prof. Ayako Yoshida in their research laboratory in the Agro-Biotechnology Research Center (AgTECH) at the University of Tokyo, Japan.

5.2.2 Experimental setup

Protein overproduction and purification

Overproduction of IolW-Strep and purification was performed similarly as described in chapter 2.2 with minor alterations. *C. glutamicum* MB001(DE3) was transformed with pPREx6-based expression plasmids for inositol dehydrogenase overproduction and cultivated in 200 mL BHI medium supplemented with 20 g/L glucose. Target gene overexpression was induced with 250 µM IPTG after 3 h, and cells were harvested after 24 h of cultivation via centrifugation at 7,500 g for 20 min at 4 °C. Cell pellets were washed and resuspended in 4 mL lysis buffer (50 mM KH_2PO_4 /K_2HPO_4 pH 7.5, 150 mM NaCl, 1 mM $MgSO_4$) per g cell wet weight and lysed by five passages through a French Press at 124 MPa. The resulting cell extract was first centrifuged at 5,000 *g* and 4 °C for 20 min and the supernatant was then subjected to ultracentrifugation at 45,000 *g* and 4 °C for 1 h. The supernatant was used for purification on an Äkta pure protein purification system (Cytiva) via StrepTactin Sepharose affinity chromatography and subsequent size exclusion chromatography.

A StrepTrap HP 5 mL column was equilibrated with binding buffer (50 mM potassium phosphate pH 7.5, 150 mM NaCl) before loading the protein extract. The column was washed with 10 column volumes (CV) of binding buffer and the remaining bound proteins were then eluted in six 0.5 ml fractions with elution buffer I (100 mM potassium phosphate pH 7.5, 150 mM NaCl, 2.5 mM desthiobiotin). The protein-containing elution fractions identified by analyzing the absorbance at 280 nm were combined and concentrated by using an AMICON Ultra centrifugal filter with a molecular mass cut-off at 10 kDa (Millipore) and centrifugation at 3,500 g and 4 °C to a final volume of 500 µL. The concentrated protein was then applied to a HiLoad 26/600 Superdex 200 pg chromatography column (GE Healthcare) that had been equilibrated with 2 CV of elution buffer II (20 mM potassium phosphate pH 7.5, 150 mM NaCl). Protein was eluted with 1.5 CV of elution buffer II and collected in 5 mL fractions. The purity and apparent molecular mass of the proteins after both purification steps were determined by 12% (wt/vol) SDS-PAGE according to standard procedures (Green and Sambrook, 2012). Protein concentrations were determined using a Bradford assay reagent (Thermofisher Scientific) and measuring concentration-dependent blue coloration at 595 nm. For crystallization, the purified protein was concentrated to a final concentration of 20 mg/mL.

Crystallization and structural determination

Crystallization was performed at 20 °C using the hanging drop vapor-diffusion method. The protein aliquot (20 mM Tris-HCl, pH 7.5, 150 mM NaCl, 10 mg/ml IolW-Strep) was mixed 1:1 with each reservoir solution. For cofactor and substrate or product binding, a final concentration of 6 mM NADPH or $NADP^+$ and 60 mM 2KMI or 60 mM SI were added. In total, we tried to obtain crystals for four different combinations: 1. IolW apo; 2. IolW + NADPH; 3. IolW + $NADP^+$ and SI; 4. IolW + NADPH and 2KMI. For crystal screening, a combination of the commercial screening kits Crystal Screen I & II and Wizard I-IV (Hampton Research, CA, USA) was used for initial screening trials. Suitable crystals were formed after four days under condition no. 4 (100 mM Tris pH 8.5, 2.0 M ammonium sulfate) in in Crystal Screen kit I. Conditions were optimized via iteratively defining optimal pH and ammonium sulfate concentration. The crystals were soaked into the cryo-protectant solution prepared by mixing the reservoir solution with 20% (v/v) ethylene glycol and then flash-frozen with a nitrogen gas stream. Diffraction data were collected at 1.000 Å with pixel array detector PILATUS3 S2M at the beamline NW12 and with PILATUS3 S6M at the beamline BL-5A of the Photon Factory, High Energy Accelerator Research Organization (KEK, Tsukuba, Japan).

Diffraction images were processed with XDS (Kabsch, 2010) and the statistics were calculated with AIMLESS (Evans and Murshudov, 2013). The structures were determined by the molecular replacement method with Phaser (McCoy et al., 2007). We used the crystal structure of IolW of *B. subtilis* (PDB:3GDO) as search models for the molecular replacement to determine the apo-IolW structure. The structure of the IolW-NADPH complex was determined by the molecular replacement methode using the apo-IolW as a search model. Manual model construction and refinement were performed with Coot (Emsley et al., 2010) and REFMAC5 (Murshudov et al., 2011). The statistics for data collection and refinement are summarized in Table 5.1. Figures were prepared using UCSF ChimeraX 1.4 software (Pettersen et al., 2021).

Table 5.1. Statistics for data collection and refinement of the crystal structure of IolW

Crystals	apo-IolW	IolW-NADPH
Data collection		
Space group	$P6_3$	$P6_3$
Cell dimensions		
a, *b*, *c* (Å)	100.7, 100.7, 127.3	101.4, 101.4, 127.3
Resolution (Å)	1.53 (46.81 – 1.53)	1.80 (47.09 – 1.80)
R_{merge}	3.6 (83.4)	5.4 (85.3)
$CC_{1/2}$	1.000 (0.894)	1.000 (0.915)
I / s(I)	31.0 (3.0)	26.4 (2.8)
Completeness (%)	100.0 (100.0)	100.0 (100.0)
Multiplicity	10.2 (10.0)	10/3 (10.5)
Refinement		
Resolution (Å)	1.53 (46.85 – 1.53)	1.80 (47.13 – 1.80)
No. reflections (total/unique)	1122438/109893	707138/68580
R_{work} / R_{free}	17.9/21.0	17.7/21.5
No. atoms		
Protein	5196	5177
NADPH	-	96
SO_4^-	10	5
Water	598	382
B-factors		
Protein	30.89	36.08
NADPH	-	61.46
SO_4^-	46.73	45.14
Water	37.66	39.29
R.m.s. deviations		
Bond lengths (Å)	0.0162	0.0103
Bond angles (°)	1.99	1.681

5.2.3 Results and Discussion

IolW of *C. glutamicum* (CgIolW) was successfully crystallized in monomeric form as the apo-enzyme and in complex with NADPH to 1.53 and 1.80 Å resolution, respectively. The monomeric structure of CgIolW is depicted in Fig. 5.2. We could not obtain crystals of CgIolW in complex with $NADP^+$, 2KMI, or SI. Administration of substrate to crystal solution as well as soaking crystals in a solution with a high 2KMI concentration was unsuccessful. We speculate that this might be due to the low solubility of 2KMI. Following the trend of the other IDHs of *C. glutamicum*, IolW might also possess a K_m in the same range (~1 - 60 mM). To effectively achieve crystallizing protein with bound substrate, excessive amounts of substrates were applied, which in the case of 2KMI is ≤140 mM, the observed maximum solubility. If possible, substrate concentrations of about ~10-fold K_m value are recommended (Chayen and Saridakis, 2008).

Structural alignment of CgIolW with the only other elucidated crystal structure of an NADPH-dependent sIDH, BsIolW from *B. subtilis* (PDB: 3GDO), revealed a close conservation of structure, as indicated by the α-carbon root mean squared deviation (rmsd) of 1.033 Å (Fig. 5.3A). The similarity of CgIolW to the best-analyzed IDH structure, BsIolG (3NT5), is also high with an rmsd of 1.312 Å (Fig. 5.3C). The structure of IolW shows the characteristic features of enzymes belonging to the GFO/IDH/MocA family (Taberman et al., 2016; van Straaten et al., 2010). The IolW monomer consists of two structural domains, the N-terminal domain (residues 1–121), which forms the typical α/β nucleotide-binding (Rossmann fold) motif (Rossmann et al., 1974). The Rossmann fold is one of the most functionally diverse structural elements, with hundreds of different functions, but it is typically involved in methylation of substrates (methyltransferase) or electron transfer from one molecule to another (oxidoreductases) (Kamiński et al., 2022). The two βαβαβ-motifs (β1α1β2α2β3 and β4α4β5α5β6) stack together to form a single six-stranded parallel β-sheet, flanked on both sides by α-helices (α1- α5) (Fig. 5.2). The Rossmann fold is completed by α10 of the C-terminal domain. The C-terminal domain (residues 122-341) contains six α-helices (α6–α11) and a mixed parallel/antiparallel six-stranded β-sheet made up of the strands β7-8+β11-14 characteristic for GFO/IDH/MocA family proteins (Taberman et al., 2016). Here CgIolW differs from other IDHs like BsIolW or BsIolG, as it also contains the two additional ß-strands ß9 and ß10, which form a loop that interrupts the stranded β-sheet (Fig. 5.2). In BsIDHs, these two strands are absent. The strands β15 and β16 of CgIolW form an additional two-stranded antiparallel β-sheet, which becomes part of the parallel/antiparallel six-stranded β-sheet,

increasing the strand number to eight. This is also true for BsIolW (Fig. 5.3A) and other members of the glyceraldehyde 3-phosphate superfamily (Buehner et al., 1974; Taberman et al., 2016), but not for BsIolG (Fig. 5.3B). In BsIolG, the stretched out β-sheet (β13-14 in BsIolG) was found to be important for tetramer formation (van Straaten et al., 2010). Both CgIolW and BsIolW (PDB 3GDO) were crystallized either as monomer or dimer, but not as a tetramer, indicating that this structural difference might affect quaternary structure arrangement.

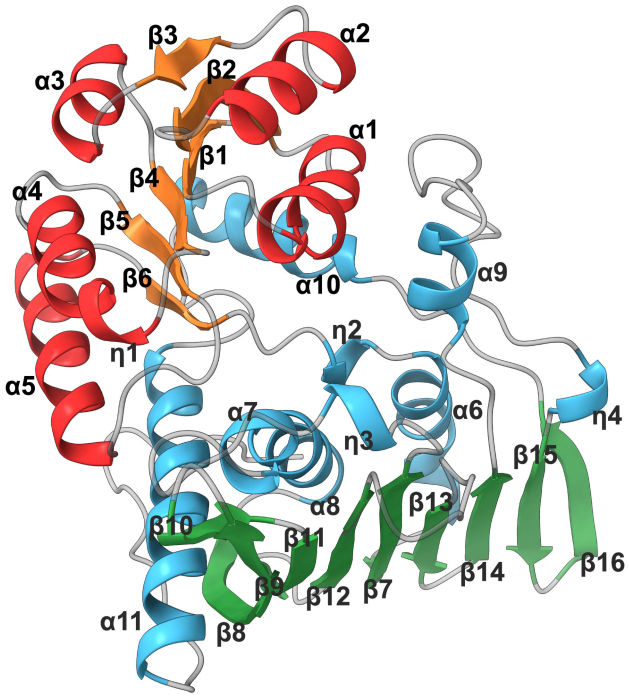

Fig. 5.2 Crystal structure of monomeric apo-CgIolW solved with a resolution of 1.53 Å in ribbon representation. Secondary structure elements of the N-terminal domain (α-helices/η-turns in red, β-strands in orange) and the C-terminal domain (α-helices/η-turns in blue, β-strands in green) indicated.

The NADPH-bound structure showed little deviation from the apo form (rmsd: 0.258A) (Fig. 5.3C). The slight change in the backbone upon binding of NADPH suggests a conformational effect, which is consistent with previous studies of IDH structures in complex with NAD(P)H (van Straaten et al., 2010; Zheng et al., 2013). This change is due to the ordered mechanism of the IDH-catalyzed reaction in which first the binding of the cofactor is necessary to build up the active center to accept the substrate (van Straaten et al., 2010). The dynamic movement upon binding of NADPH was analyzed using the DynDom database of domain motions (Veevers and Hayward, 2019). This allows comparison of the apo- and the NADPH-

bound form for specific hinge bending of domains or residues. Binding of NADPH induces a main bend at residues 118−119, which are close to the residues separating the N-terminal Rossmann fold domain (1−121) and the C-terminal domain (122−341). The C-terminal domain shows only a slight conformational change (rmsd 0.19 Å), while the N-terminal domain rotates by 2.1° about a hinge axis centered at residues 118-119 (Fig. 5.4) towards the C-terminal domain, as reported for other IDHs (Zheng et al., 2013). Effectively, binding of NADPH results in tightening the binding pocket.

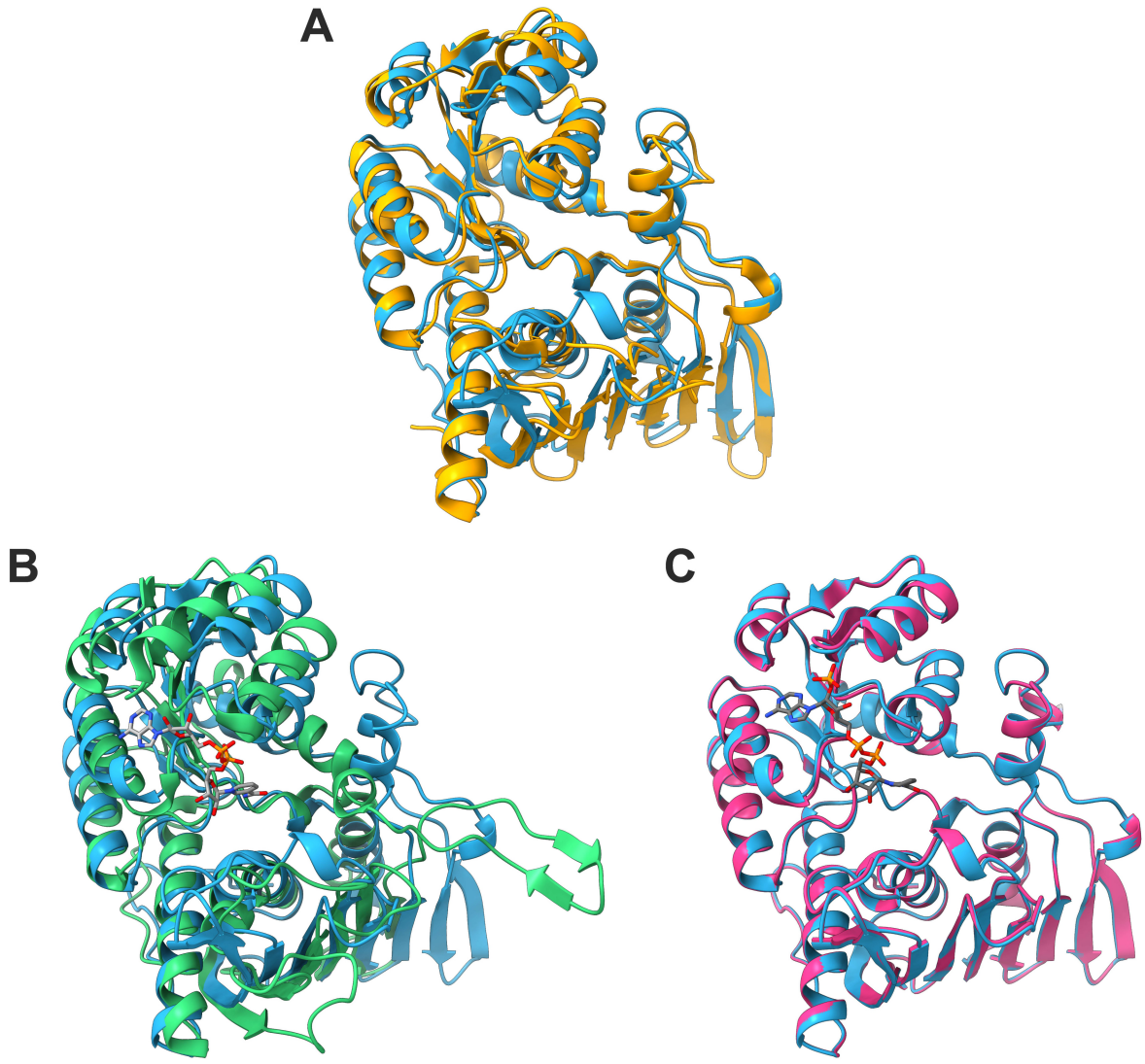

Fig. 5.3. Crystal structure of CgIolW superimposed to other IDHs. A CgIolW apo-structure (blue) superimposed to BsIolW (PDB: 3GDO, yellow). **B** CgIolW apo-structure (blue) superimposed to BsIolG with bound NADH (PDB: 3NT5, green). **C** CgIolW apo-structure (blue) superimposed to NADPH-bound form (pink) with NADPH included.

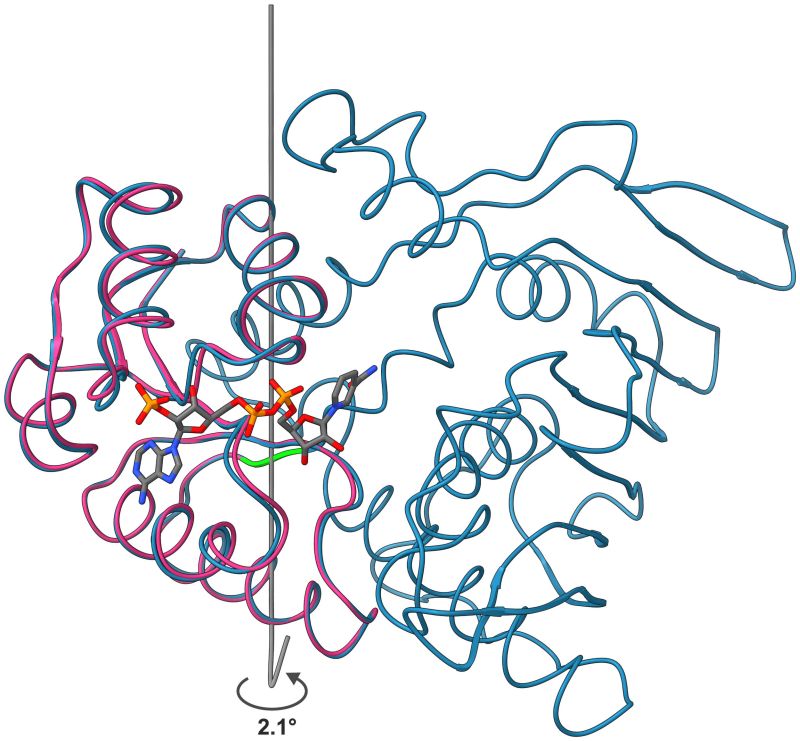

Fig. 5.4. Domain movement of CgIolW after NADPH binding calculated with DynDom. The trace of the α-carbon backbone of apo-CgIolW is shown in blue, the moving N-terminal domain of the NADPH-bound form in pink. The arrow represents the axis of rotation, hinged at residues 118-119 highlighted in green.

The binding of NADPH to CgIolW occurs in the fashion characteristic for IDHs and is very similar to NAD^+ binding to BsIolG (Fig. 5.5 and Fig. 5.6A), with hydrogen bonds formed to nearby amino acid residues and water molecules in the Rossmann-fold domain. The 2′-phosphate of NADPH is stabilized by the positive charge of Arg36 and a hydrogen bond with Ser37 at the N-terminus of the α2-helix. This site is the one that distinguishes between NADPH and NADH in GFO/IDH/MocA family proteins (Carugo and Argos, 1997; Zheng et al., 2013). In most NAD(H)- dependent members, like BsIolG, an Asp or Glu residue is present at position 35, which forms hydrogen bonds to the adenine ribose (Fig. 6B). The negative carboxyl group of Asp35 repels the 2′-phosphate of NADPH, therefore allowing only binding of NAD(H). In CgIolW, Thr40 forms an additional hydrogen bond with the 2′-phosphate of NADPH. The pyrophosphate forms hydrogen bonds with the main-chain amide of Gly13 and structurally conserved water molecules found in the GXGXXG consensus sequence motif for NAD(P)H-binding proteins (Bellamacina, 1996; Bottoms et al., 2002; van Straaten et al., 2010). The nicotinamide ribose is hydrogen-bonded to residues in the loops between β4/α4 and β5/α5. Upon NADPH binding, Ser71 rotates towards the ribose and forms a hydrogen bond to the ring oxygen, while Thr72 and Arg77 stabilize the 3'OH-group. In sugar dehydrogenases, loop β5/α5

contains the functional, conserved C95EKP (*B. subtilis* numbering) motif (Kingston et al., 1996; van Straaten et al., 2010). In CgIolW this motif mediates binding of NAD(P)H via hydrogen bonds between the 2'OH- and 3'OH-group of the ribose and the main-chain amide of Lys95. In contrast to other IDHs, CgIolW contains an Asp94 instead of the highly conserved Glu in the CEKP motif (Fig. 5.6C). The sequence alignment of all characterized IDHs (Fig. S5 of chapter 2.2) showed that CgIolW is the only IDH of that group with an Asp at that position. In IDHs the side-chain carboxyl-group of Glu or Asp makes a hydrogen bond to the carboxamide group of the nicotinamide ring of NAD(P)H (Fig. 5.6C) (van Straaten et al., 2010). In CgIolW the carboxamide group is additionally hydrogen-bonded to the sidechain amide and the hydroxyl group of Asn123.

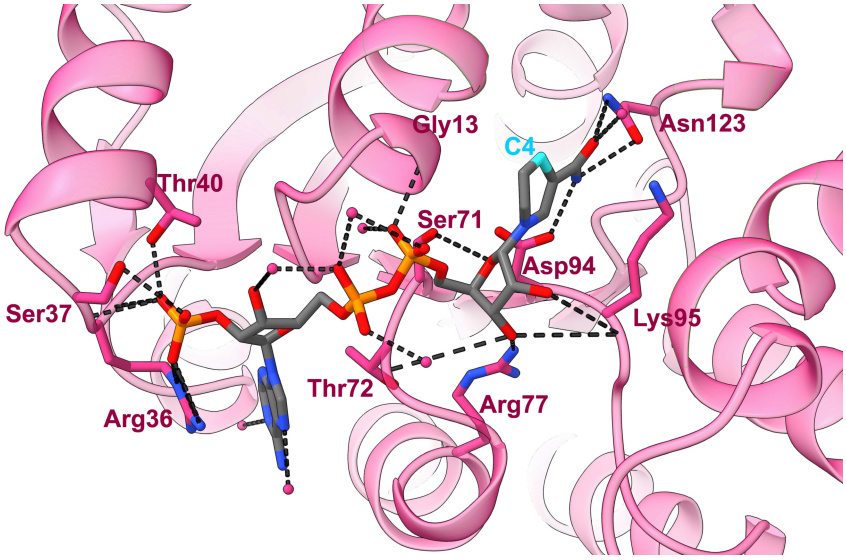

Fig. 5.5. NADPH bound to the CgIolW Rossmann-fold domain. Amino acid residues and water molecules, which form hydrogen bonds (dashed lines) with NADPH are highlighted. The C4-atom of NADPH, which is important for electron transfer is highlighted in light blue.

Another prominent difference between NADPH-dependent and NAD-dependent IDHs is the amino acid residue at position 17. In NAD-binding IDHs, a His residue seems to be conserved, while NADPH-binding enzymes contain a Phe residue (Fig. S5 in chapter 2.2). In CgIolW, the side-chain of Phe17 contained in helix α1 is located above reactive C4-atom of the nicotinamide group of NADPH. In comparison, helix α1 of BsIolG is positioned further away from NAD^+. His17 is located further away and does not interact with NAD^+. Instead, it forms a hydrogen bond with Glu96, which is hydrogen-bonded to the NAD^+ carboxamide group (Fig. 5.6C). In protein 3D structures, the delocalized π -electron system of aromatic side-chains (Phe, Tyr, Trp)

can interact with other aromatic rings via π-stacking (Al Mughram et al., 2021; Pace and Gao, 2013), which does not seem to be the case for Phe17 in CgIolW. We therefore speculate that Phe17 might play a role in correctly positioning NADPH in the active center or it contributes to binding of the substrate 2KMI. Therefore, further work will focus on site-saturation mutagenesis at this site to analyze its impact on NADPH binding and the overall activity.

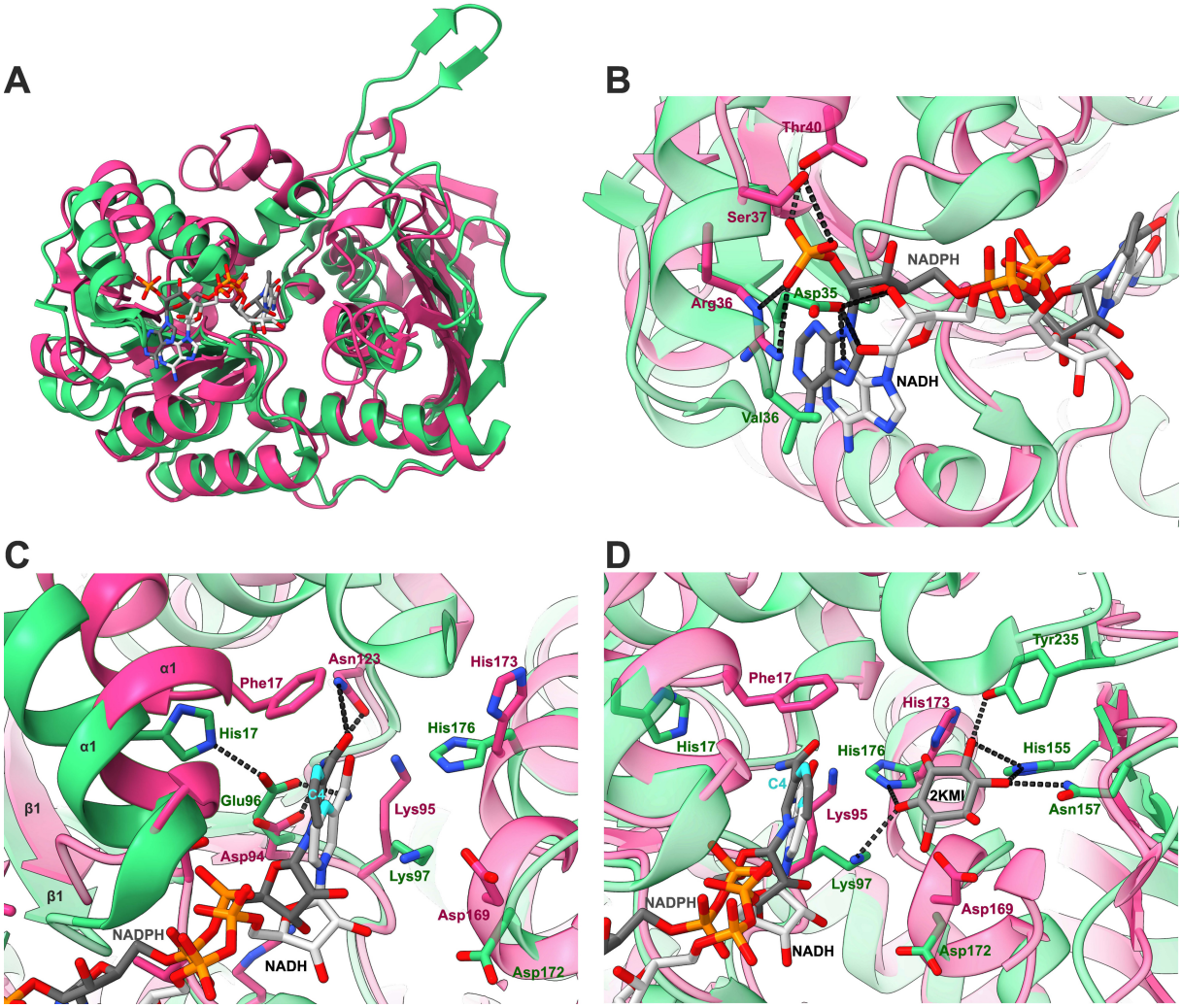

Fig. 5.6. NAD(P)H-binding in CgIolW and BsIolG. A monomeric structure of the NADPH (dark grey)-bound CgIolW (pink) superimposed to the NAD^+ (white)-bound BsIolG (3NT5, green). **B** Comparison of residues at position 35-36 and their function in distinguishing NAD^+/NADPH. **C** Comparison of cofactor positioning in relation to the catalytic triad. **D** Catalytic triad and active center of CgIolW in comparison to BsIolG bound 2-keto-*myo*-inositol (2KMI) with hydrogen bonds (dashed lines) and binding residues.

Unfortunately, we did not obtain crystals of CgIolW in complex with the substrate 2KMI, which would give more insight into the reaction mechanism. Comparison of the CgIolW active center with the one of BsIolG crystallized in complex with 2KMI (PB: 3NT5) shows a number of

differences (Fig. 5.6D). The residues of the catalytic triad, His176, Asp172, and Lys97 show a planar configuration, while the triad in CgIolW reaches more into the active center (Fig. 5.6D). Bound 2KMI in BsIolG forms hydrogen bonds with Lys97 and His176 of the catalytic triad and with His155, Asn157 and Tyr235 of the backbone. As described earlier, we identified Tyr235 as binding site in CgIolW, which potentially plays a role in inositol stereoselectivity, between the all equatorial SI and axial MI/DCI (chapter 2.2). In CgIolW, the corresponding residues (Leu152, Glu154 and Glu229) are not in proximity to 2KMI and the active center shows a more open conformation. It can be assumed that 2KMI binds differently in CgIolW than in BsIolG and to residues at other positions in the binding pocket.

Although we report the first crystal structure of an NADPH-dependent sIDH bound with NADPH, many characteristics of CgIolW are still uncertain. It remains unknown what the physiological function of NADPH-dependent synthesis of SI is or which structural features determine if an IDH prefers oxidation of inositols via reducing NAD^+ or reduction of the corresponding keto-intermediates via oxidation of NADPH. Further studies should focus on obtaining crystal structures of IolW in complex with 2KMI/SI. As an alternative, molecular docking simulations, similar to the ones described in chapter 2.2, offer an alternative possibility to identify binding sites.

5.3 References Appendix

References given in the Appendix are part of the reference list given for the general discussion.

Al Mughram, M. H., Catalano, C., Bowry, J. P., Safo, M. K., Scarsdale, J. N., Kellogg, G. E., 2021. 3D interaction homology: hydropathic analyses of the "π–cation" and "π–π" interaction motifs in phenylalanine, tyrosine, and tryptophan residues. J. Chem. Inf. Model. 61, 2937-2956.

Bellamacina, C. R., 1996. The nicotinamide dinucleotide binding motif: a comparison of nucleotide binding proteins. FASEB J. 10, 1257-1269.

Bottoms, C. A., Smith, P. E., Tanner, J. J., 2002. A structurally conserved water molecule in Rossmann dinucleotide-binding domains. Protein Sci. 11, 2125-2137.

Buehner, M., Ford, G. C., Moras, D., Olsen, K. W., Rossmann, M. G., 1974. Three-dimensional structure of D-glyceraldehyde-3-phosphate dehydrogenase. J. Mol. Biol. 90, 25-49.

Carugo, O., Argos, P., 1997. NADP-dependent enzymes. II: Evolution of the mono-and dinucleotide binding domains. Proteins 28, 29-40.

Emsley, P., Lohkamp, B., Scott, W. G., Cowtan, K., 2010. Features and development of Coot. Acta Crystallogr. D. 66, 486-501.

Evans, P. R., Murshudov, G. N., 2013. How good are my data and what is the resolution? Acta Crystallogr. D. 69, 1204-1214.

Kabsch, W., 2010. XDS. Acta Crystallogr. D. 66, 125-132.

Kingston, R. L., Scopes, R. K., Baker, E. N., 1996. The structure of glucose-fructose oxidoreductase from *Zymomonas mobilis*: an osmoprotective periplasmic enzyme containing non-dissociable NADP. Structure 4, 1413-1428.

McCoy, A. J., Grosse-Kunstleve, R. W., Adams, P. D., Winn, M. D., Storoni, L. C., Read, R. J., 2007. Phaser crystallographic software. J. Appl. Crystallogr. 40, 658-674.

Murshudov, G. N., Skubák, P., Lebedev, A. A., Pannu, N. S., Steiner, R. A., Nicholls, R. A., Winn, M. D., Long, F., Vagin, A. A., 2011. REFMAC5 for the refinement of macromolecular crystal structures. Acta Crystallogr. D. 67, 355-367.

Pace, C. J., Gao, J., 2013. Exploring and exploiting polar–π interactions with fluorinated aromatic amino acids. Acc. Chem. Res. 46, 907-915.

Pettersen, E. F., Goddard, T. D., Huang, C. C., Meng, E. C., Couch, G. S., Croll, T. I., Morris, J. H., Ferrin, T. E., 2021. UCSF ChimeraX: Structure visualization for researchers, educators, and developers. Protein Sci. 30, 70-82.

Rossmann, M. G., Moras, D., Olsen, K. W., 1974. Chemical and biological evolution of a nucleotide-binding protein. Nature 250, 194-199.

Taberman, H., Parkkinen, T., Rouvinen, J., 2016. Structural and functional features of the NAD (P) dependent Gfo/Idh/MocA protein family oxidoreductases. Protein Sci. 25, 778-786.

van Straaten, K. E., Zheng, H., Palmer, D. R., Sanders, D. A., 2010. Structural investigation of *myo*-inositol dehydrogenase from *Bacillus subtilis*: implications for catalytic mechanism and inositol dehydrogenase subfamily classification. Biochem. J. 432, 237-247.

Veevers, R., Hayward, S., 2019. Methodological improvements for the analysis of domain movements in large biomolecular complexes. Biophys. Physicobiol. 16, 328-336.

Zheng, H., Bertwistle, D., Sanders, D. A., Palmer, D. R., 2013. Converting NAD-specific inositol dehydrogenase to an efficient NADP-selective catalyst, with a surprising twist. Biochem 52, 5876-5883.

6. Acknowledgement

I would like to express my special thanks to Prof. Dr. Michael Bott and Dr. Meike Baumgart, who allowed me to work on this fascinating topic, which albeit not being the initial choice, became quite rewarding and leaves room for so much more. I am grateful for their excellent supervision, interest in my project, constant support of my work, applications and ideas, and for the countless inspiring discussions.

Furthermore, I wish to thank Prof. Dr. Vlada Urlacher for agreeing to be my co-supervisor.

I would like to thank all colleagues from the IBG-1 and other institutes for generating such a kind and fun working atmosphere and for all the technical, administrative, and scientific support.

My special thanks go to all colleagues involved in the projects: Prof. Dr. Holger Gohlke, Dr. Christoph Pfleger, and Jonas Dittrich for their tremendous support with the structural bioinformatics and molecular docking simulations without which our joint publication would not have been possible.

A big thank you to Astrid Wirtz for her mentoring and technical support, her always helpful ideas and discussions in all analytic related issues, which were essential for all my projects, and of course for all our nice, not work-related conversations while tinkering at the HPLCs.

ありがとうございました to Prof. Dr. Makoto Nishiyama, Prof. Dr. Saori Kosono, Prof Dr. Ayako Yoshida, and all members of the Agro-Biotechnology Research Center at the University of Tokyo, Japan, for their heartwarming welcome after I was waiting for so long to finally join them for these inspiring and fruitful three months. It was an incredible experience that I will never forget! Special thanks also to Heru for sharing his wisdom about life (Shoganai!) and to Babu-senpai for teaching me the true japanese spirit (Kanpai!). 素敵な時間をありがとうございました。また来ま!

My deepest gratitude goes to all former and current members of the AG Regulation who welcomed me as a Master student and supported me throughout this wonderful time as PhD-student.

Special thanks to Susana for her guidance and brilliant supervision, for the nerdy talks and being the victim of as well as assisting in all my pranks, and so much more. Of course, I want

to thank also Angela and Brita for contributing to the best office atmosphere in “Fun-Office #248”. Thanks for all the fooling around and cross-generational babbling!

I would particularly like to thank Christina Mack for her excellent performance of countless cloning and cultivation experiments as a significant contribution to our projects and even more for all the shared loud laughter and gossiping, and for tolerating my chaotic nature.

One does not simply write this acknowledgment without giving special thanks to Alex, starting under my turbulent supervision as Master student, being there from day one of this project and staying as a PhD to see its end. It’s over, it’s done!

Thank you so much to my PhD-Twin Lea, for being my lab buddy, for sharing my pain, for all the talks through our bench about everything going on in the world, for staying as Postdoc with me and for always managing my administrative issues, deadlines, certificates and of course vacation days. I would not have survived without you!

Of course I have thank Benita, Cedric, Claudia, Daniel, Friederike, Helga, Jan-Gerrit, Johanna B, Johanna MB, Karen, Kiki, Lea-Zola, Lingfeng, Lukas, Marielle, Natalie, Philipp, Rico, and Srushti. Not only for the constant scientific support but also for all the joking around to spice up the everyday work in the lab. For all the laughter, fun, jokes, joint lunches and adventures!

Thanks to my Aachener Synzell Gang: Lars, Christiane and Philipp. Not only for all the fun car rides together to and from work but all the fun evenings in the Aachener City and at home. And for still being friends after leaving Jülich!

I would like to take this opportunity to say a special thank you to all my friends who I can always rely on and who have always supported me. Thanks to my family for making this path possible for me.

Finally, yet importantly, I would like to thank Api from the bottom of my heart for her unconditional support in every difficult situation, for all her patience with me and for the all the weekends we spent together in the lab!

„*So long, and thanks for all the fish*”
- Douglas Addams, 1984

7. Erklärung

Ich versichere an Eides Statt, dass die vorgelegte Dissertation von mir selbständig und ohne unzulässige fremde Hilfe unter Beachtung der „Grundsätze zur Sicherung guter wissenschaftlicher Praxis an der Heinrich-Heine-Universität Düsseldorf“ erstellt worden ist. Die Dissertation wurde in der vorgelegten oder in ähnlicher Form noch bei keiner anderen Institution eingereicht. Ich habe bisher keine erfolglosen Promotionsversuche unternommen.

_____

Aachen, den 29.09.2022